Low Temperature and Low Pressure Bonding of Power Module and Copper Heat Spreader by Transient Liquid Phase Sintering

過渡液相焼結法による パワーモジュールと銅ヒートスプレッダの 低温及び低圧力接合

October 2017

Khairi Faiz MUHAMMAD

ムハマド　ハイリ　ファイズ

Low Temperature and Low Pressure Bonding of Power Module and Copper Heat Spreader by Transient Liquid Phase Sintering

過渡液相焼結法による パワーモジュールと銅ヒートスプレッダの 低温及び低圧力接合

October 2017

Waseda University

Graduate School of Creative Science and Engineering

Department of Modern Mechanical Engineering, Research on Transporters and Energy Plants Materials Science and Engineering

Khairi Faiz MUHAMMAD

TABLE OF CONTENTS

CHAPTER 3: METHODOLOGY

CHAPTER 4: SILVER-BASED TRANSIENT LIQUID PHASE SINTERING

CHAPTER 5: COPPER-BASED TRANSIENT LIQUID PHASE SINTERING

CHAPTER 1: INTRODUCTION

1.1 Research Background

The key factor on reducing global warming is by cutting down the emission of greenhouse gases such as carbon dioxide (CO_2), which occupies two-thirds of the global greenhouse gases, as shown in Figure 1.1 [1]. In the same report by US Environmental Protection Agency (EPA), 14% of the source was generated from transportation sector, where 95% of the world's transportation energy generated from petroleum-based fuels [1]. In recent movement on reducing global greenhouse gas emissions specifically from the transportation sector, Britain government has pledged to ban sale of all new petrol and diesel cars and vans from year 2040 due to the extreme concern of the rising levels of exhume gas that poses a major risk to public health [2].

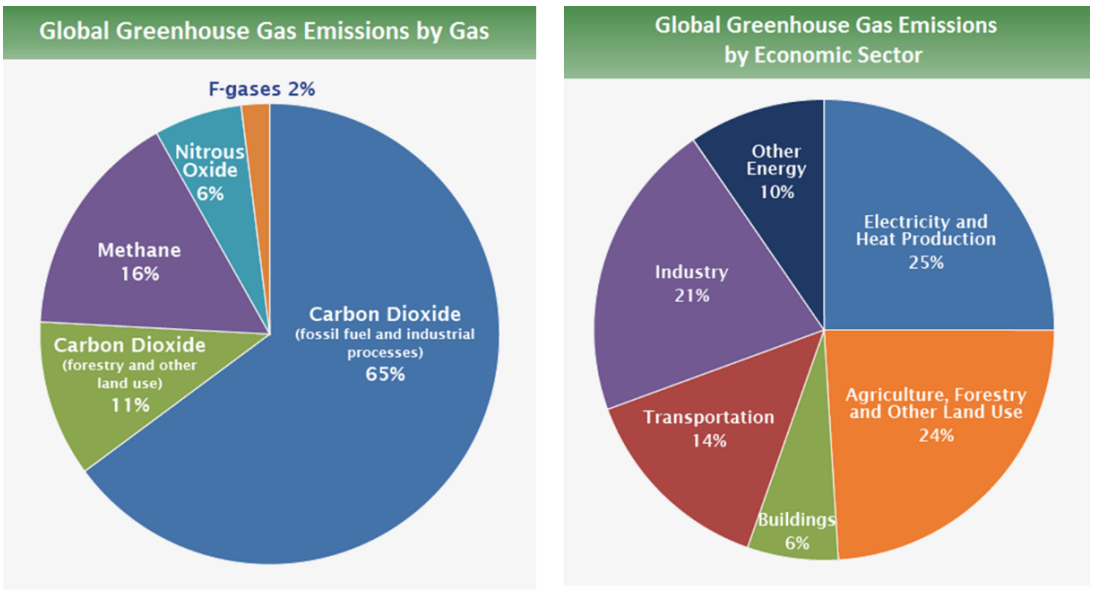

Figure 1.1 Global greenhouse gas emissions as reported by EPA on 2014 [1]

Major breakthrough of hybrid electric vehicles (HEVs) and electric vehicles (EVs) are receiving global attention to cut back CO_2. Power electronics module, which is the heart of HEVs and EVs, is one essential component that processes, converts, and control the energy in the system. One brief example on how power electronics module functions in HEVs can be seen in Figure 1.2(a) [3]. The alternate current (AC) that is generated by electric motor during traveling will be converted to direct current (DC) and will be stored in the battery. The electric energy from the battery will be used to operate the vehicle when engine demand is low, such as when starting or traveling at light load.

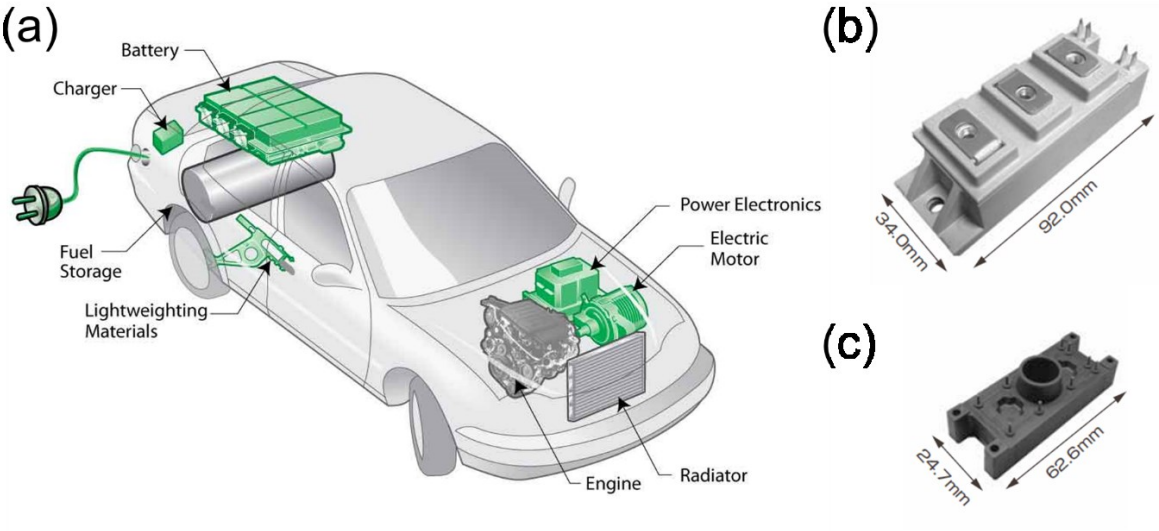

Figure 1.2 (a) An example of hybrid cars and its major components [3], (b) a Si-based module manufactured by Fuji Electric Co. Ltd, and (c) an All-SiC module from the same manufacturer [4]

In recent years, power modules has manifested a great advancements with the recent development of the state-of-the-art wide band gap devices such as silicon carbide (SiC) and gallium nitride (GaN). This has enabled power modules for not only achieving higher power density compared to the conventional Si-based devices, but also allowing miniaturization of the power modules, which

in return lead to the weight reduction of the vehicles and subsequently less emission of CO_2. In a report published by Fuji Electric Co. Ltd., the foot-print size of 1200V/100A All-SiC power module can be reduced to 50 % compared to the conventional Si-based power module with similar voltage rating, as shown in Figure 1.2(b-c) [4]. Not only that, the P-N and gate inductance are also trimmed to 75%, which displays the superiority of SiC-based power module over its future-predecessor [4].

However, one major issue need to be tackled for the next generation power module is an efficient heat dissipation system. While the major breakthrough of the power electronics devices has opened many doors of possibilities, the high heat density generated from the SiC/GaN-based during operation has triggered a new problem that need urgent solution in order to utilize the devices to their maximum limit. Packaging technology, which is one of the most important key to enable these devices to achieve their high power performances at high temperature operation, has also showed a tremendous improvement in these recent years. From conventional indirect liquid cooling-type, which used thermal grease as thermal interface material, improvised-type of power electronics modules adapted direct liquid cooling which used tin-based (Sn) solders to bond the power module to the heat spreader and/or heat sink [5]. Aluminum (Al) wire bonding has been replaced with copper (Cu) pin which can withstand higher thermal density and exhibit lower electrical resistivity. Meanwhile, thick Cu plate was incorporated in direct bonded copper (DBC) substrate to facilitate the spreading and conducting of heat to the heat sink. Additionally, the usage of low heat-resistance silicone gel has also being replaced with high heat-resistance and high rigidity epoxy resin.

Formerly, tin-silver (Sn-Ag) solder has been used as the thermal interface material [6] but recently tin-antimony (Sn-Sb) solder received great attention owing to its higher heat resistance and higher mechanical strength compared to the former [7, 8]. Sn-Sb solder exhibited two types of mechanical strengthening, i.e. solid solution strengthening and precipitation strengthening [7], and also showed a longer fatigue lifetime compared to the Sn-Ag solder [8]. On the other hand, one

considerable drawback when applying Sn-Sb solder is its high processing temperature. The processing temperature when using Sn-Sb solder may vary depending on the weight percentage (wt.%) of the Sb contained in the solder which corresponds to the liquidus temperature, e.g. the processing temperature of Sn-8wt.%Sb was up to 325°C [9]. Processing temperature should be as low as possible to avoid thermal damage to the packages especially to the epoxy-molded packages that require processing temperature less than 250°C, which is the glass transition temperature of the epoxy resin. Processing temperature that is higher than the glass transition temperature of the epoxy resin leads to rapid expansion of the resin and are suspected to induce thermo-mechanical stress to the module. Furthermore, coefficient of thermal expansion (CTE) mismatch between direct copper bonding (DCB) substrate and the heat-spreader and/or heat sink may lead to residual bending after fabrication at high temperature region. This is detrimental to the reliability of the power modules since warpage may contribute to the premature cracking in the joint materials [10]. Low melting temperature solders like Sn-57wt.%Bi (tin-bismuth, T_m:139°C), Sn-In-Bi (tin-indium-bismuth, T_m:100-109°C), Sn-9wt.%Zn (tin-zinc, T_m:198°C) might be a solution to the aforementioned problem, but as a rule of thumb, solder materials can be reliably used up to the homologous temperature of $0.8T_h$ of their absolute melting temperature before creep effects accelerate the degradation [11]. For SiC or GaN based modules which generate high heat-density during operation, high heat-resistance solders or joining technology that are thermally stable up to 125°C is in great demand.

One considerable approach to overcome this problem is by using metal nanoparticles sintering. Due to the nano-scale size of the particles, sintering can be realized at relatively low temperature compared to the melting temperature of the bulk material, with or without external pressure. Additionally, the melting point of the as-sintered materials can rise up to the bulk melting temperature, indicating the high thermal-stability of the joint. Nanoparticles sintering, particularly Ag and Cu nanoparticles has been used as die attach material because of their superior electrical and thermal

conductivities as well as higher melting temperature compared to the conventional solders [12-16]. Nevertheless, there are two major concerns when applying Ag or Cu nanoparticles as joint materials. The first one is the high external pressure exerted during sintering so that densification of the materials can occur rapidly due to the fact that the mechanisms of the sintering are solid-solid interdiffusion [11-13, 17-21]. Next, in the case of Ag nanoparticles sintering, Ag plating is inevitable. This Ag plating has twofold aims, i.e. to prevent oxidation of Cu-substrate, and to facilitate interdiffusion between Ag atoms to ensure a good joint. However, to apply metal particles sintering as joining material of epoxy-molded module is absurd since introducing high external pressure during fabrication is detrimental to the packaging and unfavorable to the industry as it complicates the production line. Furthermore, employing metal-plating to epoxy-molded module is also impractical and expensive.

On this account, transient liquid phase sintering (TLPS) has garnered attention as one of the method to achieve rapid densification without having to exert high external pressure during fabrication. Materials with low melting temperature is mixed with high melting temperature materials, and heated above the temperature of the melting temperature of the low melting temperature materials. Upon reaching the melting point, low melting temperature materials will melt and subsequently react with the matrix to form solid-solution or intermetallic compounds during isothermal solidification. The advantage of the TLPS does not only lie on the rapid densification without having to apply high sintering pressure, the remelting temperature of the as-sintered materials also increased due to the isothermal solidification [22]. Furthermore, with adequate amount of molten liquid metal, metal plating was unnecessary to form a strong interface reaction layer at the Cu-substrates [23]. TLPS technology, which possess these attractive characteristics is anticipated to be applied as thermal interface material.

In this present study, TLPS technology will be focused as a fundamental study to bond the epoxy-molded SiC-based module to the Cu heat spreader/heat sink. Five crucial points as the bonding requirements, in which this study will be centered on, are addressed as follows:

i. **Low bonding temperature (≤ 250 °C)**

ii. **Low bonding pressure (≤ 0.1 MPa)**

iii. **Plateless Cu-Cu bonding**

iv. **Fluxless bonding**

v. **High-remelting temperature (≥ 200 °C)**

Ag nanoparticle or Cu nanoparticle is mixed with eutectic Sn-Bi powders to realize the TLPS in order to fulfill all the mentioned five requirements. Influences of mixture composition and processing conditions on the mechanical properties (shear strength) and microstructure is investigated and discussed. The mechanism of transient liquid phase sintering of above materials will be elucidated and explained. Finally, mixture composition and processing conditions that passed the requirements will be proposed.

1.2 Overview of Power Electronics Module Packaging

Power electronic packaging technology is a very complex technology which consists of first level or chip-level packaging to higher level packaging such as system level packaging. On this study, the bonding of high level packaging will be the main interest. In order to comprehend the limitations that exist in the high-level packaging particularly on the future generation module, at first, the conventional type power module packaging technology will be explained in details. Then, the revolution of packaging structure to cope with the emerging problems of the newly developed power electronic devices will be introduced. Finally, demands in packaging technology of this newly developed power module will be discussed.

1.2.1 Conventional Packaging Technology

In general, the main components that constitute conventional power module are semiconductor device, electronic circuit ceramic substrate, conducting wire, solders, heat spreader, encapsulation resin, thermal interface material, and heat sink. Figure 1.3 shows the cross-sections of conventional power module packaging. Some physical properties for each components are listed in Table 1.1.

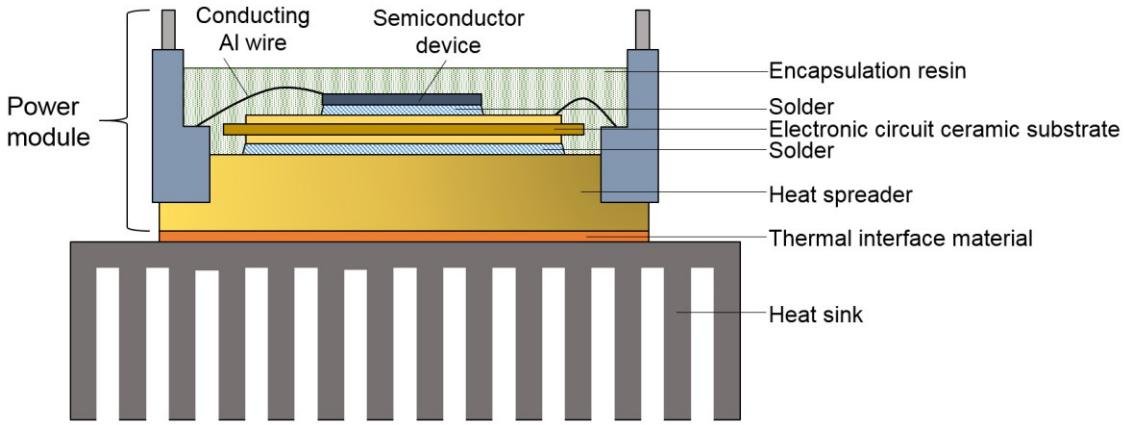

Figure 1.3 Cross-sections of conventional power module packaging [7]

Table 1.1 Physical properties of components in conventional power module

Components		Material	Thermal conductivity (W/mK)	Coefficient of Thermal Expansion (ppm/K)	References
Device		Si	83.7	3.0	24
Electronic circuit ceramic substrate	Conductance foil	Cu	393.5	16.5	24
		Al	222.0	23.6	24
	Ceramic	Al_2O_3	20.9	7.1	24
		AlN	170.0	4.6	24
		Si_3N_4	70.0	3.4	24
Solder		Sn-37wt%Pb	46.0	26.3	24
		SAC305	63.2	21.6	25
		SAC396	61.1	21.8	25
		Sn-3.5wt%Ag	54.3	22.2	26
Heat spreader		Cu	398.0	16.9	27
		Mo	140.0	5.0	27
		Al-65vol%SiC	180.0	7.5	24
Thermal interface material		AlN (60 vol%)	2.14	31.7	28
		SiC (60 vol%)	2.25	15.8	28

Power module packaging is defined as the fabrication of semiconductor devices onto DBC substrate, accompanied by the wire bonding to complete the desired electric circuit, mounting the DBC substrate onto heat spreader, and finally encapsulating the fabricated module into the case where resin is deposited into the case to protect the module, particularly the conducting wire and devices from any impurity that may cause short circuit. The fabricated power module is mounted onto the heat sink by screwing. To assist the cooling of the power module to the heat sink, thermal interface

material is deposited between the former and latter. A brief description of each component is explained as follows:

Semiconductor device

Semiconductor can be broadly classified to p-type and n-type semiconductor. Silicon (Si) which is said to be second largest abundant element in earth is one type of semiconductor. For each Si atom, there are four electrons in its outer orbital. For each electrons, they form perfect covalent bonding to the neighboring atoms which create a silvery, metallic-looking substance. However, due to the perfect covalent bonds created between each electrons, there are no free moving electrons. Thus, a pure Si lattice do not show any electricity property as there are no flow of electrons. By adding impurities to the crystal of Si, the free electrons will be created which transform the Si into a conductor. The process of adding impurities into the crystal is called "doping". For example, by doping phosphorous into the Si crystal, one free electrons will be created due to the fact that one atom of phosphorous has five outer electrons. This type of semiconductor is called n-type semiconductor, where the n is referred to the negativity of free electrons. Meanwhile, when an element with three outer electrons such as boron or gallium is doped into the Si, a hole with positive charge effect is created because one electron of Si atoms do not have pair to create a covalent bond. The p naming is referred to the positive charge that is created in the holes. When the n-type and p-type semiconductor is joint together, the insulation space which hinder the pairing of electrons and holes between former and latter is called junction. The insulation space is usually created by a thin metal-oxide layer, e.g. in Si chip, silicon oxide (SiO_2) acted as the insulation layer. The phenomenon of combining free electrons and holes through the junction at certain condition, create current flows, which would make the basis of a semiconductor devices. Figure 1.4 shows the illustration of the cross-sections of Si-based Insulated Gate Bipolar Transistor (IGBT) devices [24].

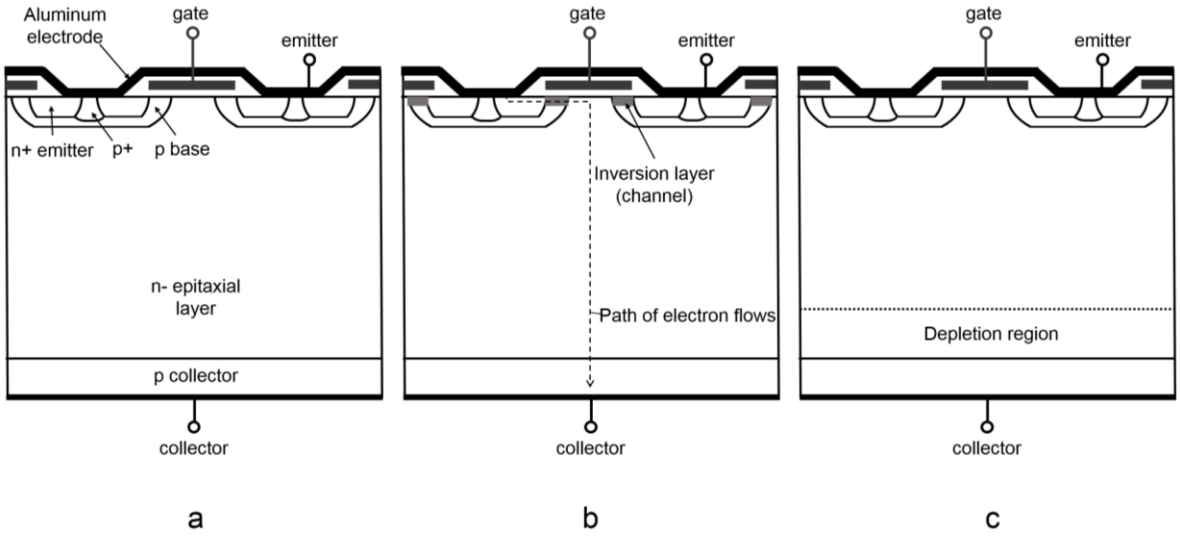

Figure 1.4 Illustration of **a** cross-sections of IGBT device, **b** IGBT under operation (Voltage at gate = V), and **c** IGBT not under operation (Voltage at gate = 0) [24]

As can be seen from Figure 1.4a, IGBT device consist of two p-n junctions: one at the emitter, and one at the collector, hence, the naming of bipolar transistor. There are three components that make up the IGBT device, i.e. emitter, collector and gate. Between the p base region and gate, there is a thin layer of metal-oxide as insulator. In order for the main current to flow from the emitter to the collector, control of voltage at the gate plays a vital role. When a positive voltage is applied to the gate, an n-type-like inversion layer will be created at the top of the p base as shown in Figure 1.4b. This will create a path for electron from n+ emitter to flow into the n- epitaxial layer, called channel. When the collector is charged with positive voltage, the holes will move up to the emitter and the electron from the emitter will move down to the collector, hence, creating a current flow. Conversely, when the voltage at gate is reduced to zero, the inversion layer will be diminished and the flow of current will be intercepted. This will produce a depletion region near the p collector and the current will not flow into the collector. Since the existence of additional p region at the collector compared

to the MOSFET device (Metal Oxide Semiconductor Field Effect Transistor), it allows the IGBT to handle higher voltages.

The main feature of semiconductor device such as IGBT as explained above is switching for the conversion and control of the electricity. For example, IGBT devices can handle and control electric current ranging from 25 to 1200A, voltage from 400 to 3300V, and frequency up to tens of kHz [24]. The ability of high-speed switching of the IGBT devices enable the realization of a smooth sinusoidal wave during converting direct current to alternating current which is the main application in rotating motor in EV/HEV. However, one major problem during switching is turn-on and turn-off loss. This switching loss is converted into heat which will accumulate with rising switching numbers (increasing frequency). This generated heat is detrimental to the devices since it will lead to the operation failure of the devices. The junction temperature, T_j of the devices can be calculated using equation (1.1) [24]:

$$T_j\,(°C) = P\,(W) \times R_{th}\,(°C/W) + T_a\,(°C) \tag{1.1}$$

where P is the switching loss, R_{th} is the thermal resistance, and T_a is temperature surrounding the devices. In general, the allowable T_j of a Si-based devices are up to 175°C and the optimum $T_{j\,op}$ is approximately 150°C. Meanwhile, for the wide-band-gap devices such as silicon carbide (SiC) devices, T_j can reach up to 300°C.

The challenges of Si-based devices for higher current and voltage applications rely on two factors. One is the poor electron hole mobility. Second is the thinning metal-oxide as insulation layer. It is understood that to reduce the increase of temperature, ΔT, of the devices, it is essential to reduce the thickness of the devices and other components, as can be seen from equation (1.2) and (1.3) [24].

$$R_{th} = t / (\lambda \times S) \quad (1.2)$$

$$\Delta T = P \times R_{th} \quad (1.3)$$

where R_{th} is thermal resistance, t is thickness, λ is thermal conductivity, S is area, and P is switching loss. SiO_2 as the gate insulator in Si-based devices begun to lose its insulating properties and has reach its limit with the miniaturization of the devices. SiC-based devices with same thickness and same area to the Si-based devices can handle higher voltage and current but with less switching loss, which in return leads to reduced temperature rise in the devices. Thus, the future of wide band gap devices such as SiC and gallium nitride (GaN) is highly anticipated to replace Si-based devices, but with the limitations of higher junction temperature up to 300°C as explained above.

Electronic circuit ceramic substrate

Electronic circuit ceramic substrates that are commonly used in power semiconductor modules are Direct Bonded Aluminum (DBA) and Direct Bonded Copper (DBC) substrate, consisting of a ceramic insulator plate that is sandwiched between two metal foils/plates. In general, the metal on the top side of the substrate are bonded into a specific pattern according to the predesigned electric circuit. On the other hand, at the bottom are kept plain. There exist twofold purposes for electronic circuit ceramic substrate: First, as an electric insulator to prevent electric circuit shock, and second, to transfer the heat from the devices and spread it to larger area before heat is dissipated at the heat sink. DBC substrate garnered attention as a replacement for the complicated assemblies based on leadframes and refractory metallized substrates. This is owing to the facile assembly and the low coefficient of thermal expansion (CTE) of DBC substrate. Although thick Cu metallization exist at both sides, the low CTE of DBC substrate which similar to the Si chip, contributes to low stress concentration during operation which in return lead to high reliability of the power module.

Cu direct-bonding to ceramic substrate is realized by the coupled fusion and diffusion process [29]. Cu foils/plates are oxidized during high temperature annealing to form thin layer of eutectic melt. The existence of 1.54 atomic percentage of oxygen in Cu reduces the melting temperature of Cu to eutectic temperature of 1065°C. When the surface-oxidized copper foils/plate is heated at the eutectic temperature, the molten Cu will react with ceramic substrate by forming a very thin Cu-ceramic layer. By diffusion of Cu and oxygen into the ceramic substrate, the direct bonding of Cu to the ceramic substrate is realized. On the other hand, the ceramic substrate also need to be oxidized by high temperature oxidation in order for the fusion-diffusion process to take place.

Conducting wire

Conducting wire is used to connect a power semiconductor devices face with each other devices or other connecting elements. Since most of the electrode plate that is used at the outer face of semiconductor devices is made of aluminum (Al) due to its high electrical conductivity, Al wire is commonly used as the conducting wire. Several Al wires may be used at the same electrode due to the limited current capability of a bond wire.

There are two methods in wire bonding process: First, is the thermal compression bonding, or also known as ball bonding. Substrates is heated and ball is placed on the substrate. Ball is pressed by the bonding tool and welding is achieved by atomic bonding forces and diffusion. Second, which is more commonly adapted in power module is the ultrasonic bonding or also called as wedge bonding. The principle of ultrasonic bonding relies on the heat generated by the friction of ultrasonic forces. The pressure exerted during bonding break the oxide layer at both Al electrode and Al wire. In contrast with thermal compression bonding, no external heat is required and no change of overall microstructure is accompanied since no melting of materials take place.

Limitations in wire bonding technology lies on the length and diameter of the wire. Heat that is generated during operation due to the electrical resistance increased with decreasing diameter and increasing length. The dissipation of heat from the wire only occur at the end of the wire, thus usage of bands are being accepted recently owing to the larger bond cross-sections.

Solders

On the first level packaging, Si-based devices are mounted onto the DBC substrate by soldering technology. At this level, high-heat resistance solder is needed due to the fact that the solder directly receives the heat that was generated from the devices during operation. Then, DBC substrate are mounted onto Cu heat substrate, also by soldering technology. However, at this level, since the heat was spread to larger area and not concentrated owing to the existence of Cu-foil at both sides of the DBC substrate, usage of lower heat-resistance solders is more common. Soldering mechanism, its advantages and challenges will be described in details later in Section 1.3.1.

Heat spreader

The main purpose of heat spreader is to conduct and spread the heat transferred from the DBC/DBA substrate to a larger area before transferring it to the heat sink. Hence, materials with high thermal conductivity such as Cu and Al has always been the choice. However, selecting a suitable material is highly dependent on matching CTE values with other components in the package to avoid high thermal stress [30]. In conventional packaging as shown in Figure 2.1, heat spreader is intimately bonded to the DBC substrate, but mounted on the heat sink by screwing. Although the bulk materials used in heat spreader contribute to efficient heat dissipation system, the problem relies on the low thermal conductivity of thermal interface material inserted below the heat spreader.

Encapsulation resin

The general purpose of encapsulation resin is to serve as electrical insulation and protecting the devices and wire bonds from impurities like dust or any materials that may cause electric circuit short. The most commonly used encapsulation resin is silicone gel [24] since it is easy to handle and cheap in cost. However, there are two major issues regarding conventional silicone gel [24]. Firstly, the silicone gel possess low heat-resistance and tends to bake-out with increasing temperature, hence leads to degradation of the silicone gel. Secondly, silicone gel is easily deformed and cannot sustain the deformation of the devices and other components in the packaging. A new encapsulation material that is compatible to constrain the deformation of other components in the packaging is highly anticipated.

Thermal interface material

In conventional packaging, power module is mounted onto the heat sink by screwing. However, the gap that exist between former and latter is the main factor that degrades the thermal contact resistance. The surface roughness of the heat sink may reach up to 100 μm [31] and the air gap is filled with thermal interface material such as thermal grease to transfer the heat. Although thermal conductivity of a thermal grease is relatively lower (refer to Table 1.1) compared to the other components in the packaging, it is better than transferring the heat by air. Thermal greases are made by mixing silicone or hydrocarbon oil with conductive particles such as silver, aluminum oxide or zinc oxide [32]. The key point in increasing thermal conductivity of thermal grease is by minimizing the contact resistance of the filler in the grease. On this account, it is desirable to mix filler with maximum particle size that is lower than the surface roughness of the heat sink. Additionally, the raw material has to be a paste-like substance for easy printing [33].

However, in addition to the low thermal conductivity, the main concern when applying thermal greases are messy, difficult to apply and remove during re-work, and tends to pump-out and migrate away from the center [32, 34]. Moreover, with increasing operation time, grease tends to dry-out and become powdery, hence, increasing thermal resistance and reducing the efficiency of heat-dissipation. Furthermore, greases that pump-out of the interface can cause electrical shorts because greases can be electrically conductive depending on the materials of the fillers.

To review, the issues relating to each component in power module and emerging problems from conventional packaging structure are summarized as follows:

i. ***Sn-based*** power semiconductor devices are approaching their physical limits in terms of operating frequency, breakdown voltage, and power density. Wide-band gap devices such as SiC and GaN-based devices are anticipated to replace Si-based devices but with a trade-off of higher junction temperature.

ii. ***DBC substrate*** is one of the adjacent component to the devices. Ceramic substrate with high thermal conductivity is a promising candidate to be introduced but the CTE must be as low as possible or match the CTE of the devices to reduce thermomechanical stress concentration due to the contraction of materials with different CTE during assembly and high temperature operation.

iii. ***Aluminum wire*** is the major connecting conductor wire that was used to connect devices to devices and other elements. However, since the junction temperature of the SiC/GaN-based devices may rise to 300°C, development of new connecting method is in great demand. In addition, due to the fact that electrical resistance is highly dependent to the diameter and length of wire, band/ribbon or pad-type connector is replacing the conventional connecting wire technology.

iv. ***Solder*** with high melting temperature was used to sustain the high heat density generated by the devices during operation. However, one major concern of the solder at the first-level packaging is creep deformation. In this section, although it is not explained in details, creep deformation will accelerated when the temperature of the solders used higher than 0.8 homologous temperature in Kelvin (K). Hence, die-attach materials that can sustain higher operation temperature for the application under SiC/GaN-based devices need to be developed. On the other hand, at substrate level packaging, substrate is bonded to the heat spreader by means of low melting temperature solders since the temperature is not a major concern in the conventional type packaging. However, for future packaging that will be explain later in Section 2.1.2, a new bonding materials is needed to cope with the newly emerging problems.

v. ***Heat spreader*** in conventional packaging is essential to spread the heat from the devices and substrate to a larger area before the heat is transferred to the heat sink. Materials with high thermal conductivity such as Cu and Al has been used as heat spreader and thickness of the heat spreader is one of the main parameter that influence the spreading of the heat. Too thin substrate led to insufficient spreading, but too thick substrate led to increasing weight of the package.

vi. ***Thermal interface materials*** such as thermal grease was inserted in between package and heat sink as a heat conductive materials to transfer the heat from the package to the heat sink. Although the heat conductivity of thermal grease was relatively lower compared to the other components in the package, it was better than conducting the heat by air. There were several issues regarding thermal grease as thermal interface material in the conventional packaging such as messy, difficult to apply and remove during re-work, and tends to pump-out and migrate away from the center.

1.2.2 Recent Trend in Packaging Technology

According to a data published by Fuji Electric Co. Ltd. in [35], due to the low thermal conductivity of the thermal grease, approximately 20% of the thermal resistance of the whole packages in conventional packaging compensated from thermal grease. One major change in recent packaging technology is the absence of thermal grease as the thermal interface material. Figure 1.5(b) and (c) shows two types of packaging that eliminate the usage of thermal grease [6]. Bulky heat spreader was also eliminated and DBC substrate were rather jointed to the heat sink by means of soldering.

Figure 1.5(b) shows open-type packaging structure where the DBC substrate was mounted onto the cooling-fin-attached heat spreader base. Then, the heat spreader was mounted onto separated water jacket. O-ring was inserted to seal the water jacket. On the other hand, Figure 1.5(c) illustrated the close-type packaging structure where DBC substrate was mounted onto heat sink with built-in cooling fin. Both types of packaging used solder as thermal interface material to join DBC substrate with heat spreader/sink. Sn-Ag solder or Sn-Sb solder were used owing to their high strength properties [36]. Although both "direct cooling" packaging showed superior heat dissipation efficiency compared to the conventional packaging, the existence of small-gap between the cooling fin ends and the bottom of the water jacket in the open-type structure led to higher thermal resistance compared to the closed-type structure. This deteriorated cooling performance was due to the gap clearance was bigger than the fin gaps that resulted in increased coolant flow where slower coolant flow at the fins were observed in the flow simulation model conducted in [6]. The closed-type packaging structure was applied to the IGBT module (1200V/500A) for HEV application [36].

Next, on realizing the downsizing of future generation SiC-based power module, issues such as heat dissipation, electrical insulation, and heat resistance were tackled by the newly developed structure as shown in Figure 1.5(d).

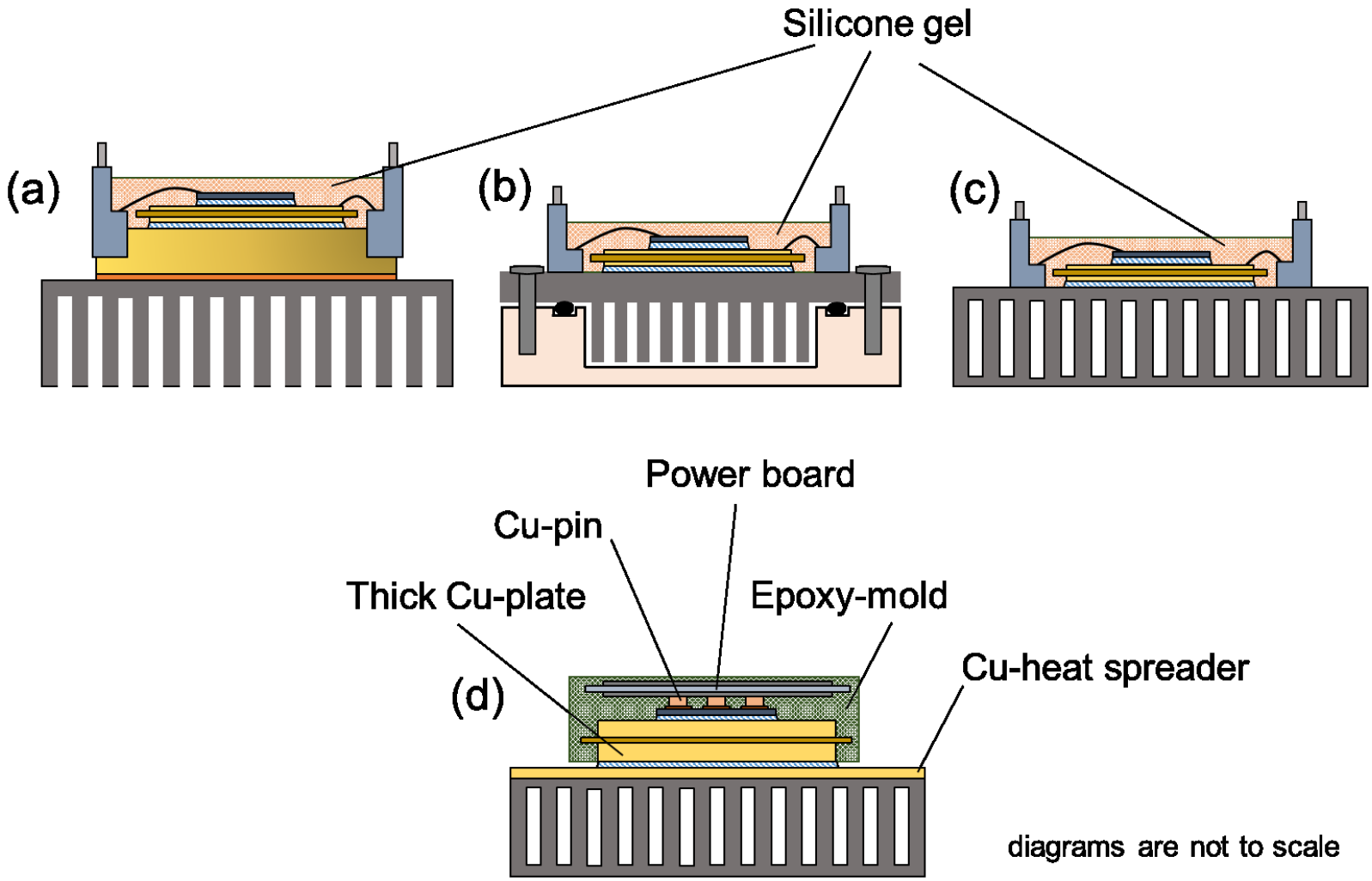

Figure 1.5 The evolution of power module packaging: (a) conventional packaging that incorporated thermal grease as thermal interface material [7], (b) direct bonding open-type packaging [6], (c) direct bonding close-type packaging [6], and (d) next generation epoxy-molded module packaging [4]

Major improvements that was implemented in this new structure compared to the conventional structure are listed in Table 1.2 based on the report published by Fuji Electric Co. Ltd. [4, 37]. One drawback of the next-generation epoxy-molded module is employing metal-plating onto the Cu-backside (Cu-thick plate) of the DBC substrate might be difficult and expensive. On the other hand, it is also expected that by a new introduction of Cu heat spreader on top of the Al heat sink, a significance increase on heat spreading to the Al sink can be anticipated, as well as a buffer to reduce the thermomechanical stress due to large CTE mismatch between Al heat sink and DBC substrate.

Table 1.2 Comparison of conventional Si-based and newly developed all-SiC based packaging

Conventional (Si-based)	New (SiC-based)	Characteristic and outcomes
Sn-Ag solder (under chip)	Ag-sintering (under chip)	▪ Capable of bonding at relatively low temperature and thermally stable up to 961°C, i.e. melting temperature of Ag ▪ Thermal conductivity is one order higher
Al wire bonding	Cu pin and power board	▪ Devices are connected to the Cu circuit in power board by Cu-pin ▪ Chips can be located near to each other which resulted in decreasing footprint size
Al_2O_3 (DBC)	Si_3N_4 (DBC)	▪ Higher thermal conductivity which led to decreasing thermal resistance up to -44%
Thin Cu foil (DBC)	Thick Cu-plate (DBC)	▪ Thick Cu-plate assists the spreading of heat more efficiently
Silicone gel	Epoxy resin	▪ Glass transition temperature of the epoxy-resin is over 200°C ▪ High-heat resistance epoxy resin is suitable to the SiC devices that generated higher junction temperature ▪ Epoxy-mold suppress deformation of the power chips and DBC substrate

From power cycling test result, it was demonstrated that the newly developed advanced structure has 50 times fatigue life capability compared to the conventional one [38]. In the same report, based on the thermal cycling test (-40°C – 175°C) results of the epoxy-molded module and conventional module, degradation of solder under chip was not observed at the former after 500 cycles, which implies that the epoxy resin molded structure has sufficient thermal cycling capability up to 175°C [38].

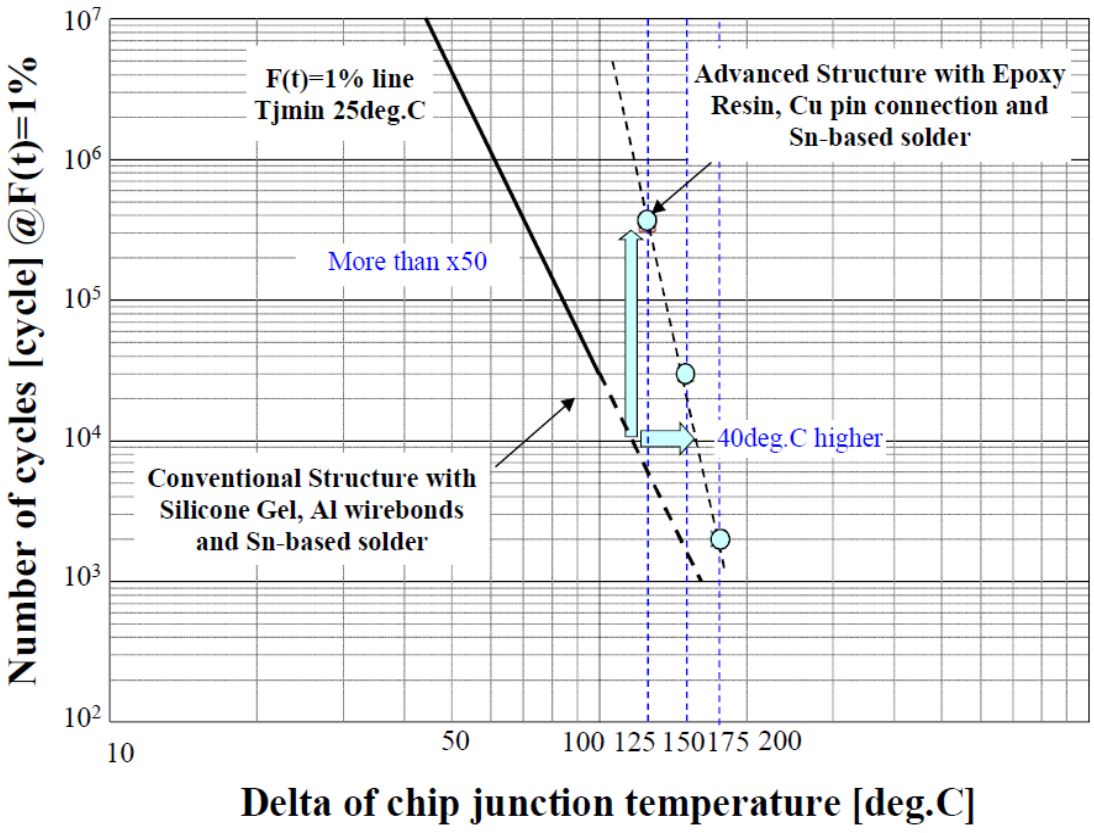

Figure 1.6 Power cycle test result of epoxy-molded all-SiC module as compared to the conventional Si-based module [38]

1.2.3 Bonding Requirements in Future-Generation Module Packaging

To summarize, various developments on several components in the packaging are giving door of opportunities for the implementations of SiC-based module and maximizing its properties for higher voltage output applications. However, several issues particularly on the requirements of joining epoxy-molded module to the heat substrate/sink must be cleared first before the SiC-based module can be utilized to its maximum limit. Issues and requirements relating to the joining of epoxy-molded module are addressed as follows:

I. Low bonding temperature

i. Due to the CTE mismatch of the components that constitute the module, processing temperature must be as low as possible to reduce the thermomechanical stress

ii. To avoid degradation of the epoxy-resin during processing, processing temperature must be lower than the glass transition temperature of the epoxy-resin

iii. ***The processing temperature need to be 250°C and lower, preferably at 200°C***, which is lower than the glass transition temperature of the epoxy-resin

II. Low bonding pressure

i. High pressure is detrimental to the epoxy-molded module since it will induce mechanical damage to the low strength epoxy-resin

ii. ***The ideal bonding pressure is pressureless, however, to provide a good adhesion, pressure of 0.1 MPa and lower may be applied***

III. Plateless Cu-Cu bonding

iii. Employing metal plating onto DBC substrate of an epoxy-molded module is difficult and expensive.

iv. ***Plateless Cu-Cu bonding is essential*** for the application on bonding epoxy-molded module to the Cu-heat spreader.

1.3 Review of Existing Bonding Technology

On reducing thermomechanical stress that is commonly induced during high temperature processing, several joining technologies that can be realized at relatively low temperature (as low as 200°C) have been the center of attention. Such joining technologies are ***low temperature soldering***, ***metal nanoparticle sintering***, and ***transient liquid phase bonding*** to name a few. In this present study, powder-based transient liquid phase bonding, or familiarly known as transient liquid phase sintering will be the main focus and will be reviewed. Restrictions and problems in previous studies will be addressed. However, it is important to understand and discuss other low temperature joining technologies as well, henceforth, in this section, advantages and limitations of each joining technology will be explained to rule out the originality and significances of this present work.

1.3.1 Soldering

Soldering which is the traditional die-attach for power semiconductor devices has also been used to mount module onto heat spreader/sink. Several Sn-based solders such as Sn-Ag solders [6], and Sn-Sb solders [7, 8] has been adapted to replace thermal grease. Depending on the composition of the solders, they possess thermal conductivity that is one order higher than the conventional thermal grease, which contribute to higher heat dissipation. For example, thermal conductivity of Sn-58wt%Bi solder is 21.0 W/mK, Sn-3.5wt%Ag is 33.0 W/mK, and In-3wt%Ag is 73.0 W/mK [39]. Since the solder used as thermal interface material under DBC substrate received direct cooling from the heat substrate/sink, solder with lower melting temperature and/or lower thermal conductivity compared to the die-attach may be applied depending on the solder composition.

However, in comparison to the conventional thermal grease which can be re-applied if the thermal grease dried-out, once module (DBC substrate) is mounted onto the heat spreader/sink by means of soldering, it is undone. Hence, due to the inevitable thermomechanical stress that generated

during fabrication and operation due to the CTE mismatch of the constituted components, high mechanical strength solders and low CTE mismatch between solders and adjoining components are usually being the optimization parameters on selecting solder to be applied as thermal interface material. Several commercially available solders that have melting temperature or liquidus temperature lower than 200°C are listed in Table 1.3.

Table 1.3 List of low melting temperature Pb-free solder (below 200°C) manufactured by solder manufacturing company in Japan as referred to the company's product list

Manufacturer	Composition, wt.%	Solidus Temperature, °C	Liquidus Temperature, °C
Senju Metal Industry [40]	Sn-58Bi	139	141
	Sn-40Bi-Cu-Ni	130	174
Nihon Handa Co. [41]	Sn-58Bi	139	139
	Sn-58Bi-1Ag	136	138
Solder Coat Co. [42]	Sn-Bi-Cu	139	170
	Sn-Bi*	138	
	Sn-In-Bi	100	109
	Sn-In-Bi*	71	
Matsuo Handa Co. [43]	Sn-9Zn	198	198
	Sn-9Zn-3Bi	190	196
	Sn-58Bi*	139	
Nihon Almit Co. [44]	Sn-8.0Zn-3.0Bi	190	199
	Sn-58Bi*	139	
Nihon Genma Mfg. Co. [45]	Sn-57Bi-0.4Ag	139	141

*solders with eutectic composition

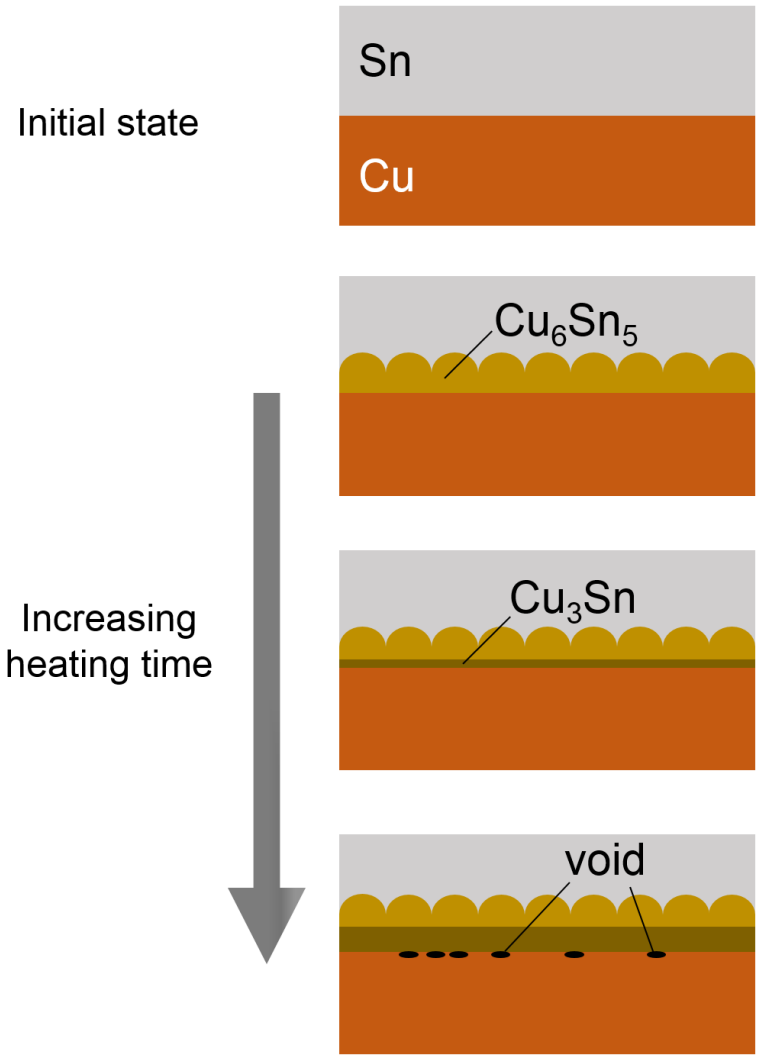

Figure 1.7 Microstructure evolution during conventional Sn-Cu system soldering process

Figure 1.7 illustrates the mechanism of soldering of the conventional Sn-Cu system, in which Sn-based solder is placed upon Cu substrate. When the joint is heated above the melting point of the solder, the rapid interdiffusion of Cu substrate into molten Sn lead to the formation of scallop-type Cu_6Sn_5 IMCs, which continue to grow towards the solder with increasing reflow time. Next, with increasing Cu-flux from Cu substrate, thin planar-type layer of Cu_3Sn IMCs are formed between Cu

substrate and Cu_6Sn_5 IMCs. Subsequently, since it takes longer time for Cu flux to be transported to the tip of scallop-type Cu_6Sn_5 IMCs, the growth of Cu_6Sn_5 IMCs are dominantly initiated at the valley of the Cu_6Sn_5 IMCs. This resulted in increasing of thickness and shape-alteration from scallop-type to planar-type of Cu_6Sn_5 IMCs [46]. Following the growth of Cu_6Sn_5 IMCs, simultaneously the Cu_3Sn IMCs also grow towards the Cu_6Sn_5 IMCs with diffusing Cu from the Cu substrate [47]. By prolonging reaction time (reflow time or annealing time), due to the inward Sn flux from Sn-rich region is smaller than outward Cu flux from Cu_3Sn IMCs, this difference in diffusion flux generates micro voids at the interface of Cu and Cu_3Sn IMCs which is usually referred as Kirkendall voids [46]. It was also found that the reaction of Cu and solder did not stop after reflow process and even continued at room temperature, where the dominating diffusion element is Cu [48]. Doosoo Kim et al. in their review of the formation of Kirkendall voids within IMC layers of solder joints, has concluded that the formation of Kirkendall voids were significant by aging, multiple reflows, annealing and electromigration in both binary and ternary solder system [46]. The formation of these two types of Cu-Sn IMCs in the Cu-Sn binary systems was predicted by a proposed kinetic model based on the principle of maximum degradation rate of the total system free energy [49]. In the same work, the first phase that was predicted to form in Cu-Sn system was Cu_6Sn_5 and followed by Cu_3Sn IMCs, which resulting in good agreement with experimental observations in the work of O.Y. Liashenko et al. [50]. It is always speculated that the excessive formation and continuous growth of IMCs is undesirable to the mechanical strength of the solder because IMC is generally known as brittle and crack will likely to propagate within IMCs phase and affecting the reliability of the joints [51]. However, in some cases of Bi-Ag solders, the lack of interfacial intermetallic reaction layer lead to the fracture along the interface of the joints [52]. In a nutshell, the formation of intermetallic reaction layer at the interface is essential to have a robust and sound joints but controlling the growth of IMCs during operation by any means is far more important to avoid the degradation of joints.

As it has been stated in section 1.2.1, it is important to prevent the semiconductor devices from heating up over the allowable maximum junction temperature, thus, solder which exhibits higher thermal conductivity has been used to replace the role of thermal grease as thermal interface material. Chandan K. Roy et al. [53] reported that the thermal resistance of two types of low melting alloys, i.e. 100wt%Ga, and In-32.5wt%Bi-16.5wt%Sn, remained constant after accelerated aging at 130°C for 3000 hours, and 1500 cycles of thermal cycling between -40°C to 80°C. This might be contributed to the formation of intermetallic compounds between Ga and In with the Cu and Ni substrate. However, one main issue regarding the process conducted in the same study was the solder was not bonded, but rather placed on Cu substrate and pressed at approximately 0.14 MPa during accelerated thermal aging, and thermal cycling test. In addition, no further metallurgical observation was conducted to investigated the change in the microstructure of the studied low melting alloys.

On contrary, Sn-Ag based solder had also been adapted as the thermal interface material under DBC substrate [6]. With eutectic composition of Ag-3.5wt%Sn, the melting point of Ag-3.5wt%Sn is 221°C, which is 38°C higher than the conventional eutectic Sn-Pb solder, i.e. 183°C. The strengthening mechanism of Ag-3.5wt%Sn solder was primarily by precipitation strengthening of randomly dispersed Ag_3Sn particles at the grain boundaries [6], and by Sn-grain refinement at the vicinity of lamellar structurally-concentrated Ag_3Sn [54]. Ag_3Sn acted as dislocation pinning where no particle bowing was observed by transmission electron microscopy (TEM) investigations, which implied the Orowan mechanism [55]. However, with increasing service time or annealing time, Sn grain enlargement in the Sn-Ag based solders was also observed in [6]. In addition, Sn-Ag based solder is known to be susceptible to heat stress and degrade thermally [56]. On this regard, tin-antimony (Sn-Sb) based solder has received attention to replace Sn-Ag based solders owing to its superior mechanical strength post-processing and after long-time of thermal aging [57]. Akira Morozumi et al. reported that supersaturated Sb precipitated as SnSb IMCs in the Sn matrix acts as

dislocation barrier which contributed to increasing tensile strength [58]. It was also reported that the strengthening mechanism of Sn-Sb binary alloys solder with supersaturated Sb was hybrid-strengthening type that included both precipitation strengthening of randomly distributed SnSb IMCs and solid solution strengthening of solute Sb in Sn matrix.

However, there remain several concerns when applying solder as thermal interface material. Such issues require countermeasures so that the requirements of low temperature bonding and high reliability of joints can be achieved. Three issues regarding on solder paste and soldering process are described as follows:

i. Usage of flux as reducing agent

With decreasing size of solder alloy particles, the oxidation states of the solder particles increased due to increasing surface area. Flux is an organic or inorganic chemical solution that is mixed together with solder alloys to reduce oxides of either solder alloy particles or the metallization at the adjoining substrate. The advantage of using flux as reducing agent is processing can be realized at ambient environment which contribute to cost-down of processing. However, there exist two issues when using flux as reducing agent: (1) the reaction of flux during processing lead to outgassing and the formation of void, and (2) flux residues is corrosive under humid environments. D. Busek et al. [58] suggested that solder with liquid volatile organic compounds as solvents evaporated at earlier temperature before the coalescence of particles, thus resulting in less void formation. Some solder manufacturers insisted that uniformly dispersed macrovoids are necessary since they can act as stress relievers and crack arresters. However, the real effects of voids is still under discussion [58]. On the other hand, no-clean flux that mainly consists of organic compounds is considered as flux which do not required post-processing residues cleaning because the aggressive additives and solids evaporate during processing. Contrarily, according to the findings from [59], flux residues of no-clean flux were

found when processed at lower temperature due to the acid part of the flux was not completely burnt-out during processing [59]. Thus, to completely remove the flux components in solders, it is essential to conduct the soldering process at high temperature, preferably higher than the melting temperature of the solder alloy.

ii. High reflow temperature compared to the melting temperature of solder alloys

In the roadmap report by Japan Electronics and Information Technology Industries Association (JEITA) in 2002 [90], the proposed soldering processing temperature of SAC305 is 20-30°C higher than its melting point. This is to make sure the temperature homogenization throughout the solder so that the productivity can be maintained [39]. For example, Pb-Sn solder with eutectic temperature of 183°C, the typical soldering processing temperature is approximately 40°C higher than its melting point. Another example of the conventional Sn-5Sb that has been used as thermal interface material below DBC substrate, the solidus temperature of Sn-Sb based solder is around 240°C, thus the processing temperature may reach 300 or above depending on the compositions. Akira Morozumi et al. processed Sn-13wt%Sb at 80°C higher than its liquidus temperature [91]. H. Beyer et al. on the other hand processed Sn-8wt%Sb at temperature as high as 325°C [92].

In addition, in real practice, it is ultimately impossible to eliminate the oxide layer on solder surface especially at high temperature since the active reaction of oxygen and the molten Sn. Due to the existence of the oxide layer at both molten solder and the substrate, surface tension between them will be increased and the wetting of the solder will be decreased. Wetting angle of molten solder on a substrate can be expressed by Young-Dupre equation as follows [93]:

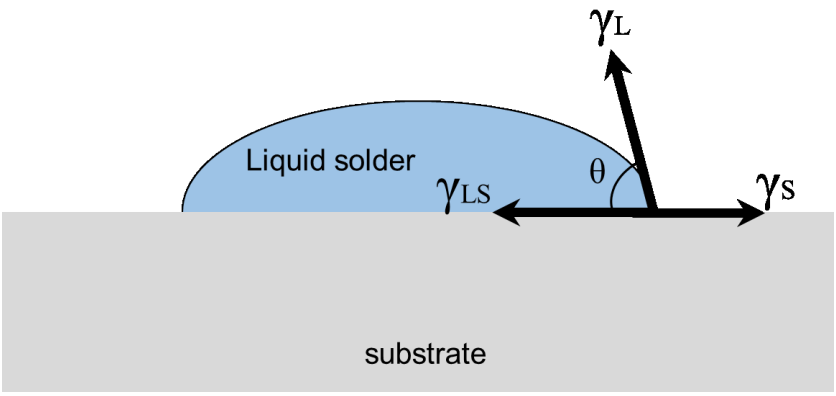

Figure 1.8 Wetting angle of molten solder (liquid) and substrate (solid)

$$\gamma_S = \gamma_L \cos\theta + \gamma_{LS} \tag{2.4}$$

$$W_{ad} = \gamma_S + \gamma_L - \gamma_{LS} \tag{2.5}$$

$$W_{ad} = \gamma_L (1 + \cos\theta) \tag{2.6}$$

where γ_L is surface tension of substrate (solid), γ_S is surface tension of molten solder (liquid), and γ_{LS} is the surface tension of between liquid and solid phase. In general when θ is lower than 90°, the systems is said to wet, and when bigger than 90°C, the system is considered non-wetting. Zinc (Zn)-contained solder is well known as solder with extremely large wetting angle, due to highly reactive particle of Zn that can easily oxidize at the surface of the molten solder [39 , 63]. Hence, to help ease the wetting of the solder so that the molten solder can penetrate grain boundaries of substrate subsequently commencing interfacial reaction between substrate, flux as oxide reducing agent has always been introduced into solder. As stated earlier, due to the corrosive properties of residue flux, it is desirable to eliminate flux during processing by increasing processing temperature, which in return lead to lowering the surface tension of the solder. Surface tension of solder containing Bi, Sb, and Pb are highly dependent to the compositions of the said elements, where with increasing

percentage of the elements, the surface tension would be lowered, resulting in lowering the wetting angle, and facilitate the spread of the solder.

iii. Operation temperature and the concern of homologous temperature

Homologous temperature, T_h of a materials is defined as the temperature of a material as a fraction of its melting point temperature in Kelvin. For example, pure Sn solder with melting temperature of 232°C has $0.6T_h$ at room temperature. In general, materials start to demonstrate creep deformation above $0.5T_h$. Thus, even at room temperature pure Sn solder exhibits creep deformation although the deformation rate might be slow. With increasing operation temperature of the solder, the fraction of T_h would also increase, hence, accelerating the creep deformation. In some harsh cases, the accumulated strain will lead to early degradation of the reliability of the solder joints. On this account, choosing solder that can operate at high operation temperature is essential. Generally, in the perspective of resistance to severe creep conditions, it would be beneficial to use solder with higher solidus temperatures.

Figure 1.9 shows the relationship of solder melting temperature and its allowable operating temperature according to $0.8T_h$. This graph was adapted from [11]. Several conventional solder that is widely used in the world is plotted in the graph. As can be seen from Figure 1.9, for a solder to be safely operated at the proximity of 125°C in a long time service, it is desirable to have a solder with melting point of 225°C and above. Sn-Sb based solder that possess solidus temperature above than 240°C is considered desirable to be applied as thermal interface material with operating temperature at about 125°C, however, due to its high processing temperature (sometimes can achieve over than 300°C), it is unfavorable to be directly applied as thermal interface material for the epoxy-molded module as explained before.

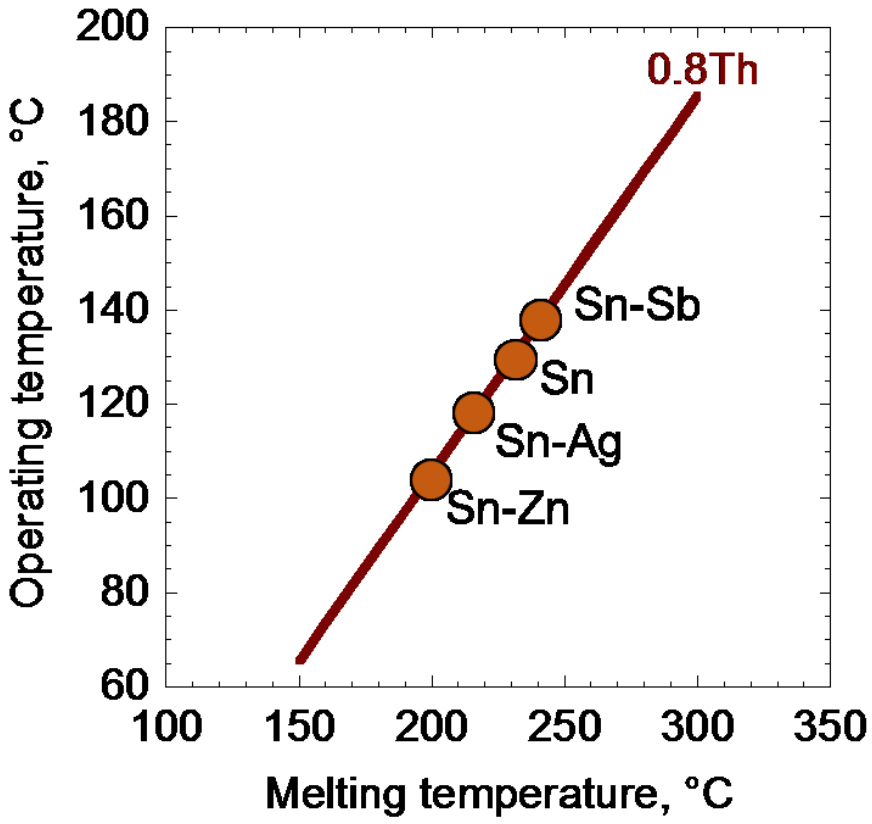

Figure 1.9 Relationship of melting temperature of solder and operating temperature (0.8 T_h)

1.3.2 Metal Particle Sintering

Metal particle sintering, in particular, nanoparticles sintering has garnered enormous attention on replacing conventional Sn-based solder as a lead-free die-attach technology. The pioneer work of utilizing metal particles to be sintered at relatively low temperature was conducted by H. Schwarzbauer and R. Kuhnert [64]. In their work, macroscale Ag particles was placed onto Ag or Au coated Mo substrate and used to bond silicon wafer with Ag or Au coating by applying pressure up to 40 MPa within few minutes to achieved bonding strength of up to 100 MPa. In recent years, by

reducing particles size to nano order, sintering pressure can also be reduced owing to the high surface energy of the nanoscale particles. On the effort of reducing production cost, studies on Cu nanoparticle sintering has also received huge attention as a replacement for the current Ag nanoparticle sintering technology.

The distinctive feature of Ag or Cu nanoparticles sintering lies on the low temperature processing ability and high temperature stability. Ag and Cu nanoparticles were prepared in paste-form by mixing it with several types of volatile organic compounds that act as viscosity adjustor or organic capping layer to protect the nanoparticles from aggregation and agglomeration. Hence, the sintering temperature of Ag or Cu nanoparticles is highly-dependent to the burn-out temperature of the organic compounds contained in the paste. With proper selection of organic compounds and processing parameters, Ag or Cu nanoparticles sintering can be realized at temperature as low as 200°C. After processing, the remaining element will be only either Ag or Cu, hence the as-sintered materials will not remelt until the melting temperature of the bulk Ag or Cu, indicating high thermal stability of the joints. Not to mention, high thermal conductivity of both materials are irresistible to be applied as thermal interface material, in particular as die-attach material, which need to resist and transfer high heat generated from the power semiconductor devices during operation.

Previous studies on Ag and Cu sintering are listed in Table 1.4 and summarized by the requirements of future generation SiC-based epoxy molded module as has been explained before, except of shear strength requirement (refer to Chapter 3, section 3.1.1 for details) . As can be seen from Table 1.4, up to author's knowledge, previous studies that fulfilled all requirements targeted in this study is not available. There exist two major concerns on applying Ag or Cu nanoparticles sintering as die-attach or substrate attach which is described as follows:

i. The necessity of Ag or Au metallization

There are twofold aim on depositing metal plating to either substrate or to the back of the die, i.e. two protect the Cu substrate from oxidization during heating, and to promote interdiffusion of Ag atoms so that a robust and strong interfacial joint can be achieved. In the case of Cu nanoparticles sintering, usually, no metallization was applied onto the Cu substrate. However, since Cu nanoparticles are easily oxidized even at low temperature, reducing or vacuum environment or organic layer coating is necessary [65].

ii. High external sintering pressure

On the occasion where Ag or Au metallization is not introduced to the Cu substrates, high external sintering pressure need to be exerted to break the oxidation layer on Cu substrate. Also, by applying high pressure during sintering, the densification of Ag or Cu nanoparticles will be accelerated, subsequently producing a joint with high mechanical properties.

Table 1.4 List of previous studies on metal nanoparticles sintering

First author [Reference]	Material(s)	Substrate	Metal plating	Sintering Parameters			*Shear Strength, MPa	Remarks on shear strength
				Temperature, °C	Pressure, MPa	Environment		
Target in this study		***Cu-Cu***	**-**	***200–250***	***≦0.1***	*None in particular*	***≧6.0***	*Refer Chapter 3, Section 3.3.1*
Min-Su Kim [66]	Ag	Cu-Cu	Ni/Au	200-400	20	Air or N_2	16.2	at 200°C under N_2
Eiichi Ide [67]	Ag	Cu-Cu	-	260-300	1-7.5	Air	11	at 260°C, 1 MPa
Hao Zhang [68]	Ag	Cu-Cu	Ni/Pd/Ag	250	0.4	Air	41	with addition of 0.6μm-sized SiC
Shuai Wang [69]	Ag	Cu-Cu	Ni/Ag	150-200	0	Air	25	at 200°C
Thomas Guangyin Lei [70]	Ag	Cu-Cu	Ni/Ag	275	0-5	Air	7.7	at 0 MPa
Matthias Knoerr [71]	Ag	Cu-Cu	Ag	275	0-5	Air or N_2	7	at 0 MPa
Toshiaki Morita [72]	Ag	Cu-Cu	-	250	1-10	Air	2.5-11	at 1 MPa (depend on Ag particle size and organic solvent
John G. Bai [73]	Ag	Cu-Cu	Ni/Ag Ni/Au	300	0	Air	40	with Ni/Ag plating
Mei, Y [74]	Ag	Cu-Cu	Ag	275	1-5	Air	24.5	at 185°C pre-sintering, and 1 MPa
Guo-Quan Lu [75]	Ag	Cu-Cu	Ni/Ag	275	0-5	Air	7.7	at 0 MPa
Yi Yan [76]	Ag	Cu-Cu	Ni/Au	280	0	Air	16.7	
E. Ide [77]	Ag	Cu-Cu	-	300	1-5	Air	25	at 1 MPa
Xiangdong Liu [78]	Cu	Cu-Cu	-	300	0.08	Formic acid	30.9	combined redox process
Nishikawa Hiroshi [79]	Cu	Cu-Cu	-	280-400	15	Air or N_2	40	at 400°C in N_2
Yan Jianfeng [80]	Cu	Cu-Cu	-	100-280	5	Air	13.5	at 220°C (fracture at Cu wire)
Shutesh Krishnan [81]	Cu	Die-Cu	-	350-400	5-10	N_2+5%H_2	1.25kgf	at 400°C, 10 MPa
Yamakawa Tomohiro [82]	Cu	Cu-Cu	-	250-400	0-15	Vac. (10^{-2}Pa)	19	at 250°C, 5 MPa
Toshitaka Ishizaki [83]	Cu	Cu-Cu	-	200-350	5	H_2	0-15	200°C (depend on organic solvent)
Jianfeng Yan [84]	Ag and Cu	Cu-Cu	Ni/Ag	250	5	Air	20	at molar ratio of Cu:Ag=1:1

*Shear strength shown in here is selected based on the conditions that best fit to the processing conditions aimed in this study.

1.3.3 Transient Liquid Phase Sintering and Bonding

Liquid phase sintering occur under condition where solid particless coexist with a wetting liquid. Compared to solid phase sintering, liquid phase sintering is one of considerable candidate to realize bonding at relatively low temperature without the application of high pressure during assembly. This is owing to the presence of liquid phase that cater the densification of the particles during isothermal solidification process. In general, according to [85], there are four types of liquid phase sintering, i.e. persistent, transient, reactive transient, and super solidus liquid phase sintering.

In this study, transient liquid phase sintering (TLPS) is focused as the possible candidate to replace solid-solid sintering to realize joining at relatively low temperature without the application of high pressure during processing. Low melting temperature material particles are mixed with high melting temperature material and heated above the melting point of the former. The liquid phase is consumed throughout the processing time by isothermal solidification with the parentheses, hence the naming of transient. One advantage of this phenomenon is the transformation of the low melting temperature material into intermetallic compounds or in some cases, solid solution with the high melting temperature material, resulted in the increase of the melting temperature of the as-processed materials. This implies the high reliability of the joint fabricated by means of TLPS to be applied at high temperature application, in particular to the SiC-based power module, which is expected to generate higher heat density compared to the conventional Si-based power module. On that account, residual low melting temperature additive materials after fabrication is unfavorable for high temperature application. Hence, sintering conditions e.g. sintering temperature and holding time, play a vital role to completely transform all low melting temperature material to other phases in order to secure a remelting temperature elevation after processing.

Similar to TLPS, transient liquid phase bonding in which low melting layer inserted between substrate, also utilized the transient liquid phase to achieve bonding that can produced joint with high

thermal stability. In this dissertation, to distinguish these two types of transient liquid phase bonding, transient liquid phase bonding that utilize layer as low melting temperature material, will be defined as layer-based transient liquid phase bonding, whereas powder-based transient liquid phase bonding will be defined as transient liquid phase sintering, or TLPS. The mechanism of both transient liquid phase bonding is schematically illustrated in Figure 1.10.

In layer-based transient liquid phase bonding technology, low melting temperature layer is inserted between high melting substrate either at one side or at both sides. This low melting temperature layer might be applied as foil, ion sputtering, or metal plating. On contrary, low melting particles are mixed with high melting particles either in dry-state or prepared as paste and deposited onto the substrate. By heating the joints over than the melting point of the low melting material in both TLP bonding, low melting materials will melt and begin to react with the high melting materials. During isothermal solidification stage, the low melting temperature will be consumed to form either organic compounds or solid solution, depending on the material selection and processing parameters, e.g. processing temperature and processing time. Further homogenization may be applied to release thermomechanical stress or to achieve the desired microstructure.

Previous studies on layer-based transient liquid phase sintering and TLPS are listed in Table 1.5 and Table 1.6, and summarized in the similar manner to Table 1.4. Usage of flux in both TLP bonding was also reviewed. As explained in earlier section, usage of flux might resulted in voiding if not processed properly. Hence, in this study, the usage of flux as reducing agent will be eliminated and reducing environment will be used to facilitate the wetting of low melting materials.

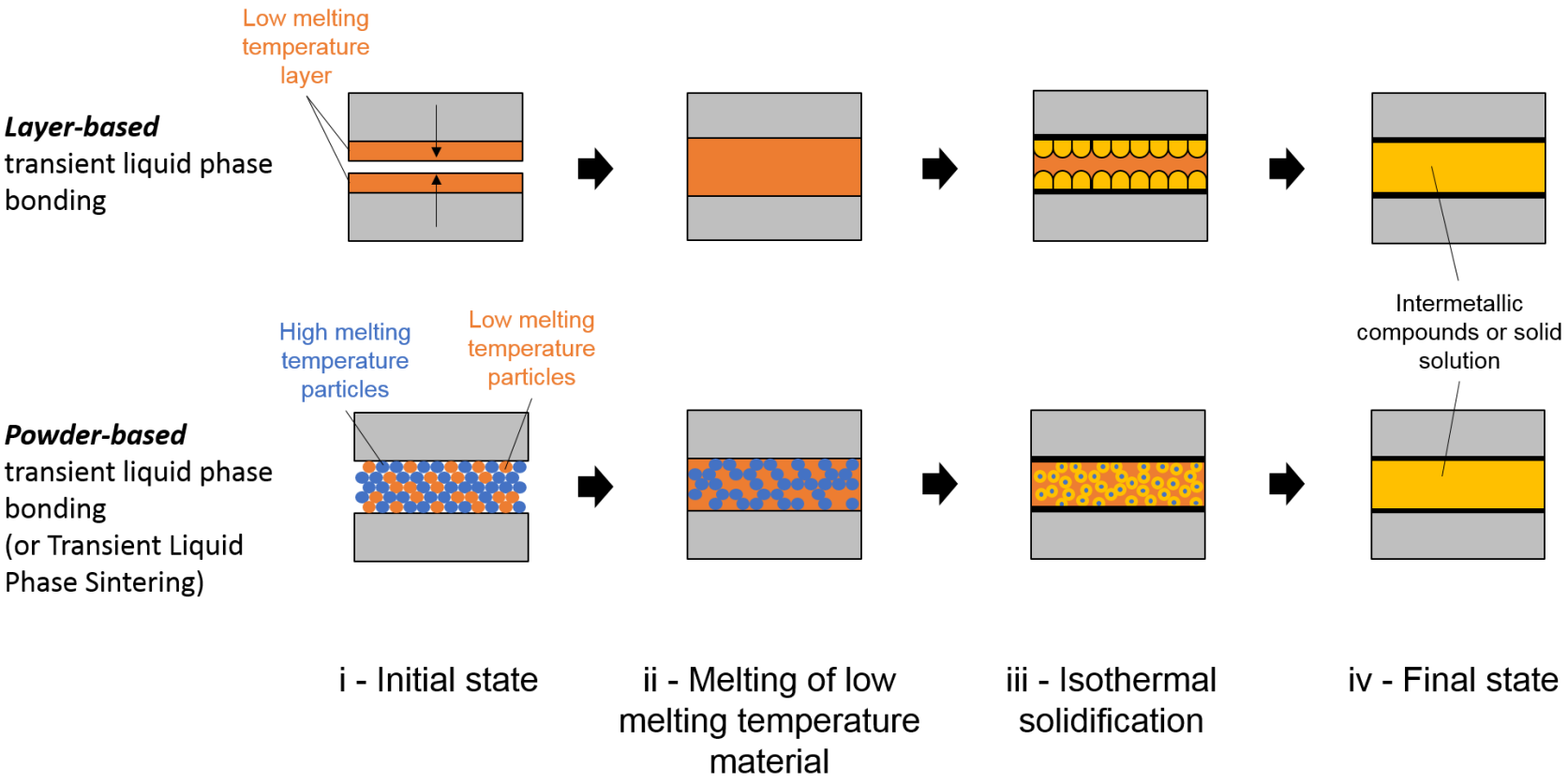

Figure 1.10 Evolution during the process of two types of transient liquid phase bonding

Table 1.5 List of previous studies on transient liquid phase bonding (***layer-based***)

First author [Reference]	Joining layer material	Substrate	Metal plating	Sintering Parameters			Usage of flux	*Shear Strength MPa	Remarks on shear strength
				Temperature °C	Pressure MPa	Environment			
Target in this study		***Cu-Cu***	***-***	***200–250***	***≦0.1***	*None in particular*	***No***	***≧6.0***	*Refer Chapter 3, Section 3.3.1*
Huakai Shao [86]	Sn	Cu-Cu	Ag	260-340	0.1	Vac. (2e-3)	No	60.2	420 min bonding time
Habib A. Mustain [87]	In, Ag	SiC-DBC	Au-Ag	210	0.3	N_2 and H_2	No	9.1kgf	after annealing at 400°C for 100h
H.Y. Zhao [88]	Sn	Cu-Cu	-	250	0.2	Air	No	-	
J.H. Liu [89]	Sn	Cu-Cu	-	250	0.4	Air	No	60.1	by ultrasonic-assisted TLP process
L. Mo [90]	Sn	Cu-Cu	-	260	0	Vac. (93kPa)	No	-	
Kunmo Chu [91]	Sn	Cu-Cu	-	280	2.7	N_2	No	41	with 2 μm metallization thickness
Hongjun Ji [92]	Sn-0.7wt%Cu	Si-Cu	Ni/Ag on Si side	250	0.2	Air	No	69	with 10s ultrasonic vibration
J.S. Kang [93]	Sn	Cu-Cu	-	275-325	0	Air	No	-	
J.F. Li [94]	Sn	Cu-Cu	-	260-340	0.01	N_2+2%H_2	No	-	
H. Liu [95]	Sn	Cu-Cu	-	270-330	0	Vacuum	No	-	
N.S. Bosco [96]	Sn	Cu-Cu	-	400	0	Vac. (2e-6torr)	No	-	
F. Brem [97]	Sn	Cu-Cu	-	300	0.1	Vacuum	No	-	
S.W. Park [98]	Sn/Zn	Cu-Cu	-	250	0.1	N_2	No	37.4	after 30 min bonding time
A. A. Bajwa [99]	Sn/Ag/Sn In/Ag/In	Si-DBC	Ni/Au	210-235	5-10	Vac. (2e-4mbar)	No	32	for Sn/Ag/Sn with 5 MPa bonding pressure
W. Liu [100]	Sn-Ag/Ag	Cu-Cu	-	300-380	0-0.3	N_2	No	50.1	

*Shear strength shown in here is selected based on the conditions that best fit to the processing conditions aimed in this study.

Table 1.6 List of previous studies on transient liquid phase bonding (***powder-based or known as TLPS***)

First author [Reference]	Material		Substrate	Metal plating	Sintering Parameters			Usage of flux	*Shear Strength MPa	Remarks
	Base	Additive			Temperature °C	Pressure MPa	Environment			
Target in this study			***Cu-Cu***	***-***	***200−250***	***≦0.1***	*None in particular*	***No***	***≧6.0***	*Refer Chapter 3, Section 3.3.1*
Hannes Greve [101]	Cu	Sn	Cu-Cu	-	280	0	Air	No	13.1	Cu-60wt%Sn
Hannes Greve [102]	Cu	Sn	Cu-Cu	-	300	0.33	Air	No	-	
S. Ali Moeini [103]	Cu	Sn	Si-DBC Si-DBA	Ni at DBC/A	300	0.5	Air	No	-	
Hannes Greve [104]	Cu	Sn	Cu-Cu	-	300	0.5	Air	No	-	
Hannes Greve [105]	Cu	Sn	Si-Ni	Ag at Si-side	300	0.2	Air	No	35	Paste C (composition is unmentioned)
Hannes Greve [106]	Cu	Sn	Cu-Cu	-	280	0	Air	No	8.0	Cu-40wt%Sn
Fengqun Lang [107]	Cu	Sn	Cu-Cu	Au	260	0-0.5	Air	No	35	at 0.1MPa bonding pressure
Toshitaka Ishizaki [108]	Cu	Sn	Cu-Cu	Ni	250-350	0	Air	No	10	Cu-10wt%Sn
Omid Mokhtari [109]	Cu	Sn-Bi	Cu-Cu	-	200	2.5	N_2	Yes	42	Thermo-compression reflow
Tianqi Hu [110]	Cu	Sn	Cu-Cu	-	250	0	Air	No	29.3	
Xiangdong Liu [111]	Sn-coated Cu		Cu-Cu	-	200	5-20	Formic acid	No	18	with 5MPa pressure and 20 min bonding
Masahisa Fujino [112]	Ag	Sn	Si-Cu	Ti/Ni/Au at Si-side	260-300	5	Air	No	18	Ag-30wt%Sn at 260°C
C-Xiang Yang [113]	Ag	Sn	Cu-Cu	Ag	235	0	Air	No	22	Ag-4wt%Sn
Ahmed Sharif [114]	Ag	Sn	Cu-Cu	-	250	1.2	Air	Yes	31	Ag-40wt%Sn
Koji Kondo [115]	Ag	Sn	Cu-Cu	-	320	1.5-10	Vac.(0.2kPa)	No	-	

*Shear strength shown in here is selected based on the conditions that best fit to the processing conditions aimed in this study.

As can be seen from Table 1.5 and 1.6, up to author's knowledge, there is no previous studies that fulfilled the target of this study, except for the work of S.W. Park et al. [98] and Tianqi Hu et al. [110], which will be reviewed in details later.

One major drawback of layer-based transient liquid phase bonding is the necessity to keep the insert-layer as thin as possible as the diffusion is highly dependent to processing time as can be explained by Fick's second law. According to the law, length of diffusion l is proportional to the square root of the product of the time t and diffusion coefficient D. Thus, keeping the layer as thin as possible is essential to shorten the processing time, if not, low melting layer will residue in the middle of the joints, degrading the thermal reliability of the joints. J.F. Li et al. [94], inserted Sn layer with thickness of 25 μm between two Cu substrates, pressed with relatively low pressure of 0.01 MPa and heated the joints under forming gas environment at 340°C for at least 480 min to completely transform the Sn layer into Sn-Cu IMCs. This relatively high processing temperature (approximately 110°C higher than the melting temperature of the Sn, i.e. 232°C) and long processing time is not compatible to the industry and the needs on bonding epoxy-molded module.

Similarly, J.H. Liu et al. bonded two Cu plates with Sn layer with thickness of 20 μm at 250°C in vacuum furnace with application of pressure of 0.04 MPa and completely transform the Sn into Cu-Sn within relatively shorter time of 60 min as can observed in Figure 1.11(a-c) [89]. In addition, in the same work, they reported that the reaction time of isothermal solidification can be shorten to 4 s (see Figure 1.11(d-f)) with the assistance of ultrasonic vibration during processing at 250°C. The rapid formation of IMCs joints were attributed to the effects of acoustic cavitation phenomenon at the interfacial of molten Sn and Cu substrate. The horizontal ultrasonic frequency was fixed to 20 kHz and applied onto upper Cu plate with fixed pressure of 0.4 MPa. The collapse of micro-bubbles when the ultrasonic vibration is applied was thought to create a tiny localize hot-spot that can reach up to 5000 K in which accelerate the diffusion [89].

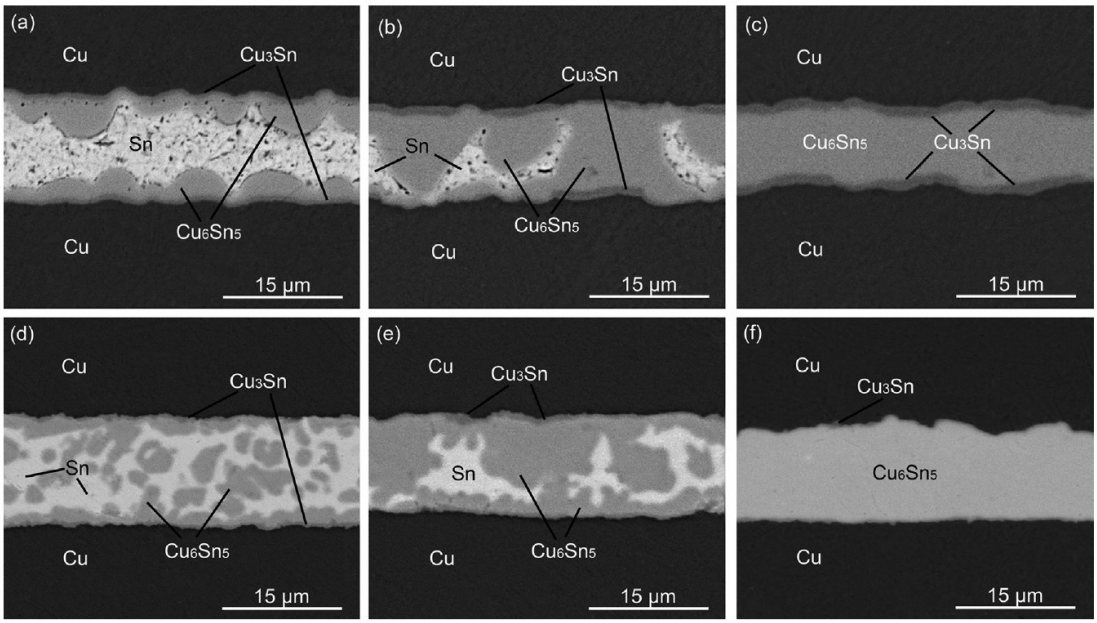

Figure 1.11 Cross-sectional SEM images of the joints bonded by layer-based transient liquid phase bonding at 250°C, at (a) 20 min, (b) 40 min, (c) 60 min, and joints bonded by ultrasonic-assisted layer-based transient liquid phase bonding processed at 250°C for (d) 2 s, (e) 3 s, (f) 4 s [89]

Meanwhile, S.W. Park et al. [98] had successfully bonded Cu-Cu substrates with Sn-plated Zn sheet. Sn with thickness of 10 μm was electroplated onto Zn sheet and inserted between the Cu-substrate, realizing the bonding at 250°C with application of low pressure of 0.1 MPa. The bonding mechanism was rather quasi-transient liquid phase bonding, instead of transient liquid phase bonding, since the β-Sn matrix still exist in the bonded joints after processing. Although the bonding had been realized at 250°C taking into account of the melting point of Sn, lowering the processing temperature to 200°C is impossible since the Sn will not melt and the reaction will only occur at solid-phase, which is relatively slower than quasi-transient liquid phase bonding.

To conclude, while layer-based transient liquid phase bonding sounds promising as possible candidate on realizing low temperature and low pressure bonding, several issues that might hinder the application can be addressed as follow:

i. The necessity on thin layer

Extremely thin insert layer is needed to shorten the reaction time to complete the isothermal solidification process. Although by exploiting ultrasonic vibration during sintering may shorten the reaction, a trade-off with bonding pressure that is exerted by ultrasonic horn during vibration is inevitable.

ii. Limited choice of low melting temperature material

Thin layer may be realized by metal plating or ion-sputtering which is more feasible compared to foil, but come with limited selection of low melting temperature material. Solder paste may also be used, but fine particle-sized solder alloy as small as 20 μm might be needed and must be applied at the thickness of one layer of the solder particles which is impractical.

On this account, TLPS which used particles to shorten the diffusion length compared to the layer-based transient liquid phase bonding, may contribute to shorter processing time, in particular if nanoparticles is utilized. However, the main disadvantage of this processing technique is the susceptibility of void formation from the initial spot of the low melting temperature that melt and spread into the skeleton-structure of the sintered structure, and the void formation from trapped gas of residual organic compounds. Cheng-Xiang Yang et al. [113] successfully performed the bonding of Cu substrate and Si chip with Sn-doped Ag paste at processing temperature as low as 235°C, slightly above the melting point of the Sn. High shear strength of the joint was obtained with 4% mass fraction of Sn. However, the Cu substrate was coated with Ag to promote the interdiffusion of Ag atoms since the amount of liquid Sn was extremely small and not sufficient to wet and form interfacial layer with Cu substrate. On the other hand, Ahmed Sharif et al. [114] had demonstrated bonding of plateless Cu-Cu substrate with Sn-added Ag-based TLPS. The bonding of bare Cu-Cu substrate was

achieved by the addition of at least 25% mass fraction of Sn to create interfacial reaction of Cu-Sn IMCs, and with addition of 40wt% of Sn, thick layer of Cu-Sn IMCs can be observed and the joint fractured at the Ag_3Sn IMC phase in the matrix.

Meanwhile, Omid Mokhtari et al. [109], has successfully bonded plateless Cu-Cu substrates by Sn-Bi solder joints with added Cu particles at temperature as low as 200°C. Cu-Cu joints that were bonded at 200°C with Sn-Bi-30Cu for 50 min without the application of pressure during reflow exhibited shear strength of 20 MPa. However, from cross-sectional observation as shown in Figure 1.12(c), extremely large macroscale voids were observed. The mean void area fraction was 49%, which is detrimental to joints as macroscale voids do not transfer heat and act as crack-initiation site when thermomechanical stress is induced during operation. The formation of voids were thought to occur due to the coalescence of solvent-depleted regions at the vicinity of the added-Cu particles. The solvent-included flux was used to reduce the oxidation of Sn-Bi solder and Cu substrates which in return led to the formation of voids. The formation voids were reduced by applying thermo-compression reflow method. Pressure less than 2.5 MPa was applied during reflow process in which contributed to the decrease of void area fraction to 28.5%, which was still rather high for the application as die-attach material.

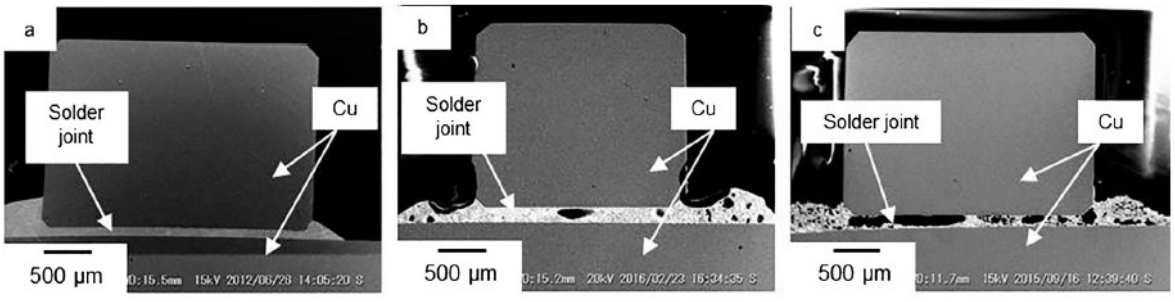

Figure 1.12 Cross-section of (a) eutectic Sn-Bi solder bonded at 170°C for 1 min, (b) Sn-Bi-based TLPS bonded at 170°C for 1 min, and (c) Sn-Bi-based TLPS bonded at 200°C for 50min [63]

Tianqi Hu et al. [110] had successfully performed bonding of plateless Cu-Cu substrate by Sn-coated Cu particles at temperature of 250°C for 40 min without the application of pressure. Sn-coated Cu particles were firstly compressed into a preform and placed onto Cu substrate. When the reflow temperature exceeded the melting temperature of Sn, Sn reacted with Cu particles to form Cu-Sn IMCs in which after 40 min of reflow time, the microstructure of the joints constituted of macro-sized Cu particles and Cu_3Sn extensive networks (Figure 1.13). However, since the melting of Sn begin only after 232°C, lowering processing temperature is impossible. Xiangdong Liu et al. [111], took an effort on lowering the sintering temperature of the same bonding techniques with Tianqi Hu et al. [110]. The bonding of plateless Cu-Cu substrates was conducted with Sn-coated Cu particles under the application of pressure as high as 10 MPa, since the bonding mechanism is no longer transient liquid phase sintering, but rather solid-phase sintering. Formic acid atmosphere was used to reduce the oxide layer on both Sn coating and Cu substrates.

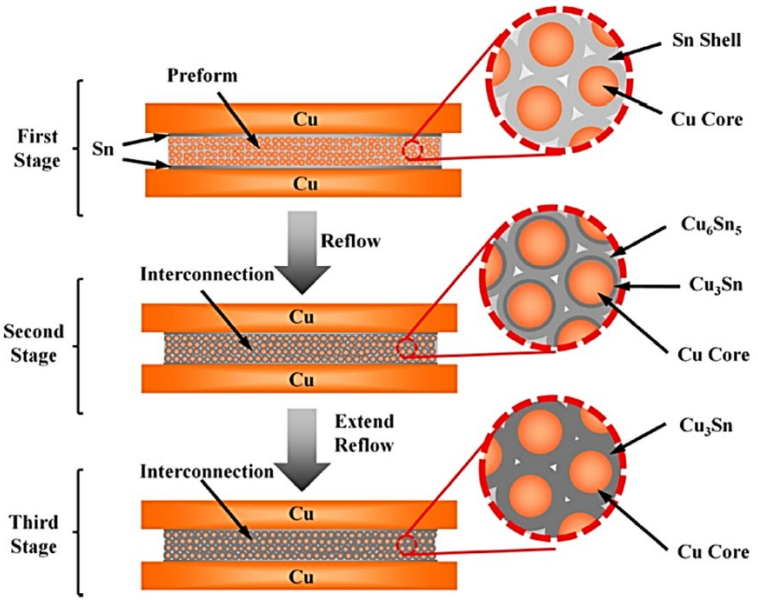

Figure 1.13 Schematic diagram of bonding process using Sn-coated Cu particles as reported by Tianqi Hu et al. [110]

To conclude, powder-based transient liquid phase bonding or transient liquid phase sintering, is a promising approach to enable bonding of plateless Cu-Cu substrate. Based on literature review conducted, advantages of TLPS are addressed as follows:

i. ***Processing temperature as low as 200°C*** can be realized with proper selection of low-melting temperature material.
ii. Realization of bonding ***plateless Cu substrates*** with adequate addition of liquid phase.
iii. ***High pressure is unnecessary*** since the densification of the sintered structure was performed by the isothermal solidification of the liquid phase with matrix grains.
iv. Processing time can be shorten with adapting nanoscale particles since the diffusion path will be shorten to complete the isothermal solidification process, henceforth, ***higher remelting temperature*** can be expected.

1.4 Summary

A review of power electronics module technology, packaging technology evolution, and existing bonding technologies associating to the packaging technology has been conducted and can be summarized as follows:

1. Si-based module has reached its limit and SiC-based module is anticipated to replace the former in future. However, a new packaging structure is needed to comply with the high heat density generated by the SiC-devices during operation.
2. Packaging technology has evolved from thermal indirect packaging using thermal grease thermal interface material between module and heat sink, to direct packaging in which the module is connected to the heat sink via solder.
3. Due to the CTE mismatch in power module, low temperature bonding is one major requirement that need to be met, particularly in future generation SiC-based module where module is molded with epoxy-resin.
4. On top of ***low temperature bonding***, ***low pressure bonding***, ***plateless Cu-Cu bonding***, and ***fluxless bonding*** are also required for future generation SiC module packaging. ***High remelting temperature*** of the bonded materials is also necessary to cope with the high operation temperature of SiC-based module.
5. Existing bonding technologies such as soldering, metal particle sintering, and layer-based transient liquid phase bonding cannot meet the bonding conditions of SiC-based epoxy-molded module.
6. Transient liquid phase sintering technology is one of the promising bonding technology that is expected to meet the current demand on bonding epoxy-molded module to the Cu heat-spreader/sink.

References

[1] United States Environmental Protection Agency, Global Greenhouse Gas Emission Data, https://goo.gl/zFF2Zi (accessed on 15 August 2016)

[2] Britain to ban sale of all diesel and petrol cars and vans from 2040, https://goo.gl/8zG2Rg (accessed on 27 August 2017)

[3] Application of Power Electronics in Automotive Applications, https://goo.gl/Cdbrj0 (accessed on 31 August 2017)

[4] Nakano Hayato, Hinata Yuichiro, Horio Masafumi, Ultra-compact, high-reliability all-SiC module, Fuji Electric Review vol. 59 no. 4 (2013) 221-225

[5] Arai Hirohisa et al., 3rd-Generation Direct Liquid Cooling Power Module for Automotive Applications, Fuji Electric Review, Vol. 61, No. 4 (2015) 252-257

[6] Gohara Hiromichi et al., Packaging Technology of 3rd-Generation Power Module for Automotive Applications, Fuji Electric Review, Vol. 61, No.4 (2015) 258-262

[7] Gohara Hiromichi et al., Packaging Technology of IPMs for Hybrid Vehicles, Fuji Electric Review, Vol. 59, No. 4 (2013) 235-240

[8] A. Morozumi, H. Hokazono, Y. Nishimura, E. Mochizuki and Y. Takahashi, "Influence of Cooling Rates on Reliability of Solder Joints Using Sn–13wt.% Sb Binary Alloy for Power Semiconductor Modules," in IEEE Trans. Compon. Packag. Manuf. Technol **6**, 1139 (2016)

[9] H. Beyer, V. Sivasubramaniam, D. Hajas, E. Nanser and F. Brem, "Reliability Improvement of Large Area Soldering Connections by Antimony Containing Lead-Free Solder," in PCIM Europe 2014; International Exhibition and Conference for Power Electronics, Intelligent Motion, Renewable Energy and Energy Management; Proceedings of, Nuremberg, Germany, 2014, pp. 1-8.

[10] Li Jiang et al., Evaluation of Thermal Cycling Reliability of Sintered Nanosilver versus Soldered Joints by Curvature Measurement, IEEE Trans. Compon. Packag. Manuf. Technol. **4**, 751 (2014)

[11] M. Knoerr and A. Schletz, "Power semiconductor joining through sintering of silver nanoparticles: Evaluation of influence of parameters time, temperature and pressure on density, strength and reliability," in Integrated Power Electronics Systems (CIPS), 2010 6th International Conference on, Nuremberg, 2010, pp. 1-6

[12] T. G. Lei, J. N. Calata, G. Q. Lu, X. Chen and S. Luo, "Low-Temperature Sintering of Nanoscale Silver Paste for Attaching Large-Area 100 mm^2 Chips," in IEEE T Compon. Pack. T **33**, 98 (2010)

[13] Min-Su Kim, Hiroshi Nishikawa, Effects of bonding temperature on microstructure, fracture behavior and joint strength of Ag nanoporous bonding for high temperature die attach, Mat. Sci. Eng. A-Struct **645**, 264 (2015)

[14] Yunhui Mei, Gang Chen, Lu Guo-Quan, Xu Chen, Effect of joint sizes of low-temperature sintered nano-silver on thermal residual curvature of sandwiched assembly, Int. J. Adhes. Adhes. **35**, 88 (2012)

[15] Zhang, H., Nagao, S., Suganuma, K., J. Electron Mater **44**, 3896 (2015)

[16] A. Hu, J. Y. Guo, H. Alarifi, G. Patane, Y. Zhou, G. Compagnini, C. X. Xu, Low Temperature sintering of Ag nanoparticles for flexible electronics packaging, Appl. Phys. Lett. **97**, 153117 (2010)

[17] T. Herboth, M. Guenther, A. Fix and J. Wilde, "Failure mechanisms of sintered silver interconnections for power electronic applications," in 2013 IEEE 63rd Electronic Components and Technology Conference, Las Vegas, NV, 2013, pp. 1621-1627

[18] Yoshio Kobayashi, Yuki Abe, Takafumi Maeda, Yusuke Yasuda, Toshiaki Morita, J Mater Research Technol **3**, 114 (2014)

[19] Nishikawa Hiroshi, Hirano Tomoaki, Takemoto Tadashi, Bonding process of Cu/Cu joint using Cu nanoparticle paste, Trans JWRI **40**, 33 (2011)

[20] Shutesh Krishnan, A. S. M. A. Haseeb, Mohd Rafie Johan, Preparation and Low-Temperature Sintering of Cu Nanoparticles for High-Power Devices, IEEE T Compon Pack T **2**, 587 (2012)

[21] Yan Jianfeng, Zou Guisheng, Hu Anming, Y. Norman Zhou, Preparation of PVP coated Cu NPs and the application for low-temperature bonding, J Mater Chem **21**, 15981 (2011)

[22] Cheng-Xiang Yang, Xin Li, Guo-Quan Lu, Yun-Hui Mei, Enhanced pressureless bonding by Tin Doped Silver Paste at low sintering temperature, Mat. Sci. Eng. A-Struct **660**, 71 (2016)

[23] Ahmed Sharif, Chee Lip Gan, Zhong Chen, Transient liquid phase Ag-based solder technology for high-temperature packaging applications, J. Alloy. Compd. **587**, 365 (2014)

[24] Takahashi et al., Introduction to Reliability of Energy Devices, Nikkan Kogyo Publication Production (2012) pp125-193, *in Japanese*

[25] Tadashi Sawamura, Takeo Igarashi, Difference between various Sn/Ag/Cu Solder Compositions, 29 June 2005, https://goo.gl/NVqVwC (accessed on 20 August 2016)

[26] Mulugeta Abtew, Guna Selvaduray, Lead-free solders in microelectronics, Materials Science and Engineering, 27 (2000) 95-141

[27] Thomas Siewert, Stephen Liu, David R. Smith, Juan Carlos Madeni, Properties of lead-free solders, Database for solder properties with emphasis on new lead-free solders, National Institute of Standards and Technology, Release 4.0 (2012) pp1-77

[28] Geon-Woong Lee, Min Park, Junkyung Kim, Jae Ik Lee, Ho Gyu Yoon, Enhanced thermal conductivity of polymer composites filled with hybrid filler, Composites: Part A 37 (2006) 727–734

[29] Jurgen Schulz-Harder, Advantages and new development of direct bonded copper substrates, Microelectronics Reliability 43 (2003) 359–365

[30] Allan Ward, Douglas J. Nelson, Development of heat spreader for high power electronic modules using thermal vias, in Intersociety Conference on Thermal Phenomena, 520 (1998)

[31] Yoshitaka Nishimura, Mitsukane Oonota, Fumihiko Momose, Thermal Management Technology for IGBT Modules, Fuji Electric Review 56, 79 (2010)

[32] Chandan K. Roy, Sushil Bhavnani, Michael C. Hamilton, R.Wayne Johnson, RoyW. Knight, Daniel K. Harris, Applied Thermal Engineering 99 (2016) 72–79

[33] Martin Schulz, Improved Thermal Transfer for Power Modules, in Article Power Electronic Europe 03, (2013)

[34] K. Vijay, Solder-TIMs (Thermal Interface Materials) for superior thermal management in power electronics, 18th European Microelectronics & Packaging Conference, Brighton, 2011, pp. 1-8

[35] Takahisa Hitachi, Hiromichi Gohara, Fumio Nagaune, Direct Liquid Cooling IGBT Module for Automotive Applications, Fuji Electric Review, Vol 58 No. 2 (2012) p55-59

[36] A. Morozumi, H. Hokazono, Y. Nishimura, Y. Ikeda, Y. Nabetani and Y. Takahashi, "Direct liquid cooling module with high reliability solder joining technology for automotive applications," 2013 25th International Symposium on Power Semiconductor Devices & IC's (ISPSD), Kanazawa, 2013, pp. 109-112

[37] Masafumi Horio, Yuji Iizuka, Yoshinari Ikeda, Packaging technologies for SiC power modules, Fuji Electric Review, vol. 48 no. 2 (2012) pp75-78

[38] Y. Hinata, M. Horio, Y. Ikeda, R. Yamada and Y. Takahashi, "Full SiC power module with advanced structure and its solar inverter application," 2013 Twenty-Eighth Annual IEEE Applied Power Electronics Conference and Exposition (APEC), Long Beach, CA, 2013, pp. 604-607

[39] Mulugeta Abtew, Guna Selvaduray, Lead-free solders in microelectronics, Materials Science and Engineering, 27 (2000) 95-141

[40] http://www.senju-m.co.jp/product/ecosolder/index.html (Accessed on 9 February 2016)

[41] http://www.nihonhanda.com/pg301.html (Accessed on 9 February 2016)

[42] http://www.soldercoat.co.jp/pages/product.html (Accessed on 9 February 2016)

[43] http://www.matsuo21.com/?page_id=10 (Accessed on 9 February 2016)

[44] http://www.almit.co.jp/product/sold_past.html (Accessed on 9 February 2016)

[45] http://www.genma.co.jp/wp/wp-content/uploads/2015/01/SB6-HLGQ-20.pdf (Accessed on 9 February 2016)

[46] Doosoo Kim, Jong-hyeon Chang, Jungil Park, James Jungho Pak, Formation and behavior of Kirkendall voids within intermetallic layers of solder joints, J Mater Sci: Mater Electron (2011) 22:703–716

[47] Liu Mei Lee, Habsah Haliman, Ahmad Azmin Mohamad, Interfacial reaction of a Sn-3.0Ag-0.5Cu thin film during solder reflow, Soldering & Surface Mount Technology, 25/1 (2013) 15–23

[48] K.N. Tu, R.D. Thompson, Kinetics of interfacial reaction in bimetallic Cu Sn thin films, Acta Metall. 30, 947 (1982)

[49] Tsutomu Sasaki, Masamoto Tanaka, Yasuhide Ohno, Intermetallic compound formation between lead-free solders (Sn) and Cu or Ni electrodes, Materials Letters 61 (2007) 2093–2095

[50] O.Y. Liashenko, S. Lay, F. Hodaj, On the initial stages of phase formation at the solid Cu/liquid Sn-based solder interface, Acta Materialia 117 (2016) 216-227

[51] P. Sebo, P. Svec Sr., D.Janickovic, E.Illekova´, M.Zemankova, Yu.Plevachuk, V.Sidorov, P. Svec, The influence of silver content on structure and properties of Sn–Bi–Ag solder and Cu/solder/Cujoints, Materials Science & Engineering A 571 (2013) 184–192

[52] Yaowu Shi, Weiping Fang, Zhidong Xia, Yongping Lei, Fu Guo, Xiaoyan Li, Investigation of rare earth-doped BiAg high-temperature solders, J Mater Sci: Mater Electron (2010) 21:875–881

[53] Chandan K. Roy, Sushil Bhavnani, Michael C. Hamilton, R.Wayne Johnson, RoyW. Knight, Daniel K. Harris, Thermal performance of low melting temperature alloys at the interface between dissimilar materials, Applied Thermal Engineering 99 (2016) 72–79

[54] B. Yeung, Jin-Wook Jang, Correlation between mechanical tensile properties and microstructure of eutectic Sn-3.5Ag solder, Journal of Materials Science Letters 21, 2002, 723– 726

[55] J. Keller, D. Baither, U. Wilke, G. Schmitz, Mechanical properties of Pb-free SnAg solder joints, Acta Materialia 59 (2011) 2731–2741

[56] A. Morozumi, K. Yamada, T. Miyasaka, S. Sumi and Y. Seki, "Reliability of power cycling for IGBT power semiconductor modules," in IEEE Transactions on Industry Applications, vol. 39, no. 3, pp. 665-671, May-June 2003

[57] H. Beyer, V. Sivasubramaniam, D. Hajas, E. Nanser and F. Brem, "Reliability Improvement of Large Area Soldering Connections by Antimony Containing Lead-Free Solder," PCIM Europe 2014; International Exhibition and Conference for Power Electronics, Intelligent Motion, Renewable Energy and Energy Management, Nuremberg, Germany, 2014, pp. 1-8

[58] D. Bušek, K. Dušek, D. Růžička, M. Plaček, P.Macha, J. Urbánek, J. Starý, Flux effect on void quantity and size in soldered joints, Microelectronics Reliability 60 (2016) 135–140

[59] K. S. Hansen, M. S. Jellesen, P. Moller, P. J. S. Westermann and R. Ambat, "Effect of solder flux residues on corrosion of electronics," 2009 Annual Reliability and Maintainability Symposium, Fort Worth, TX, 2009, pp. 502-508

[60] Japan Electronics and Information Technology Industries Association, “Lead-free Roadmap 2002, Roadmap 2002 for Commercialization of Lead Free Solder” September 2002

[61] A. Morozumi, H. Hokazono, Y. Nishimura, E. Mochizuki and Y. Takahashi, "Influence of Cooling Rates on Reliability of Solder Joints Using Sn–13wt.% Sb Binary Alloy for Power Semiconductor Modules," in IEEE Trans. Compon. Packag. Manuf. Technol **6**, 1139 (2016)

[62] H. Beyer, V. Sivasubramaniam, D. Hajas, E. Nanser and F. Brem, "Reliability Improvement of Large Area Soldering Connections by Antimony Containing Lead-Free Solder," in PCIM Europe 2014; International Exhibition and Conference for Power Electronics, Intelligent Motion, Renewable Energy and Energy Management; Proceedings of, Nuremberg, Germany, 2014, pp. 1-8.

[63] Katsuaki Suganuma, Introduction to Lead-free Soldering, Osaka University Publication, (2013) pp74-76

[64] H. Schwarzbauer and R. Kuhnert, "Novel large area joining technique for improved power device performance," in IEEE Transactions on Industry Applications, vol. 27, no. 1, pp. 93-95, Jan/Feb 1991

[65] Shlomo Magdassi, Michael Grouchko, Alexander Kamyshny, Copper Nanoparticles for Printed Electronics: Routes towards Achieving Oxidation Stability, Materials 2010, 3, 4626-4638

[66] Min-Su Kim, Hiroshi Nishikawa, Effects of bonding temperature on microstructure, fracture behavior and joint strength of Ag nanoporous bonding for high temperature die attach, Materials Science & Engineering A 645 (2015) 264–272

[67] Eiichi Ide, Akio Hirose, Kojiro F. Kobayashi, Influence of Bonding Condition on Bonding Process Using Ag Metallo-Organic Nanoparticles for High Temperature Lead-Free Packaging, Materials Transactions, Vol. 47, No. 1 (2006) pp. 211 to 217

[68] Hao Zhang, Shijo Nagao, Katsuaki Suganuma, Addition of SiC Particles to Ag Die-Attach Paste to Improve High-Temperature Stability; Grain Growth Kinetics of Sintered Porous Ag, Journal of ELECTRONIC MATERIALS, Vol. 44, No. 10, 2015

[69] Shuai Wang, HongjunJi, MingyuLi, ChunqingWang, Fabrication of interconnects using pressureless low temperature sintered Ag nanoparticles, Materials Letters 85 (2012) 61–63

[70] Thomas Guangyin Lei, Jesus Noel Calata, Guo-Quan Lu, Xu Chen, Shufang Luo, Low-temperature sintering of nanoscale silver paste for attaching large-area (100 mm2) chips, IEEE TRANSACTIONS ON COMPONENTS AND PACKAGING TECHNOLOGY, VOL. 33, NO. 1, MARCH 2010

[71] Matthias Knoerr, Andreas Schletz, Power semiconductor joining through sintering of silver nanoparticles, evaluation of influence of parameters time, temperature and pressure on density, strength and reliability, in CIPS 2010, Nuremberg/Germany

[72] Toshiaki MORITA, Eiichi IDE, Yusuke YASUDA, Akio HIROS1 Kojiro KOBAYASHI, Study of Bonding Technology Using Silver Nanoparticles, Japanese Journal of Applied Physics Vol. 47, No. 8, 2008, pp. 6615–6622

[73] John G. Bai, Jesus N. Calata, Guo-Quan Lu, Processing and Characterization of Nanosilver Pastes for Die-Attaching SiC Devices, IEEE TRANSACTIONS ON ELECTRONICS PACKAGING MANUFACTURING, VOL. 30, NO. 4, OCTOBER 2007

[74] Mei, Y., Chen, G., Cao, Y. et al, Simplification of Low-Temperature Sintering Nanosilver for Power Electronics Packaging, Journal of Elec Materi (2013) 42: 1209

[75] Guo-Quan Lu, Meihua Zhao, Guangyin Lei, Jesus N. Calata, Xu Chen, Susan Luo, Emerging Lead-free, High-temperature Die-attach Technology Enabled by Low-temperature Sintering of Nanoscale Silver Pastes, in 2009 International Conference on Electronic Packaging Technology & High Density Packaging (ICEPT-HDP)

[76] Yi Yan, Xu Chen, Xing Sheng Liu, Guo-Quan Lu, Die Bonding of Single Emitter Semiconductor Laser with Nano-Scale Silver Paste, in 2011 International Conference on Electronic Packaging Technology & High Density Packaging,

[77] E. Ide, S. Angata, A. Hirose, K.F. Kobayashi, Metal–metal bonding process using Ag metallo-organic nanoparticles, Acta Materialia 53 (2005) 2385–2393

[78] Xiangdong Liu, Hiroshi Nishikawa, Low-pressure Cu-Cu bonding using in-situ surface-modified microscale Cu particles for power device packaging, Scripta Materialia 120 (2016) 80–84

[79] Nishikawa Hiroshi, Hirano Tomoaki, Takemoto Tadashi, Bonding process of Cu/Cu joint using Cu nanoparticle paste, Transactions of JWRI, Vol. 40 (2011) No.2 pp33-36

[80] Yan Jianfeng, Zou Guisheng, Hu Anming, Y. Norman Zhou, Preparation of PVP coated Cu NPs and the application for low-temperature bonding, J. Mater. Chem., 2011, 21, 15981

[81] Shutesh Krishnan, A. S. M. A. Haseeb, Mohd Rafie Johan, Preparation and Low-Temperature Sintering of Cu Nanoparticles for High-Power Devices, IEEE TRANSACTIONS ON COMPONENTS, PACKAGING AND MANUFACTURING TECHNOLOGY, VOL. 2, NO. 4, APRIL 2012

[82] Yamakawa Tomohiro et al, Low temperature bonding using Cu nanoparticle paste and reliability evaluation on the joints, in 26th Japan Electronics Packaging Conference

[83] Toshitaka Ishizaki and Ryota Watanabe, A new one-pot method for the synthesis of Cu nanoparticles for low temperature bonding, J. Mater. Chem., 2012, 22, 25198

[84] Jianfeng Yan, Guisheng Zou, Yingchuan Zhang, Jiaxin Li, Lei Liu, Aiping Wu, Y. Norman Zhou, MetalMetal Bonding Process Using Cu+Ag Mixed Nanoparticles, Materials Transactions, Vol. 54, No. 6 (2013) 879-883

[85] Randall M. German, Sintering: From Empirical Observation to Scientific Principles, Butterwoth-Heinemann (2014) pp247

[86] Huakai Shao et al, Interfacial reaction and mechanical properties for Cu/Sn/Ag system low temperature transient liquid phase bonding, J Mater Sci: Mater Electron (2016) 27:4839–4848

[87] Habib A. Mustain, William D. Brown, Simon S. Ang, Transient Liquid Phase Die Attach for High-Temperature Silicon Carbide Power Devices, IEEE TRANSACTIONS ON COMPONENTS AND PACKAGING TECHNOLOGIES, VOL. 33, NO. 3, SEPTEMBER 2010

[88] H.Y. Zhao, J.H. Liu, Z.L. Li, Y.X. Zhao, H.W. Niu, X.G. Song, H.J. Dong, Non-interfacial growth of Cu3Sn in Cu/Sn/Cu joints during ultrasonic assisted transient liquid phase soldering process, Materials Letters 186 (2017) 283–288

[89] J.H. Liu, H.Y. ZhaoZ.L. Li, X.G. Song, H.J. DongY.X. Zhao, J.C. Feng, Study on the microstructure and mechanical properties of Cu-Sn intermetallic joints rapidly formed by ultrasonic-assisted transient liquid phase soldering, Journal of Alloys and Compounds 692 (2017) 552-557

[90] L. Mo, Z. Chen, F. Wu, C. Liu, Microstructural and mechanical analysis on CueSn intermetallic micro-joints under isothermal condition, Intermetallics 66 (2015) 13-21

[91] Kunmo Chu, Yoonchul Sohn, Changyoul Moon, A comparative study of Cn/Sn/Cu and Ni/Sn/Ni solder joints for low temperature stable transient liquid phase bonding, Scripta Materialia 109 (2015) 113–117

[92] Hongjun Ji, Yunfei Qiao, Mingyu Li, Rapid formation of intermetallic joints through ultrasonic-assisted die bonding with Sn–0.7Cu solder for high temperature packaging application, Scripta Materialia 110 (2016) 19–23

[93] J.S. KANG, R.A. GAGLIANO, G. GHOSH, M.E. FINE, Isothermal Solidification of Cu/Sn Diffusion Couples to Form Thin-Solder Joints, Journal of ELECTRONIC MATERIALS, Vol. 31, No. 11, 2002

[94] J.F. Li, P.A. Agyakwa, C.M. Johnson, Interfacial reaction in Cu/Sn/Cu system during the transient liquid phase soldering process, Acta Materialia 59 (2011) 1198–1211

[95] H. Liu, K. Wang, K.E. Aasmundtveit, N. Hoivik, Intermetallic Compound Formation Mechanisms for Cu-Sn Solid–Liquid Interdiffusion Bonding, Journal of ELECTRONIC MATERIALS, Vol. 41, No. 9, 2012

[96] N.S. Bosco, F.W. Zok, Strength of joints produced by transient liquid phase bonding in the Cu–Sn system, Acta Materialia 53 (2005) 2019–2027

[97] F. Brem, C. Liu and D. Raik, "Influence of Cu joining partner in transient liquid phase bonding," 2012 4th Electronic System-Integration Technology Conference, Amsterdam, Netherlands, 2012, pp. 1-5.

[98] S.W. Park, S. Nagao, Y. Kato, H. Ishino, K. Sugiura, K. Tsuruta, K. Suganuma, Quasi-transient liquid-phase bonding by eutectic reaction of Sn-plated Zn on Cu substrate for high-temperature die ttachment, Journal of Alloys and Compounds 637 (2015) 143–148

[99] A. A. Bajwa, Y. Y. Qin, R. Zeiser, Wilde, "Foil Based Transient Liquid Phase Bonding as a Die-Attachment Method for High Temperature Devices," CIPS 2014; 8th International Conference on Integrated Power Electronics Systems, Nuremberg, Germany, 2014, pp. 1-6

[100] W. Liu, N. C. Lee and P. Bachorik, "An innovative composite solder preform for TLP bonding — Microstructure and properties of die attach joints," 2013 IEEE 15th Electronics Packaging Technology Conference (EPTC 2013), Singapore, 2013, pp. 635-640

[101] H. Greve, L. Y. Chen, I. Fox and F. P. McCluskey, "Transient liquid phase sintered attach for power electronics," 2013 IEEE 63rd Electronic Components and Technology Conference, Las Vegas, NV, 2013, pp. 435-440

[102] H. Greve, S. A. Moeini, F. P. McCluskey and S. Joshi, "Microstructural Evolution of Transient Liquid Phase Sinter Joints in High Temperature Environmental Conditions," 2016 IEEE 66th Electronic Components and Technology Conference (ECTC), Las Vegas, NV, 2016, pp. 2561-2568

[103] S. A. Moeini, H. Greve and F. P. McCluskey, "Reliability and failure analysis of Cu-Sn transient liquid phase sintered (TLPS) joints under power cycling loads," 2015 IEEE 3rd Workshop on Wide Bandgap Power Devices and Applications (WiPDA), Blacksburg, VA, 2015, pp. 383-389

[104] H. Greve, S. A. Moeini and F. P. McCluskey, "Reliability of paste based transient liquid phase sintered interconnects," 2014 IEEE 64th Electronic Components and Technology Conference (ECTC), Orlando, FL, 2014, pp. 1314-1320

[105] H. Greve and P. McCluskey, "Reliability of Sn based LT-TLPS Joints for High Temperature Electronic Systems," CIPS 2014; 8th International Conference on Integrated Power Electronics Systems, Nuremberg, Germany, 2014, pp. 1-6

[106] Hannes Greve, F. Patrick McCluskey, Transient liquid phase sintered joints for power electronic modules, Proceedings of the ASME 2013 International Technical Conference and

Exhibition on Packaging and Integration of Electronic and Photonic Microsystems InterPACK2013 July 16-18, 2013, Burlingame, CA, USA, IPACK2013-73209

[107] F. Lang, H. Yamaguchi, H. Nakagawa and H. Sato, "High temperature resistant joint technology for SiC power devices using transient liquid phase sintering process," 2012 13th International Conference on Electronic Packaging Technology & High Density Packaging, Guilin, 2012, pp. 157-161

[108] Toshitaka Ishizaki, Ryota Watanabe, Pressureless Bonding by Use of Cu and Sn Mixed Nanoparticles, Journal of ELECTRONIC MATERIALS, Vol. 43, No. 12, 2014, pp4413-4420

[109] Omid Mokhtari, , Hiroshi Nishikawa, The shear strength of transient liquid phase bonded Sn–Bi solder joint with added Cu particles, Advanced Powder Technology 27 (2016) 1000–1005

[110] Tianqi Hu, Hongtao Chen, Mingyu Li, Die attach materials with high remelting temperatures created by bonding Cu@Sn microparticles at lower temperatures, Materials and Design 108 (2016) 383–390

[111] Xiangdong Liu, Siliang He and H. Nishikawa, "Low temperature bonding using microscale Cu particles coated with thin Sn layers at 200 °C," 2016 International Conference on Electronics Packaging (ICEP), Sapporo, 2016, pp. 306-309

[112] Masahisa Fujino, Hirozumi Narusawa, Yuzuru Kuramochi, Eiji Higurashi, Tadatomo Suga, Toshiyuki Shiratori, Masataka Mizukoshi,

[113] Cheng-Xiang Yang, XinLi, Guo-QuanLu, Yun-HuiMei, Enhanced pressureless bonding by Tin Doped Silver Paste at low sintering temperature, Materials Science & Engineering A 660 (2016) 71–76

[114] Ahmed Sharif, Chee Lip Gan, Zhong Chen, Transient liquid phase Ag-based solder technology for high-temperature packaging applications, Journal of Alloys and Compounds 587 (2014) 365–368

[115] Koji Kondo, Yoshitaro Yazaki, Yoshihiko Shiraishi, Development of a new multi-layer substrate (PALAP) using Ag-Sn liquid phase sintering process, J. Jpn Soc. Powder Powder Metallurgy Vol. 57 No.10 (2010) pp678-682 (in Japanese)

CHAPTER 2: SIGNIFICANCE OF STUDY

2.1 Research Motivation

Based on the literature review on current packaging technologies and associated low temperature bonding technology that has been conducted in previous chapter, the motivation of this research is addressed as follows.

On increasing the efficiency of thermal dissipation in power module, usage of low thermal conductance of thermal grease has been eliminated and replaced with higher thermal conductance of soldering technology. Sn-Ag, Sn-Sb based Pb-free solder has been used as the thermal interface material to bond DBC substrate of power module to the heat substrate/sink, owing to their high thermal conductivity and superior mechanical strength. However, the processing temperature was rather high and can reached over than 300°C, depending on the composition of the solder alloys. Since the components that constitute power modules comprised of different CTE values, thermomechanical stress is inevitable during fabrication.

In addition, on coping with increasing junction temperature of wide-band gap SiC-based devices, several improvements have been developed in packaging technology. This includes the replacement of low thermal resistance of silicone gel to higher thermal resistance of epoxy-resin. However, bonding epoxy-molded module by using conventional Sn-Ag or Sb-Sb solder comes with one drawback. The glass transition temperature of the epoxy-resin is around 200°C, but the processing temperature of the conventional solder exceeded the glass transition temperature of the epoxy-resin. Research on increasing the glass transition temperature of the epoxy-resin is still ongoing, however, it is preferable for the processing temperature of the epoxy-molded module to be realized at the

vicinity of 200°C. This has twofold aims which are to lower the thermomechanical stress, and to avoid the thermal damage of epoxy-resin the same time.

On the other hand, exerting high pressure during fabrication is unfavorable to the epoxy-molded module as it will induced pre-mature cracking, and also it complicates the production line. Furthermore, metal plating is costly and depositing metal plating to the epoxy-molded module is impractical. To top that, excluding flux from the sintering paste favors the industry as the flux residue cleaning works after fabrication can be omitted and ensure high reliability of the bonded materials since it is well known that flux residue is corrosive.

Last but not least, since the junction temperature of SiC-based module can reach up to 300 °C, in which the case temperature is expected to rise up to 125 °C, a thermally stable bonding material up to 125 °C is required. On this regards, a new bonding technology that can be realized at temperature lower than 250°C, or preferably as low as 200°C, and in the same time satisfies the requirement of bonding future generation SiC/GaN-based epoxy-molded power module as explained above is in great demand. Taking $0.85T_h$ of the bonding material as the maximum application temperature, when the maximum case temperature is 125 °C, the melting temperature of the bonding material should be over than 200 °C.

Table 2.1 compiles several existing low temperature bonding technologies according to the requirements that need to be met in this study. As can be seen in Table 2.1, up to author's knowledge, as being introduced in Chapter 1, there is no precedent work on TLPS that can accomplish all those requirements. This study is thought to be the first in the world to satisfy all the processing conditions, and in the same time meeting the requirements for the high temperature application.

Table 2.1 Previous studies on low temperature bonding technology as reviewed in Chapter 1

Bonding technology	Processing parameters		Plate-less	Flux-less	High temp. application (Melting temp.: ≧ 200 °C)
	Temperature (200 – 250 °C)	Pressure (≦0.1 MPa)			
Target in this study	○	○	○	○	○
Soldering	○	○	○	×	×
Ag nanoparticles sintering	△	×	×	○	○
Cu nanoparticles sintering	△	×	○	×	○
Transient liquid phase bonding (layer-based)	△	△	○	○	○
Transient liquid phase sintering (powder-based)	○	△	○	○	×

○: Able; △: Partially able, depending on certain conditions; ×: Unable

2.2 Transient Liquid Phase Sintering Proposed in This Study

In this study, Ag or Cu nanoparticles are mixed with eutectic Sn-Bi micro-sized powders to achieve the TLPS in order to join plateless Cu-Cu substrate. The reasons of choosing these materials are addressed as follows:

Silver, Ag

- High thermal conductivity
- Noble metal, hence, sintering is thought to be conducted in non-reductive atmosphere
- High melting temperature

Copper, Cu

- High thermal conductivity
- Similar element to the substrate of interest, hence, metal plating is thought to be unnecessary
- High melting temperature

Eutectic Tin-Bismuth, Sn-Bi

- Low eutectic temperature (139 °C) providing possibility of TLPS at low temperature
- Low wetting angle

It is well established from Bi-Ag (Figure 2.1(a)) and Cu-Bi (Figure 2.1(b)) binary alloy phase diagrams that Ag or Cu do not solute into Bi, and vice versa. Hence, it is not exaggeration to state that when Sn-Bi particles melt and wet the Ag or Cu nanoparticles, only Sn but Bi diffuse into Ag or Cu. Rapid solubility of Ag or Cu nanoparticles into molten Sn leads to the formation of IMCs where Bi is precipitated throughout the process. The precipitated Bi is thought to fill the sintering voids, hence the densification of the sintering structure can be achieved. The densification of the sintering structure is assumed to strengthen the joints. The expected microstructure to be achieved once the sintering is completed is depicted in Figure 2.2.

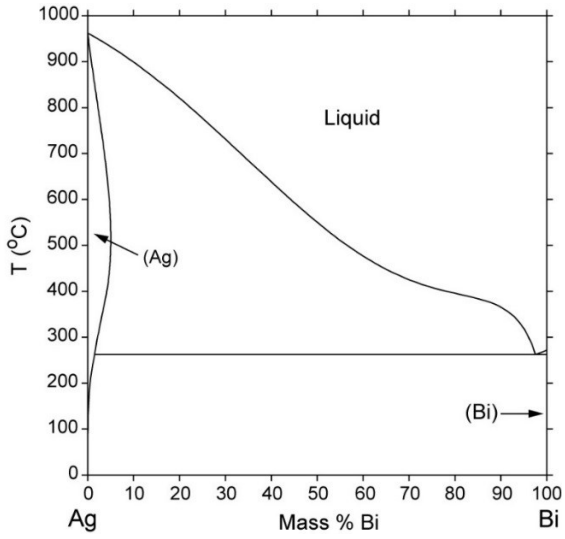

(a) Bi-Ag binary phase diagram [1, 2]

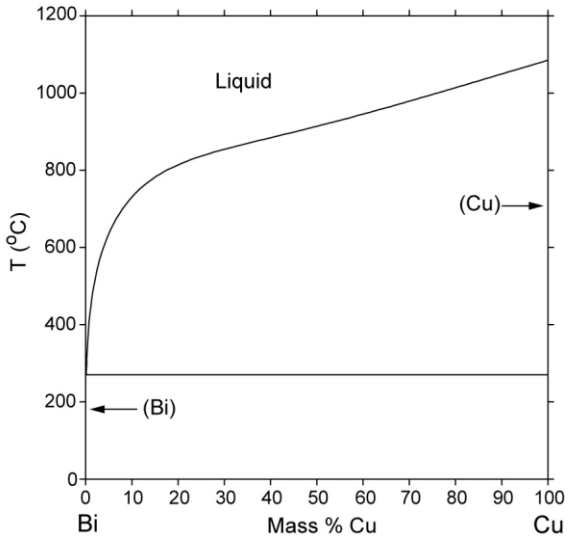

(b) Cu-Bi binary phase diagram [3, 4]

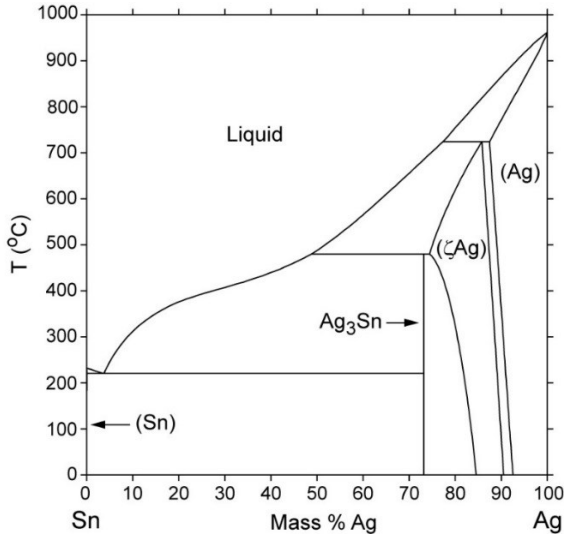

(c) Ag-Sn binary phase diagram [5]

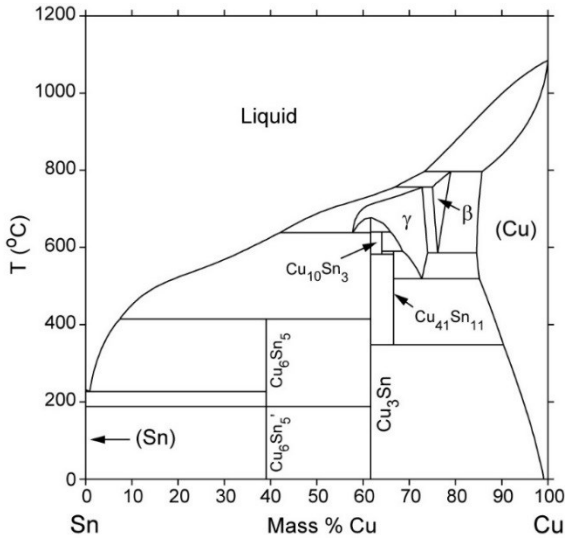

(d) Cu-Sn binary phase diagram [5]

Figure 2.1 Binary phase diagrams of elements of interest in this study

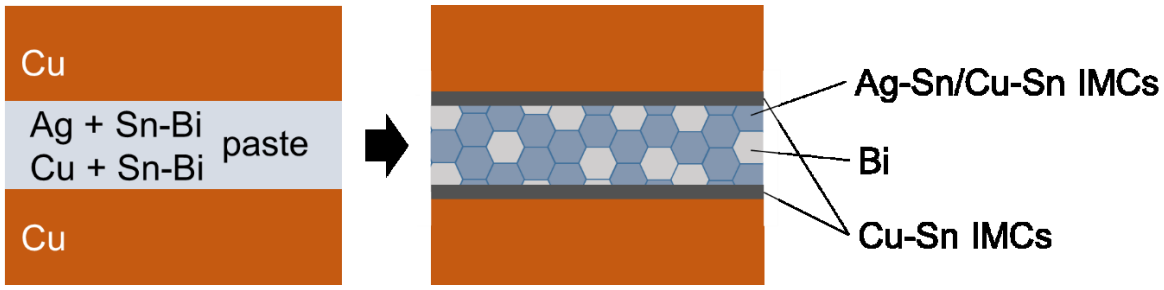

Figure 2.2 Expected microstructure by TLPS proposed in this study

In order to realize the fluxless bonding, formic gas reducing environment has been incorporated during the processing. Formic gas has been reported to reduce copper oxide at temperature as low as 150 °C [6, 7]. The reducing environment is essential to remove the unavoidable oxide layer that may exist on the Cu substrate and Cu nanoparticles, as well as Sn-Bi powder, prior to and during heating. Five significance characteristics from the Sn-Bi added Ag or Cu TLPS as proposed in this study are described as follows:

1. Enabling low temperature bonding

Sn-Bi eutectic temperature is 139 °C, hence, once the Sn-Bi is melted, the isothermal solidification will begin and densification of the sintering structure can be expected at temperature lower than 200 °C.

2. Enabling low pressure bonding

Sn-Bi is well-known as one of the solder that possess low wetting angle, hence, once melted, it is expected that the spreading of the molten Sn-Bi will be accelerated, facilitated by the capillary effect that exist in the sintering structure. High pressure is unnecessary for densification since the densification of the sintering structure will be accommodated by the liquid phase from.

3. Allowing plateless Cu-Cu bonding

The existence of molten Sn is expected to react with plateless Cu-substrate to form interfacial interaction layer consisting of Cu-Sn IMCs which is one of the important conditions, although not definitely a must, on achieving a good bonding.

4. Replacing flux-contained bonding

By the introduction of formic gas during sintering, rather than mixing the paste with flux, the reduction of Cu substrate, Cu nanoparticles, as well as Sn-Bi powders can be anticipated. Residue flux-cleaning procedure post-processing is no longer necessary.

5. Increasing remelting temperature

With the formation of Ag-Sn or Cu-Sn IMCs at the expense of Sn from the molten Sn-Bi, the remelting temperature of the as-sintered joints is expected to rise higher than the eutectic temperature of the Sn-Bi, i.e.139 °C.

2.3 Objective of Study

The objective of this dissertation is to utilize transient liquid phase sintering to achieve bonding between plateless Cu-Cu substrates at low temperature without the application of high pressure during fabrication. Macroscale Sn-Bi eutectic alloy particles as low melting temperature material is mixed with high melting temperature material of Ag or Cu nanoparticles with volatile organic compounds to realize the TLPS. Flux as reducing agent is not introduced in preparing the sintering paste, whereas reducing environment was incorporated during processing to reduce the oxidation of added particles and Cu substrates. This special reducing environment has allowed the reduction reaction takes place at as low as 150°C which is relatively lower than hydrogen atmosphere, which is can only be realized at temperature higher than 250°C. Following items are investigated in this study.

i. ***Effect of processing environment***. Major issue on fluxless bonding lies on the difficulty of achieving the wetting of the additive materials due to the oxide layer that form on the surface of the particles and also the Cu substrate. Since poor wetting lead to poor interfacial reaction at both substrates and within grains, choosing the suitable environment is essential. Non-reactive inert environment and reducing environments are compared to investigate the wetting of the Sn-Bi particles prior to bonding of plateless Cu-Cu substrates.

ii. ***Organic compound selection and paste preparation***. In this present work, commercially available Ag paste is used to mix with Sn-Bi particles. On contrary, for Cu and Sn-Bi mixed TLPS, Cu and Sn-Bi is mixed with several types of organic compounds. Shear strength and the remelting temperature of the mixture is firstly evaluated to find the suitable addition amount for further investigations. Organic compounds composition that shows the highest shear strength is selected for the paste preparation.

iii. ***Influence of alloy composition***. To realize the bonding of plateless Cu-Cu substrate, the formation of interfacial reaction layer is essential to ensure a robust and sound joint. The

formation of this interfacial reaction layer is thought to be highly dependent on the liquid phase amount that formed during heating. Hence, the minimum addition amount of additive Sn-Bi particles is investigated. Effect of alloy composition to the shear strength of the joints and remelting temperature of the as-sintered material is also evaluated. Excessive addition of eutectic Sn-Bi particles may lead to low temperature remelting event, hence, alloy composition is a crucial parameter to be assessed. Microstructural observation and elemental analysis is conducted to correlate the effect of alloy composition to the strengthening mechanism of the proposed TLPS.

iv. ***Effects of sintering parameters***. Sintering parameters such as sintering temperature, and sintering holding time, are varied to find the effects on the shear strength of the joints and remelting temperature of the as-sintered materials. Sintering temperature are kept at 250°C and lower, meanwhile the sintering pressure is kept below than 0.1 MPa with the application of weight throughout processing. Minimum sintering time is investigated to have a joint with high shear strength or at least exceeded the minimum requirement of MIL-STD-883K. These findings are adapted to screen the best conditions for the application on large area bonding and reliability assessment in future works.

v. ***Elucidation of the mechanism of Sn-Bi added TLPS***. To further understanding the strengthening mechanism of the proposed TLPS, and the factors that contribute to the increasing of the remelting temperature, the mechanism of the Sn-Bi added TLPS process is made clear by microstructure observation and elemental analysis.

2.4 Organization of Dissertation

The outline of this dissertation is described as follows.

Chapter 3 explains about the materials under test, sintering paste preparation procedure, experimental methods, and evaluation methods used in this study. A preliminary investigations on the wetting of Sn-Bi powders under difference heating environment is also conducted and discussed.

Chapter 4 discusses about the silver-based transient liquid phase sintering. Alloys composition is selected according to the expected microstructure of the sintered structure and the associated expected remelting temperature. Influence of alloy composition and several sintering parameters to the shear strength and remelting temperature is evaluated and discussed. Preliminary screening was conducted based on the alloy composition and sintering conditions that showed the highest shear strength. The mechanism of Ag and Sn-Bi mixed TLPS that showed the highest shear strength is elucidated and explained.

Chapter 5 talks about Cu and Sn-Bi mixed transient liquid phase sintering. The advantages of using nanoscale Cu particles are explained. The selection of alloy composition is discussed based on the expected microstructure and remelting temperature of the sintered material. Organic compounds selection and optimization in preparing sintering paste is explained. Effects of composition, sintering time, and sintering temperature to the shear strength and microstructure are investigated and discussed. Similar to Ag-based TLPS as explained in Chapter 4, the mechanism of Cu and Sn-Bi mixed TLPS that showed the highest shear strength is elucidated and explained.

Chapter 6 compares the Ag-based and Cu-based TLPS, in term of liquid phase volume fraction and strengthening mechanism. The mechanism of reduction of oxide film will also be proposed and explained.

Chapter 7 is the summary and conclusion of each chapter. Future works for this study will also be addressed.

References

[1] Ag-Bi system, https://goo.gl/JkKuM5 (accessed on 1 August 2016)

[2] U.R. Kattner and W.J. Boettinger, J. Electron. Mater. 23 (1994) 603-610

[3] Bi-Cu system, https://goo.gl/HPwczz (accessed on 1 August 2016)

[4] O. Teppo, J. Niemelä and P. Taskinen, Thermochim. Acta 173 (1990) 137-150

[5] Ursula R. Kattner, Phase diagrams for lead-free solder alloys, The Journal of The Minerals, Metals & Materials Society, Volume 54, Issue 12 (2002) 45–51

[6] Wenhua Yang, Hiroyuki Shintani, Masatake Akaike, Tadatomo Suga, Low Temperature Cu-Cu Direct Bonding using Formic Acid Vapor Pretreatment, 2011 Electronic Components and Technology Conference, 2079-2083

[7] Naoya Matsuoka, Masahisa Fujino, Masatake Akaike, Tadatomo Suga, Process Parameters for Formic Acid Treatment with Pt Catalyst for Cu Direct Bonding, ICEP-IAAC 2015 Proceedings, 460-463

CHAPTER 3: METHODOLOGY

In this chapter, all materials under test and the preparation of Ag-based and Cu-based sintering pastes that will be used for investigations in Chapter 4 and 5 will be explained. A method on deciding sintering profile for both as-prepared sintering pastes was performed by means of thermogravimetric-differential thermal analysis (TG-DTA). In addition, a preliminary experiment on wetting of Sn-Bi by formic gas has also been conducted and discussed. Using the outcomes of the TG-DTA and preliminary experiment, sintering profile was determined and demonstrated. Sample preparation for shear test, remelting temperature determination, and cross-sectional microstructural observation and elemental analysis are also described in details. All explanations stated in this chapter are applicable to the investigations in Chapter 4 and 5, unless otherwise specified.

3.1 Materials and Sintering Paste Preparation

In this work, as explained in prior chapter, on aiming for the application to bond plateless DBC substrate with plateless Cu-heat spreader/heat sink at low temperature and low pressure, transient liquid phase sintering of Ag or Cu mixed with Sn-Bi was proposed. For Ag-based TLPS study that will be discussed in Chapter 4, commercial available Ag sintering paste was mixed with Sn-Bi powders. On the other hand, for Cu-based TLPS study that will be discussed in Chapter 5, sintering paste was developed from scratch by mixing Cu nanoparticles and Sn-Bi with specific organic solutions. Commercially available Ag sintering paste, Cu nanoparticles, and Sn-Bi powders used in this work are listed in Table 3.1. Pictures of as-received Ag sintering paste in syringe and as-received methanol-dispersed Cu nanoparticles in bottle are shown in Figure 3.1.

The particle size of the Ag particles in the green paste ranged from several hundred nm to several μm with random shape, i.e. flake and sphere. Figure 3.2 shows the Ag particles size distribution and SEM image used to calculate the size distribution using image analysis software (ImagePro Premier 9.2). 300 particles were measured. Taking into account of the mode value, the particle size of Ag particles is defined as 0.2 μm. Meanwhile, primary particle size of Cu particles used in this study was 50 nm, as reported by the manufacturer. Sn-Bi powders in this study was produced by atomization method and the mean particle size was 2 μm according to the material data sheet obtained from the manufacturer. Figure 3.3 demonstrates the SEM images of Sn-Bi used in this study.

Table 3.1 Materials under test in this work

Material	Product name	Manufacturer	Particle size
Silver, Ag	Loctite Ablestik SSP2020	Henkel AG & Co. KGaA	200 μm
Copper, Cu	SFCP-10AX	Fukuda Metal Foil & Powder Co. Ltd.	50 nm
Tin-bismuth eutectic alloy, Sn-57wt.% Bi	Custom order	Fukuda Metal Foil & Powder Co. Ltd.	2 μm

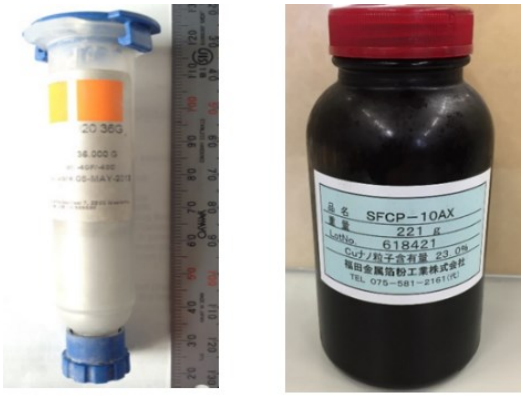

a **b**

Figure 3.1 Picture of as-received **a** Ag sintering paste, and **b** methanol-dispersed Cu nanoparticles

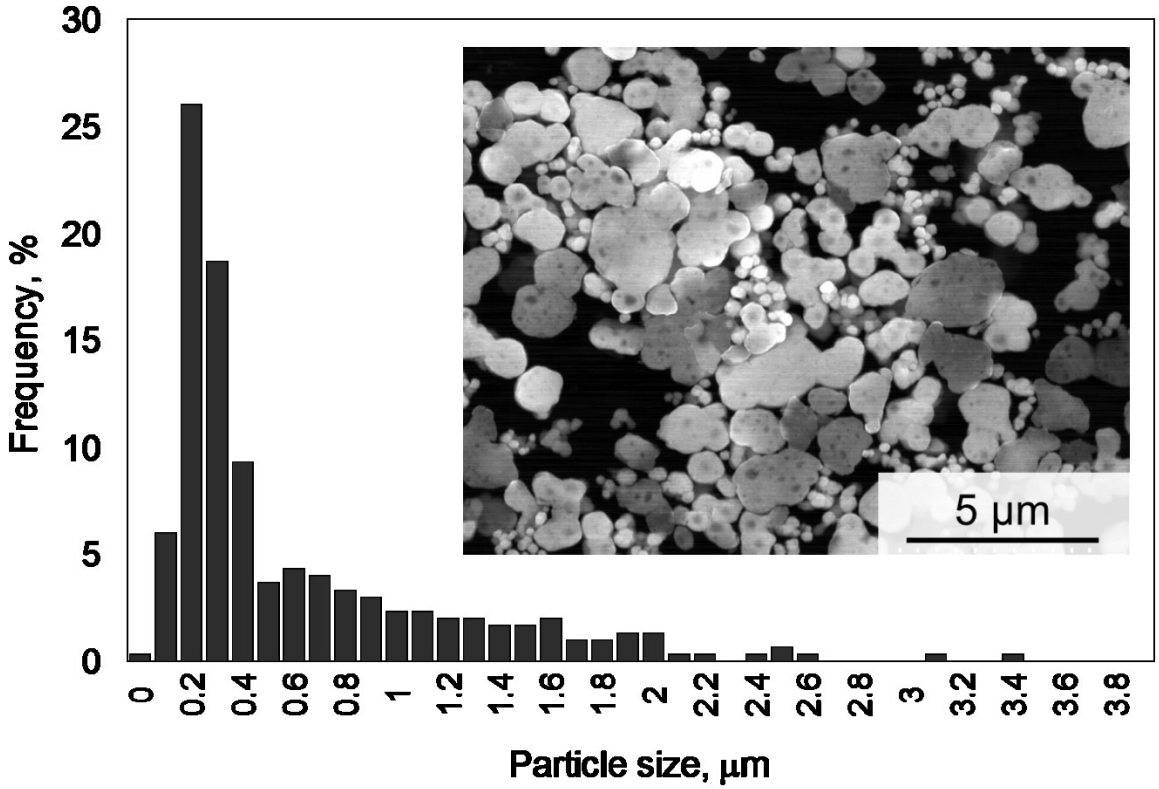

Figure 3.2 Particle size distribution of Ag particles (inset is the SEM image used to calculate the particle size distribution

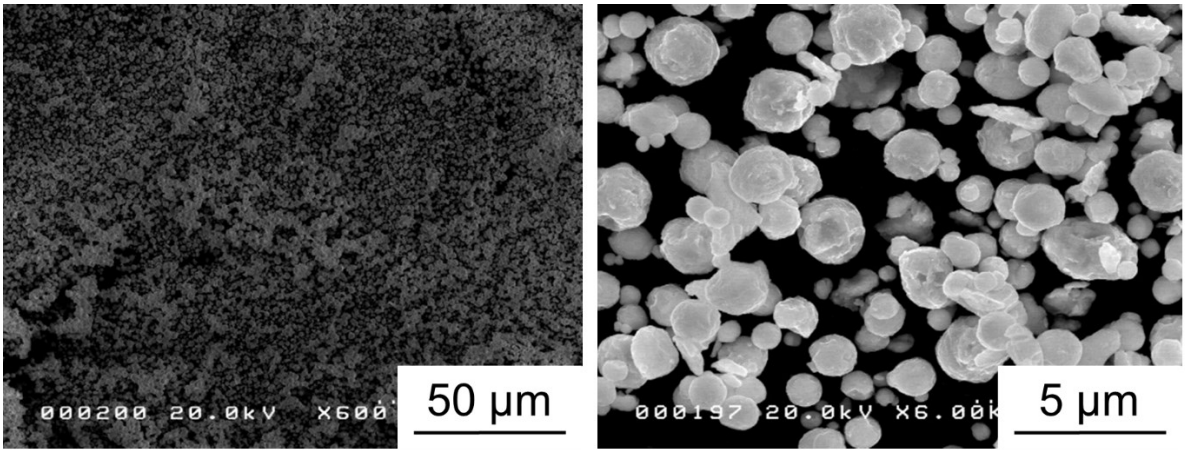

Figure 3.3 SEM images of Sn-Bi with different magnification (left: 600×; right: 6000×)

3.1.1 Silver-based Sintering Paste

Since the organic compounds in the commercially available Ag sintering paste are unknown, adding organic compounds that exhibit certain effects such as reduction effects need to be prevented since the unknown reaction that might likely happen between unknown organic compounds and the newly added organic compounds might be detrimental to the sintering paste. Mixture paste preparation in this study was very simple and it is presumed that this method might be applicable to all commercially available Ag sintering paste. In brief, the added Sn-Bi was firstly dispersed in an ethanol solution and the Ag sintering paste was added into the dispersion. Finally, the added ethanol from the mixture was evaporated by means of high speed centrifugal planetary rotation. Details on preparing the Ag-based mixture paste are explained as follows. Figure 3.4 illustrates the mixture paste preparation procedure corresponding to the steps explained as per below for quick guide.

i. On a zero-adjusted glass plate, Ag sintering paste was weighed. After weighing, the weight of Ag particles was determined from the value obtain from TG-DTA analysis, which will be explained in section 3.2.1.

ii. On a separate zero-adjusted plastic container, Sn-Bi powders was weighed. The plastic container used in this study complies with the planetary centrifugal mixer (Thinky Mixer AR-100) for subsequence mixing.

iii. Ethanol was added into the plastic container from step ii sufficiently to create a Sn-Bi dispersion. The amount of ethanol may vary depending on the amount of Sn-Bi.

iv. Sn-Bi powders in ethanol solution was dispersed in an ultrasonic bath accompanied by stirring with glass rod to break any lumps in order to obtain a uniformly dispersed Sn-Bi dispersion. The ultrasonic agitation was conducted for at least 3 min.

v. Ag sintering paste from step i was added into the Sn-Bi dispersion from step iv.

vi. Without closing the lid of the plastic container, the mixture was mixed in the planetary centrifugal mixer for minimum 5 minutes. Mixing and deaeration mode were utilized to facilitate the evaporation of added ethanol.

The evaporation of ethanol by centrifugal mixing is thought to occur by the pressure difference in the bottom and upper part of plastic container. The purpose of mixing with open case is to assist the evaporated ethanol out of the sintering paste. Deaeration mode assisted the ethanol in the sintering paste to resurface and by continuous mixing for several minutes, the ethanol is assumed to completely evaporate.

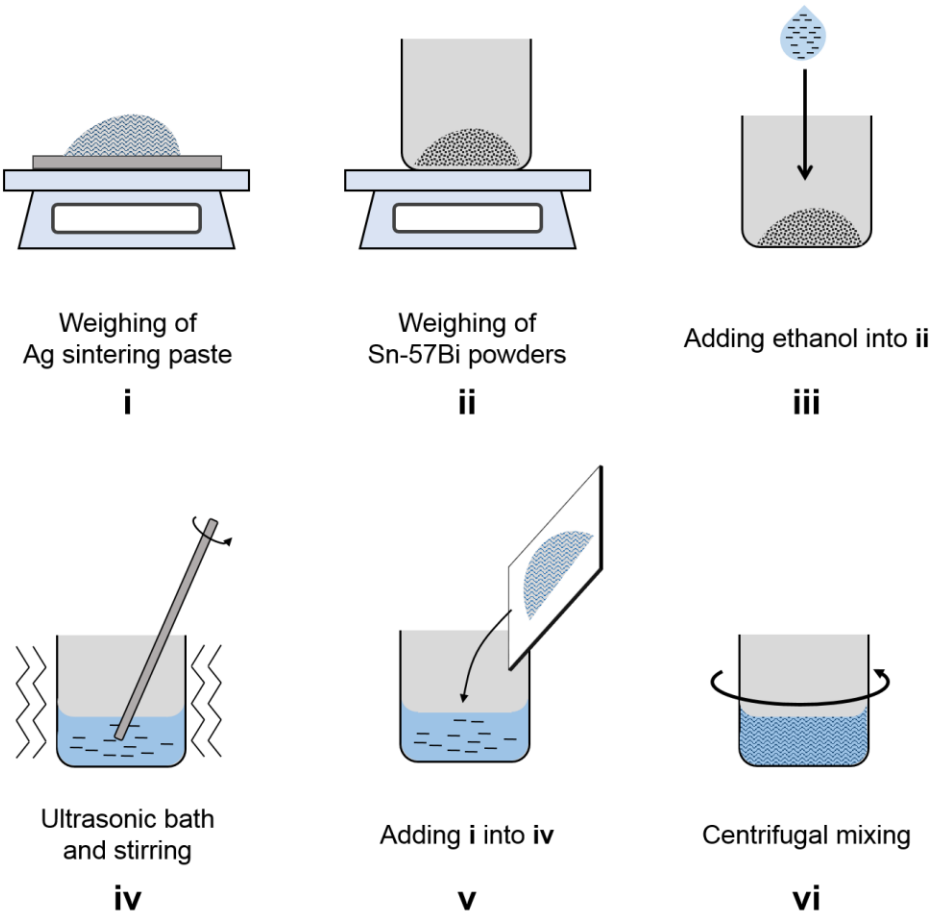

Figure 3.4 Schematic illustration of Ag-based sintering paste preparation method

3.1.2 Copper-based Sintering Paste

As explained earlier, compared to the preparation of Ag-based sintering paste, Cu-based sintering paste in this study was prepared by mixing Cu nanoparticles and Sn-Bi. In this study, organic capping layer or surface activation layer that is commonly deposited onto nanoparticles to prevent agglomeration or aggregation of nanoparticles was not introduced. One may suspect that the agglomeration or aggregation of Cu particles is inevitable and might hinder the rapid solution of Cu nanoparticles into the molten Sn-Bi. However, it is also assumed that since the as-received Cu nanoparticles was dispersed in methanol solution, the oxidation of Cu nanoparticles might also be unavoidable. The stable copper oxide layer that exist on the outer layer of the Cu nano particles might prevent the agglomeration/aggregation of the Cu nanoparticles. Illustrations of preparing mixture paste corresponding to each step explained below are depicted in Figure 3.5.

i. Approximately 3 g of the as-received methanol-dispersed Cu nanoparticles were weighed in a zero-adjusted plastic container. The plastic container used here complies with planetary centrifugal mixer (Thinky Mixer AR-100) for the subsequence mixing.

ii. Without closing the lid of the container, the methanol solution containing Cu nanoparticles was centrifuged at 2000 rpm for several minutes until all the methanol was evaporated and there was no change of weight from the collected dry-Cu nanoparticles.

iii. The collected dry-Cu nanoparticles was weighed to two places of decimals.

iv. Approximately 3 ml of ethanol was added to the mixed Cu nanoparticles. Ethanol addition amount may vary up to 5 ml according to the amount of Cu nanoparticles.

v. Cu nanoparticles in ethanol solution was dispersed in an ultrasonic bath accompanied by stirring with glass rod to break any lumps in order to obtain a uniformly dispersed Cu nanoparticles dispersion. The ultrasonic agitation was conducted for at least 3 min.

vi. On a separate zero-adjusted weighing paper, Sn-Bi powders were weighed accordingly to the pre-determined Cu weight at iii.

vii. Sn-Bi powders were added to the container that contained the dispersed Cu nanoparticles (v).

viii. Organic solution(s) to control the viscosity of the paste was/were added into the Cu and Sn-Bi mixed suspension. The weight ratio of organic compound(s) to the Cu and Sn-Bi mixed particles are determined in Chapter 5 Section 5.2.

ix. Once again, the mixed powders and organic solution(s) was/were ultrasonicated in bath for 3 min. During dispersion in the ultrasonication bath, the Cu and Sn-Bi mixed suspension were stirred using a glass rod to break any lumps and ensure a uniformly dispersed solution.

x. Finally, the mixed solution was mixed homogeneously in the same mixer as stated above for 5 min or more according to the added amount of ethanol in step vi. Deaeration mode and mixing mode were utilized to completely vaporize the ethanol solution.

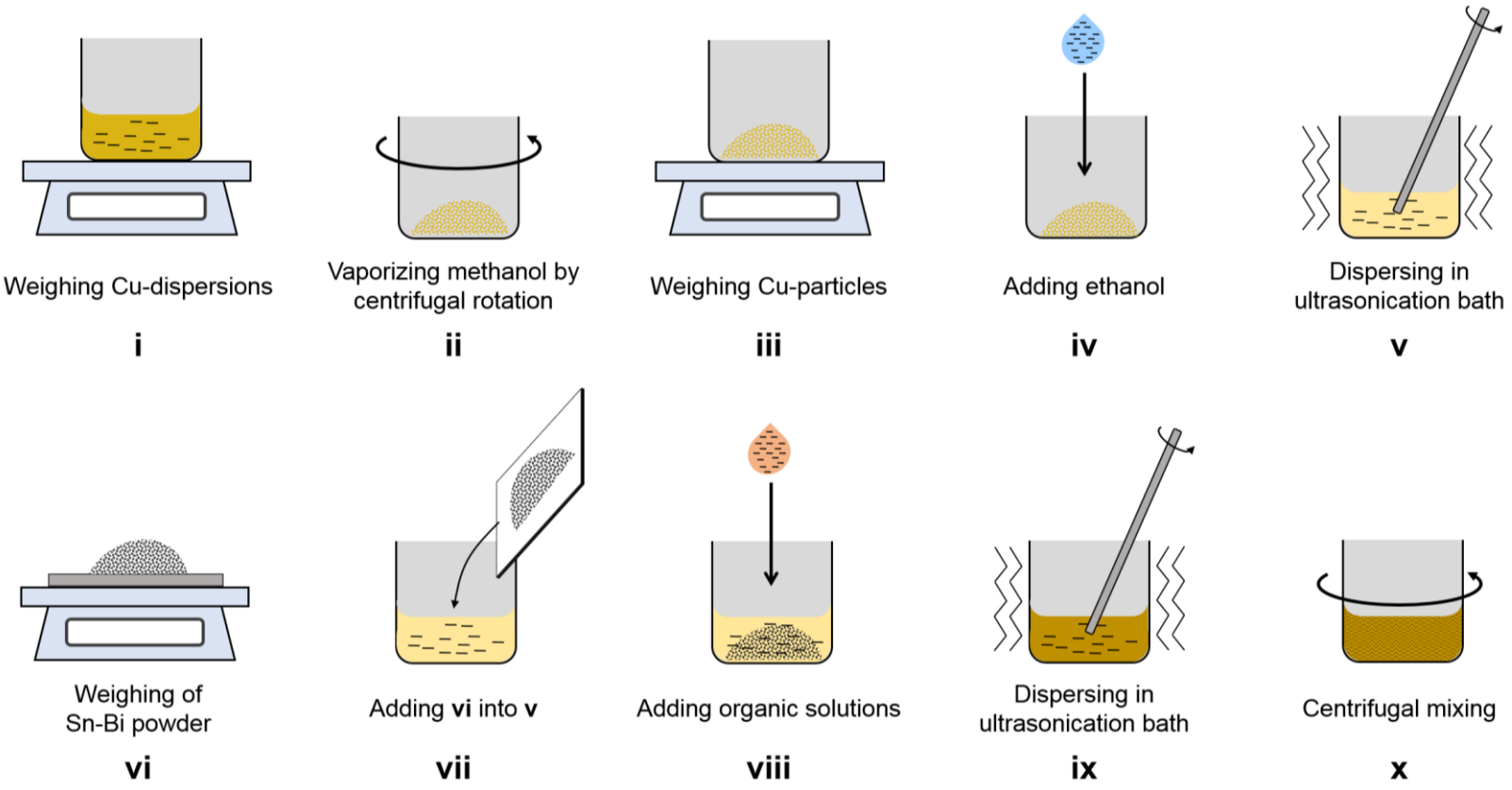

Figure 3.5 Schematic illustration of Cu-based sintering paste preparation method

3.2 Sintering Profile Determination

In order to initiate the sintering of Ag or Cu particles, the organic solutions that contained in the sintering paste need to be burnt-out, particularly the organic capping layer that contained in the commercially available Ag sintering paste. Hence, it is essential to figure out the approximate burn-out temperature of the organic compounds. One method to determine the burn-out temperature of the organic compounds is by determining the relative weight decrease of sintering paste from its initial (green) state. When the weight decrease is in plateau state, it can be interpreted as the initially contained organic compounds have been completely evaporated. TG-DTA is one powerful method to determine the weight change and the temperature difference of the sintering paste against temperature, simultaneously. The plotted temperature difference of the sintering paste between the reference samples provides information on the exothermic or endothermic reaction that takes place during the temperature change through-out the analysis.

In this study, to determine the suitable sintering profile of the as-prepared Ag-based and Cu-based sintering paste, firstly, TG-DTA was conducted on both pastes. Next, using the outcome of the TG-DTA, a sintering profile was suggested.

3.2.1 Thermogravimetric-Differential Thermal Analysis

TG-DTA analysis of both Ag sintering paste (without addition of Sn-Bi) and Cu-based sintering paste (with 65 wt% addition of Sn-Bi) was conducted from room temperature to 300°C with heating rate of 5°C/min. Two types of dynamic gas stream was flowed to the heating chamber to determine the effects of the heating environment to the thermal reaction of the Ag sintering paste. The two types of dynamic gas stream was inert N_2 and ambient air. For Cu-based sintering paste, TG-DTA was performed under N_2 environment only. The gas flow was set to constant at 250 ml/min. Approximately 10 mg of sample was heated in an aluminum pan. Reference material for the DTA

was aluminum oxide, Al_2O_3 with same amount to the sample. All test was performed by Thermo Plus EVO TG8120, Rigaku Corporation at constant heating rate of 5 °C/min.

Figure 3.6 shows the TG-DTA result of Ag sintering paste without any addition of Sn-Bi. As can be seen from the weight loss curve, at all analysis environment (N_2 and ambient air), the final weight was kept constant over 250 °C without any increase at high temperature region. However, the final weight was different depending on the dynamic gas flow. For sample that was heated in an N_2 gas flow, the final weight was lower than sample that was heated in ambient air gas flow. This difference might be resulted from the oxidation of the Ag particles at high temperature. On preparing the mixed sintering paste, the weight of pure Ag particles is needed, so, the final weight loss of sample that was heated in N_2 was defined as the weight percentage of the Ag particles in the Ag sintering paste.

Next, exothermic reaction peak can be observed at two different temperature depending on the analysis environment. At N_2 environment, the exothermic reaction peak can be observed at approximately 250 °C, while at the ambient air, the reaction peak was observed at lower temperature, which was at 200 °C. Both reactions were accompanied by final weight loss which indicated the burn-out of the organic capping layer. The existence of high concentration of oxygen in ambient air compared to the inert atmosphere is expected to accelerate the burning-out process of the organic compounds by the accelerated combustion. However, if the sintering process is conducted in air, the Cu-substrate and added Sn-Bi particles will be oxidized and the desired transient liquid phase sintering will not be achieved because the oxidize surface will hinder the wetting of Sn-Bi particles to both Ag particles and Cu substrate. However, if the reduction environment is carefully controlled, sintering at 200 °C might be achieved. In this study, firstly, for Ag-based TLPS, sintering was conducted at 250 °C in an N_2 environment and combined formic gas to assist the wetting of Sn-Bi particles.

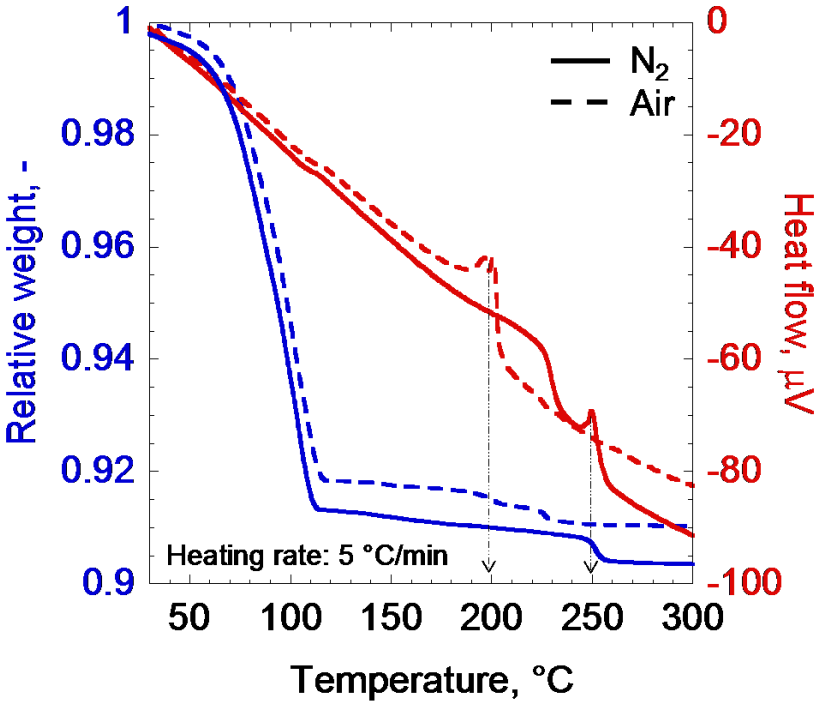

Figure 3.6 TG-DTA result of commercially available Ag sintering paste (SSP2020)

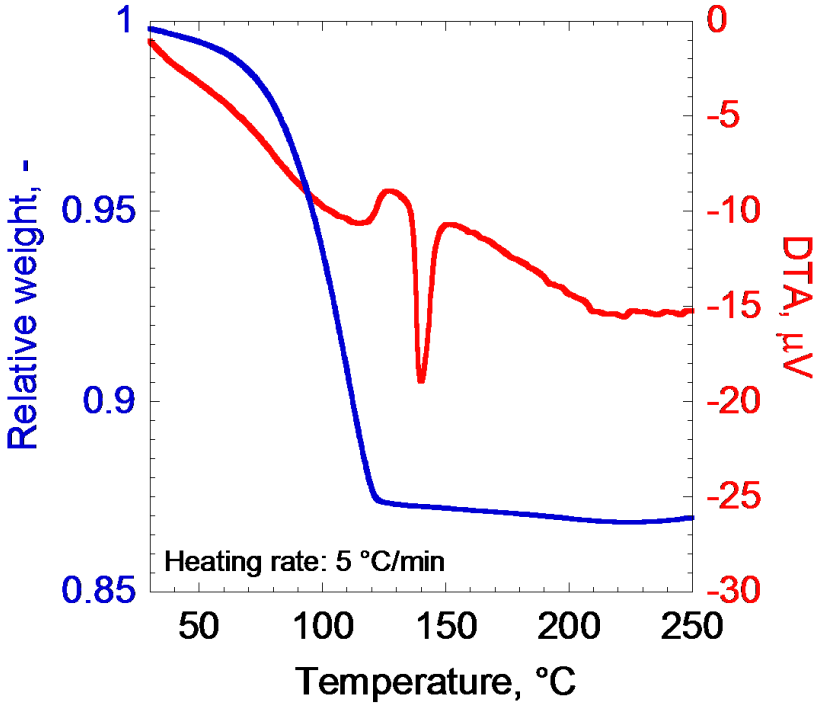

Figure 3.7 TG-DTA result of Cu-based sintering paste (Cu-65wt%SnBi)

Meanwhile, Figure 3.7 demonstrates the TG-DTA result of Cu-based sintering paste. As can be seen in Figure 3.7, the relative weight exhibited a sudden drop to approximately 0.87 from temperature range between 70 to 120 °C, and begin to decrease slowly and almost plateaued from 200 °C, despite the fact that the theoretical boiling point of terpineol at 1 atm. is 219 °C. This finding suggests the possibility of low temperature bonding.

On the other hand, one interesting finding from the TG-DTA result of the Cu-based sintering paste was a sharp endothermic peak that can be observed at about 140 °C, inferring the melting of the eutectic Sn-Bi. This suggested that in a dynamic N_2 gas flow, melting and/or wetting Sn-Bi to the Cu nanoparticles can be expected. However, oxide layer might hinder the sintering process as will be described in next section.

To summarize, since both Ag-sintering paste and Cu-based sintering paste demonstrated small weight change over 120 °C, the drying stage was set at 150 °C for 15 min accompanied by alternating gas exchange to assist the evaporation of the organic compounds that contained in both pastes. Once the temperature reached the sintering temperature, it is expected that all organic compounds might be completely burnt-out.

3.2.2 Preliminary Experiment on Wetting of Sn-Bi by Formic Gas

As explained in Section 3.2.1, one interesting finding from the TG-DTA result of Cu-based sintering paste (Figure 3.7) was a sharp endothermic peak that can be observed at about 140 °C, inferring the melting of the eutectic Sn-Bi. However, on a separate experiment to confirm the wetting of Sn-Bi powders on Cu substrate under N_2 environment, the wetting of Sn-Bi on Cu substrate was not observed. Figure 3.8b showed the Sn-Bi powders after heating under N_2 environment that was heated up to 300 °C. Some powders from the heated sample was collected and observed under SEM. The SEM image is shown in Figure 3.8e. As can be seen from the SEM image, rather than wetting the Cu substrate, the Sn-Bi powders contracted to each other and the particles became larger up to 30 μm. This might be resulted of the oxide layer that existed on both Cu substrate and Sn-Bi powders that hinder the wetting between former and latter.

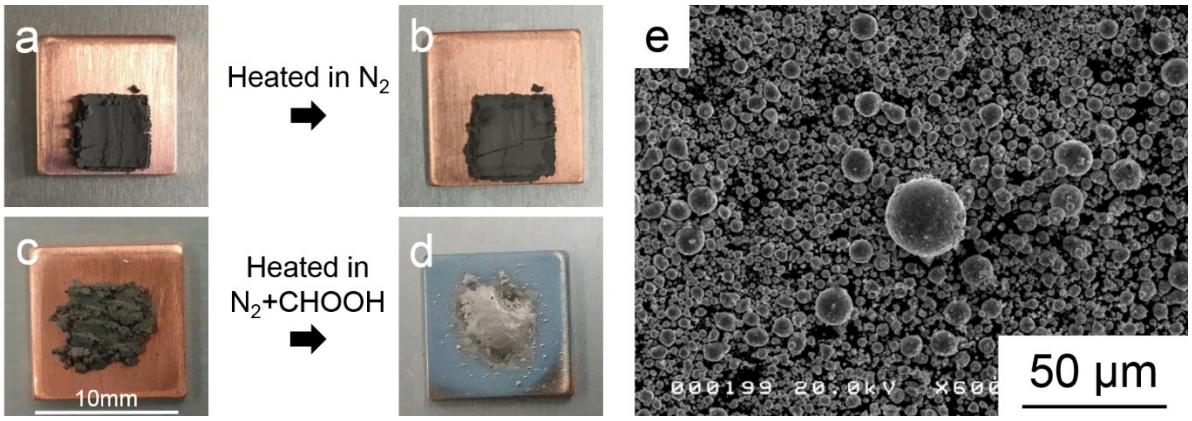

Figure 3.8 Sn-Bi powders **a** before, and **b** after heating in N_2 environment up to 300 °C; **c** Sn-Bi before, and **d** after heating in N_2 and formic gas environment up to 200 °C; **e** SEM image of Sn-Bi that was collected from **b** after heated in N_2 environment

Next, reducing environment of N_2 + 3 vol.% formic gas was introduced to assist the wetting of the Sn-Bi powders. It was reported that the reduction reaction using formic gas took place at as low as 150°C which is highly desired for low temperature processing [1, 2]. Figure 3.8c and d shows the before and after heating up to 200°C of Sn-Bi under reducing environment of N_2 + 3 vol.% formic gas. Wetting of Sn-Bi had been successfully done even at temperature as low as 200°C as can be seen in Figure 3.8d. The reduction of oxide surface by formic gas, CH_2O_2 can be explained by the following reaction [1]:

$$HCOOH + \frac{1}{2}O_2 \rightarrow CO_2 + H_2O \quad (4.5)$$

To summarize, although Sn-Bi was heated under N_2 higher than its eutectic temperature, the wetting was not observed, hence, at drying stage to facilitate the evaporation of organic compounds, the environment can be set to N_2 so that no molten Sn-Bi will interfere with the evaporation.

3.2.3 Sintering Profile and Procedure

Sintering profile is described as follows: Firstly, in an inert N_2 environment, samples were heated from room temperature to 150 °C (first heating stage). Then, the temperature was hold for 15 min. This stage was defined as drying stage to facilitate the evaporation of organic solutions contained in the paste. During drying stage, chamber was depressurized and N_2 gas was displaced alternately. Following drying stage, samples were again heated (second heating stage) to sintering temperature and hold at specific time (sintering stage). After drying stage until sintering was completed, sintering was conducted in a reducing environment (97% N_2+3% formic gas, CH_2O_2). Heating rate was set to

5 °C/min for both heating stages, while cooling rate was set to 10 °C/min. Sintering was performed in reflow solder system (RSS-210, UniTemp GmbH). Throughout the sintering process, a Cu-block was placed onto the samples to ensure a good contact between the substrate and the paste while giving a low pressure to the samples. Weight of the Cu-block was adjusted so that each sample was pressurized uniformly at *0.02 MPa for Ag-based TLPS* and *0.1 MPa for Cu-based TLPS*. A Teflon sheet with 3 mm-thickness was inserted between the Cu-block and the samples as a heat insulator to suppress thermal loss to the Cu-block. Figure 3.9 illustrates the reflow solder system used in this study and the method of bonding the sample as explained above. An illustration for a quick guide of the sintering profile is shown in Figure 3.10. It should be noted that for Cu-based TLPS investigated in Chapter 5, instead of N_2 gas, Ar gas was used.

To confirm the wetting and spreading of Sn-Bi using this proposed sintering profile, Ag mixed with 30wt% of Sn-Bi was printed onto a Cu substrate and heated. During heating, the spreading of Sn-Bi from the Ag-based sintering paste was observed via the observation window. Five observation points are depicted in (a), (b), (c), (d), and (e) in Figure 3.10. Point (a) is the initial point at 25 °C. When heated up to 150°C (point (b)) prior entering the drying stage, and to the end of the drying stage (point(c)), spreading of Sn-Bi was not observed although the temperature of the drying stage exceeded the melting temperature of Sn-Bi particles (139°C). When the heating was continued, at approximately 170 °C (point (d)), spreading of Sn-Bi was observed as can be seen in the white area in Figure 3.10(d). Upon reaching the sintering temperature of 250°C, the spreading of Sn-Bi were significant. It is assumed that the introduction of formic gas has facilitated the reduction of oxide layer on the Cu substrate and improved the spreading of Sn-Bi. The observed spreading phenomenon of the molten Sn-Bi indicated that the oxide layer on both Sn-Bi powders Cu-substrate was removed and facilitate the wetting of Sn-Bi. It can be anticipated that the isothermal solidification process can be realized during the TLPS by the introduction of formic gas by the proposed sintering profile.

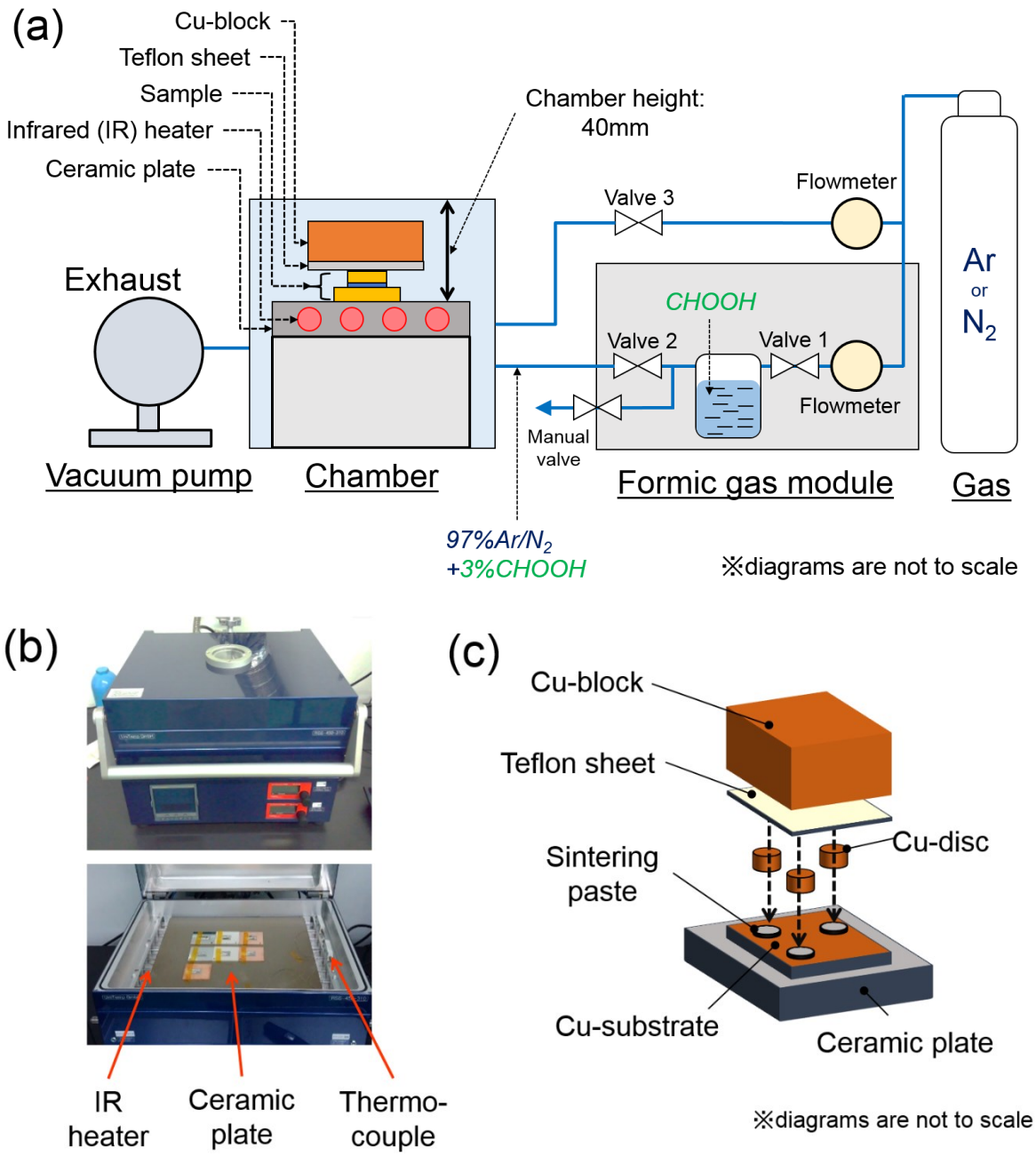

Figure 3.9 (a) Illustration of reflow solder system, (b) outer appearance of the reflow solder system, and (c) bonding method applied in this study

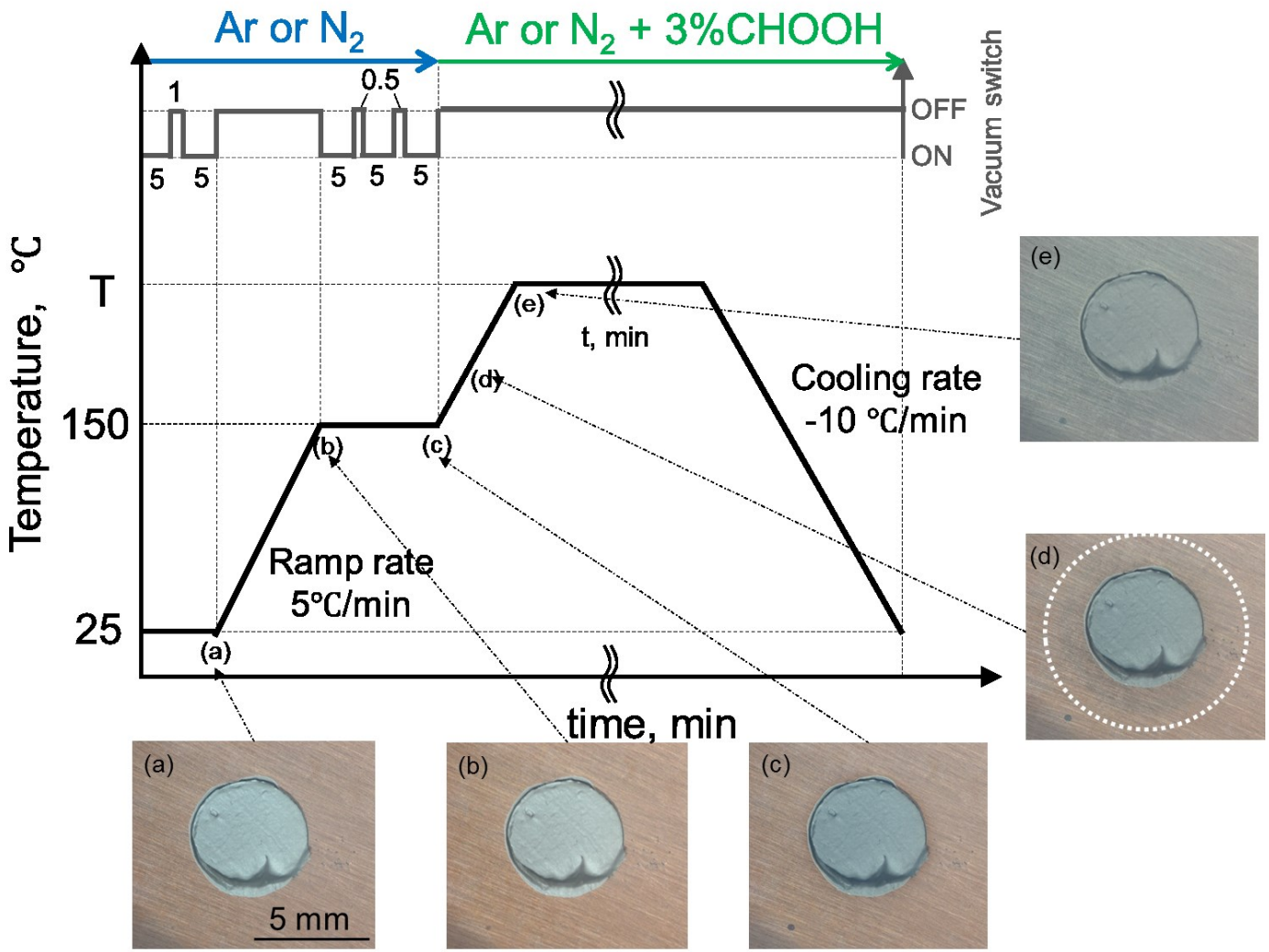

Figure 3.10 Sintering profile used in this study. (Temperature at each point is as follows: (a) 25°C, (b) 150°C i.e. beginning of drying stage, (c) 150°C i.e. end of drying stage, (d) 170°C, and (e) 250°C i.e. beginning of sintering stage)

3.3 Sample Preparation and Evaluation Methods

The aim of this work is to bond Cu substrates without metal plating since the metal-plating cannot be subjected to the epoxy-molded materials as explained in Chapter 2. Thus, in this work, all bonding for shear test and microstructural observation was conducted with plateless Cu substrates. All Cu substrates used in this work were oxygen-free Cu, C1020. For shear strength evaluation, Cu-discs with dimension of 5 mm × 3 mmt and Cu-plates with dimension of 20 mm × 20 mmt × 2 mmt were used. On the other hand, for microstructural observation, Cu substrates with dimension of 10 mm × 10 mmt × 1 mmt and 5 mm × 5 mmt × 1 mmt were used. All Cu-substrates were subjected to mechanical grinding and chemical polishing prior to paste-printing and sintering. Mechanical grinding was performed by SiC abrasive paper of #800, #1000, and #1200 in unidirectional. Subsequently, Cu-discs and substrates were soaked into 15 vol.% aqueous sulfuric acid solution and ultra-sonicated for 3 min, rinsed with deionized water, and repeatedly ultra-sonicated in acetone for 3 min. All chemical solutions were acquired from Wako Pure Chemical Industries, Ltd. DSC and XRD test was conducted at The Materials Characterization Central Laboratory, Waseda University [3].

3.3.1 Shear Test

As a preparation for shear test samples, a stainless-mask with 0.2 mm-thickness was used to print the mixture paste onto the Cu substrate. Next, Cu-discs were placed onto the paste printed on the Cu substrate. Three samples were placed to form a triangular pattern, and a Cu-block was placed onto the samples to ensure a good contact between the substrate and the paste while giving a low pressure to the samples as explained earlier in Section 3.2.3.

All samples were subjected to shear test at room temperature. Shear height was 0.2 mm and shear speed was 0.1 mm/s. Shear test was conducted using DAGE 4000Plus Bond tester (Figure 3.11)

and maximum force recorded at failure divided by the bonding area was defined as the shear strength. Each plot in shear test results that will be shown later in Chapter 4 and 5 exhibits the average shear strength, and error bars present the highest and lowest shear strength for each condition. For each condition, number of samples will be written in the graph. In this study, MIL-STD-883K, Method 2019.9 was used to evaluate the shear strength obtained in each investigations. According to the standard, for bonding area larger than 4 mm^2, minimum force in kilograms required to pass the requirements is 5.0 kg. Since all samples for shear test in this study have dimension of 5 mm in diameter, ***minimum shear strength of 2.5 MPa*** is required to pass the requirement as stated above. Additionally, as reference, high temperature Pb-based solder will also be used a benchmark in this study. In the work reported by Eiichi Ide et al., shear strength of Pb-5Sn was approximately 18 MPa, hence, bonding conditions that exhibit ***shear strength higher than 20 MPa*** will also be the criterion to evaluate the shear strength of the proposed Ag-based and Cu-based TLPS in this study.

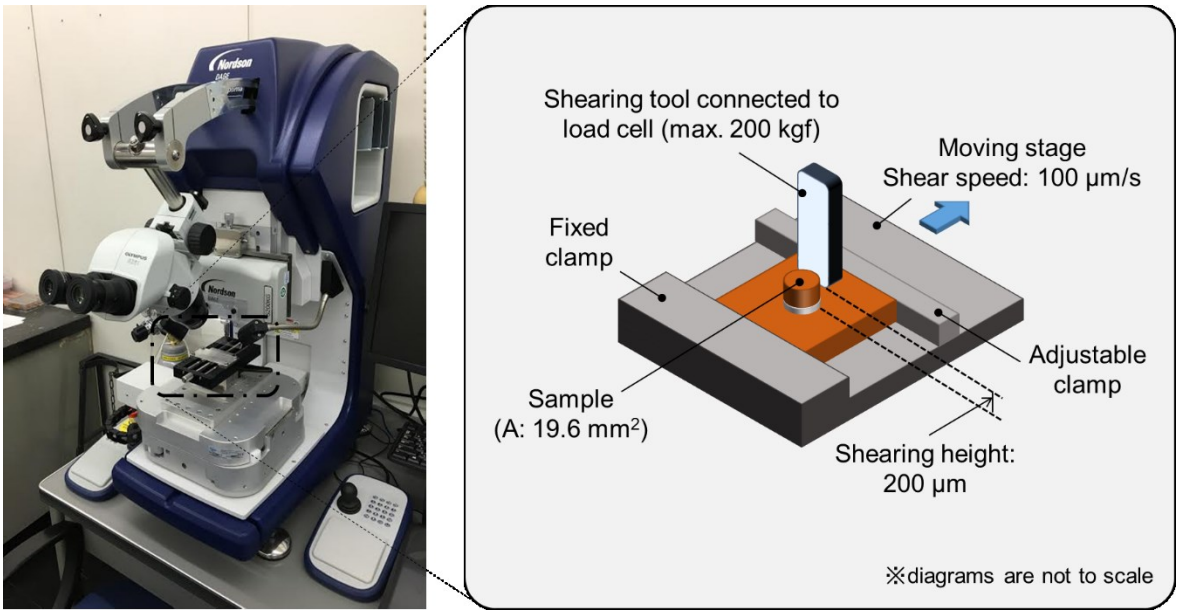

Figure 3.11 Shear test machine (DAGE 4000Plus Bond tester) used in this study and an illustration of shear test conditions

3.3.2 Differential Scanning Calorimetry Analysis

As a parameter of thermal stability for high temperature application, the remelting temperature of the as-sintered samples was investigated by means of differential scanning calorimetry, DSC analysis (DSC8500, Perkin Elmer Inc.). Samples for DSC analysis were prepared separately on a glass substrate where the samples was not pressurized. Note that samples for DSC analysis was sintered paste, not bonded joints. Omid Mokhtari et al. [5] reported that DSC results of sample that was prepared separately without the Cu substrate (sandwiched-sample) showed almost no difference compared to the one that was sandwiched with Cu substrates. Each sample was prepared on an aluminum pan, where it was sealed with an aluminum lid by punching. The mass of the sample used in DSC analysis ranged from 3.0 to 10.0 mg. The analysis was performed from 50°C to 350°C for 1 cycles with heating and cooling rate of 10°C/min in an inert N_2 environment. Heating and cooling were performed continuously where no isothermal period was applied.

As explained in Section 1.3.1, as a rule of thumb, solder should be used below than the $0.8T_h$ to prevent the degradation by accelerated creep effects [6]. On contrary, Omid Mokhtari stated that solder should be used below than $0.86T_h$ [5]. The discrepancy on the actual value might depend on the real application. In this study, $0.85T_h$ is set as an evaluation criterion. Considering the maximum T_c in the SiC-based module to be 125 °C, the remelting temperature of the proposed Ag-based and Cu-based TLPS should be higher than 195 °C ($0.85T_h$). In this study, ***remelting temperature higher than 200 °C*** is set to be the criterion for the possibility in the application at high operation temperature.

3.3.3 Microstructural Observation and Elemental Analysis

For cross-section microstructural observation, two bare Cu-plates (5 mm × 5 mm × 1 mm and 10 mm × 10 mm × 1 mm) were prepared and bonded together with similar manner to the shear test samples. Following sintering process, these samples were mounted in cold-mount epoxy.

Subsequently, mechanical grinding of (#80, and #320) and mechanical polishing (diamond particles of 9, 3, and 1 μm) were subjected to the samples. Finally, colloidal silica oxide suspension were used for minor etching.

The cross-sectional microstructure of the bonded joints were observed and evaluated qualitatively and quantitatively using electron probe micro analyzer (JXA-8230, JEOL), and energy-dispersive X-ray spectrometry (EDAX, Ametek Inc.) that is attached to a field emission scanning electron microscopy, FE-SEM (S-4000, Hitachi High-Technologies Corporation).

To define the phase in the sintered samples qualitatively and quantitatively, X-ray diffraction (XRD) analysis was conducted. Sintered samples (not bonded samples) for the XRD analysis were prepared separately on a glass substrate without the application of pressure. Stainless-mask was used for paste printing on the glass substrate. After sintering, samples were pounded and powder concentration method was adapted to perform the analysis using a diffractometer (Rigaku SmartLab) with Co-Kβ radiation at an accelerating voltage of 40 kV. Scanning 2θ range was 20-110° with scanning step of 0.02°. Reference intensity ratio (RIR) method was utilized to qualitatively determine the phase in the sintered samples. Powder diffraction files number (#PDF) that were used in this study are listed in Table 3.2.

Table 3.2 List of #PDF adapted in this study

Phase	Symbol (Composition in at%)	#PDF (Quality marks)
Silver	Ag	01-071-4612 (I)
Silver Tin	Ag_3Sn	01-074-9567 (S)
Silver Tin	$Ag_{0.87}Sn_{0.13}$	01-072-5168 (I)
Silver Tin	$Ag_{80}Sn_{20}$	01-072-5167 (I)
Tin	Sn	00-004-0673 (S)
Bismuth	Bi	01-085-1330 (S)
Copper	Cu	03-065-9026 (I)
Copper Tin	Cu_3Sn	01-074-6752 (I)
Copper Tin	Cu_6Sn_5	01-081-8262 (S)

S = Star, I = Indexed

References

[1] Wenhua Yang, Hiroyuki Shintani, Masatake Akaike, Tadatomo Suga, Low Temperature Cu-Cu Direct Bonding using Formic Acid Vapor Pretreatment, 2011 Electronic Components and Technology Conference, 2079-2083

[2] Naoya Matsuoka, Masahisa Fujino, Masatake Akaike, Tadatomo Suga, Process Parameters for Formic Acid Treatment with Pt Catalyst for Cu Direct Bonding, ICEP-IAAC 2015 Proceedings, 460-463

[3] Izutani, C. et al., The Materials Characterization Central Laboratory: An Open-Ended Laboratory Program for Fourth-Year Undergraduate and Graduate Students, Journal of Chemical Education 93, 1667 (2016)

[4] Eiichi Ide, Akio Hirose, Kojiro F. Kobayashi, Influence of Bonding Condition on Bonding Process Using Ag Metallo-Organic Nanoparticles for High Temperature Lead-Free Packaging, Mater. Trans. 47, 211 (2006)

[5] Omid Mokhtari, Hiroshi Nishikawa, J Mater Sci: Mater Electron 27, 4232 (2016)

[6] M. Knoerr and A. Schletz, "Power semiconductor joining through sintering of silver nanoparticles: Evaluation of influence of parameters time, temperature and pressure on density, strength and reliability," in Integrated Power Electronics Systems (CIPS), 2010 6th International Conference on, Nuremberg, 2010, pp. 1-6

CHAPTER 4: SILVER-BASED TRANSIENT LIQUID PHASE SINTERING

In this chapter, TLPS of Ag nanoparticles mixed with eutectic Sn-Bi for the application on bonding DBC substrate and Cu heat-spreader/sink will be discussed. As explained in Chapter 1 Section 1.3.2, the conventional Ag nanoparticles sintering required Ag plating at the Cu substrates to facilitate the solid-solid diffusion to obtain a robust joint at the interface. However, in this present study, Ag plating might be unnecessary since the interfacial layer is expected to be formed by the formation of IMCs between Cu and Sn. It is essential to properly select the Sn-Bi addition amount to achieve a uniform interfacial reaction layer since the Sn will not only react with the Cu substrate, but also with the matrix Ag nanoparticles. On contrary, an excessive addition of Sn-Bi will cause the as-sintered microstructure to remelt at the Sn-Bi eutectic temperature due to the unreacted Sn-phase will remain in the microstructure. This might harm the mechanical properties of the joints at temperature higher than the eutectic temperature of the Sn-Bi. Hence, in this chapter, at first, the selection procedure of the suitable amount of Sn-Bi will be discussed. Next, influences of composition, and several sintering parameters to the shear strength and microstructure will be discussed. Remelting temperature of the sintered material will be examined as an insight of high temperature application of the developed Ag-based TLPS in this study. Finally, microstructure evolution during the sintering process of the composition that showed the highest shear strength at room temperature will be made clear and the associated strengthening mechanism and factors that contribute to the rising of remelting temperature will be discussed.

4.1 Alloy Composition Selection Procedure

The amount of Sn-Bi that is mixed with Ag will influence the final microstructure and the shear strength of the bonded joints. Also, if the Sn-Bi amount is not properly chosen, the remelting temperature of the sintered materials will occur at the eutectic temperature of the Sn-Bi. Hence, it is important to properly choose the amount of Sn-Bi to be added into the Ag sintering paste. It is well established from the binary alloy phase diagram of Ag-Bi that the solubility of Ag and Bi with each other is negligible small as can be seen in Figure 2.1(a). Taking this into account, it is not an exaggeration to consider that when the added Sn-Bi melted when reaching its melting temperature, only the molten Sn will react with the Ag particles to form intermetallic compounds (IMCs) and subsequently Ag-solid solution, while Bi will be precipitated simultaneously. In addition, according to [1], three melting events can be observed in Ag-Sn-Bi ternary alloy system. The reactions, and corresponding temperature and phases are summarized in Table 4.1. The three invariant reactions at Ag-Sn-Bi ternary system are defined as below:

$$U_1: \ L + (Ag) \leftrightarrow \xi Ag + (Bi) \tag{4.1}$$

$$U_2: \ L + \xi Ag \leftrightarrow Ag_3Sn + (Bi) \tag{4.2}$$

$$E: \ L \leftrightarrow Ag_3Sn + (Sn) + (Bi) \tag{4.3}$$

As can be seen from Table 4.1, the ternary eutectic invariant reaction (4.3) occurred at the temperature equivalent to the Sn-Bi eutectic temperature, due to the existence of Sn solid solution phase (Sn). This implies that the excessive addition of Sn into the Ag-based TLPS might result in the remelting event at near the Sn-Bi eutectic temperature. To prevent the remelting event at the said temperature, the added Sn must be make sure to completely react with Ag particles to form Ag_3Sn.

Table 4.1 Calculated invariant reaction in Ag-Sn-Bi ternary system from [1]

Ag-Bi	Ag-Sn-Bi	Ag-Sn	Sn-Bi

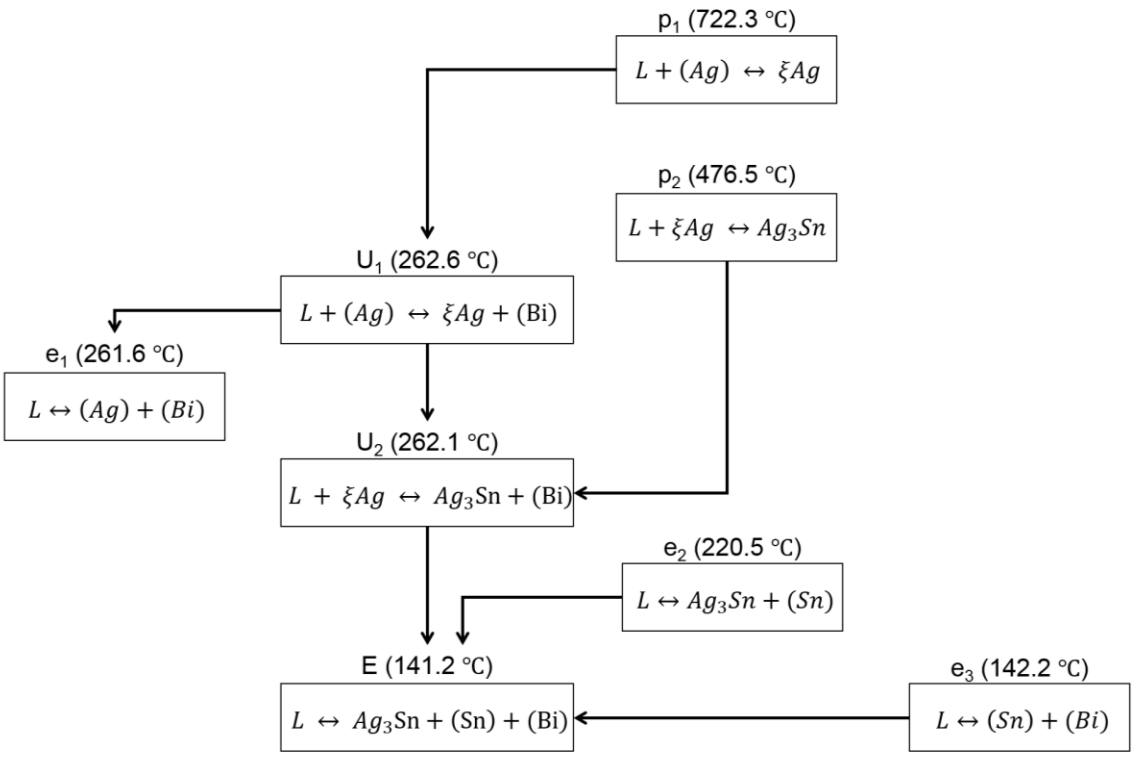

U: Ternary Four Phase Equilibria Type 2 (Quasi-peritectic)

E: Ternary Four Phase Equilibria Type 1 (Ternary eutectic)

If the solubility of Ag into Bi and vice versa is totally neglected, the weight percentage of Sn to Ag, X_{Sn} can be calculated as follows:

$$X_{Sn} = \frac{0.43\beta}{(0.43\beta)+\alpha} \cdot 100 \tag{4.4}$$

where α is the weight percentage of Ag nanoparticles and β is the weight percentage of added Sn-Bi particles. From equation (4.4), weight percentage of Sn to Ag, X_{Sn} with different addition amount of Sn-Bi are listed in Table 4.2. It must be noted that the corresponding phase(s) that are mentioned in Table 4.2 are expected phase(s) from the Ag-Sn binary system. The formation of Sn-solid solution at the addition of 50 wt% Sn-Bi is an indicator of excessive amount of Sn, which will solidify as Sn-Bi in Ag-Sn-Bi ternary system. Hence, it is important to control the amount of Sn to be completely react with Ag to form Ag-Sn IMCs. As can be seen in Table 4.2, to prevent the remelting event at the temperature of Sn-Bi eutectic temperature, the addition weight percentage of Sn-Bi powders into Ag sintering paste must be kept at least 45 wt.% and below. In this study, for the sake of convenience, hereinafter, each notation of composition will be refer as the addition amount of Sn-Bi powder to the Ag. For example, for a mixture with composition of 90 wt% Ag and 10 wt% Sn-Bi, the naming of the composition will be written as Ag-10SnBi. For Ag without any addition of Sn-Bi, it will be referred as 100Ag.

Table 4.2 Weight percentage of Sn to Ag, X_{Sn} with different addition amount of Sn-Bi as calculated using equation (4.4) and corresponding expected phase(s) in equilibria Ag-Sn system

Addition amount of Sn-Bi (wt.%)	X_{Sn} (wt.%)	Corresponding expected phase(s)
10	4.6	Ag solid solution
20	9.7	Ag solid solution and ζ-Ag
30	15.6	ζ-Ag
40	22.3	ζ-Ag and ε-Ag
45	26.0	ζ-Ag and ε-Ag
50	30.1	ε-Ag and Sn solid solution

4.2 Effects of Alloy Composition

To investigate the effect of addition amount of Sn-Bi to the shear strength, microstructure, and remelting temperature of the proposed Ag-based TLPS, plateless Cu-Cu substrates were bonded with 100Ag, Ag-10SnBi, Ag-20SnBi, Ag-25SnBi, Ag-30SnBi, Ag-35SnBi, and Ag-45SnBi using the sintering profile as explained before in Section 3.2.3 (Figure 3.10). For all compositions, sintering was conducted at constant sintering temperature of 250°C and sintering holding time of 60 min.

4.2.1 Effects on Shear Strength and Microstructure

Figure 4.1 shows the effect of addition amount of Sn-Bi to Ag nanoparticles on the shear strength of the plateless Cu-Cu joints at room temperature. It was demonstrated that excluding Ag-10SnBi, average shear strength that was obtained for all compositions exceeded 10 MPa and passed the requirements of MIL-STD-883K, which requires shear strength greater than 2.5 MPa for bonding area larger than 4.1 mm^2 (bonding area in this study was 19.6 mm^2) [2]. Moreover, some samples from Ag-20SnBi, Ag-25SnBi, Ag-35SnBi and Ag-45SnBi, and all samples from Ag-30SnBi shows shear strength higher than conventional Pb-5wt.%Sn solder (18MPa) [3]. Notably, with addition of 30 wt. % of Sn-Bi, the highest shear strength was 26.7 MPa. Additionally, with the same addition amount of low melting temperature materials i.e. 30wt. %, Ag-30SnBi shows higher shear strength compared to Ag-30Sn examined by A. Sherif et al. (17 MPa) [4]. Interestingly, in their study, 1.2 MPa of sintering pressure was applied during sintering at 250°C whereas in present study, merely 0.02 MPa was applied at the same sintering temperature. Meanwhile, when the addition of Sn-Bi exceeded 30 wt%, the average shear strength dropped lower than 20 MPa. Ag-45SnBi which comprised of the highest Sn-Bi addition amount investigated in this study exhibited approximately 15 MPa of average shear strength, which was similar to the one without any Sn-Bi addition. On the

other hand, shear strength of Ag-10SnBi decreased abruptly to 7.8 to 9.6 MPa, in fact lower than the 100Ag alone. To elucidate the factors that influenced the strength, microstructure observation of the fracture surface and cross-section was conducted and discussed.

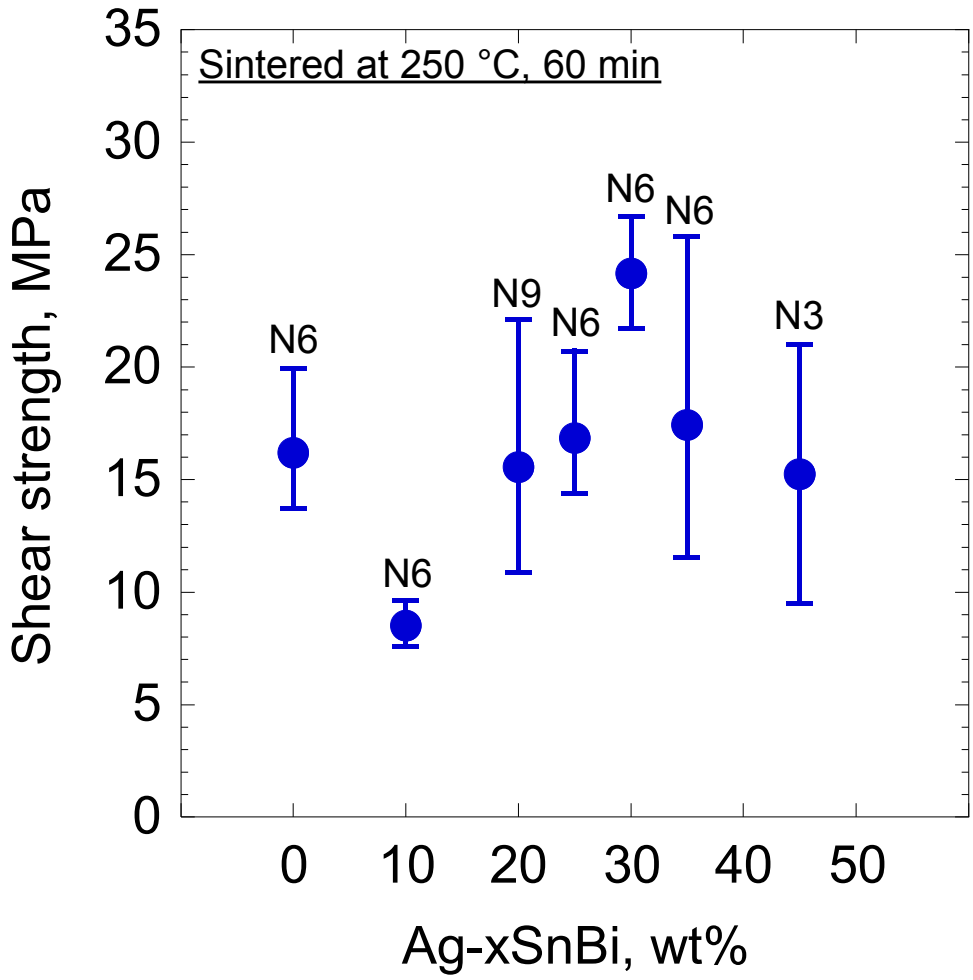

Figure 4.1 Effects of Sn-Bi addition amount to the shear strength in Ag-SnBi TLPS

Optical micrograph images of the fracture surface from 100Ag, Ag-10SnBi, Ag-20SnBi, Ag-30SnBi, and Ag-45SnBi samples from Figure 4.1 that demonstrated the highest shear strength are shown in Figure 4.2. As can be seen from lower images (Cu-) for each conditions, brownish color of Cu substrate in the fracture surface is clearly visible from 100Ag and Ag-10SnBi samples indicating adhesive fracture, while for Ag-20SnBi and Ag-30SnBi grayish color is more prominent implying cohesive fracture. These suggest that the likelihood of lower shear strength shown by 100Ag and Ag-10SnBi was caused by the poor joint at the interface while higher shear strength for the Ag-20SnBi and Ag-30SnBi was resulted by the sound joint at interface, which might be the formation of Cu-Sn IMCs. On contrary, with the addition of 45 wt% Sn-Bi, the fracture surface was at first thought to be similar to Ag-30SnBi, but in spite of the increased amount of Sn, the fracture surface was rather resembled to that of 100Ag and Ag-10SnBi. The color of Cu substrate that was exposed from the adhesive fracture was slightly different to the one observed in 100Ag and Ag-10SnBi. On the other hand, similar observation was found on the lower Cu substrate of the sample with Sn-Bi addition, in which greyish color outside of the joint perimeter can be seen. It is assumed that these greyish color spreading might be the spreading of molten Sn-Bi, as confirmed in Figure 3.10.

To further investigate the constituent phases that influenced the strength of the joints, elemental mapping of the fracture surface that is shown in Figure 4.2 was conducted by EDX. Fracture surface of the upper Cu-disc side was firstly observed by FE-SEM and subsequently elemental mapping by EDX was performed.

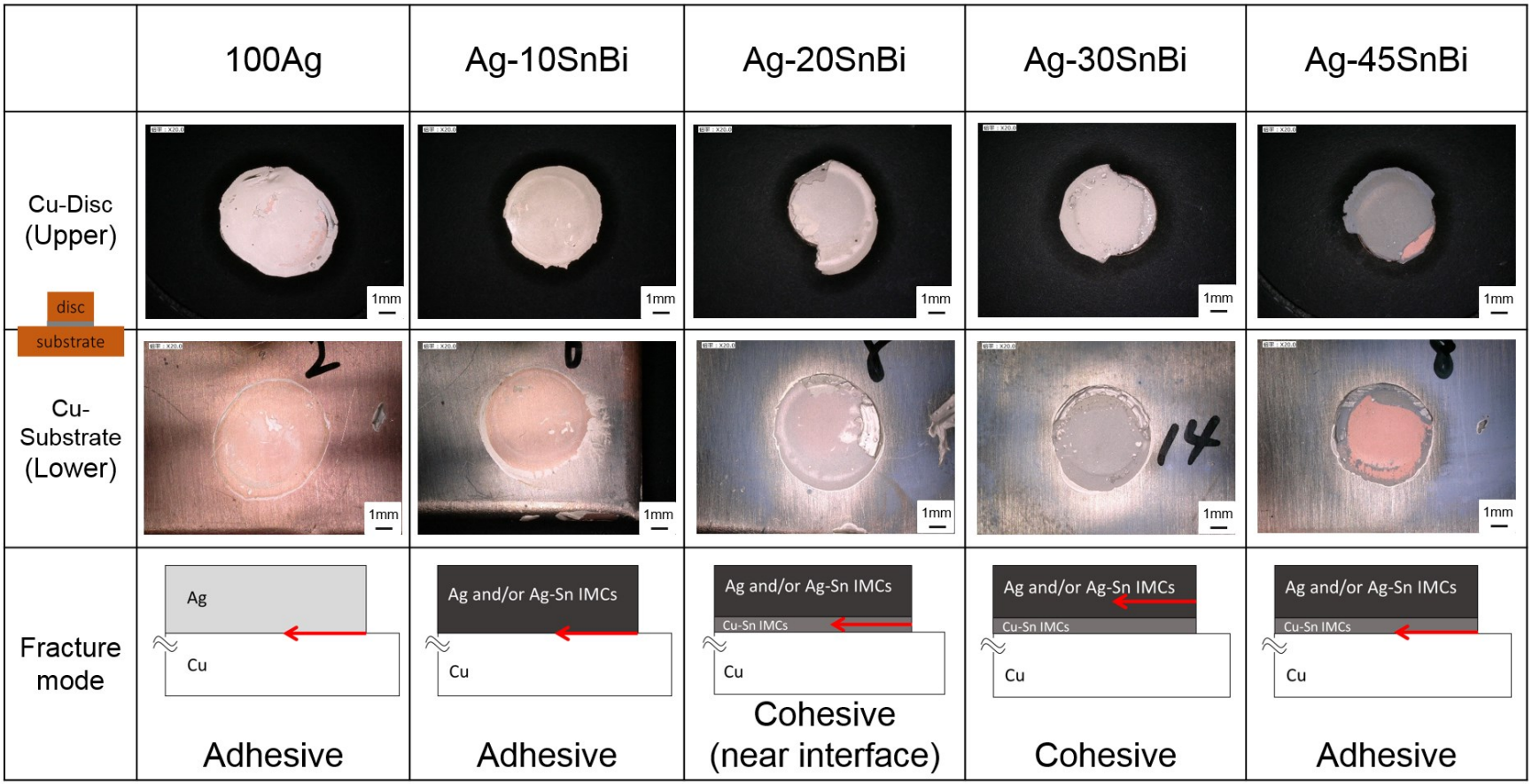

Figure 4.2 Optical micrograph images showing fracture surface of samples from Figure 4.1 and illustration of fracture mode as presumed from the elemental mapping as conducted in Figure 4.4

Figure 4.3 depicts the secondary electron SEM images of the fracture surface that is shown in Figure 4.2. Fracture surface of 100Ag, Ag-10SnBi, and Ag-30SnBi that is shown in Figure 4.3a, b, and d, respectively, exhibited similar microstructure, in which skeleton-type microstructure equivalent to the sintering structure can be observed. On the other hand, for Ag-20SnBi, two types of fracture surface can be extinguished. The first one is similar to the skeleton-type structure as observed in 100Ag, Ag-10SnBi, and Ag-30SnBi, on the other hand, the second one is more densified microstructure as depicted in the red-dash line, as can be seen in Figure 4.3c. Meanwhile, SEM image of the fracture surface of Ag-45SnBi projected an entirely different microstructure. An almost uniformly densified microstructure with scattered voids can be observed as shown in Figure 4.3e.

Elemental mapping of these fracture surfaces are shown in Figure 4.4. As can be seen in Figure 4.4a, the element of Cu can be detected at the fracture surface of Cu-disc, implying that limited Cu-atom transportation (diffusion) to the Ag nanoparticles sintering structure might occurred during the solid-solid sintering of 100Ag on Cu-substrate. However, as established in equilibrium Ag-Cu binary system, Ag and Cu solution to each other is negligible small, hence, the formed interfacial reaction layer might be very thin. Shear strength up to 20 MPa shown by 100Ag might be contributed by the mechanical inter-locking or anchor effect due to the surface roughness of Cu substrate. It is known from Figure 3.2 that the mode particle size of Ag nanoparticles sintering paste used in this study was about 200 nm, so, the nanoparticles might penetrate inside the Cu-surface roughness and acted like an anchor once Ag nanoparticles started to sintered with each other and further densified.

Similarly, Cu element was also detected on the fracture surface of Ag-10SnBi as demonstrated in Figure 4.4b. The distribution of Sn in Ag-10SnBi implied that Ag-Sn IMCs and/or Cu-Sn IMCs might also formed at the fracture surface. However, according to Figure 4.6b which will be explained later, Cu-Sn IMCs phases were not observed, thus ruled-out that the fracture surface of Ag-10SnBi might consist of Ag-Sn IMCs, Ag-Cu interdiffusion phases, and Bi-rich phases. This suggests that

the low strength exhibited by Ag-10SnBi might be caused by the formation of Ag-Sn IMCs at the expense of Ag-Cu interdiffusion layer. In addition, the amount of Sn in Ag-10SnBi is thought to be insufficient to form Cu-Sn IMCs at the interface.

On the other hand, elemental mapping of Ag-20SnBi as shown in Figure 4.4c strong signal of Cu and Sn was detected. This demonstrated that the fracture might occurred within Cu-Sn IMCs interfacial reaction layer, which might suggest that the amount of Sn to react with Cu substrate was insufficient to form a strong interfacial reaction layer.

At Ag-30SnBi, fracture was likely to occur within the matrix, but near to the Cu-Sn IMCs interfacial reaction layer as the Cu distribution was less detected, as can be seen in Figure 4.4d. The fracture surface majorly consisted of Ag-Sn IMCs and Bi-rich phases as proved by the distribution of Ag, Sn, and Bi element.

Finally, elemental mapping of Ag-45SnBi as shown in Figure 4.4e provides an insight of interfacial fracture or adhesive fracture between Cu-Sn IMCs and the Cu substrate. It was also supported by the observation of the optical micrograph image of Ag-45SnBi (Figure 4.2) on the Cu-substrate side that prevailed the Cu-substrate (brown color). In addition, the Ag element distribution was mainly detected at the void, suggesting that the dense structure which might be Cu-Sn IMCs was sufficiently thick for electron beam from the SEM to reach the Ag-Sn IMCs sintering structure that existed beneath the Cu-Sn IMCs, as compared to the Ag-20SnBi in which the signal of Ag was strongly detected. A schematic illustration summarizing the fracture mode of each composition as explained above is shown in the lower part of Figure 4.2.

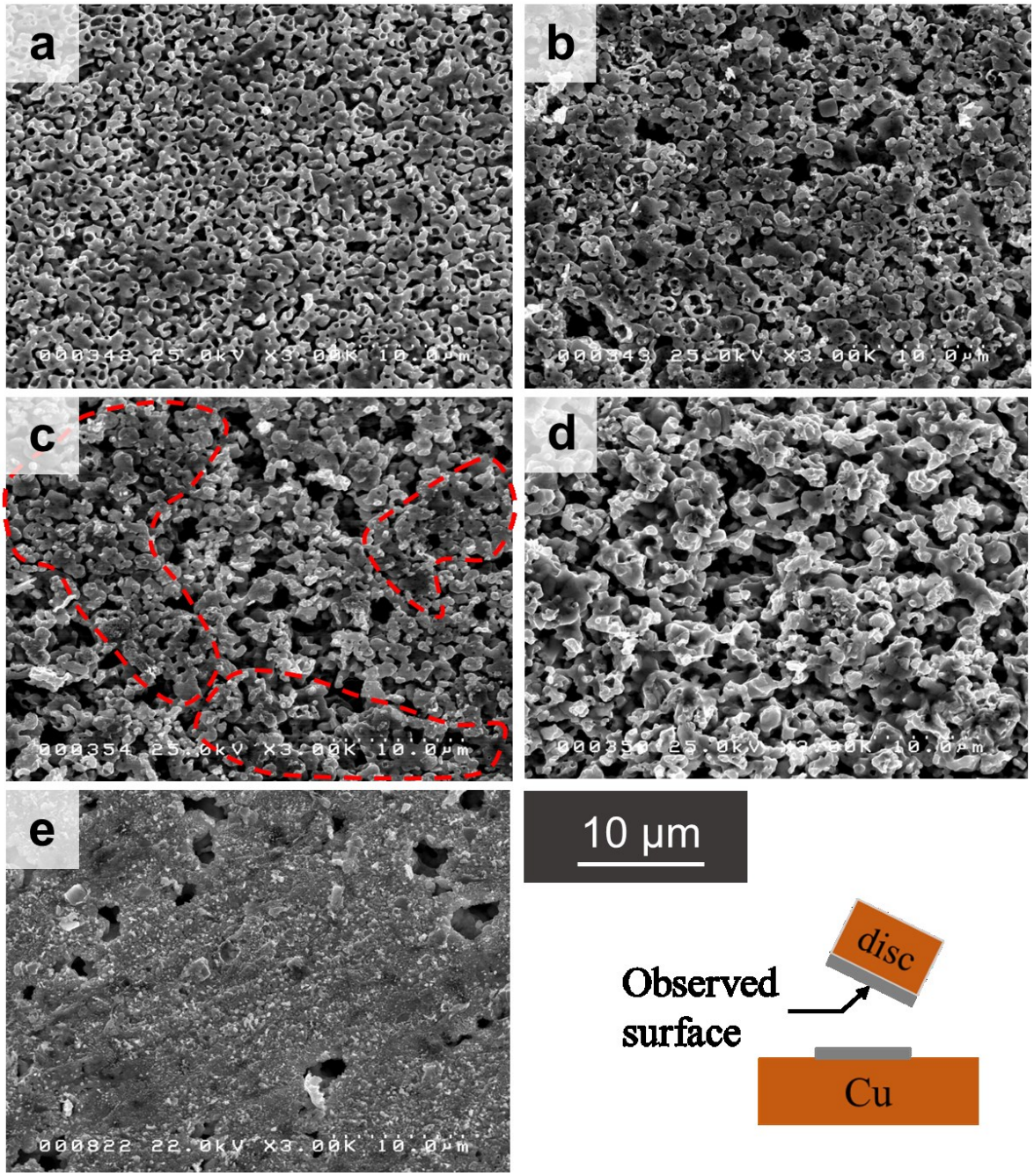

Figure 4.3 SEM secondary electron (SE) images of fracture surface shown in Figure 4.2: (a) 100Ag, (b) Ag-10SnBi, (c) Ag-20SnBi, (d) Ag-30SnBi, and (e) Ag-45SnBi

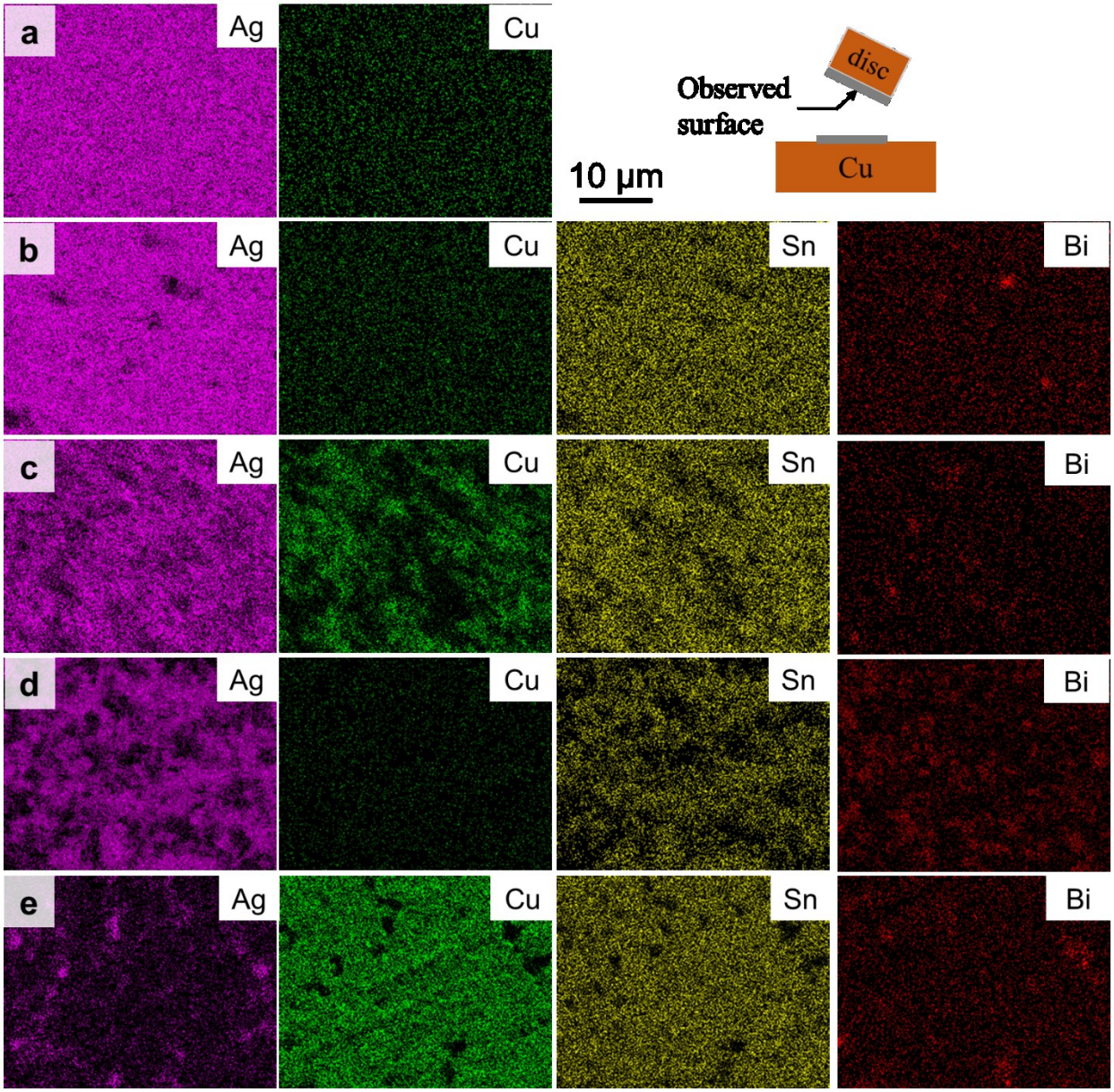

Figure 4.4 Elemental mapping of SEM images shown in Figure 4.3: **a** 100Ag, **b** Ag-10SnBi, **c** Ag-20SnBi, **d** Ag-30SnBi, and **e** Ag-45SnBi

To further investigate the contributing factor of the fracture mode, an elemental mapping analysis by using EPMA at the cross-sections for each samples was conducted. Figure 4.5 shows back-scattered electron (BSE) SEM images of each samples and the corresponding elemental mapping images are shown in Figure 4.6. A "Red-Green-Blue composite function" was used to qualitatively reveal the microstructures of the cross-sections. Detected elements of Ag (blue), Cu (green), and Sn (red) were combined and microstructures that consist of two or more elements are shown in different combination of colors of cyan, magenta, yellow, or gray. Cyan may refer to the formation of Cu-Ag interdiffusion layer. Magenta and yellow on the other hand represents the formation of Ag-Sn IMCs and Cu-Sn IMCs, respectively. Meanwhile, the co-existence of Sn, Cu, and Ag were depicted in gray color. As can be seen from BSE images (Figure 4.5a-d), with increasing addition amount of Sn-Bi, white phases that are randomly distributed although not concentrated locally, are also increased. The white phases were identified as Bi-rich phase which possibly precipitated during isothermal solidification. From elemental mapping images of 100Ag (Figure 4.6a) and Ag-10SnBi (Figure 4.6b), interface layer consists of Cu-Ag interdiffusion layer (cyan) with no Cu-Sn IMCs phase (yellow). This may be resulted to the Cu-Ag interdiffusion during sintering, as explained earlier. Figure 4.7 shows atomic percentage of Ag and Cu at the interface of 100Ag at each point shown in Figure 4.5a, pointing out that the interface of 100Ag consist of interdiffusion layer of Ag and Cu at extremely small thickness, approximately 1 μm. It is also established from binary phase diagram that Ag and Cu solubility to each other is negligible small and show no alloying behavior. Meanwhile, the non-existence of Cu-Sn phase at the interface of Ag-10SnBi supported earlier argument that the low shear strength of Ag-10SnBi might be caused by the formation of Ag-Sn IMCs at the expense of Ag-Cu interdiffusion layer or the formation of Cu-Sn IMCs interfacial reaction layer.

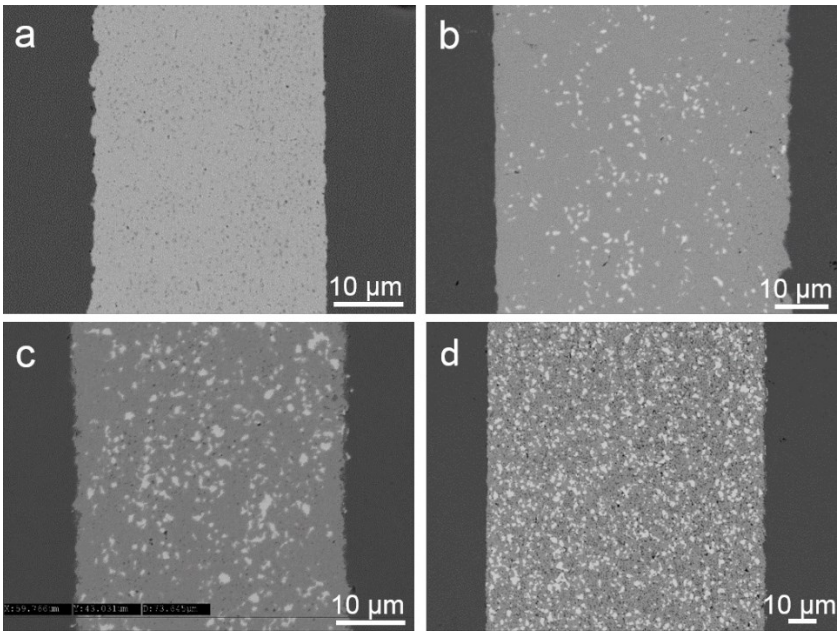

Figure 4.5 SEM (BSE) images of cross-sections of samples sintered at 250 °C for 60 min: a 100Ag, b Ag-10SnBi, c Ag-20SnBi, and d Ag-30SnBi

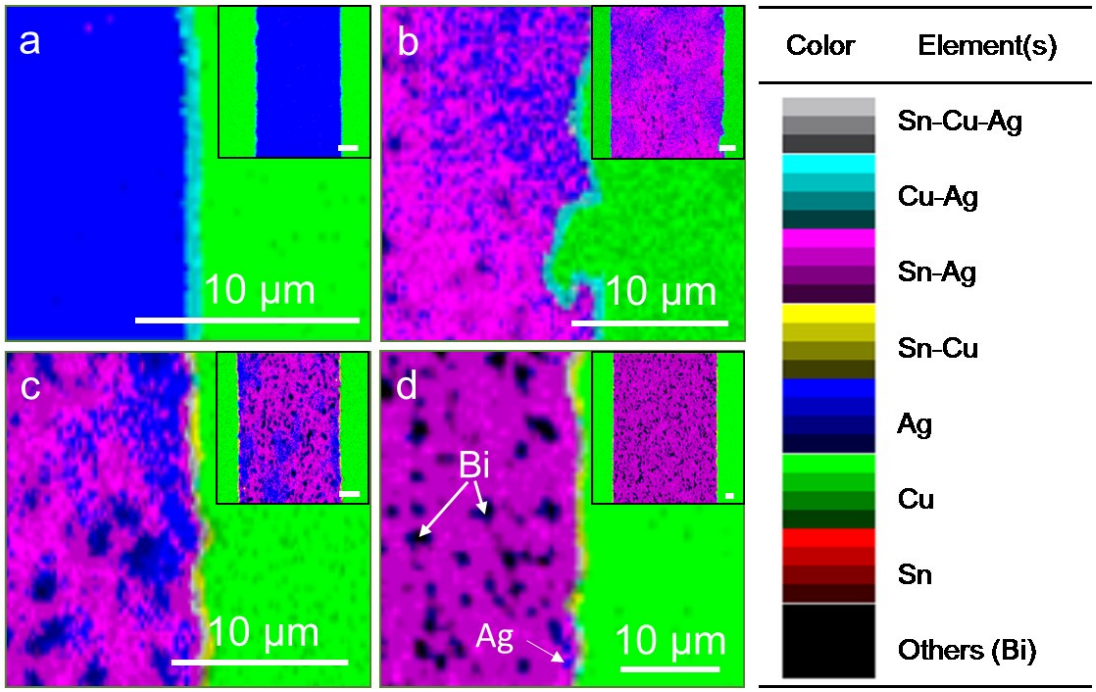

Figure 4.6 Magnified images of EPMA elemental mapping of cross-sections shown in Figure 4.5: a 100Ag, b Ag-10SnBi, c Ag-20SnBi, and d Ag-30SnBi. Inset shows the whole mapping images (Images were magnified near the scale bar from the whole images)

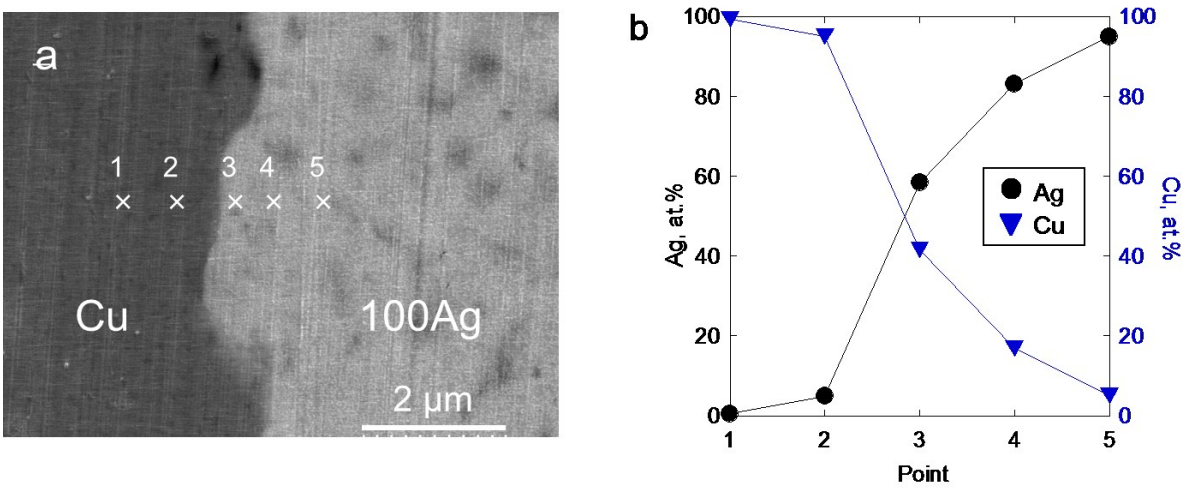

Figure 4.7 **a** Cross-sectional SEM (SE) image of 100Ag, and **b** corresponding detected Cu and Ag in atomic percentage (at %) at each point shown in **a**

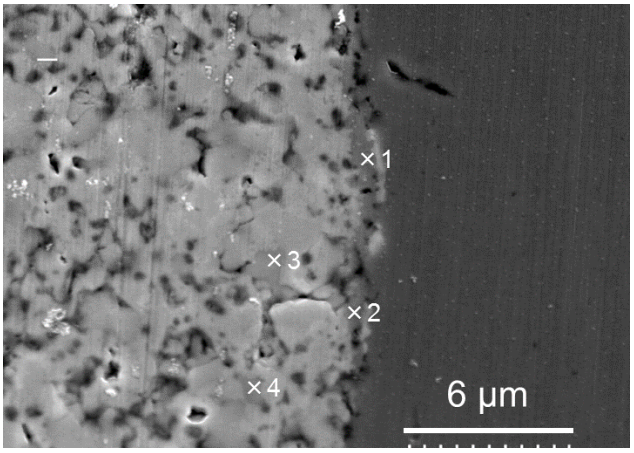

Figure 4.8 Cross-sectional SEM (SE) image of Ag-30SnBi sintered at 250 °C for 60 min

Table 4.3 Elemental analysis (EDX) result at points shown in Figure 4.12

Point	Ag, at.%	Sn, at.%	Bi, at%	Cu, at.%	Predicted phase
1	-	20.4	-	79.6	Cu_3Sn
2	-	21.9	-	78.1	Cu_3Sn
3	84.9	15.1	-	-	Ag_5Sn
4	85.4	14.6	-	-	Ag_5Sn

In general, one essential condition to achieve a sound joint is firstly to have a strong interfacial reaction layer [5]. In most cases when plateless Cu-substrates were bonded with Sn-based solder, Cu-Sn IMCs are expected to form at the interface [5]. Although one of the main aims of adding Sn-Bi in this study is to promote an intermetallic joint between molten Sn and Cu, there was likely insufficient molten Sn to react with Cu to form IMCs in the case of Ag-10SnBi. Furthermore, as reference, the interdiffusion coefficient at 200°C of Ag into Sn, i.e. 9.5×10^{-11} m^2s^{-1} [6], was higher than Cu into Sn, i.e. 5.4×10^{-16} m^2s^{-1} [7], up to fifth orders. This indicates that Ag preferentially diffuse into Sn five times faster compared to Cu, which in return retarded the formation of Cu-Sn IMC interfacial reaction layer. To top that, the Ag nanoparticles solution into Sn-liquid phase is thought to be higher compared to that of Cu-substrate due to the high curvature of the nanoparticles. It is assumed that the preferential formation of Ag-Sn IMCs at the expense of the formation of Cu-Sn IMCs interfacial reaction layer and/or Ag-Cu interdiffusion layer might resulted in the low shear strength of Ag-10SnBi.

On the other hand, when there is sufficient amount of molten Sn, Cu-Sn IMCs layers are expected to be formed, as can be seen in Ag-20SnBi and Ag-30SnBi (yellow), hence leading to strong interface joint (refer to Figure 4.6c-d). Ahmed Sharif et al. also observed similar phenomenon to the interface of Cu substrates that were bonded with Ag-40wt%Sn [4]. Figure 4.8 shows the SEM image of cross-sections of Ag-30SnBi sample and corresponding elemental analysis at points shown in the figure are listed in Table 4.3. It is assumed that, although the ratios were slightly different, Cu_3Sn phases are dominant at the interface. No ratio of Cu_6Sn_5 was detected indicating that the interface consisted of, although not limited to, planar-type Cu_3Sn. This observation was different to conventional Sn-based solder where former and latter were the major constituents that typically formed at the interface, as explained in Section 1.3.1.

The mechanism of densification throughout liquid phase sintering has been discussed in details in [8]. In general, there are three mechanisms to densify the structure i.e. contact flattening,

dissolution of small grains and solid state bonding. Additionally, capillary action plays a vital role for the spreading of the molten metal liquid where small pore is preferable for the filling of molten liquid [8]. On the other hand, the higher solubility rate of the solid into the liquid will lead to rapid sinter densification, particularly the particles with high curvature or with small radius (nano range size).

The strengthening of Ag with the addition of Sn-Bi in Ag-20SnBi and Ag-30SnBi might be attributed to the formation of Ag-Sn IMCs (magenta) and Cu-Sn IMCs (yellow) as can be seen from the elemental mapping images (Figure 4.6c and d). However, Ag-30SnBi demonstrated superior shear strength compared to Ag-20SnBi, as can be seen in Figure 4.1. In addition, the elemental mapping of the fracture surface of Ag-20SnBi, as shown in Figure 4.4c revealed that the fracture occurred within the Cu-Sn IMC interfacial reaction layer. This indicates that with the increasing addition amount of Sn-Bi, the formation of Cu-Sn IMC interfacial reaction layer was promoted, but with 20 wt% addition amount of Sn-Bi was not enough to form a strong interface. With 30 wt% addition amount of Sn-Bi, it is assumed that a uniform Cu-Sn IMC interfacial reaction layer was formed and contribute to the strengthening at the interface. On the other hand, as shown in Figure 4.8, micro-sized voids can be found scattered in the sintering structure. It is thought that although the interface was strengthened by the formation of Cu-Sn IMCs, the strength of the sintering structure might be highly influenced by the existence of the randomly distributed micro-sized voids. According to D.C. Lin et al [9], the existence of macro-sized and micro-sized voids are detrimental to strength and durability as the fine micro-sized voids might eventually form fine microscopic cracks that lead to failure.

Figure 4.9 shows the elemental mapping by EDX of the cross-section of Cu-Cu joints bonded with Ag-45SnBi. The white phase that can be observed in the SEM (BSE) image is Bi-phase as detected by the EDX. Microscale voids were scattered in the matrix of Ag-Sn IMCs and Bi. At the interface, a uniform layer of Sn can be seen, which is assumed to be the Cu-Sn IMCs interfacial reaction layer. The thickness is approximately 2 μm. Although the uniformly formed Cu-Sn IMCs at

first was assumed to strengthen the interface of the joints, the formation of Kirkendall voids at the interface is assumed to weaken the interface, particularly at Ag-45SnBi joints. The adhesive fracture mode shown by this composition despite the existence of the Cu-Sn IMCs interfacial reaction layer is thought to be influenced by the formation of Kirkendall voids that can be observed at the vicinity of the interface, as shown in Figure 4.10.

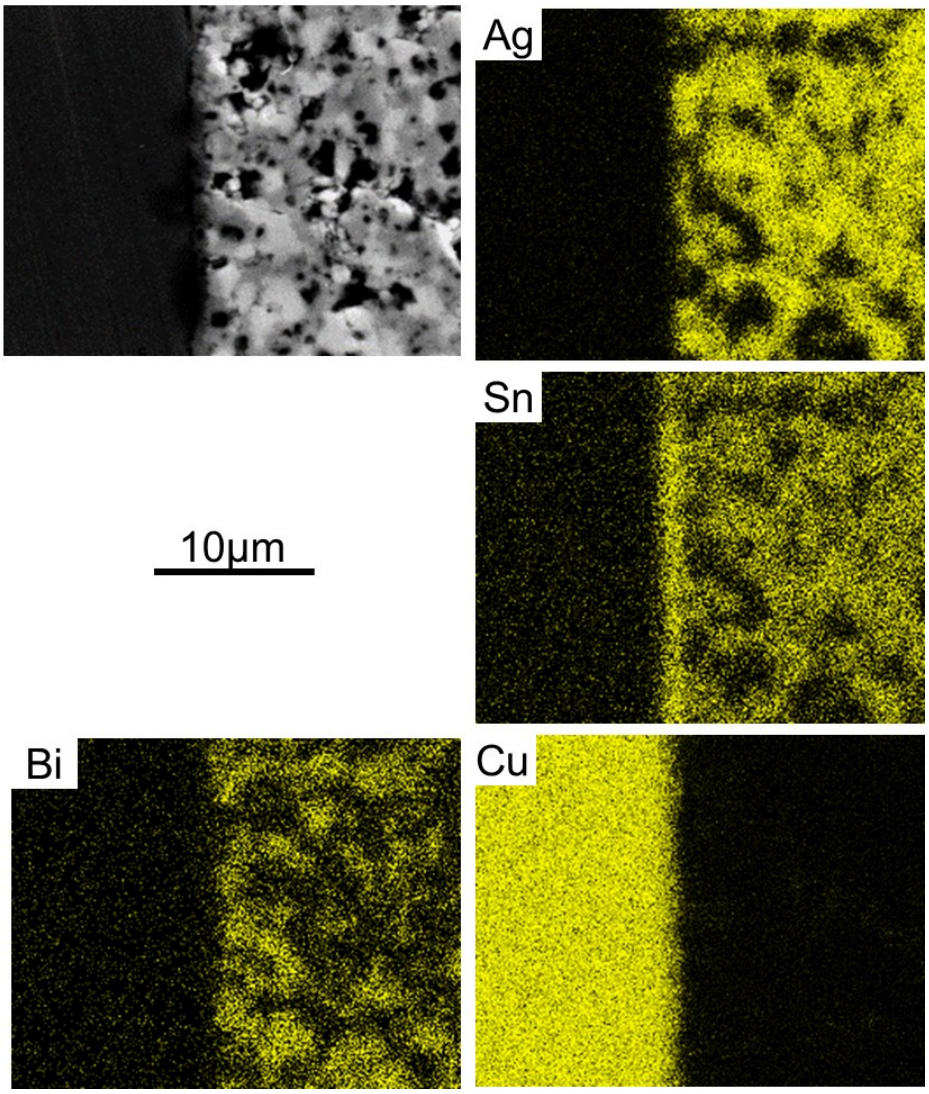

Figure 4.9 Elemental mapping by EDX of samples bonded with Ag-45SnBi at 250°C for 60 min sintering holding time and pressured with 0.1 MPa (upper left image is the SEM-BSE image)

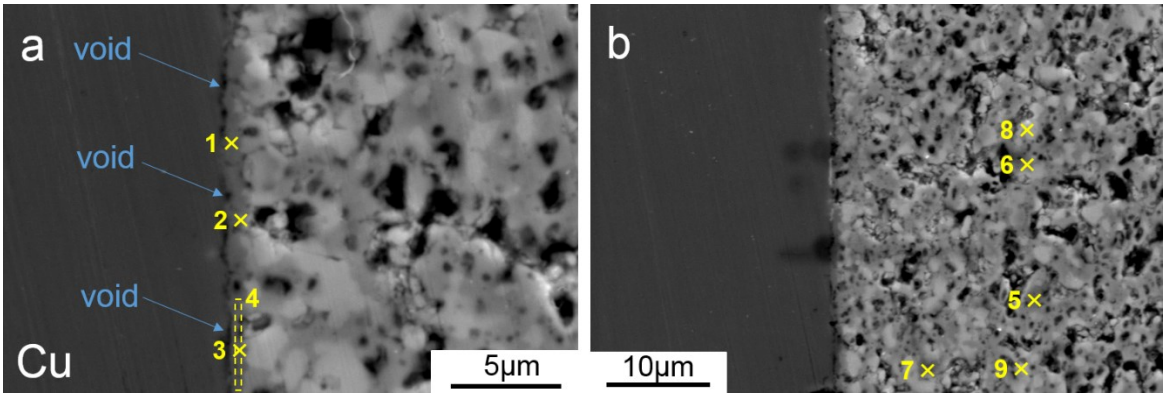

Figure 4.10 SEM (SE) images of Ag-45SnBi bonded with Cu substrate at 250°C for 60 min with different magnification

Table 4.4 Elemental analysis results corresponding to the points shown in Figure 4.10

Point	Ag, at.%	Sn, at.%	Cu, at%	Bi, at.%	Assumed phase
1	6.19	18.7	74.4	0.93	Cu_3Sn
2	6.46	18.2	73.6	1.71	Cu_3Sn
3	2.11	19.4	74.5	4.06	Cu_3Sn
4	5.02	18.0	74.6	2.43	Cu_3Sn
5	69.3	21.4	1.83	7.43	Ag_3Sn
6	68.3	21.9	2.91	6.89	Ag_3Sn
7	66.2	21.1	3.32	9.01	Ag_3Sn
8	41.2	10.7	3.02	44.3	Bi-rich
9	40.0	8.57	2.40	49.1	Bi-rich

Figure 4.10 shows two SEM images with different magnification of the same cross-sectional Cu-Cu joints bonded with Ag-45SnBi at 250 °C and 60 min. Table 4 listed elemental analysis results corresponding to the points and area shown in Figure 4.10. In the matrix, the main phase that existed was Ag_3Sn and at the interface was Cu_3Sn. No Cu_6Sn_5 phase was identified by the EDX analysis. The formation of Ag_3Sn in the matrix is consistent with the earlier assumption that was addressed in Section 4.1.As can be seen from Figure 4.10a, continuous voids can be observed at the interface between Cu and Ag-45SnBi. The formation of these voids can be assumed as follows.

In the conventional Sn-based solder system as explained in Chapter 1 Section 1.3.1 (Figure 1.7), the firstly formed Cu-Sn IMC at the interface is Cu_6Sn_5 due to the abundance of Sn resource in the matrix. Subsequently, with the diffusion of Cu-flux from the Cu-substrate, Cu_3Sn formed between the formerly formed Cu_6Sn_5 and Cu substrate with increasing reaction time at high temperature (soldering temperature).

Taking this into account, when the Sn-Bi melted and start to form IMCs with Ag matrix and Cu-substrate, it is assumed that the Cu_6Sn_5 was also formed at the interface due to the abundance of Sn in Ag-45SnBi. With prolonging sintering time, i.e. 60 min in this study, it is expected that the Cu-flux from the Cu-substrate diffused into the Cu_6Sn_5 to form Cu_3Sn. This observation is in good agreement with the interface at Ag-30SnBi which is shown in Figure 4.8. However, in comparison with Ag-30SnBi, Ag-45SnBi have more Sn resources, thus, the expected Cu_6Sn_5 IMC that firstly formed at the interface was assumed to be thicker than Ag-30SnBi. This means that subsequently more Cu-fluxes are transported from Cu substrate to the Cu_6Sn_5. At 60 min sintering holding time, the transported Cu-flux (Cu atoms) from the Cu substrate resulted in the formation of void at the Cu substrate side. This void is familiarly known as Kirkendall void due to the indifference of diffusion coefficient between Cu and Sn into the Cu_6Sn_5. Santosh Kumar et al. reported that the diffusion coefficient of Sn was half smaller compared to the Cu in the Cu/η system at 200 °C [10], which

supported above statement on the formation of Kirkendall void at the interface. A schematic presentation on the formation of Kirkendall voids in Cu-Cu joints that was bonded with Ag-45SnBi is illustrated in Figure 4.11. As confirmed by the point-by-point elemental analysis that was conducted in Figure 4.10, Cu_3Sn that was formed at the expense of Cu from the Cu substrate is thought to generate the voids at the interface. 60 min sintering holding time is enough to completely transform the Cu_6Sn_5 into Cu_3Sn.

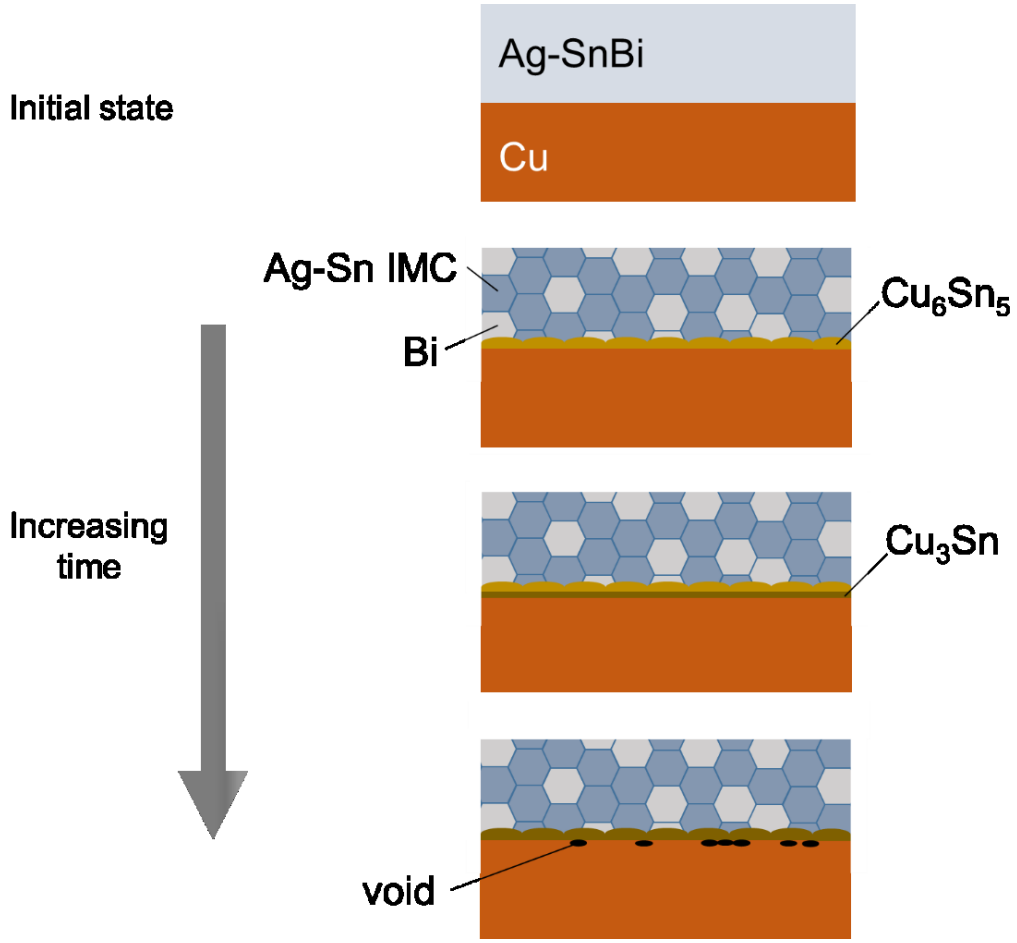

Figure 4.11 An assumption of Kirkendall void formation mechanism in Ag-SnBi joints

4.2.2 Effects on Remelting Temperature

Next, the remelting temperature of the as-sintered Ag-45SnBi was investigated by means of DSC. Ag-45SnBi was chosen to be evaluated because it has the largest Sn-Bi addition amount among the investigated composition in this study. According to the lever rule in the Ag-Sn binary system, no Sn solid solution will be formed with the addition of 45wt% Sn-Bi when the reaction between Ag and Bi is totally neglected. Hence, as formerly explained in Section 4.1, the expected remelting event of Ag-45SnBi should be observed at approximately 262 °C.

Figure 4.12 illustrates the DSC test result of the Ag-45SnBi sintered at 250 °C for 60 min. No endothermic peak of Sn-Bi eutectic was observed at 139°C, indicating that reaction between molten Sn, and Ag particles has been completed during sintering process. An endothermic reaction peak was observed at the proximity of 262°C, which is in good agreement with the reaction (4.1) and (4.2), as explained in Section 4.1. It can be concluded that all Sn-phase from the Sn-Bi has been transformed to Ag-Sn IMCs and Bi phase during the sintering process. Both invariant reactions were compared with experimental data [11] which showed very good agreement between both works. According to Z. Li et al., reaction (4.1) occurs at 262.6°C which is slightly higher than Ag-Bi binary eutectic (261.6°C) and reaction (4.2) occurs at 262.1°C [1]. In present study, the onset and peak temperature both covered the temperature range of above reactions, showing that both reactions might take place in Ag-45SnBi where both Ag_3Sn and Ag_5Sn (ζ Ag) might co-exist in the sintered microstructure, as well as Ag-Bi binary phase.

To conclude, in this study, it has been revealed that a complete shift of remelting temperature from Sn-Bi eutectic temperature to about 262 °C can been achieved by addition up to 45 wt% Sn-Bi. As a rule of thumb, Ag-based TLPS may be used up to 155°C (by considering 0.8 T_h) before creep effects accelerate degradation; 98°C higher than Sn-Bi eutectic solder, and 20°C higher than conventional Sn-Sb solder.

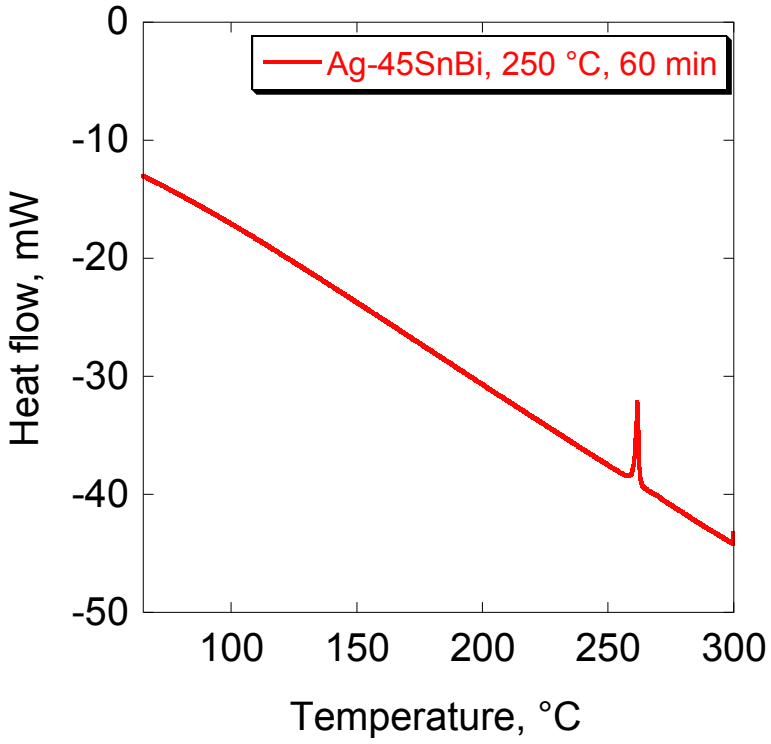

Figure 4.12 DSC results of Ag-45SnBi sintered at 250 °C for 60 min

4.3 Effects of Sintering Parameters

In this section, by focusing on Ag-30SnBi, which exhibited the highest shear strength among other compositions investigated in earlier section, several influences of sintering parameters i.e. sintering environment, sintering holding time, and sintering temperature to the shear strength, microstructure and remelting temperature will be discussed.

4.3.1 Sintering Holding Time

To investigate the effect of sintering time to the shear strength of the bonded joints, plateless Cu-Cu joints was bonded with Ag-30SnBi at different sintering holding time at 250°C and shear test was conducted. Three samples for each condition were prepared using the same sintering profile shown in Figure 3.10. Upon reaching the desired sintering holding time, the samples were cooled with the same cooling rate as described in Figure 3.10.

Figure 4.13 shows the shear strength of Ag-30SnBi that was sintered at 250 °C for different sintering holding time. It was found that longer sintering holding time led to higher shear strength. Interestingly, it can be observed that even at 0 min sintering time, the shear strength of Ag-30SnBi was similar to the 100Ag that was sintered for 60 min (refer Figure 4.1 for shear strength of 100Ag). On the other hand, for 45 min sintering time, the mean shear strength was equivalent to conventional Pb-free SnAg (Sn-1Ag-0.4Cu, wt.%) solder bonded with plateless Cu substrates [12]. Shear strength reached the highest when the sintering holding time was 60 min, which is the longest sintering time considered in this investigation. Sintering holding longer than 60 min was not conducted to minimize the processing time, as well as the obtained shear strength for 60 min sintering holding time was more than 20 MPa, which is in good agreement with the demand in the industry.

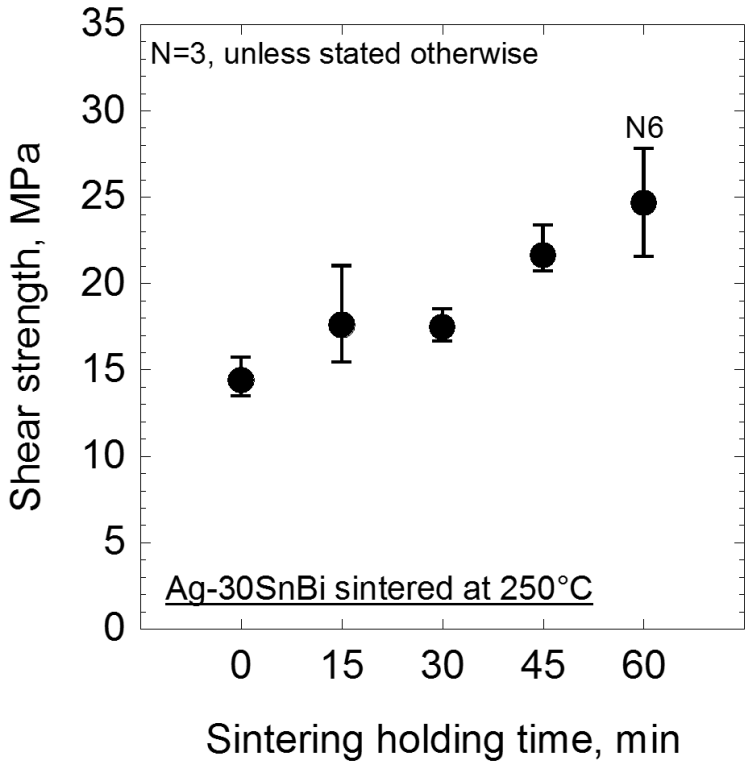

Figure 4.13 Shear strength of Ag-30SnBi sintered at 250 °C with different sintering holding time

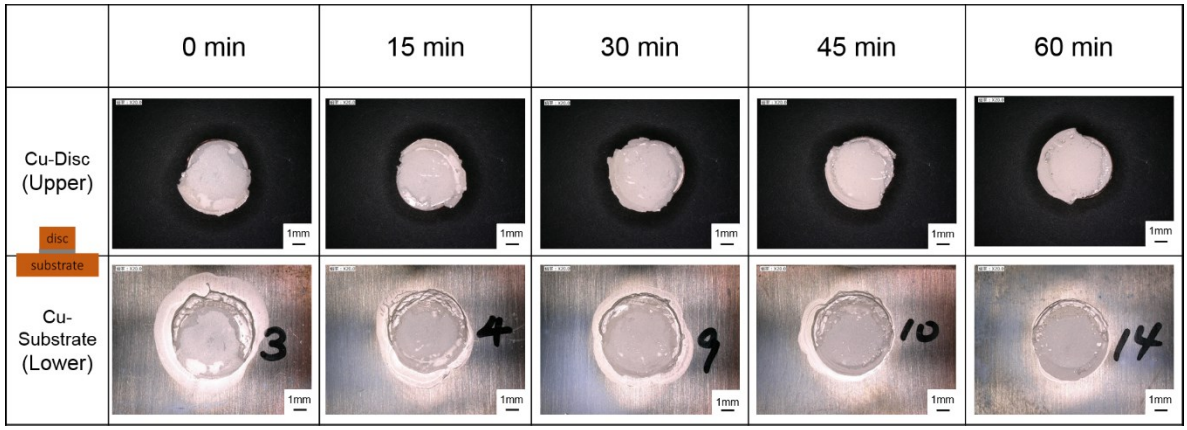

Figure 4.14 Optical micrograph images of Ag-30SnBi sintered at 250 °C with different sintering holding time

Figure 4.14 represents the fracture surface of sample showing the highest shear strength for each condition. Even for 0 min sintering time, the fracture mode demonstrated by Ag-30SnBi was cohesive failure. Up to 60 min sintering holding time, similar fracture mode was observed, which indicated that with prolonging sintering holding time up to 60 min, the interface was not weakened and the strengthening mechanism lied in the sintering structure. A detailed observation on the sintering structure will be addressed in Section 4.3.3 and the factor contributing to the strengthening will be discussed.

Figure 4.15 shows an example of fracture surface of Ag-30SnBi that was sintered for 60 min. At least two kinds of fracture morphology can be observed i.e. typical skeleton structure of sintered microstructure and dense microstructure which is shown in the area inside the dashed line. The dense structure may resulted from localized concentration of Sn-Bi. The fracture mode was similar to the brittle fracture behavior. Particularly at the dense structure, either Ag-Sn IMCs or Bi-rich phases were rather sheared throughout the particles, conforming transgranular fracture. However, at the skeleton structure, fracture might occur at the sintering neck inferring that intergranular fracture might be prominent. From qualitative elemental analysis (EDX) as shown in Table 4.3, the dense microstructure consist of Bi-rich phases and Ag_5Sn IMCs phases. However, at the skeleton structure (point 4), it was rather difficult to identify the phase existed due to the nature of the irregularity of analysis surface. If the Bi atomic percentage is neglected, the likely formed phase was Ag_5Sn which similar to the phase found at the dense structure.

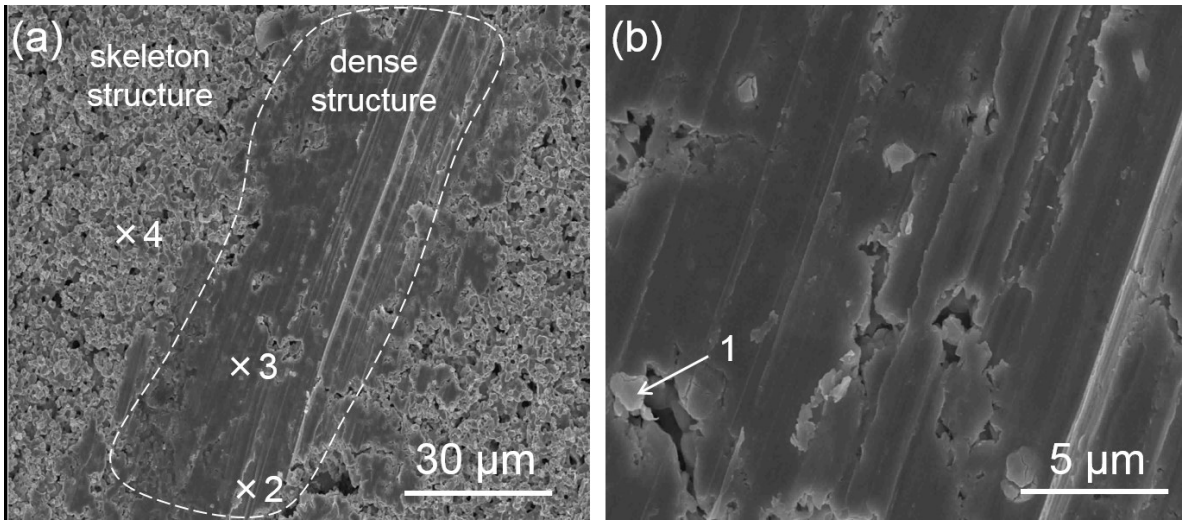

Figure 4.15 (a) SEM (SE) image of fracture surface of Ag-30SnBi sintered at 250°C and 60 min sintering holding time, and (b) magnified image of dense area shown (a)

Table 4.5 Elemental analysis (EDX) at points shown in Figure 4.18

Point	Ag, at.%	Sn, at.%	Bi, at.%	Predicted phase
1	26.15	2.67	71.18	Bi-rich
2	22.66	1.63	75.71	Bi-rich
3	84.24	13.15	2.61	Ag_5Sn
4	76.52	12.32	11.16	Ag_3Sn or Ag_5Sn*

* if Bi percentage is neglected

4.3.2 Sintering Temperature

On lowering thermomechanical stress induced during high temperature processing, the effect of sintering temperature to the shear strength was investigated in order to establish a minimum sintering temperature allowed while retaining high shear strength, or at least passing the requirements of MIL-STD-883K (minimum shear strength of 2.5 MPa). Plateless Cu-Cu was bonded with Ag-30SnBi with three different final sintering temperature, i.e. 200, 225, and 250°C with 60 min sintering holding time. Three samples for each conditions were prepared, except six samples for 250°C.

Figure 4.16 demonstrates the effects of sintering temperature on the strength of Cu-Cu that was bonded with Ag-30SnBi at the same sintering holding time. The increase in sintering temperature from 200 to 250°C resulted in the increasing of shear strength. Average shear strength of samples sintered at 200, 225, and 250 °C was 9.1, 15.4, and 19.3 MPa, respectively. Although samples that were sintered at 200°C exhibited the lowest shear strength, even lower than 100Ag sintered at 250 °C (refer Figure 4.1), all samples investigated here fulfilled the requirement of MIL-STD-883K. Low shear strength shown by sintering temperature of 200°C might be caused by the slower diffusion rate compared at higher temperature region. It was assumed by prolonging reaction time, which is sintering holding time, it is expected that the shear strength might also increase. To further investigate this assumption, sintering at 200 °C has been prolonged to 90 min and the shear strength was assessed.

Figure 4.17 shows the shear strength of Ag-30SnBi that was sintered at 200 °C for 60 and 90 min. The obtained shear strength for both sintering holding time at 200 °C was similar, implying that prolonging sintering holding time provide almost no influence to the sintered microstructure at 200 °C. The detailed observation of the microstructure at sintering temperature of 200 °C with different sintering holding time will be discussed in the next section.

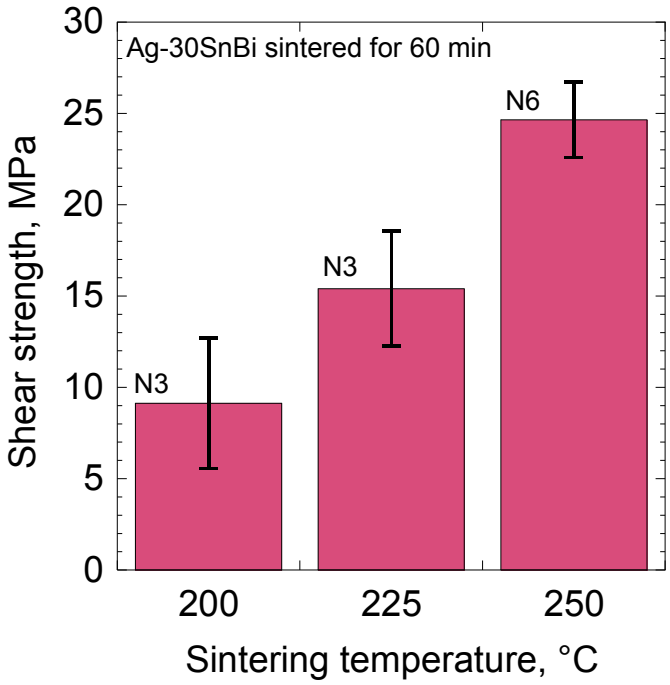

Figure 4.16 Influence of sintering temperature of Ag-30SnBi on the shear strength

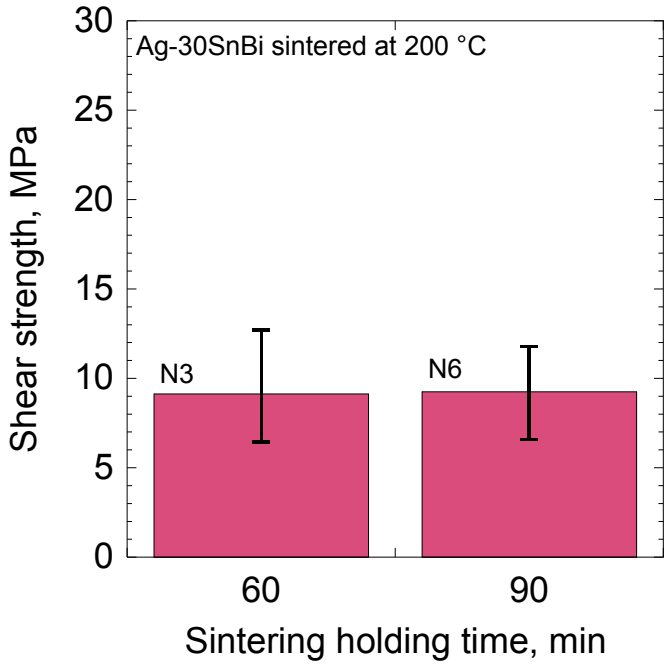

Figure 4.17 Shear strength of Ag-30SnBi that was sintered at 200 °C with different sintering holding time

4.3.3 Microstructure Evolution during Sintering Process

In Section 4.3.1, it has been demonstrated that the shear strength of Ag-30SnBi increased with increasing sintering holding time up to 60 min when sintered at 250 °C. Meanwhile, it Section 4.3.2, it has also been shown that the shear strength of Ag-30SnBi became higher with the increase of sintering temperature within the same sintering holding time, i.e. 60 min. In addition, when Ag-30SnBi was sintered at 200 °C for 60 min and 90 min, the shear strength was almost unaffected.

In order to understand the mechanism behind the strengthening of Ag-30SnBi under the influence of sintering temperature and sintering holding time, in this section, an investigation of the microstructure evolution during the TLPS process has been conducted and the factors that contributed to the strengthening in the matrix of Ag-30SnBi joints will be discussed. Note that the strengthening at the interface is omitted and the discussion in this section will solely focus on the strengthening mechanism in the matrix. The strengthening at the interface is assumed to provide less influence to the strength joint of Ag-30SnBi as observed in Figure 4.14, where the mode of fracture of Ag-30SnBi remained consistent as cohesive fracture despite sintered at different sintering holding time.

In this investigation, Ag-30SnBi was printed with dimension of 10 × 10 × 0.2 mm on a glass plate. Three samples were prepared for each conditions. Eleven sintering conditions that were varied in this investigations are shown in Figure 4.18. Condition 1 and 2 were conducted under N_2 environment to imitate the sintering profile (drying stage) that has been used in this study. Meanwhile, after the drying stage, the remaining sintering process was conducted under formic gas reducing environment. At 200 °C and 250 °C, in addition to the 0 min sintering holding time, samples were also hold for 90 min to investigate the microstructure evolution with prolonging sintering holding time.

Ag-30SnBi was heated at 5 °C/min to specific temperature and time as shown in Figure 4.18, and upon reaching the desired temperature and time, the samples were abruptly cooled with 50 °C/min

cooling rate. The samples were then collected, and SEM observation was conducted. The upper surface of the sample was set as the observation surface, as shown in Figure 4.18. Next, the samples were pounded in a mortar for XRD and DSC analysis. The condition for XRD and DSC analysis are explained in Chapter 3 Section 3.3.3.

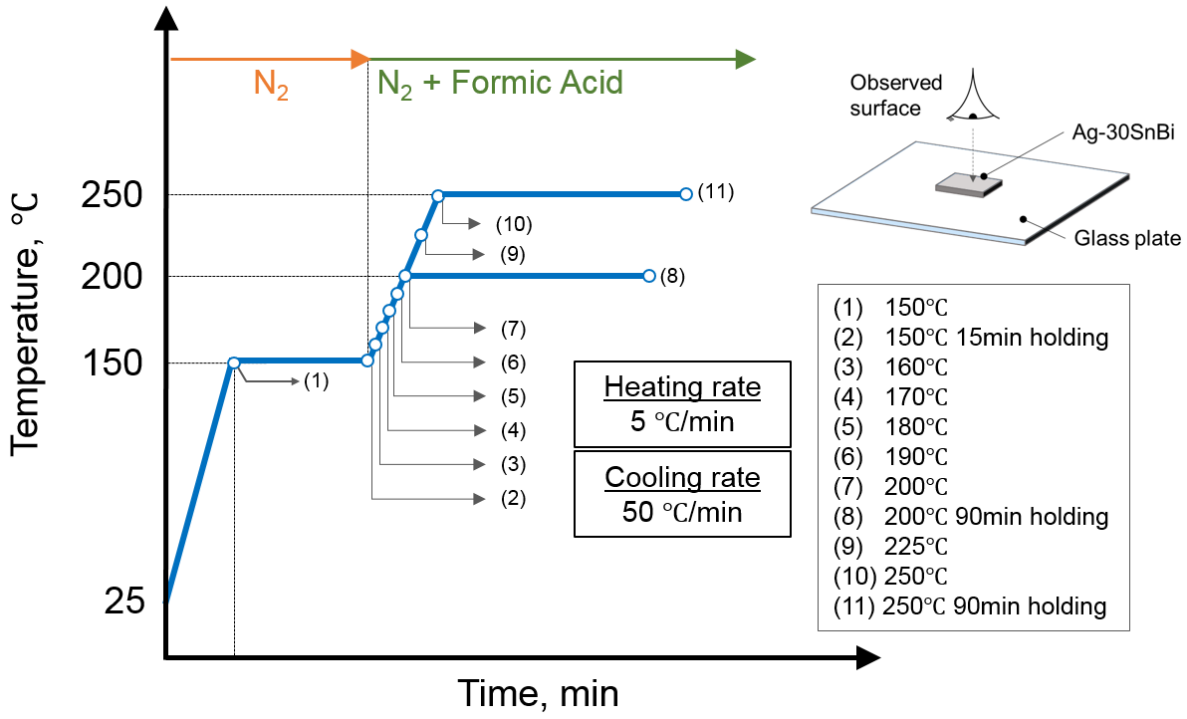

Figure 4.18 Sintering conditions used in the investigation on elucidating the evolution of microstructure during the sintering process and the sample preparation method

Figure 4.19 shows the SEM (SE) images of Ag-30SnBi that was sintered at different sintering temperature (sintering holding time: 0 min). At 150 °C, several Sn-Bi powders can be seen despite the temperature has exceeded the eutectic temperature of the Sn-Bi. This might be caused by the oxide layer that hinder the wetting of Sn-Bi onto the Ag particles. On the other hand, when the temperature was raised to 160 °C and formic gas was introduced, Sn-Bi powders was not detected, owing to the reducing effect of the formic gas. The sintering microstructure evolution with increasing sintering time can be described as follows. With increasing sintering temperature, the sintering necks extension between particles became larger and contributed to the densification. In particular, at 150 °C, the most particles existed as a single particles and almost no sintering necks can be observed. However, at 250 °C, almost all particles had sintered to each other and a densified sintering structure can be distinguished despite the existence of sintering voids.

Figure 4.20 represents the SEM (SE) images of Ag-30SnBi that was sintered at three different sintering temperature, and a prolonged sintering holding time associated with the sintering temperature. At the drying stage where sintering temperature was hold for 15 min, the Sn-Bi powders still can be detected. Note that at this drying stage, the sintering environment was N_2 environment. At 250 °C, an improvement of densification of the sintering microstructures can be observed with the increasing sintering holding time. It is not an exaggeration to state that at 250 °C 90 min condition, a densified sintering structure can be observed as compared to other conditions. On the other hand, in comparison to Ag-30SnBi that was sintered at 250 °C for 90 min, the one that was sintered at 200 °C for 90 min exhibited less extensive sintering necking between particles. The decreased sintering necking area might weaken the matrix as shown by the shear strength in Figure 4.16. Interestingly, at 200 °C no significance different can be explained in the microstructure regardless of the sintering holding time. The densification between particles were not as prominent as compared to the one at 250 °C. This might explained the plateau shear strength of Ag-30SnBi as demonstrated in Figure 4.20.

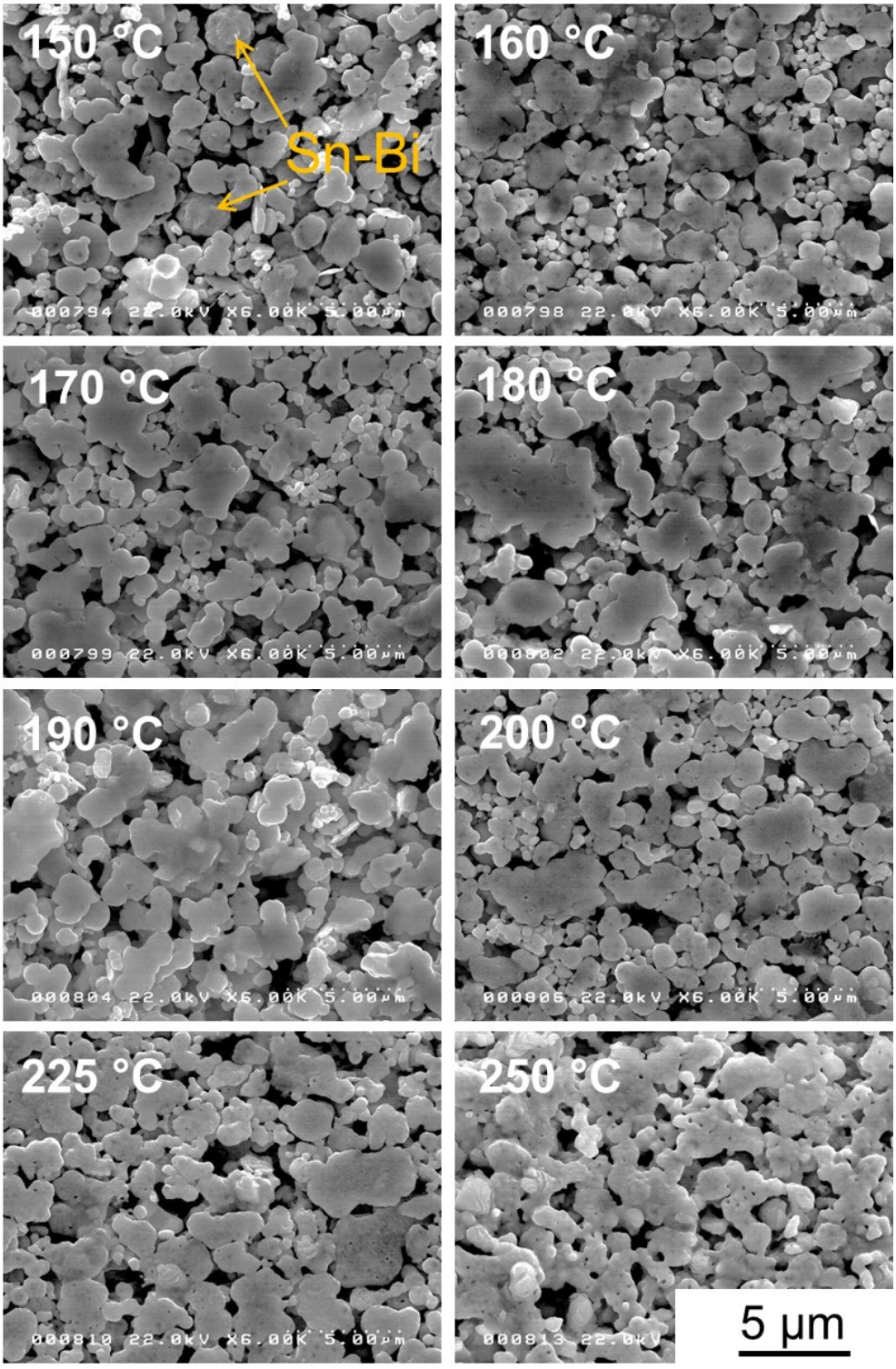

Figure 4.19 SEM (SE) images of sintering surface of Ag-30SnBi that was sintered at different sintering temperature (sintering holding time is 0 min for each condition)

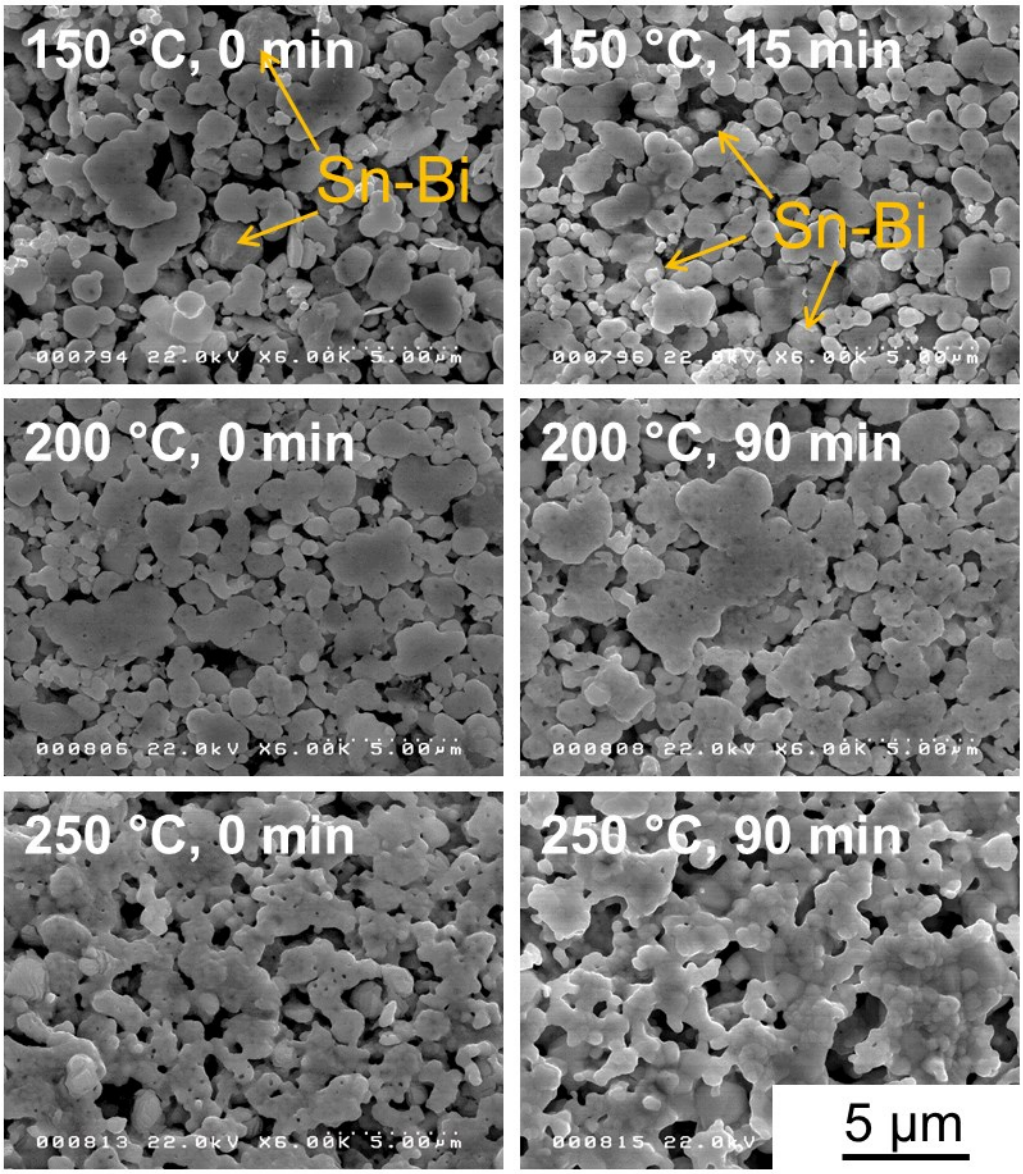

Figure 4.20 SEM (SE) images of sintering surface of Ag-30SnBi that was sintered at different sintering temperature and different sintering holding time

Next, the phase change in Ag-30SnBi sintering microstructure during the sintering process will be explained. Figure 4.21 shows the XRD pattern of Ag-30SnBi that was sintered at several sintering conditions as described in Figure 4.18. At 150 °C, regardless of sintering temperature exceeding the eutectic temperature of Sn-Bi, Sn (200) plane at 35.7 °, Sn (101) plane at 37.3 °, Sn (220) plane at 51.3 °, and Sn (211) plane at 52.6 ° can be detected, which indicated the Sn phase in Sn-Bi powders. These findings are in good agreement with the SEM observation in Figure 4.20. These Sn planes, however, were no longer detected at sintering temperature of 160 °C, in which the introduction of formic gas might facilitate the wetting of molten Sn-Bi onto the Ag particles and subsequently commencing the isothermal solidification process. The isothermal solidification process is thought to complete within 2 min time frame during heating from 150 °C to 160 °C with ramp rate of 5 °C/min.

On the other hand, the intensity peak of Ag (111) plane, and Ag (200) plane at 44.6 °, and 51.9 ° can be observed, respectively, until sintering temperature of 200 °C and 0 min sintering holding time. At 200 °C, with prolonging sintering holding time up to 90 min, these Ag planes were almost not detected. Similarly, with increasing sintering temperature from 225 °C to 250 °C, these Ag planes were almost not detected. The Ag (111) plane at 44.6 ° coincided with Bi (104) plane, hence the small peak that can be observed at temperature range from 200 °C to 250 °C might indicated the Bi (104) plane, since the Ag was assumed to react with Sn to form Ag-Sn IMCs.

After drying stage, formic gas was introduced and expected to facilitate the wetting of Sn-Bi. Sn will react with Ag and assumed to firstly form the Ag_3Sn. With increasing sintering temperature and sintering time, the interdiffusion between Ag and Sn will resulted in the transformation of Ag_5Sn from Ag_3Sn. This assumption was confirmed by the identified Ag_3Sn (201) plane at 40.5 ° from temperature range of 160 °C to 200 °C, but subsequently diminished when the sintering holding time was prolonged to 90 min at 200 °C or when the sintering temperature was raised to higher temperature.

Meanwhile, the intensity peak of Ag_5Sn (100) plane at 41.3 ° became clearly visible from sintering temperature of 200 °C and higher, which implied that the increase of temperature might facilitated the interdiffusion between Ag and Sn atoms to transform the Ag_3Sn phase into Ag_5Sn phase, as explained in the earlier assumption. Interestingly, Ag_5Sn (002) plane peak at 43.9 ° can be clearly observed from 160 °C, indicating that the formation of Ag_5Sn might occur at even lower temperature than 200 °C. The intensity peak became relatively higher towards increasing sintering temperature and sintering holding time. Similar observation can be found with Ag_5Sn (101) plane at 47.1 °.

At 200 °C and 250 °C with 90 min sintering holding time, and at 225 °C and 250 °C with 0 min sintering time, no Ag_3Sn phase can be observed, implying that the microstructure in the matrix of Ag-30SnBi consisted of Ag_5Sn. It can be inferred that the final phases existing in the matrix of Ag-30SnBi that was sintered at 250 °C and 60 min sintering, which showed the shear strength of about 25 MPa (Figure 4.1), were Ag_5Sn and Bi. These constituent phases were at first thought to be the strengthening factor of Ag-30SnBi, however, at 200 °C and 90 min, the identified phases were similar to that of 250 °C and 90 min. Ag-30SnBi that was sintered at 200 °C and 90 min sintering holding time exhibited shear strength about 9 MPa (Figure 4.17), which was 2.8 times lower than the one sintered at 250 °C and 60 min (Figure 4.1), albeit the identified constituent phases were similar. Hence, the constituent phase might provide less influence to the strengthening mechanism, but poor densification of the sintering structure in the matrix of Ag-30SnBi that was sintered at 200 °C compared to that of 250 °C (Figure 4.20), might result in poorer shear strength.

To summarize, the strengthening mechanism of Ag-30SnBi strongly affected by the extensive formation of sintering necks and densification of the sintering microstructure with increasing sintering temperature, at least up to 250 °C as investigated in this study.

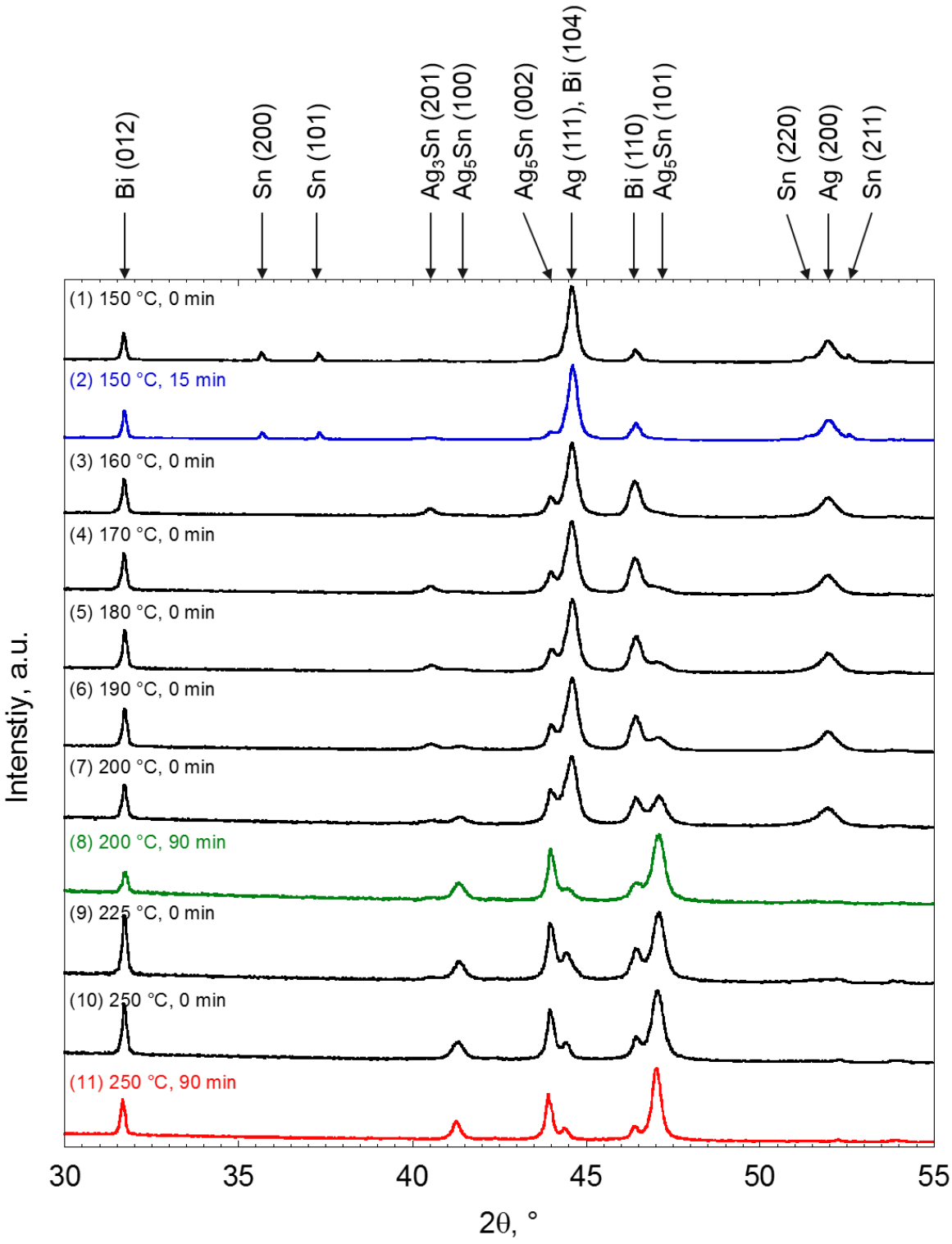

Figure 4.21 XRD pattern of Ag-30SnBi sintered at different sintering conditions as shown in Figure 4.18

Finally, the effect of sintering temperature and sintering time to the remelting temperature of Ag-30SnBi will be discussed. Figure 4.22 shows the DSC result of Ag-30SnBi that was sintered at several sintering temperatures. Onset temperature and peak temperature of the melting event that was observed in each sintering condition were summarized in Table 4.6. Apart from the one sintered at 150 °C for 15 min, remelting event was only observed at the proximity of 262 °C, which might indicate the melting event of reaction (4.1) or (4.2) as explained in Section 4.1. Meanwhile, as confirmed by the DSC test result of Ag-30SnBi that was sintered at 160 °C, no remelting event of Sn-Bi can be observed, implying that isothermal solidification process might be finished before reaching 160 °C. The rapid diffusion of Ag nanoparticles into the Sn liquid phase is thought to contribute to this rapid completion of the isothermal solidification process.

On the other hand, Ag-30SnBi that was sintered up to the completion of drying stage (150 °C, 15 min) exhibited two remelting events, i.e. at approximately 139 °C and 262 °C. During drying stage, no formic gas was introduced, thus, the melting event at the Sn-Bi eutectic temperature (139 °C) was expected due to the poor wetting of Sn-Bi on the Ag particles that hindered the isothermal solidification process. However, during the DSC analysis, the second remelting event that occurred at 262 °C indicates that the reaction (4.1) or (4.2) might happen during the DSC analysis, or the transformation of Ag into Ag-Sn IMCs to initiate the above mentioned reactions might occur partially during the drying stage. This finding suggests that although without the introduction of formic gas, the Sn-Bi might partially wet the Ag particles, and subsequently react with Ag to form Ag-Sn IMCs, either during the drying stage or during the re-heating in the DSC analysis. To further investigate the effect of formic gas reducing environment onto the mechanism of TLPS of Ag-SnBi and its effect on the shear strength, an investigation was carried out and will be discussed in the next section.

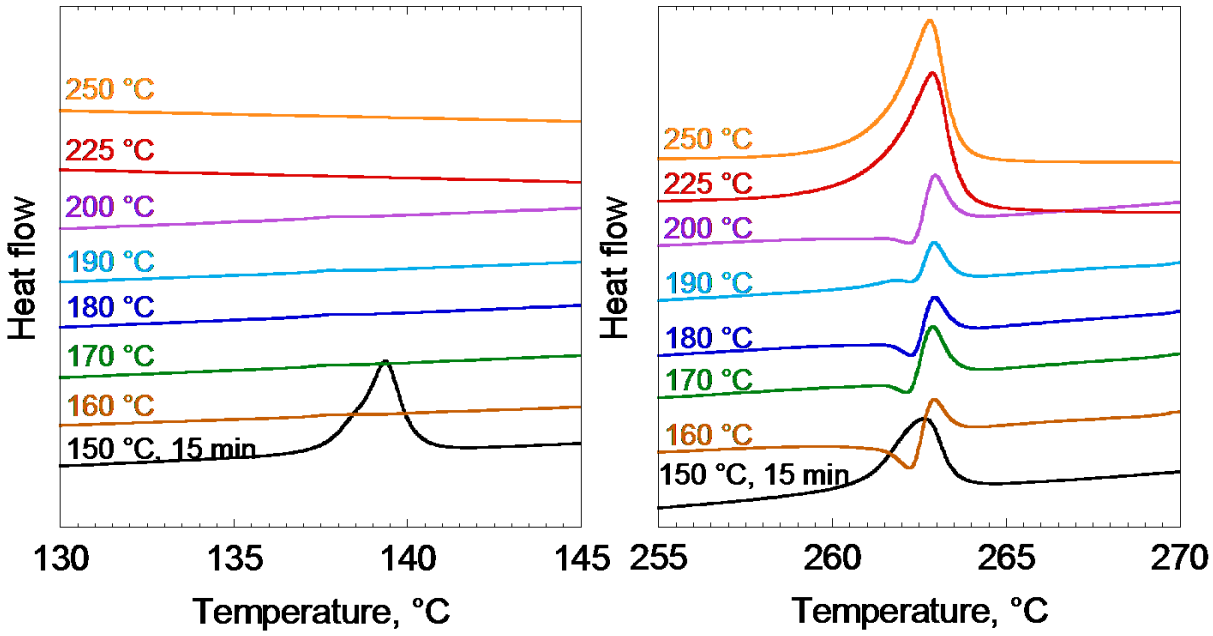

Figure 4.22 DSC analysis results of Ag-30SnBi at different sintering temperature (Except of at 150 °C, sintering holding time was 0 min)

Table 4.6 Onset temperature and peak temperature of endothermic reaction corresponding to the DSC analysis results shown in Figure 4.

No.	Sintering Condition		First melting event		Second melting event	
	Temperature °C	Holding time min	Onset temperature °C	Peak temperature °C	Onset temperature °C	Peak Temperature °C
1	150	0	138.15	139.30	260.93	262.61
2	150	15	138.16	139.37	260.87	262.63
3	160	0	-	-	261.20	262.23
4	170	0	-	-	262.40	262.89
5	180	0	-	-	262.55	262.94
6	190	0	-	-	262.45	262.94
7	200	0	-	-	262.54	262.97
8	200	90	-	-	260.66	262.66
9	225	0	-	-	261.06	262.90
10	250	0	-	-	261.23	262.82
11	250	90	-	-	262.37	263.43

4.3.4 Sintering Environment

In the preliminary experiment on the wetting of Sn-Bi under different environment that was conducted in Chapter 3 Section 3.2.2, the wetting of Sn-Bi on the Cu substrate was not observed when sintered under N_2 environment (Figure 3.8b, e). The spreading of Sn-Bi on the Cu substrate was firstly observed after the introduction of formic gas, as confirmed in Figure 3.10. However, in Section 4.3.3, according to DSC result shown in Figure 4.22, it was clear that Ag-30SnBi that was sintered at 150 °C showed two melting events, i.e. at the Sn-Bi eutectic temperature and at 262 °C. The first melting event is expected to occur due to the residual Sn-Bi. However, the second remelting event might be attributed by two phenomena. First, during drying stage under N_2, there might exist some reaction between molten Sn and Ag, resulted in the formation of Ag-Sn IMCs and Bi. Second, although DSC test was conducted under N_2, the first remelting event of Sn-Bi subsequently resulted in the formation of Ag-Sn IMCs and Bi. These Ag-Sn IMCs and Bi is thought to trigger the remelting event at 262 °C.

To further clarify the effect of formic gas influence on the shear strength of Ag-30SnBi and the TLPS process of Ag mixed with Sn-Bi, Ag-30SnBi was sintered under fully N_2 environment and compared to the one with the introduction of formic gas. Figure 4.23 presents the effect of sintering environment with formic gas influence on the shear strength of Ag-30SnBi that was sintered at 250 °C and sintering holding time of 60 min. Without the introduction of formic gas, the shear strength was about 5 MPa. In addition, out of 6 samples, 2 samples delaminated before the shear test was even conducted. Furthermore, all samples that was sheared exhibited adhesive failure mode. The delamination and low shear strength demonstrated by the Ag-30SnBi that was sintered without the introduction of formic gas was caused by the oxide layer on the Cu substrate that is assumed to suppress the formation of intermetallic reaction layer. This implies that formic gas reducing environment is essential on achieving a sound and robust joint at the interface in the proposed work of Ag-30SnBi.

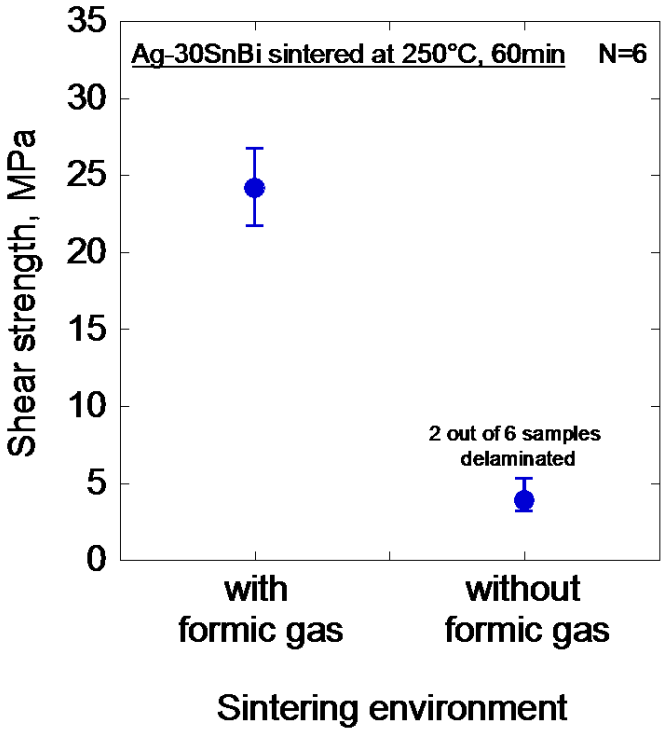

Figure 4.23 Effect of formic gas on the shear strength of Ag-30SnBi sintered at 250 °C for 60 min

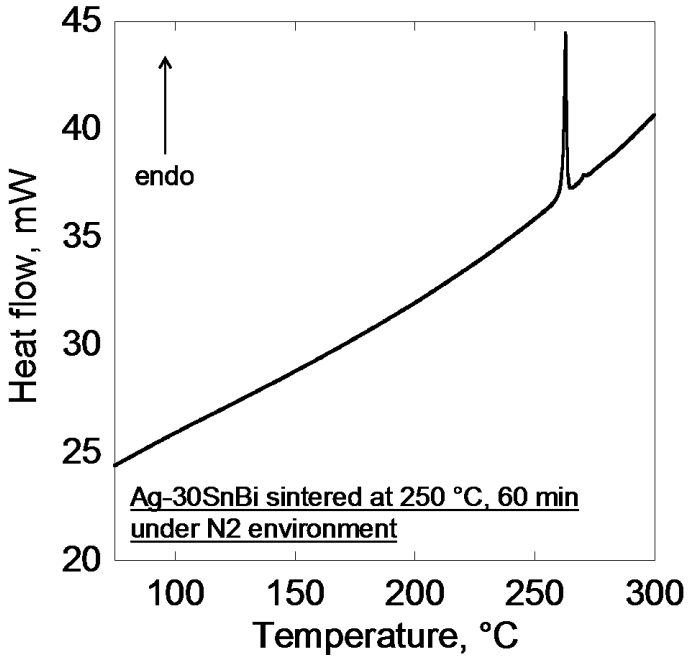

Figure 4.24 DSC result of Ag-30SnBi sintered at 250 °C for 60 min under N_2 environment without the introduction of formic gas

Figure 4.24 demonstrates the DSC result of Ag-30SnBi that was sintered at 250 °C for 60 min sintering holding time under N_2 environment. The remelting event at the Sn-Bi eutectic temperature was not totally observed which implied that although under N_2 environment Sn-Bi is presumed to react with Ag nanoparticles during the isothermal solidification process despite no introduction of formic gas to reduce the oxide layer on the outer surface of Sn-Bi powders. This findings indicated that the oxide layer on the Sn-Bi powders might exist partially, and the wetting of molten Sn onto the Ag particles might be introduced via the surface without oxide layer. With increasing sintering time and temperature throughout the sintering frame time, the rapid diffusion of Ag into Sn aided the isothermal solidification process to completely consume the Sn into forming Ag-Sn IMCs. This resulted in the remelting event at about 262 °C, which is similar to the one sintered under the influence of reducing formic gas.

Figure 4.25 shows the SEM (SE) images of Ag-30SnBi that was sintered under two different sintering environment. The image was taken from a sample that was prepared separately on a glass plate. Sintering was conducted at 250 °C and 60 min sintering holding time for both conditions. As can be seen from the SEM image of the sintering microstructure of Ag-30SnBi that was sintered without the introduction of formic gas, the sintering microstructure was less densified compared to that of with the introduction of formic gas. Sintering necks between supposedly Ag-Sn IMCs particles were limited in number and the sintering microstructure was rather similar to the Ag nanoparticles at the early stage of sintering, as observed in Figure 4.19 at 150 °C. This implied that oxide layer that existed on the Ag-Sn IMCs particles hindered the densification of particles, but improved by the reducing effect of the formic gas.

From above findings, it was comprehended that formic gas reducing environment is essential on realizing fluxless bonding. The reducing effect of oxide layer existed on both Cu substrate and Ag-Sn IMCs microstructure can be achieved by the introduction of formic gas during sintering.

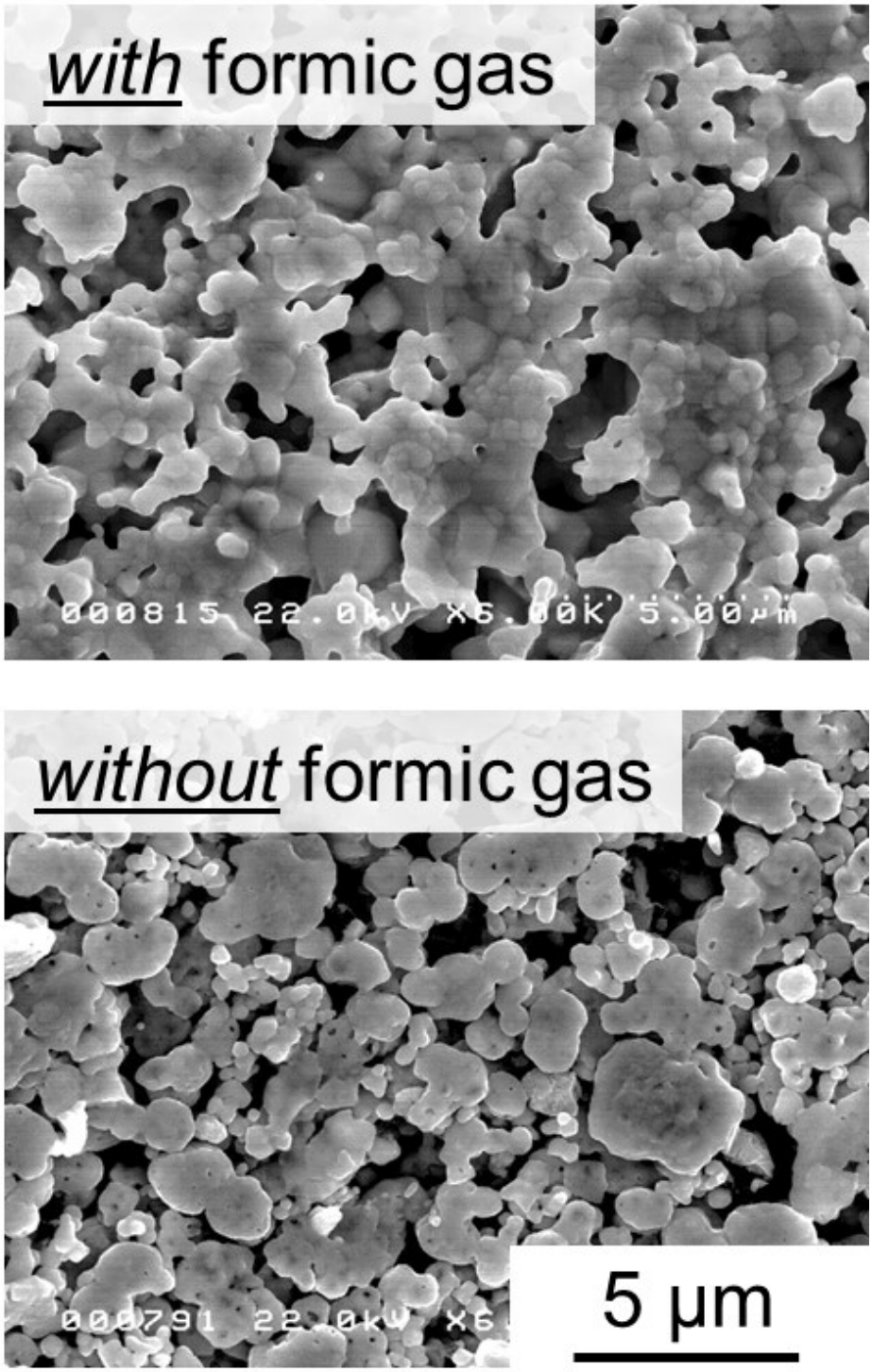

Figure 4.25 SEM images of sintering surface of Ag-30SnBi sintered under different environment (observation was conducted on sample that was prepared separately on a glass plate)

4.4 Bonding with Ni-plating

Up to this point, the aim of this study is to bond plateless Cu-Cu for the application of bonding DBC substrate of the module onto the Cu heat-spreader/sink. Thus, all investigations on the shear strength were conducted by bonding of plateless Cu-Cu substrate. Ag-30SnBi has demonstrated the highest shear strength when bonded at 250 °C and 60 min sintering holding time. As explained in Chapter 1 Section 1.2.3, the Cu heat-spreader that was attached on the Al-sink was aimed to spread the heat from the module to larger area before being cooled at the Al heat sink, and also performed as a buffer to reduce the thermomechanical stress due to the large CTE mismatch between Al heat-sink and ceramic substrate. However, the bonding of Cu heat spreader onto the Al heat sink is still an undergoing research and yet to be realized. On this account, the bonding of module onto a Ni-plated Al heat-sink is also demanded in the industry. At first, to investigate the effect of Ni-plating on the bonding strength of the Ag-30SnBi, a preliminary experiment on plateless Cu and Ni-plated Cu (Cu-Ni/Cu) bonding was conducted. Plateless Cu disc with diameter of 5 mm and Ni-plated Cu substrate with dimension of 20 × 10 × t3 mm was bonded with Ag-30SnBi at 250 °C for 60 min.

Figure 4.26 shows the obtained shear strength of six samples that was bonded with Ag-30SnBi, and Figure 4.27 represents the corresponding fracture surface of each sheared sample. The average shear strength of Ag-30SnBi used to bond Cu-Ni/Cu was 15.8 MPa, which was approximately 35% lower than that of Cu-Cu bonding. Out of six samples, the lowest shear strength obtained was about 13 MPa, which is higher than the maximum shear strength value of MIL-STD-883K (2.0×) [2]. Cu substrate can be clearly seen from the fracture surface of sample #3, which demonstrated the highest shear strength. For other samples, Cu substrate can also be observed, although not as clear as sample #3. This implied that the Ni-plating on the Cu substrate peeled off and influenced the shear strength. Effects of the thickness of Ni-plating and/or surface roughness of Cu substrate on the joint strength of the Ni-plating should be investigated in the future.

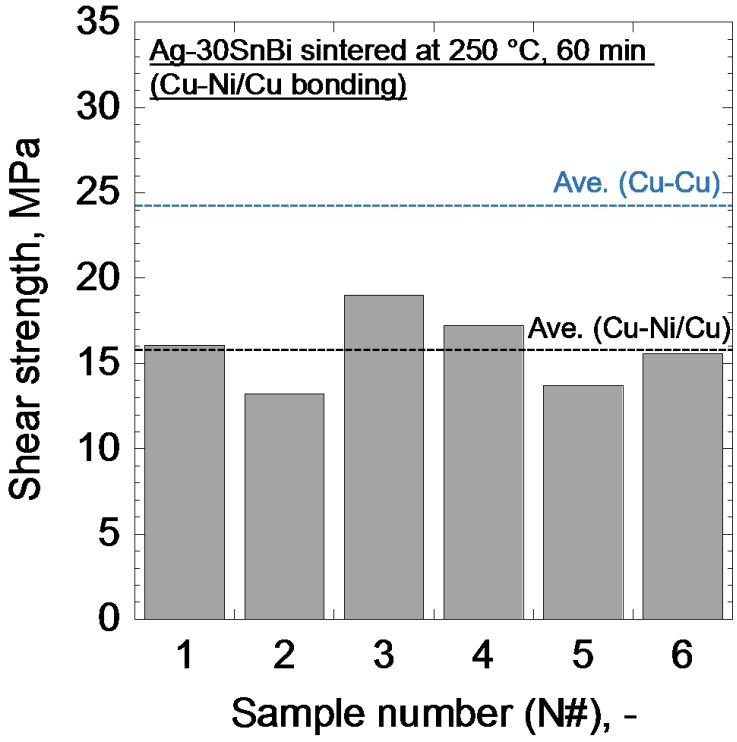

Figure 4.26 Shear strength of Ag-30SnBi used to bond plateless Cu disc with Ni-plated Cu substrate

N#	1	2	3	4	5	6
Cu-Disc (Upper)	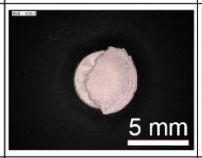	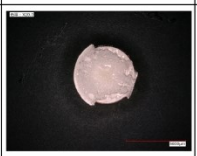		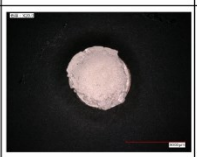	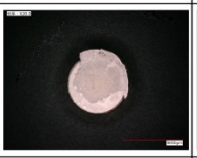	
disc / substrate						
Cu-Substrate (Lower)	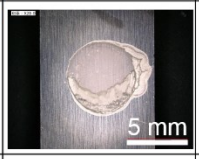	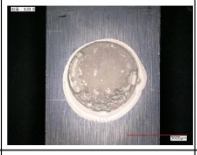	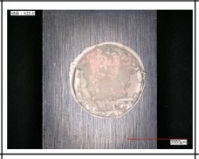			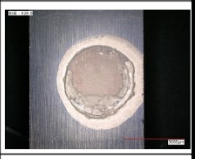
Shear strength MPa	16.0	13.2	19.0	17.2	13.8	15.6

Figure 4.27 Optical micrographs image of the fracture surface of Ag-30SnBi samples that used to bonded plateless Cu disc and Ni-plated Cu substrate (N# corresponds to the sample number in Figure 4.26)

4.5 Summary

In this study, a new strategy to joint SiC-based epoxy-molded modules (Cu-backside of DBC substrates) to Cu heat-substrate/sink has been developed. Fluxless mixture of Sn-Bi eutectic alloy and Ag particles were applied to bond plateless Cu-Cu substrates at 250 °C and lower processing temperature with the application of pressure as low as 0.02 MPa by TLPS process. The influences of Sn-Bi addition amount and sintering holding time to the shear strength and microstructure were investigated. Remelting temperature was also examined as a parameter for the possibility of high temperature application. Alloy composition and sintering conditions that demonstrated the highest shear strength are summarized in Table 4.7. The results obtained in this study are summarized as follows:

1. At sintering temperature of 250 °C and sintering holding time of 60 min, Ag-30SnBi demonstrated the highest shear strength (24.2 MPa), however, with increasing Sn-Bi addition amount from 30wt% to 45%, shear strength dropped. Ag-10SnBi showed the lowest shear strength out of all compositions investigated in this study.

2. The fracture mode of Ag-30SnBi was cohesive mode, meanwhile, Ag-45SnBi exhibited fracture at the interface (adhesive mode).

3. Formation of Cu-Sn IMCs at the interface of Ag-30SnBi is assumed to contribute to the strengthening at interface, while densification of sintering microstructure in the matrix was thought to contribute to the strengthening in the matrix.

4. It is expected that with 60 min sintering holding time, diffusion of Cu-atoms from the Cu substrate into the Cu_6Sn_5 interfacial reaction layer resulted in the formation of Cu_3Sn, and subsequently Kirkendall voids at the interface, which is thought to weaken the interface.

5. Shear strength of Ag-30SnBi increased with increasing sintering holding time (0 to 60 min) and sintering temperature (200 °C to 250 °C).

6. The decrease in the shear strength of Ag-30SnBi with decreasing sintering holding time and temperature was due to the lack of sintering necks formation and poor densification in the sintering microstructure in the matrix.

7. From XRD analysis of Ag-30SnBi sintered at 200 °C and 250 °C with the same sintering holding time of 90 min, the constituent phases in the matrix were same, i.e. Ag_5Sn and Bi, despite the fact that the obtained shear strength was lower when sintered at former. The difference of shear strength despite consisting same phases in the matrix was thought to be caused by the poor densification of the sintering microstructure.

8. Remelting temperature of all alloy compositions assessed in this study was approximately at 262 °C, implying the possibility of high temperature application. Isothermal solidification process was thought to complete within 2 min after the introduction of formic gas to remove the oxide layer on Sn-Bi powders.

9. Formic gas reducing environment has been proved to assist the wetting of Sn-Bi to the Ag particles and Cu substrates at temperature, and also the densification of the matrix particles.

10. In Cu-Ni/Cu bonding, the obtained shear strength of Ag-30SnBi was about 35% lower than that of Cu-Cu bonding. The observed fracture surface revealed the fracture between Ni-plating and Cu substrate, rather than the fracture within the matrix.

Table 4.7 Alloy compositions of Ag-SnBi and sintering conditions that satisfied the requirement of processing conditions, and the obtained shear strength and remelting temperature

Alloy composition	Sintering conditions			Bonding Conditions		Shear strength (Max.) MPa		Remelting temperature °C
	Temperature °C	Pressure MPa	Holding time min	Fluxless	Plateless Cu-Cu	≥ 20*	≥ 2.5**	(T_c max=125)
Target in this study	*≤ 200*	*≤ 0.1*	*n/a*	○	○	○	○	*≥ 200***
Ag-30SnBi	× (250)	○ (0.02)	60	○	○	○ (26.7)	○	○ (262)
Ag-30SnBi	○ (200)	○ (0.02)	60	○	○	× (12.7)	○	○ (262)

* Equivalent to the Pb-based solder [3]

** MIL-STD-883K (1.0 ×) [2]

*** Considering $T_c = 0.85T_h$

A patent has been applied for the Cu-based TLPS that has been discussed in this chapter. The submitted patent application information is as follows (in Japanese):

Kato Ryoichi, Gohara Hiromichi, Ikeda Yasunari, Mochizuki Eiji, Takahashi Kazuyoshi, Yoshida Makoto, Muhammad Khairi Faiz, 2017-000281, Power Electronics Module Manufacturing Method and Power Electronics Module

References

[1] Zuoan Li, Zhanmin Cao, Sabine Knott, Adolf Mikula, Yong Du, Zhiyu Qiao, Thermodynamic investigation of the Ag–Bi–Sn ternary system, Calphad 32, 152 (2008)

[2] MIL-STD-883K, EverySpec, http://everyspec.com/MIL-STD/MIL-STD-0800-0899/MIL-STD-883K_54326/ Accessed on 10 October 2016

[3] Eiichi Ide, Akio Hirose, Kojiro F. Kobayashi, Influence of Bonding Condition on Bonding Process Using Ag Metallo-Organic Nanoparticles for High Temperature Lead-Free Packaging, Mater. Trans. 47, 211 (2006)

[4] Ahmed Sharif, Chee Lip Gan, Zhong Chen, Transient liquid phase Ag-based solder technology for high-temperature packaging applications, J. Alloy. Compd. 587, 365 (2014)

[5] Suganuma Katsuaki, Introduction to Lead-free Soldering, Osaka University Press (2013) p85-91 (*in Japanese*)

[6] Brian F. Dyson, Diffusion of gold and silver in tin single crystals, J Appl. Phys. 37, 2375 (1966)

[7] Santosh Kumar, Carol A. Handwerker, and Mysore A. Dayananda, Intrinsic and Interdiffusion in Cu-Sn System, J Phase Equilib. Diff. 32, 309 (2011)

[8] Randall M. German et al., Review: liquid phase sintering, J. Mater. Sci 44, 1 (2009)

[9] D.C. Lin, S. Liu, T.M. Guo, G.-X. Wang, T.S. Srivatsan, M. Petraroli, Mat. Sci. Eng. A-Struct 360, 285 (2003)

[10] Santosh Kumar et al., Intrinsic and Interdiffusion in Cu-Sn System, Journal of Phase Equilibria and Diffusion, Vol. 32, No. 4 (2011) 309-319

[11] S. Hassam, E. Dichi, B. Legendre, Experimental equilibrium phase diagram of the Ag–Bi–Sn system, J. Alloy. Compd. 268, 199 (1998)

[12] J. Keller, D. Baither, U. Wilke, G. Schmitz, Mechanical properties of Pb-free SnAg solder joints, Acta Mater. 59, 2731 (2011)

CHAPTER 5: COPPER-BASED TRANSIENT LIQUID PHASE SINTERING

In previous chapter, Ag-based TLPS as a new bonding approach for the application on mounting module to the Cu heat-spreader/sink has been addressed. However, it is well known that Ag as one of the metal with high thermal conductivity (i.e., 429 W/mK), is extremely high in cost. Aiming for cost down strategy to benefit the industry, in this chapter, TLPS of mixed Cu nanoparticles and Sn-Bi eutectic alloy powders (hereinafter, Cu-SnBi) is focused on and will be discussed. Cu which possess thermal conductivity second to Ag but cost cheaper than Ag is highly anticipated to replace Ag nanoparticles sintering or Ag-based TLPS as a new bonding technology. In this study, firstly, sintering paste of Cu nanoparticles mixed with microscale Sn-Bi powders was prepared by mixing the particles with several types of organic compounds. The optimization of organic compounds addition amount was conducted by evaluating the shear strength and remelting temperature of the sintered sample. Using the optimized particles to organic compounds ratio, next, the influence of alloy composition on the shear strength and microstructure was investigated. The remelting temperature of each composition was also assessed. Several sintering parameters were varied and the effect to the shear strength and remelting temperature to the alloy composition that showed the highest shear strength in the previous investigation was examined, and the microstructure evolution during sintering process is made clear. Finally, the alloy composition and sintering conditions that are thought to fulfill the requirements as explained in Chapter 1 will be summarized.

5.1 Alloy Composition Selection Procedure

Cu nanoparticle selection reasoning

Previous work on Sn-Bi solder mixed with Cu particles by Omid Mokhtari et al. has derived a mathematical calculation of the sufficient amount of Cu particles to be added into Sn-Bi solder to completely convert the Sn-phase to Cu-Sn IMCs [1]. It was revealed that by addition of at least 30 wt% of Cu into Sn-Bi, not only the Sn will be completely converted to Cu-Sn IMCs, but 18.64 at% of Cu will remained unreacted in the soldered microstructure. However, in the same study, the DSC test of 30wt%Cu-70wt%SnBi soldered at 200 °C and for 50 min revealed the remelting event of Sn-Bi eutectic phase. The authors assumed that the observed remelting event at the Sn-Bi eutectic temperature was resulted by the residual Sn-Bi solders that remain unreacted with the Cu particles that was added into the solders [1]. In their study, microscale Cu particles with diameter of 5 μm was used to realize the transient liquid phase bonding at 200 °C. It was claimed that the usage of microscale Cu-particles resulted in the residual Sn-Bi due to the low solubility rate of Cu micro particles into the molten Sn during soldering. In addition to that, in a different work by the same authors, the cluster of Cu particles that was assumed to form during soldering was speculated to create solvent-depleted regions which in return led to the formation of macro-scale voids [2].

It was understood that by using nanoparticles, the reaction between molten Sn and Cu particles is expected to be accelerated, hence, unreacted Sn-phase that might lead to the remelting event at 139 °C can be avoided. The phenomenon of accelerated reaction by using nanoparticles can be explained by Gibbs-Thomson capillarity effect equation. This has been explained in detail in [3]. For further reading on deriving the equation, one may refers to the reference. The final form of Gibbs-Thomson is expressed as follows:

$$Cu_r = Cu_\infty \exp\frac{2\gamma V_{Cu}}{RTr} \tag{5.1}$$

where Cu_r is the concentration of solute Cu nanoparticles in molten Sn with a spherical interface. Cu_∞ is the concentration of solute Cu with planar interface, hence, the infinity symbol of radius. γ is the interfacial energy between solute Cu and molten Sn, V_{Cu} is the molar volume of Cu, R is the gas constant with value of 8.314 J K^{-1} mol^{-1}, T is the temperature of interest in Kelvin, and r is the radius of the Cu particles. Assuming that the exponential value is extremely small i.e., $2\gamma V_{Cu}/RTr << 1$, equation (5.1) can be expressed as:

$$Cu_r \approx Cu_\infty\left(1 + \frac{2\gamma V_{Cu}}{RTr}\right) \tag{5.2}$$

$$\frac{Cu_r}{Cu_\infty} \approx 1 + \frac{2\gamma V_{Cu}}{RTr} \tag{5.3}$$

From equation (5.3) the ratio of solubility of Cu particles with high curvature particles to planar particles is highly influenced by the radius of the Cu particles. The smaller the particles, the higher the ratio, indicating higher solubility rate of Cu particles into molten Sn. For example, taking into consideration of typical values of γ = 2500 mJ/m^2 [2], V_{Cu} = 7.12 × 10^{-6} m^3 mol^{-1} [4], and T = 523 K, for r = 25 nm, and 2.5 μm, Cu_r/Cu_∞ can be estimated as 1.3, and 1.003, respectively. These results show that particles with small radius particularly in nano range exhibit additional effects on achieving equilibrium at higher rate.

On this regard, in this study, in order to accelerate the isothermal solidification process so that the Sn-phase will be completely remove to prevent the remelting event at 139 °C, nano-size Cu particles with primary particle size of 50 nm was selected to be mixed with Sn-Bi. The material under test is described in details in Chapter 3.

Determining the Sn-Bi addition amount

It is well established from Bi-Cu binary alloy phase diagrams (Figure 2.1) that Cu do not solute into Bi, and vice versa. Hence, it is not exaggeration to state that when Sn-Bi particles melt and wet the Cu nanoparticles, only Sn but Bi diffuse into Cu. Rapid solubility of Cu nanoparticles into molten Sn leads to the formation of two types of IMCs: Cu_6Sn_5 and Cu_3Sn, where Bi is precipitated throughout the process. If the solubility of Bi, and Cu-flux from Cu substrate are neglected, with the addition amount of Sn-Bi particles, the weight percentage of Sn to Cu, X_{Sn} can be calculated as follows:

$$X_{Cu} = 100 - \frac{0.43\beta}{(0.43\beta) + \alpha} \cdot 100 \tag{5.4}$$

where α is the weight percentage of Cu nanoparticles and β is the weight percentage of added Sn-Bi particles. From equation (5.4), weight percentage of Cu to Sn, X_{Cu} with different addition amount of Sn-Bi, and the phases that are expected to form in equilibrium state, are listed in Table 5.1. However, these phases will only be achieved if sufficient time is given for the reaction to reach an equilibrium condition. In practice, it is rather impossible and unattainable to achieve the equilibrium state within short processing time. Prolonging processing time is costly and unfriendly to the industry.

Table 5.1 Weight percentage of Cu to Sn, X_{Cu} with different addition amount of Sn-Bi and corresponding expected phases according to the equilibrium state Cu-Sn phase diagrams

Addition amount of Sn-Bi (wt. %)	X_{Cu} (wt. %)	Corresponding expected phases
10	95.4	Cu solid solution, Cu_3Sn
20	90.3	Cu solid solution, Cu_3Sn
30	84.4	Cu solid solution, Cu_3Sn
40	77.7	Cu solid solution, Cu_3Sn
50	69.9	Cu solid solution, Cu_3Sn
60	60.8	Cu_6Sn_5, Cu_3Sn
70	49.9	Cu_6Sn_5, Cu_3Sn
80	36.8	Cu_6Sn_5, Sn solid solution

According to [5], in Cu-Sn-Bi ternary system, a remelting event will occur at approximately 138.8 °C when unreacted Sn remained in the system. The calculated invariant equilibria is expressed as follows:

$$L \leftrightarrow Cu_6Sn_5 + (Sn) + (Bi) \tag{5.5}$$

The (Sn) and (Bi) is the solid solution of each phase at the eutectic temperature. Meanwhile, the composition in liquid was calculated as 56.90wt.% of Bi, 0.01wt.% of Cu, and 43.09wt.% of Sn. From above reaction, it can be interpreted that when there are three phases, i.e. Cu_6Sn_5, (Sn), and (Bi) locally co-exist, the remelting event will occur at the similar temperature of the Sn-Bi eutectic temperature. Moreover, the solubility of Cu in the liquid was extremely small, which implies that

albeit the mixture is ternary, the liquid phase is constantly exist as Sn-Bi binary system. Meanwhile, when the reaction between Sn and Cu was completed, the remelting event will occur at higher temperature than reaction (5.5). The calculated invariant reaction was expressed as below [5]:

$$L + Cu_3Sn \leftrightarrow Cu_6Sn_5 + (Bi) \quad (5.6)$$

where the melting event in reaction (5.6) occurred at 195.9 °C. It is obvious from reaction (5.6) that when all (Sn) phases was consumed to form both Cu_6Sn_5 and Cu_3Sn, the locally co-exist Cu_6Sn_5 and (Bi) shifted the remelting temperature from 138.8°C to much higher temperature. On the other hand, reaction (5.7) and reaction (5.8) that takes place at 270.3 °C and 270.2 °C, respectively expressed that with the absence of Cu_6Sn_5 phase, the remelting temperature will be shifted to a higher temperature.

$$L + Cu \leftrightarrow Cu_{41}Sn_{11} + (Bi) \quad (5.7)$$

$$L + Cu_{41}Sn_{11} \leftrightarrow Cu_3Sn + (Bi) \quad (5.8)$$

On this account, based on above background, to avoid the remelting event at 138.8°C as shown in reaction (5.5), the addition amount of Sn-Bi was selected to be below than 70wt%. It can be assumed that the formation of Cu_3Sn indicates that the amount of Cu is sufficient enough to be consumed by molten Sn, hence, not leaving any (Sn) phases. In addition, by selecting nanoscale compared to microscale Cu particles, the consumption of Cu particles into the Sn phase is assumed to be accelerated. However, in preliminary experiments on choosing the minimum addition amount of Sn-Bi, by decreasing the Sn-Bi, the liquid phase was insufficient to form a robust joint. In order to

investigate the influences of composition to the shear strength and microstructure, 50 wt.% was selected as the minimum addition amount of Sn-Bi. Cu nanoparticles, Sn-Bi microscale particles, and composition examined in this study are listed in Table 5.2.

Table 5.2 Composition of mixed Cu and Sn-Bi investigated in this study

Sn-Bi addition amount (wt. %)	Final Composition (wt. %)	Notation hereinafter (wt. %)
50	Cu-21.5Sn-28.5Bi	Cu-50SnBi
55	Cu-23.7Sn-31.4Bi	Cu-55SnBi
60	Cu-25.8Sn-34.2Bi	Cu-60SnBi
65	Cu-28.0Sn-37.1Bi	Cu-65SnBi
70	Cu-30.1Sn-39.9Bi	Cu-70SnBi

5.2 Selection of Organic Compounds

In the early stage of this study, several attempts has been made to prepare Cu and Sn-Bi mixture paste. In this section, organic compounds selection and the optimization of the added amount will be discussed. First, terpineol-added mixture paste will be discussed. Next, ethylene glycol-added mixture paste will be discussed. For each organic compounds, the advantages and drawbacks of the organic compounds will be explained. Finally, considering the preliminary experiments based on former and latter organic compounds, terpineol and ethylene glycol-added mixture paste will be discussed. The results from these preliminary experiments were used to investigate the effects of composition, sintering temperature, and sintering time to the shear strength and microstructure, which will be discussed in details in next section.

5.2.1 Terpineol-added Mixture Paste

Nanoscale particles are prone to agglomerate or aggregate even at low temperature due to their high surface energy. Compared to the bulk material, materials that exist in nanoscale comprised of higher surface area per volume. Even without applying high thermal energy to the system, nanoscale particles are easily agglomerated and/or aggregated to each other even at room temperature. The difference between agglomeration and aggregation is depicted in Figure 5.1.

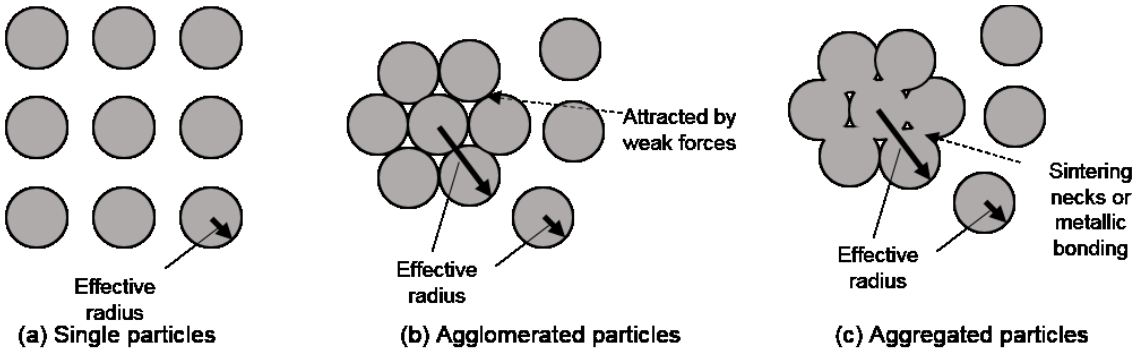

Figure 5.1 Differences of agglomeration and aggregation of particles

Agglomeration of particles occurred due to weak forces such as Van der Walls or electrostatic forces. Meanwhile, aggregation might occur due to the metallic bond which can be observed by the formation of sintering necks between particles. Both agglomeration and aggregation can be considered as defects if exist in green sintering paste. As can be seen in Figure 5.1, the effective radius of both types of defects in nanoscale is bigger than the primary particle size, hence, the benefits of using nanoscale particles cannot be realized, particularly on solid-solid sintering. The agglomeration of particles can be re-dispersed by external mechanical forces, but the aggregation of particles cannot be undone. Hence, it is common in the preparation of sintering paste of nanoparticles to apply an organic capping layer or surface activate agent to lower the surface energy of the nanoparticles. During sintering, the organic capping layer will burn-out at certain temperature depending on the chemical composition of the organic compound, thus, allowing the sintering of nanoparticles. Here, the selection of organic capping layer is essential to determine the minimum sintering temperature. Organic compound with low carbon chain is feasible to burn-out thus allowing sintering at relatively low temperature. Organic compounds with lower carbon chains are able to compose at lower temperature, however, the low number of carbon atoms in the carbon chains is insufficient to prevent the agglomeration and aggregation of the particles at low temperature. On this account, organic compounds with higher carbon chains were always chosen, by compromising high sintering temperature.

In this study, as explained in section 5.1, the addition amount of Sn-Bi into Cu nanoparticles is rather high, i.e. higher than 50 wt%. Taking into account that the average particles size of Sn-Bi is 2 μm, and bulk density of Sn-Bi is 8.54 g/cm^3 [6], which is equivalent to bulk Cu i.e. 8.96 g/cm^3, even 50 wt% addition of Sn-Bi is sufficient enough to wet all Cu nanoparticles and consumed it to form new phases. Hence, in this study, the usage of organic capping layer is intentionally omitted to achieve sintering at relatively low temperature. On contrary, one may suspect that at the early stage,

Cu nanoparticles would agglomerate and/or aggregate, but due to the nature of abundance of liquid phase that will be formed when heated, the influences of former and latter may be neglected since the mechanism of the sintering will switch to liquid phase sintering, instead of solid-solid sintering. In addition to that, the introduction of formic gas as explained in Chapter 3 and Chapter 4 is thought to facilitate the reduction of oxide layer at both Cu and Sn-Bi particles.

α-Terpineol, $C_{10}H_{18}O$ (hereinafter, TPO) was chosen to be mixed with Cu nanoparticles and Sn-Bi. Several studies had also adapted TPO as the solvent to mix particles owing to its viscosity at room temperature that is suitable for printing when mixed with appropriate amount of particles (the viscosity of TPO is 36.50 cP [7]). According to [7], boiling point of TPO at 1 atm. is 218 °C, vapor pressure is 5 mmHg, and temperature for vapor pressure is 80 °C. Although the theoretical boiling point of the TPO is higher than 200 °C, which is the target processing temperature in this study, the burn-out of the TPO might be achieved at rather lower temperature if the chamber pressure is lowered.

To find the suitable addition amount of TPO, three different ratio of TPO to the total particles of Cu-50SnBi was prepared and evaluated by means of shear strength. The varied weight ratios of Cu-50SnBi to TPO were 7:3, 8:2, and 9:1. Bonding was conducted with the same manner as described in Figure 3.10. Figure 5.2 shows the shear strength of Cu-50SnBi samples with different TPO ratio that were bonded at 250°C for 90 and 150 min. As can be seen in Figure 5.2, the shear strength was at the lowest at both sintering times when bonded with weight ratio of 9:1. The shear strength reached its peak when bonded with weight ratio of 8:2. At weight ratio of 8:2, the obtained shear strength of samples bonded at 150 min was approximately 10 MPa, with the highest recorded was up to 16 MPa.

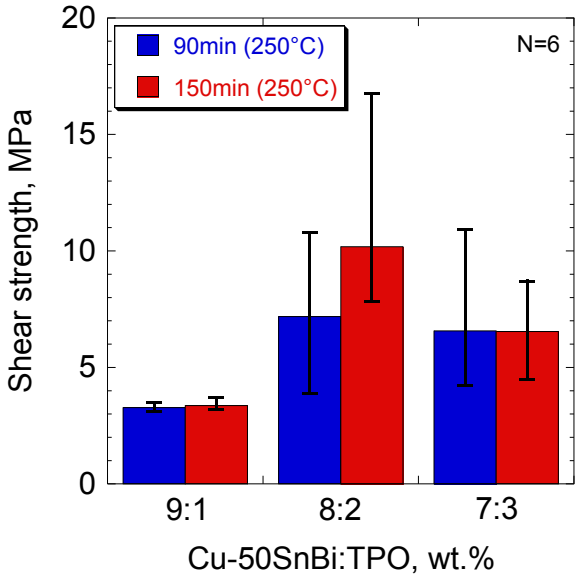

Figure 5.2 Shear strength of Cu-50SnBi with different weight ratio of particles:TPO bonded at 250°C for 90 and 150 min

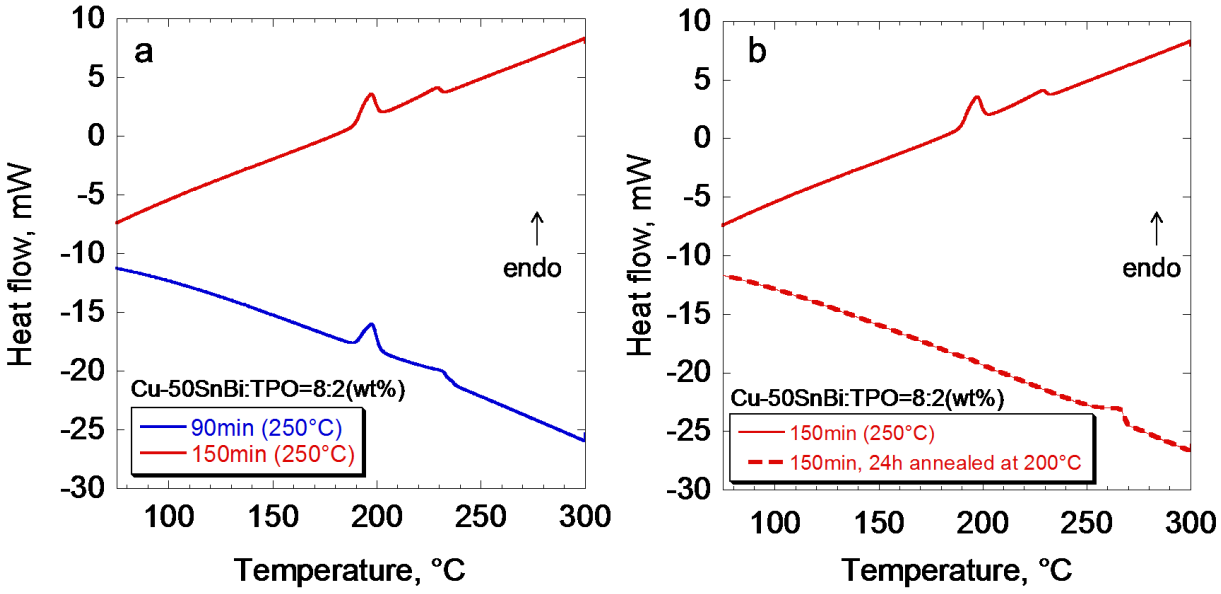

Figure 5.3 DSC test results of Cu-50SnBi with Cu-50SnBi:TPO=8:2 (a) sintered at 250 °C at two different sintering temperatures, and (b) annealed at 200 °C for 24h after sintered at 250 °C for 150 min

Figure 5.3a shows the DSC results of Cu-50SnBi with weight ratio of particles:TPO=8:2 sintered at 250°C for 90 and 150 min, which showed the highest shear strength as can be seen in Figure 5.2. At both sintering holding times, the remelting event of Cu-50SnBi was observed at approximately 195.0 °C. It was lower than expected remelting temperature, i.e. approximately 270°C, as explained by reaction (5.8) due to the expected phase to be formed in Cu-50SnBi were Cu_3Sn and Bi-rich phase. The remelting event at 195.0 °C coincide well with the temperature of invariant reaction (5.6), which implied that instead of Cu_3Sn, the major phases existed in the Cu-50SnBi even after sintering at 250 °C for 150 min was Cu_6Sn_5 and Bi. Figure 5.3b shows the DSC results of Cu-50SnBi sintered at 250°C for 150 min, with and without annealing process at 200°C for 24 hours. As can be seen from the heat flow curve of annealed sample, the remelting temperature shifted from 195°C (without annealing) to approximately 268°C. This indicated that sufficient time had been given to allow the diffusion of Cu and Sn to convert the Cu_6Sn_5 to Cu_3Sn.

The remelting event at 195 °C instead of 270 °C might be resulted by the slow solubility rate of Cu nanoparticles into the molten Sn although with the introduction of formic gas. It was assumed that the as-received Cu nanoparticles in the methanol solution was initially oxidized at the surface. Formic gas was introduced to reduce the oxide layer and improve the wetting between the molten Sn and Cu to further the isothermal solidification process by the formation of Cu_6Sn_5 and subsequently phase transformation to Cu_3Sn. However, in the case of TPO mixed paste, it was thought that the sintering time might be insufficient to completely reduce the oxide layer and delayed the wetting to commence the reaction between Cu and Sn.

To achieve the desired phases within sintering time, organic compound with reducing effect need to be introduced into the paste so that oxide layer on both Cu and Sn particles can be reduced as early as possible during the heating, and further assisted with the reducing effect by formic gas. This will be explained in the next section.

5.3.2 Ethylene Glycol-added Mixture Paste

As described in Figure 3.10, formic gas was introduced into the chamber from 150 °C. Hence, it is more favorable if the reduction effects of can take place at lower temperature to assist the wetting of the Sn-Bi to the Cu nanoparticles and Cu-substrates at relatively earlier time compared to the reduction by formic gas which will occur at temperature higher than 150°C. To realize the reduction of oxidize surface of Cu and Sn-Bi, organic compounds that can act as a reductant need to be introduced into the paste to assist the reduction process at lower temperature. One approach that can be applied is by referring to the method of synthesizing nanoparticles. Synthesis of nanoparticles has been conducted by several approaches, such as chemical vapor deposition (CVD), physical vapor deposition (PVD), chemical reduction, and many others. In chemical reduction method, metal precursor was added into reductant and heated to obtain the metal particles. Here, literature review focusing on synthesis of nanoparticles by chemical reduction method has been conducted to find the suitable reductant. Some studies related to synthesis of nanoparticles by chemical reduction method are listed in Table 5.3.

According to Table 5.3, ethylene glycol (EG), $C_2H_6O_2$ and its polyether (PEG), $H{-}(O{-}CH_2{-}CH_2)_n{-}OH$ had been used vastly as a reductant in reducing metal precursor to synthesis nanoparticles. Organic capping layer is also essential to protect the newly synthesized nanoparticles from agglomerated and/or aggregated to each other. In chemical reduction method, metal precursor, reductant, and organic capping layer are put together in organic solvent and heated to the boiling point of the reductant for several minutes or hours. The reduction of metal precursor by the reductant, and the organic capping layer as a protective layer resulted in monodispersed nanoscale materials in the organic solvent. Finally, after centrifugation and vacuum drying, dry samples of nanoscale particles are collected. The usage of ethylene glycol was proved as a good reducing agent to reduce oxide material to its metal state. The reaction of reduction by using ethylene glycol is described as follows:

Table 5.3 Reducing agent and organic capping layer that were used in previous studies on synthesis of nanoparticles by chemical reduction method

First author	Reducing agent	Organic capping layer	References
Yusuke Sakuda	Ascorbic acid	Hexylamine Octylamine Decylamine	[8]
Tomohiro Yagishita	PEG200 PEG400 EG, DEG, TEG	-	[9]
Yan Jiafeng	Sodium hypophosphile	PVP	[10]
T. Ishizaki	Ethylene glycol	Fatty acid fatty amine	[11]
Toshitaka Ishizaki	Ethylene glycol	Oleic acid Oleyl amine	[12]
Chengcai Luo	PEG	-	[13]
Monica Popa	PEG200	-	[14]

$$2CH_2OH\text{-}CH_2OH \rightarrow 2CH_3CHO + 2H_2O \quad (5.9)$$

$$2CH_3CHO + M(OH)_2 \rightarrow CH_3COCOCH_3 + 2H_2O + M \quad (5.10)$$

Acetaldehyde, CH_3CHO, which is produced by the dehydration of ethylene glycol as shown in reaction (5.9) exhibits strong reducing agent when heated [24]. If this characteristic is utilized well, the oxidize surface of Sn-Bi powders and Cu nanoparticles can be reduced at relatively lower temperature than the formic gas reduction onset temperature.

In this study, ethylene glycol was introduced into the Cu-based sintering paste to realize the reduction of the oxide layer of the Sn-Bi and Cu particles during heating, even earlier than the introduction of formic gas at temperature higher than 150 °C. This is thought to assist the reduction

of the oxide layer at lower temperature as possible. In order to achieve bonding at lower temperature, the selection of ethylene glycol or its polyether is essential since the boiling point is different with increasing molecular weight. It was also understood that with increasing molecular weight, i.e. with increasing chain length, physical properties of the polyethylene such as viscosity would also change. Thus, selecting the suitable ethylene glycol or polyethylene glycol is important. Table 5.4 shows several properties of ethylene glycol and its polyether [15].

As can be seen from Table 5.4, MEG or DEG is suitable candidate to be added into Cu-SnBi mixture paste owing to their boiling point that are lower than 250°C, which is the maximum target processing temperature in this study. In addition, the viscosity of DEG is equivalent to TPO (36.50 cP [7]), which imply that DEG is also suitable as replacement for the TPO. In this study, to achieve bonding at temperature as low as 200°C, MEG is the perfect choice since its boiling point is lower than 200°C. As a preliminary study, Cu-50SnBi was mixed with ethylene glycol (hereinafter, EG). Three different weight ratios of particles (Cu-SnBi) to the EG was prepared i.e., particles:EG = 95:5, 9:1, 8:2) Shear strength and remelting temperature were examined for each condition. Figure 5.4 shows the DSC results of Cu-50SnBi mixed with EG sintered at 200°C for 90 min. The weight ratio of the particles:EG was 9:1. For the sake of comparison, DSC result of Cu-50SnBi that were mixed with TPO with same weight ratio is also depicted in the same figure. Note that the sintering temperature of the TPO-mixed Cu-50SnBi was different, i.e. 250°C at 90 min. It can be seen from the DSC result that remelting temperature of Cu-50SnBi mixed with EG can be observed at approximately 270°C, indicating the melting event of Bi-rich phase as shown in reaction (5.8). Thus proving that mixing EG into the mixture paste was effective to accelerated the oxide surface reduction and wetting of Sn-Bi particles. However, the obtained shear strength at all weight ratio was extremely low which the highest was approximately 3.3 MPa, shown by 9:1 weight ratio. For weight ratio of 95:5 and 8:2, the shear strength cannot be determined since all samples delaminated from early stage

of shear test. This is somehow understandable since the viscosity of the EG is approximately half of the TPO. Although same weight ratio was used, the low viscosity of EG means more inter-particles spacing, which in return lead to low shear strength since the particles were highly spaced between each other and metallic bonding is expected to be limited.

Table 5.4 Properties of ethylene glycol and its polyether [15]

	Monoethylene glycol MEG	Diethylene Glycol DEG	Triethylene Glycol TEG	Tetraethylene Glycol TETRA EG
Formula	$C_2H_6O_2$	$C_4H_{10}O_4$	$C_6H_{14}O_4$	$C_8H_{18}O_5$
Molecular weight, g/mol	62	106.12	150	194.2
Boiling point at 1 atm, °C	197	245	288	329
Viscosity at 25°C, cP	16.9	35.7	49.0	58.3

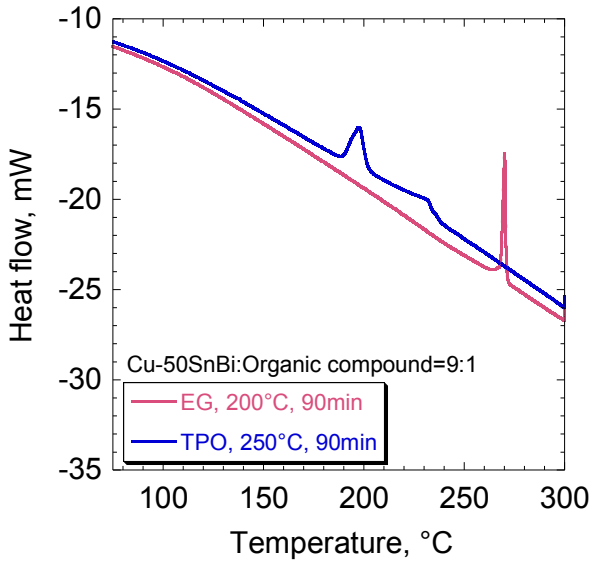

Figure 5.4 DSC results of Cu-50SnBi mixed with TPO or EG with weight ratio of (9:1)

5.3.3 Terpineol and Ethylene Glycol-added Mixture Paste

Since it was comprehended that mixing particles with EG alone was not suitable to prepare the mixture paste due to the low viscosity of the EG, both EG and TPO was mixed together to achieve a printable mixture paste with reduction effect at relatively low temperature compared to the formic gas reduction effect. This newly proposed combination is expected to enable bonding at sintering temperature lower than 250°C, and achieve the desired remelting temperature depending on the composition within processing time, without the application of further annealing process. As a preliminary study, Cu-50SnBi were mixed with TPO and EG with the following weight ratio, i.e. Cu-50SnBi:TPO:EG=80:15:5. Weight percentage of particles was chosen as 80 wt% based on results obtained in Figure 5.2, in which Cu-50SnBi exhibited the highest shear strength. Remelting temperature was examined to verify the effectiveness of combining both organic compounds to achieve the aims as stated above. Sintering of Cu-50SnBi was conducted at 250 °C with 30 min sintering holding time.

Figure 5.5 shows the DSC analysis result of Cu-50SnBi. Even at sintering time of 30 min, remelting temperature was observed at the expected temperature, i.e. at the Bi-rich phase melting temperature. It can be concluded that the newly improvised mixture paste was effective to promote the sintering paste to obtain the designated microstructure within sintering process.

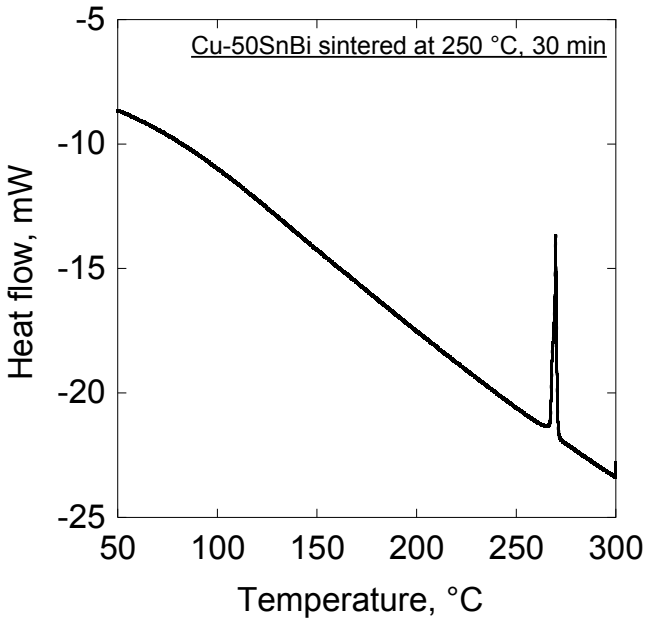

Figure 5.5 DSC analysis of Cu-50SnBi (Cu-SnBi:TPO:EG=80:15:5) sintered at 250°C for sintering time of 30 min

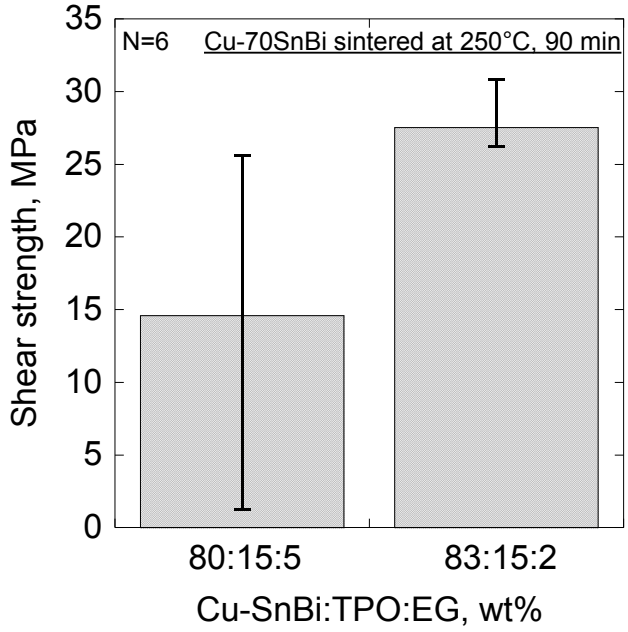

Figure 5.6 Shear strength of Cu-70SnBi with different weight ratio of Cu-SnBi:TPO:EG

Next, in order to search the optimum weight ratio of the newly proposed mixture paste, focusing on Cu-70SnBi, mixture paste with weight ratio of Cu-70SnBi:TPO:EG=83:15:2 was prepared. Weight percentage of TPO was kept constant while increasing the weight percentage of particles and decreasing the weight percentage of EG. Figure 5.6 shows the shear strength of Cu-70SnBi with two different weight ratios of Cu-70SnBi to the TPO and EG bonded at 250°C for 90 min. It was clear from Figure 5.6 that by increasing the weight precentage of particles (Cu nanoparticles and Sn-Bi particles), the shear strength was also increased. The DSC analysis of the Cu-70SnBi with weight ratio of particles:TPO:EG=83:15:2 sintered at 250 °C with different sintering time, which is not shown here demonstrated that the remelting temperature was observed at approximately 139 °C and 200 °C (the remelting at 139 °C will be discussed in the next section). Hence, from above finding, it can be concluded that, even with 2 wt.% addition of EG, the expected remelting event can be achieved within short period of time while increasing the shear strength of the bonded materials owing to increasing weight percentage of particles in the mixture paste.

Since it was clear that the effect of increasing weight percentage of particles while keeping the weight percentage of EG to 2 wt.% can lead to increasing shear strength and the desired remelting temperature can also be achieved within processing time, next, the weight ratio of the particles, TPO, and EG was examined in details. Cu-70SnBi was focused on to investigate the effect of the weight ratio of the mixture paste to the shear strength. Four kinds of weight ratio of particles:TPO:EG was investigated, i.e. 83:15:2, 85:13:2, 87:11:2, and 89:9:2. Weight percentage of EG was kept constant so that the effects of reduction by EG can be realized. Weight percentage of particles was increased and weight percentage of TPO was decreased accordingly. Shear test was conducted to examine the influences of the weight ratio of the mixture paste to the shear strength. Figure 5.7 shows the shear strength of Cu-70SnBi with different weight ratio of particles:TPO:EG bonded at 250°C for 60 min.

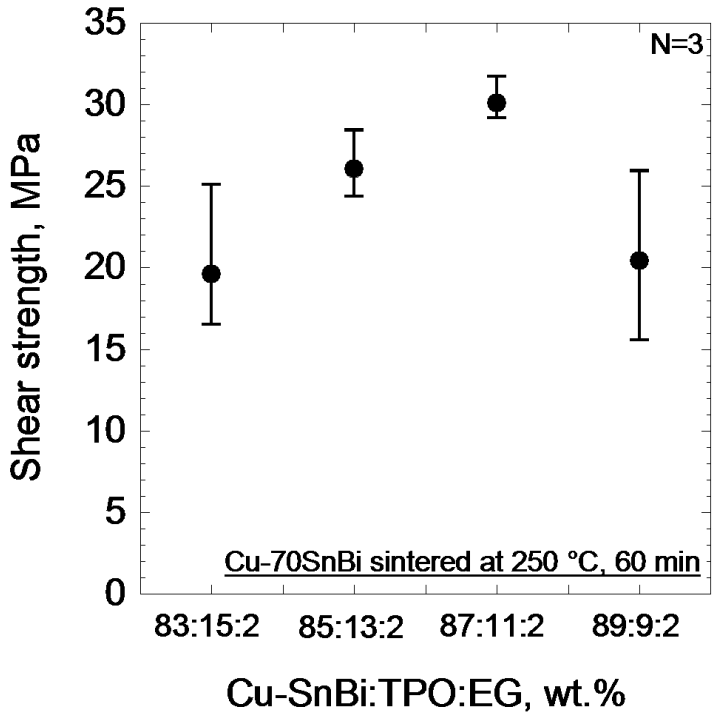

Figure 5.7 Shear strength of Cu-70SnBi with different weight ratio of particles:TPO:EG bonded at 250°C for 60 min

As can be seen, from Figure 5.7, with increasing weight percentage of the particles in the mixture paste, the shear strength was also increased. Shear strength reach its peak when the weight percentage of the particles is 87 wt.%. It is thought that with increasing weight percentage of the particles, the inter-particles spacing would also be increased, thus, in return led to a more packed and dense microstructure. However, when the weight percentage of the particles exceeded some threshold values, the particles tend to agglomerate and/or aggregate with each other. The mixture paste viscosity would also be decreased, and it was rather hard to stencil-printing the paste. As a conclusion, weight ratio of the particles:TPO:EG=87:11:2 can be expressed as the suitable weight ratio in preparing the mixture paste for further investigation.

5.3 Effects of Alloy Composition

5.3.1 Effects on Shear Strength and Microstructure

Figure 5.8 shows the influence of the Sn-Bi addition amount on the shear strength of Cu-SnBi that was sintered at 250 °C. As seen in Figure 5.8, with increasing amount of Sn-Bi, the shear strength was also increased. Cu-65SnBi and Cu-70SnBi exhibited average shear strength higher than 20 MPa regardless of sintering holding time, which was higher than conventional Pb-5wt%Sn solder (18 MPa) [16]. Although average shear strength shown by Cu-55SnBi was 4.8 MPa, it is remarkable to state that the average shear strength of all composition obtained in this study passed the specification of MIL-STD-883K [17]. Omid Mokhtari et al. bonded plateless Cu-Cu substrates using Cu-70wt%SnBi with conventional reflow process at 200°C [2]. The average shear strength obtained in their study was approximately 25 MPa, which in a good agreement with the shear strength of Cu-65SnBi in our study. However, in their study, the mean large void area fraction in solder joints after conventional reflow was approximately 49.0%, which will be detrimental for solder as a heat-conductance material since the contact area between the solder and substrates were reduced. On contrary, in our study, large voids were less observed as will be explained in the next section.

Figure 5.9 illustrates the XRD pattern of Cu-55SnBi, Cu-60SnBi, and Cu-65SnBi samples that was sintered at 250°C. As seen in Figure 5.9, at 35°, Cu_6Sn_5 (11-3) plane was not detected in Cu-55SnBi whereas the peak intensity at the same angle became larger with increasing Sn-Bi amount, implying that Cu_6Sn_5 phases became more prominent in Cu-65SnBi. On contrary, the peak intensity of Cu_3Sn (101) plane at 32° and (120) plane at 43° were getting smaller towards Cu-65SnBi, which manifested that the amount of Cu_3Sn IMCs in Cu-65SnBi were fewer compared to the Cu-55SnBi. Using reference intensity ratio (RIR) method, the amount of each phase detected in XRD data were quantitatively calculated.

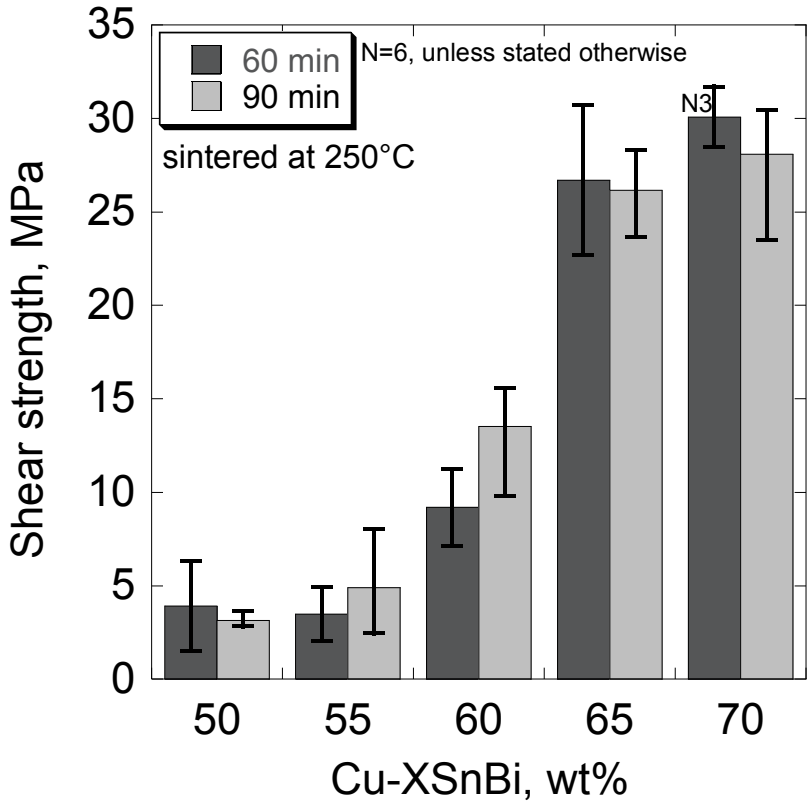

Figure 5.8 Effects of Sn-Bi addition amount to the shear strength of Cu-based TLPS sintered at 250 °C with different sintering holding time

Figure 5.10 demonstrates the weight percentage of each constituent phase for each condition as calculated by RIR method. Error bar presents the standard deviation. The weight percentage of Cu at all condition was less than 0.5%, which indicated that almost all Cu nanoparticles was converted to Cu-Sn IMCs during isothermal solidification. On the other hand, the amount of Cu_3Sn and Cu_6Sn_5 IMCs decreased and increased respectively with increasing addition amount of Sn-Bi, in which the tendency agreed well with the earlier assumption explained by equation (5.4). However, the measured value did not coincide well with the value calculated according to the lever rule.

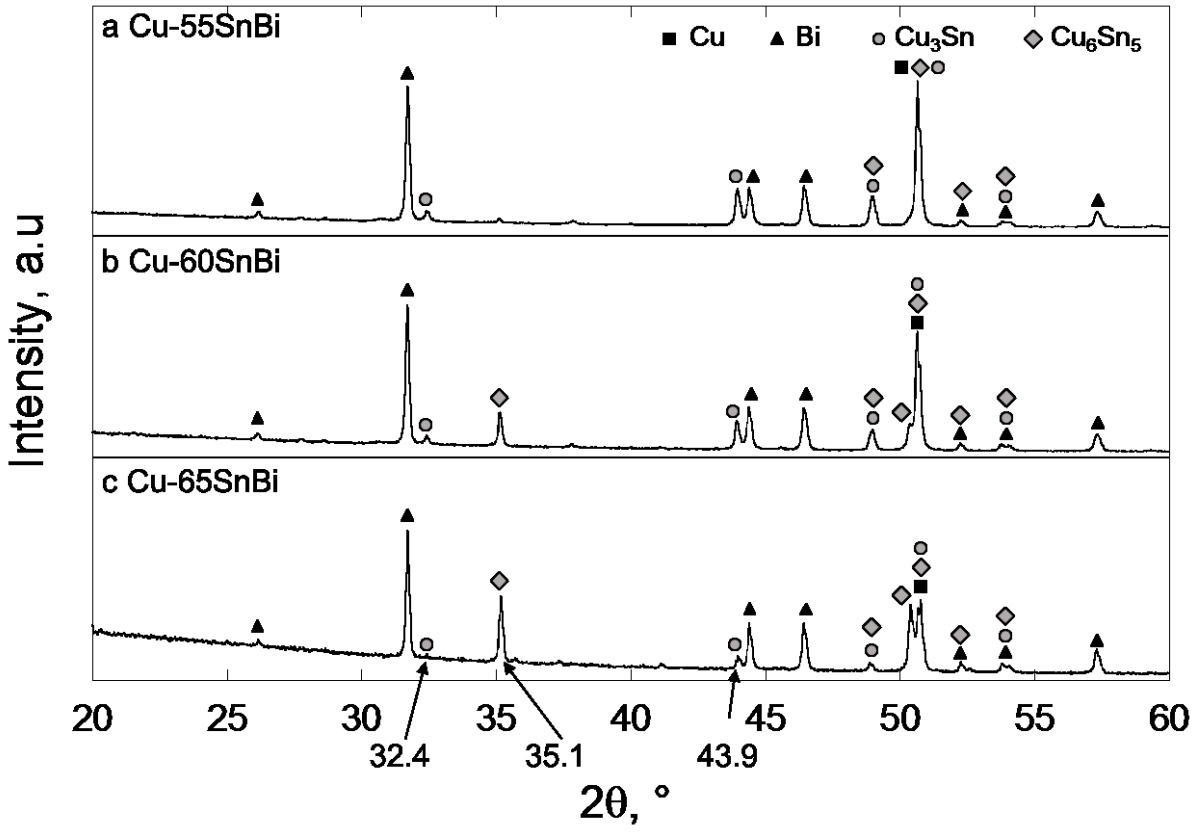

Figure 5.9 XRD pattern of Cu-55SnBi, Cu-60SnBi, and Cu-65SnBi sintered at 250 °C with different sintering holding time

Figure 5.11 presents the cross-sectional SEM image of samples with different alloy composition that was sintered at 250°C. As can be seen in Figure 5.11a, Cu-55SnBi exhibited a porous skeleton-type structure mixed with unevenly distributed densified microstructure, consisted of Cu_3Sn and Bi-phase. Meanwhile, Cu-60SnBi (Figure 5.11b) and Cu-65SnBi (Figure 5.11c) showed densified microstructure in which Cu-Sn IMCs can be observed at the interface and distributed randomly in the matrix of the Bi phase (white phase). Several voids with irregular shape can be found scattered in the matrix at both alloy compositions.

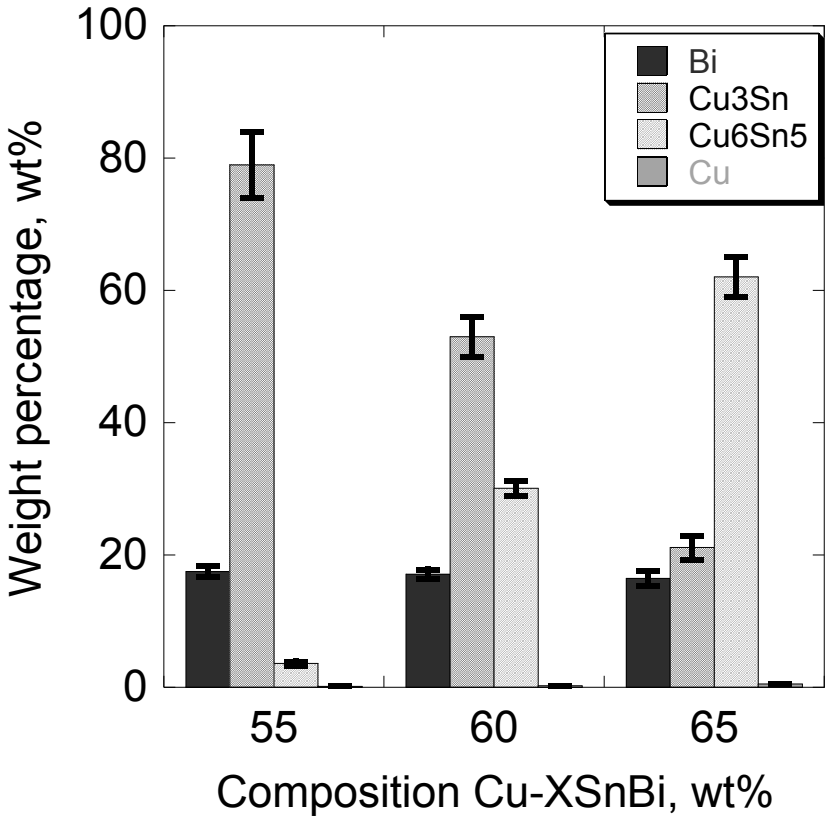

Figure 5.10 Weight percentage of phases in Cu-55SnBi, Cu-60SnBi, and Cu-65SnBi sintered at 250 °C with different sintering holding time as calculated by the RIR method from the XRD analysis conducted in Figure 5.9

The difference of microstructure between these three alloy compositions might be explained as follows. According to T. D'Hondt et al. [18] and National Institute of Standards and Technology [5], in ternary Cu-Sn-Bi, a new melting event is introduced over 195.9 °C as a result of the localize reaction between Bi and Cu_6Sn_5 as shown in the reaction (5.6). For above reaction to take place, the Bi must be above 99.89wt% [5]. In this investigation, all Cu-SnBi mixture were sintered at 250 °C. It can be expected that due to the rapid solubility of Cu nanoparticles into molten Sn, the isothermal solidification was completed within few minutes after the melting of Sn-Bi resulting in the formation

of Cu_6Sn_5 and Bi. Subsequence heating to the sintering temperature i.e. 250 °C, giving way for reaction (5.6) to take place over the provided temperature, i.e. at temperature higher than 195 °C. This newly generated liquid phase was thought to facilitate the rapid densification of the microstructure since the diffusion of atom in liquid phase is generally faster compared to the diffusion in solid phase.

In Cu-55SnBi where Cu nanoparticles were abundance and assisted by the rapid solubility of nanoparticles into molten Sn, it was predicted that after the isothermal solidification process was completed, not only Cu_6Sn_5, but Cu_3Sn was also formed. This resulted in unevenly distributed Cu_6Sn_5, Cu_3Sn, and Bi-phase. When reaction (5.6) took place, only the locally concentrated Cu_6Sn_5 and Bi reacted to form liquid phase, which produced the unevenly distributed densified microstructure, as observed in Figure 5.11a. Meanwhile, in Cu-60SnBi and Cu-65SnBi where the amount of molten Sn is greater, it was suspected that almost no Cu_3Sn phase was formed after the isothermal solidification process was completed, and the homogenously formed Cu_6Sn_5 and Bi were assumed to assist the densification of the microstructure via liquid phase introduced by reaction (5.6).

The difference of microstructure observed in Figure 5.11 is thought to influence the strengthening mechanism of each alloy composition. Low shear strength shown by Cu-55SnBi as demonstrated in Figure 5.8 might be caused by the voids-dominated porous microstructure. Such voids can be the site for stress concentration and crack initiation, and eventually influence the strength of the joints. Although some voids can also be observed in Cu-60SnBi and Cu-65SnBi, the higher shear strength exhibited by Cu-65SnBi compared to the Cu-60SnBi might be attributed by the greater composition of Cu_6Sn_5 as shown in Figure 5.10. It was understood that the hardness of Cu_6Sn_5 was higher than Cu_3Sn [19], hence the greater composition of Cu_6Sn_5 in Cu-65SnBi might contribute in higher shear strength.

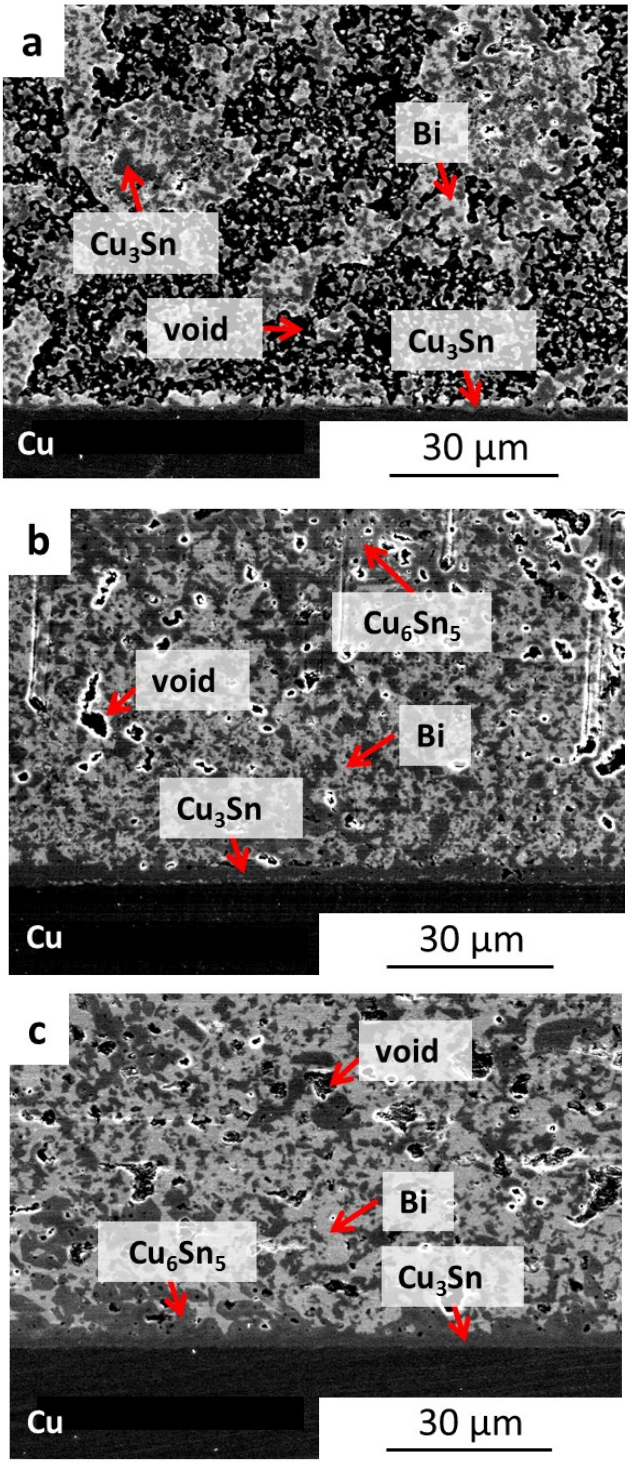

Figure 5.11 SEM (SE) images of (a) Cu-55SnBi, (b) Cu-60SnBi, and (c) Cu-65SnBi, that was sintered at 250 °C and 90 min

5.3.2 Effects on Remelting Temperature

Figure 5.12 illustrates the DSC analysis result of Cu-SnBi with different Sn-Bi addition amount sintered at 250 °C for 90 min. Remelting temperature of Cu-50SnBi and Cu-55SnBi was observed at approximately 270 °C, implying the remelting of Bi-phase as shown in Reaction (5.8). This finding is in good agreement of the early assumption that predict the formation of Cu_3Sn and Bi phase in the microstructure after sintering was completed, as shown in Table 5.1.

On the other hand, according to Figure 5.12, Cu-60SnBi shows one remelting event, i.e. at approximately 200 °C, while Cu-65SnBi and Cu-70SnBi exhibit two remelting event, i.e. at approximately 138 °C and 200 °C. The melting event at 138 °C shown by Cu-65SnBi and Cu-70SnBi is thought to be the melting of the solidified liquid phase from reaction (5.6) due to the solidification in non-equilibrium state. According to [18], although the liquid phase was ternary in nature, the solubility of Cu in the liquid phase is negligible small, and remained to act as binary Sn-Bi. Hence, during the cooling stage, which is thought to be in non-equilibrium state, the liquid phase was expected to solidify as 78.10Bi-21.87Sn-(0.03Cu), and once heated, remelt again at the eutectic temperature (at approximately 138 °C). In this study, cooling stage was conducted with cooling rate of 10 °C/min. From the cooling curves of DSC test which will be explained later in Figure 5.21b, undercooling was observed, indicating a non-equilibrium state during the cooling. Note that the cooling rate in DSC test conducted in this study was slower, i.e. at 5 °C/min.

The locally co-existing Cu_6Sn_5 and Bi is the main precursor on initiating the reaction (5.6). Although the final microstructure in Cu-60SnBi is assumed to be a mixture of Bi, Cu_6Sn_5, and Cu_3Sn, the remelting event at 138 °C by the reaction (5.6) was not found, as shown in Figure 5.12. The volume fraction of the liquid from reaction (5.6) in Cu-60SnBi was thought to be negligible small to be detected by the DSC test.

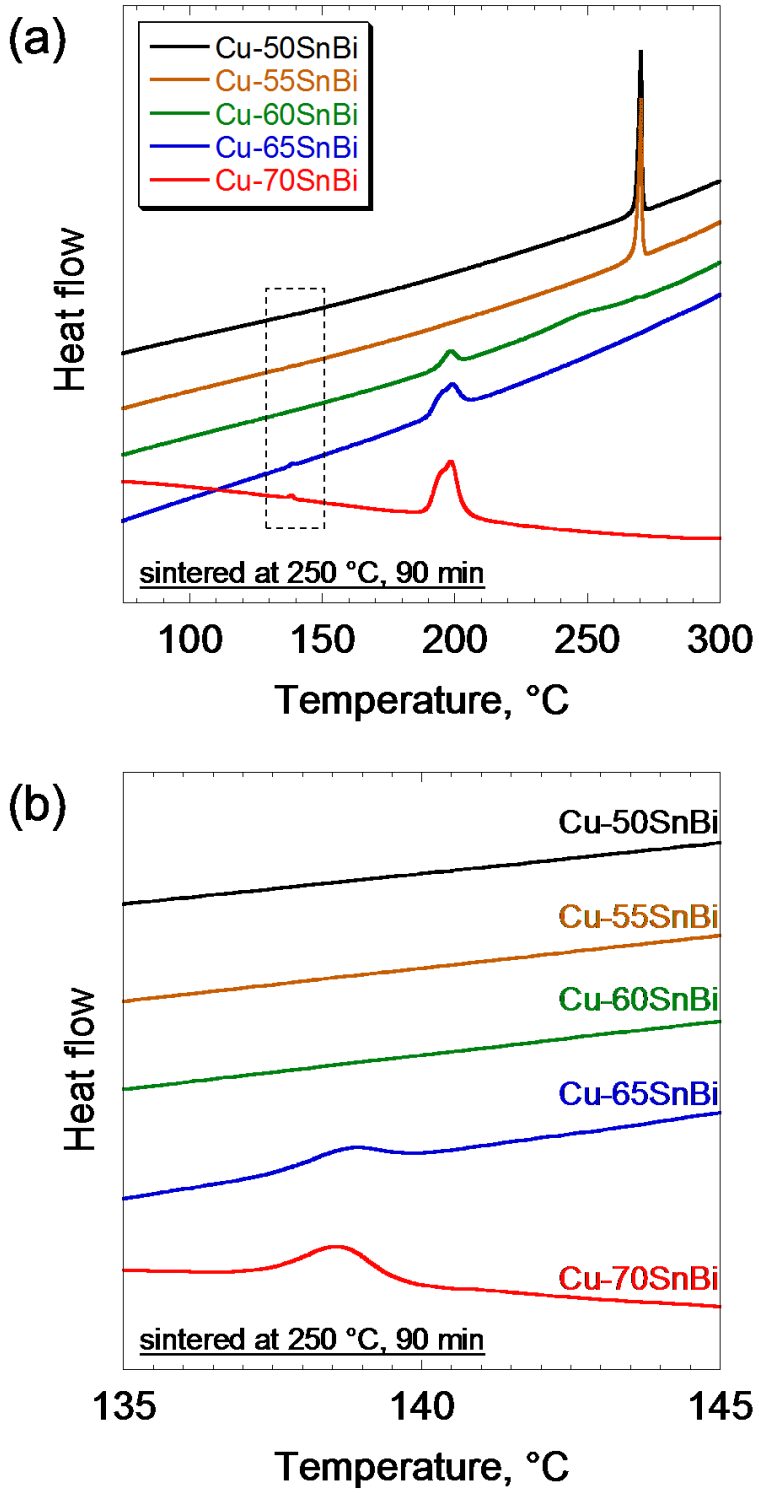

Figure 5.12 (a) DSC result of Cu-SnBi with different Sn-Bi addition amount sintered at 250 °C for 90 min. and (b) shows the DSC result of the magnified area shown in (a)

5.4 Effects of Sintering Parameters

5.4.1 Sintering Holding Time

Figure 5.13 demonstrates the effect of sintering holding time to the shear strength of Cu-65SnBi samples bonded at sintering temperature of 250 °C. From 0 to 30 min, shear strength increased abruptly with 64% rise in average shear strength. Then, the rise percentage declined to approximately 11% from 30 to 60 min. Subsequently, from 60 to 90 min, the shear strength was maintained at approximately 26 MPa. It is noteworthy to state that the average shear strength of Cu-65SnBi achieved at all sintering holding time passed the specification of MIL-STD-883K, which requires shear strength greater than 2.5 MPa for bonding area more than 4.1 mm^2 (bonding area in this study was 19.6 mm2) [17].

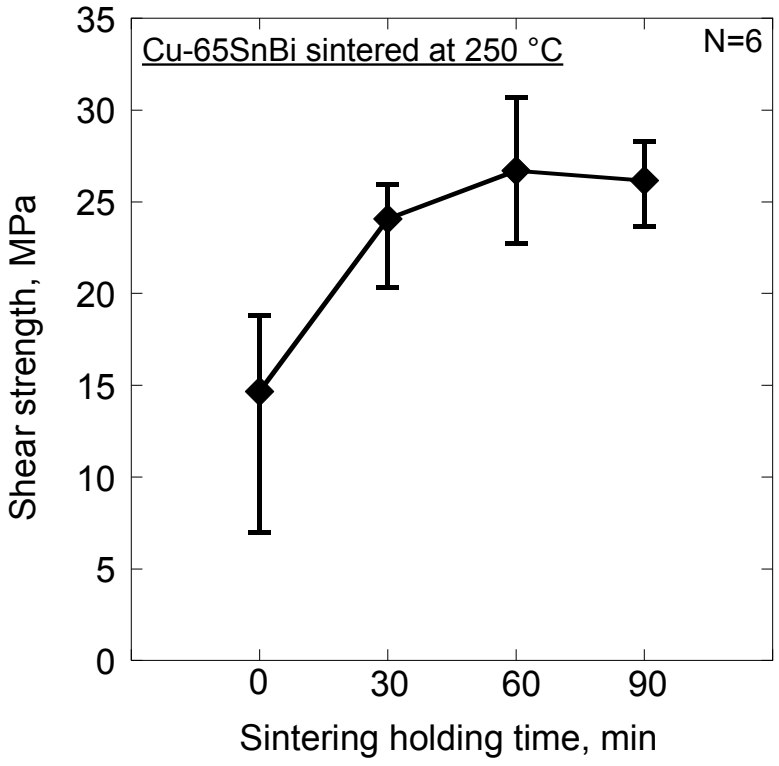

Figure 5.13 Shear strength of bonded Cu-65SnBi with different sintering holding time at sintering temperature of 250°C

On the other hand, average shear strength of Cu-70SnBi when sintered at 90 min decreased by approximately 3 MPa, compared to that of 60 min, as illustrated in Figure 5.8. Meanwhile, as seen in Figure 5.8, the shear strength of Cu-55SnBi and Cu-60SnBi when sintered for 90 min was slightly increased as compared to that of 60 min.

Figure 5.14 shows SEM images of Cu-65SnBi sintered at 250°C for 0 and 90 min sintering holding time. No significance difference of cross-sectional microstructure can be observed between 0 and 90 min sintering holding time. Gray shades which represent the Cu-Sn IMCs were smaller and scattered at 0 min as compared to the 90 min sintering holding time, as seen in Figure 5.14a and c. By prolonging sintering time, it is assumed that interdiffusion between Cu-Sn IMCs leads to grain growth and rearrangement of the grains, which also resulted in grain growth of Bi-rich phases. Although microscale voids were still visible in both conditions, they were less prominent in 90 min sintering holding time owing to the densification of the grains. This phenomenon was similarly observed in Ag sintering where the densification of solid-solid sintering was achieved by prolonging sintering time [20]. Meanwhile, at the interface, Cu_3Sn IMCs layer were thicker at 90 min with increasing sintering holding time as can be observed in Figure 5.14b and d. The Cu_3Sn layer thickness was approximately 1 μm at 0 min but increased to approximately 4 μm with 90 min sintering holding time. However, no Kirkendall voids were observed at Cu substrate and Cu_3Sn IMCs interface that were usually found in conventional solder, despite the 90 min sintering time [21].

As a conclusion, the factors that contributed to the strengthening of Cu-65SnBi with prolonging sintering holding time was unclear, but densification of the microstructure via liquid phase that was formed by reaction (5.6) is assumed to play a vital role.

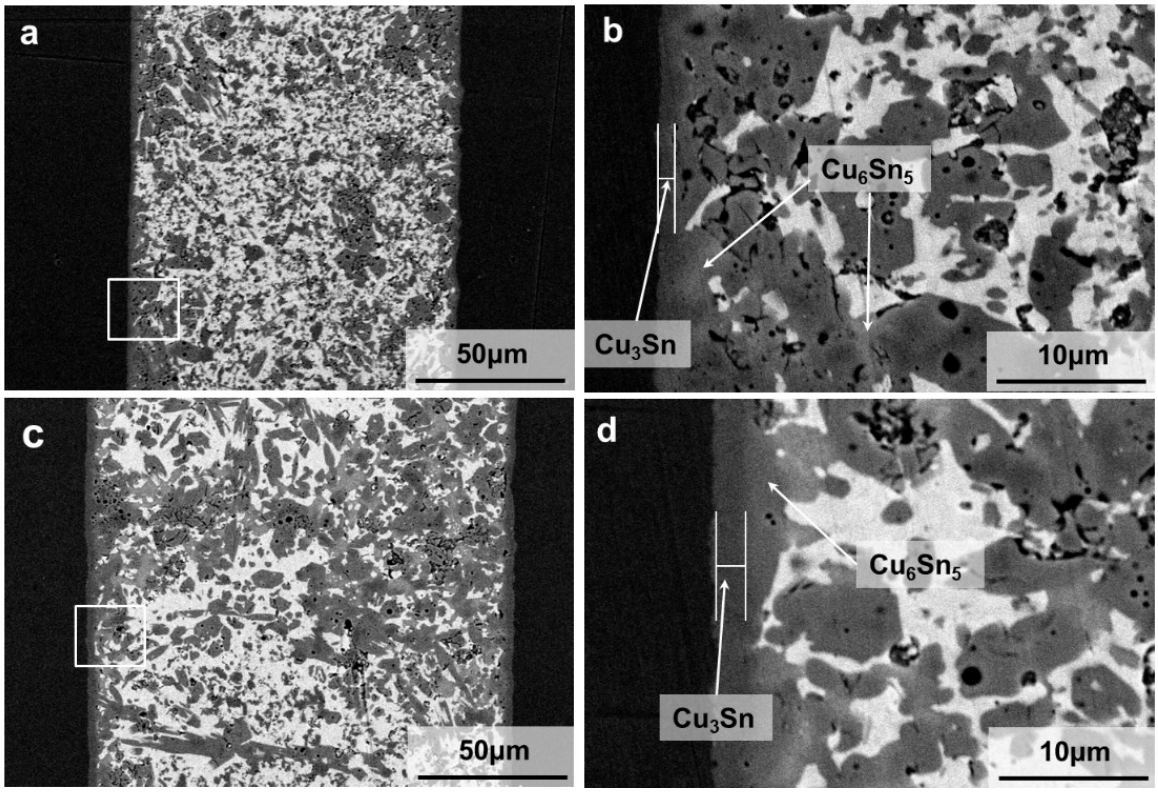

Figure 5.14 **a**, **c** SEM images of Cu-65SnBi sintered at 250°C with 0 min and 90 min sintering holding time, respectively, and **b**, **d** magnified image in area (white box) shown in a and c

5.4.3 Sintering Temperature

Next, to investigate the influence of sintering temperature on the shear strength, Cu-65SnBi and Cu-70SnBi that demonstrated shear strength higher than 20 MPa as seen in Figure 5.8 was selected and sintered at four different sintering temperatures. Figure 5.15 shows the influence of sintering temperature on the shear strength of Cu-65SnBi and Cu-70SnBi that was sintered from 180°C to 250°C. It was demonstrated that with increasing sintering temperature, the shear strength was also increased for both compositions. At all sintering temperature, Cu-70SnBi projected shear strength slightly higher than Cu-65SnBi. Average shear strength showed by the samples sintered at 180°C for both compositions was lower than 5 MPa, which was the lowest. Although the average shear strength of Cu-65SnBi and Cu-70SnBi sintered at 200°C was 15.3 MPa and 17.2 MPa, respectively, it is noteworthy to state that the highest shear strength obtained was 21.2 MPa and 22.3 MPa, which was equivalent to the conventional Pb-based solder [16]. Toshitaka Ishizaki et al. reported that the shear strength of Cu-10wt%Sn also increased by increasing sintering temperature [22]. The highest shear strength obtained in their study, which equivalent to the shear strength of samples sintered at 250 °C in this work, was achieved at sintering temperature of 350 °C. On the other hand, in the same work, it was demonstrated that in hydrogen atmosphere at sintering temperature of 350 °C, Ni layer that was deposited on the Cu plates facilitated the reducing of CuO of Cu-particles to Cu, hence, contributing to higher shear strength in comparison to the plateless Cu substrates. However, in our study, formic gas environment was introduced to assist the wetting of added Sn-Bi particles and suppressed the oxidation of both Cu nanoparticles and Cu substrates at relatively lower temperature compared to hydrogen environment. It was also reported that the reduction reaction using formic gas took place at as low as 150 °C which is highly desired for low temperature processing [23].

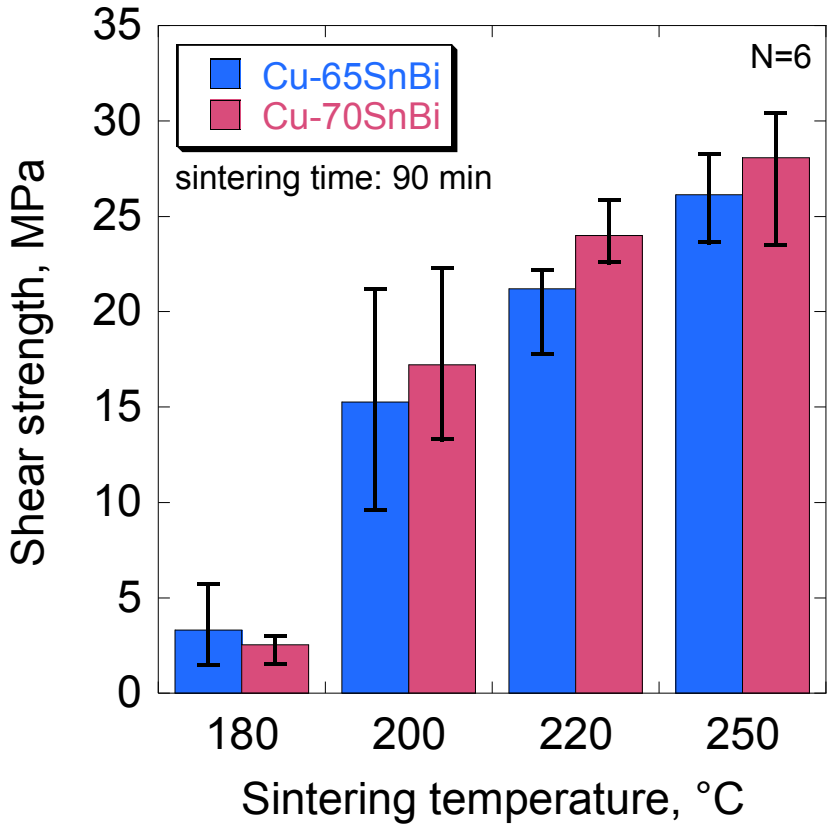

Figure 5.15 Shear strength of Cu-65SnBi and Cu-70SnBi sintered at different sintering temperature

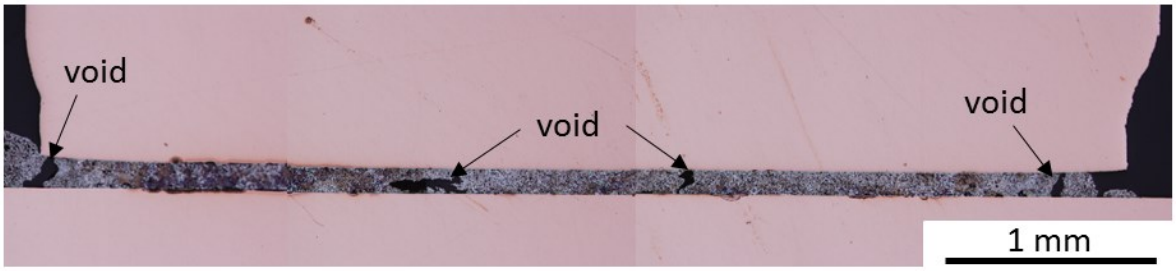

Figure 5.16 Cross-sectional optical micrograph image of Cu-65SnBi sintered at 200°C for 90 min sintering holding time

Figure 5.16 presents the cross-sectional optical micrograph image of Cu-65SnBi sintered at 200°C for 90 min sintering holding time. Although some large voids can be observed, it was relatively smaller in area than the voids observed in the work of Omid Mokhtari et al. in [2]. In their work, mean void area fraction in solder joints after conventional reflow process (pressureless bonding) was 49.0%, which will be detrimental for solder as heat-conductance material. They speculated that the formation of large voids in the solder was the result of solvent-depleted regions that were trapped between Cu micro-particles clusters. Compared to nanoparticles, solubility rate of micro-particles into molten Sn is slower, therefore, the formed Cu clusters remained throughout the reflow process and led to the formation of large voids with the merging of vicinity voids. It is noteworthy to state that in the same work, voids increased in size with increasing reflow time (up to 50 min), but in our work, although the sintering time took place for 90 min, the formation of large voids was relatively smaller in area. This indicates that the process and the usage of Cu nanoparticles as proposed in this study is advantageous to lower the formation of voids.

Figure 5.17a-d illustrates cross-sectional back-scattered electron (BSE) SEM images of Cu-65SnBi that was sintered at 180, 200, 220, and 250 °C, respectively. As can be seen in Figure 5.17a, the microstructure of Cu-65SnBi that was sintered at 180 °C was different compared to that of 200 °C, 220 °C, and 250 °C as shown in Figure 5.17b-d. The microstructure of Cu-65SnBi that was sintered at 180 °C was typical skeleton-type sintering structure, consisting of Cu_6Sn_5 and Bi-phase, but a relatively densified microstructure can be observed at higher sintering temperatures. It is assumed that the difference of microstructure with increasing sintering temperature might be explained by reaction (5.6) as discussed in earlier section. When the sintering temperature is higher than 195.9 °C, due to the reaction of Cu_6Sn_5 and Bi, a new liquid phase was generated and facilitated the diffusion of atoms to form a denser microstructure, as can be seen in the microstructure that was sintered at 200 °C and above (Figure 5.17b-d). As explained in Figure 5.15, Cu-65SnBi demonstrated greater

shear strength with increasing sintering temperature, however, the observed microstructure was rather similar, in which microscale voids were found scattered in the matrix. The reason of the difference is unclear, but the shape and size of voids might play a role in determining the shear strength. Additionally, it is presumed that the volume fraction of liquid phase that generated in reaction (5.6) increased with increasing sintering temperature and promoted the densification of the microstructure.

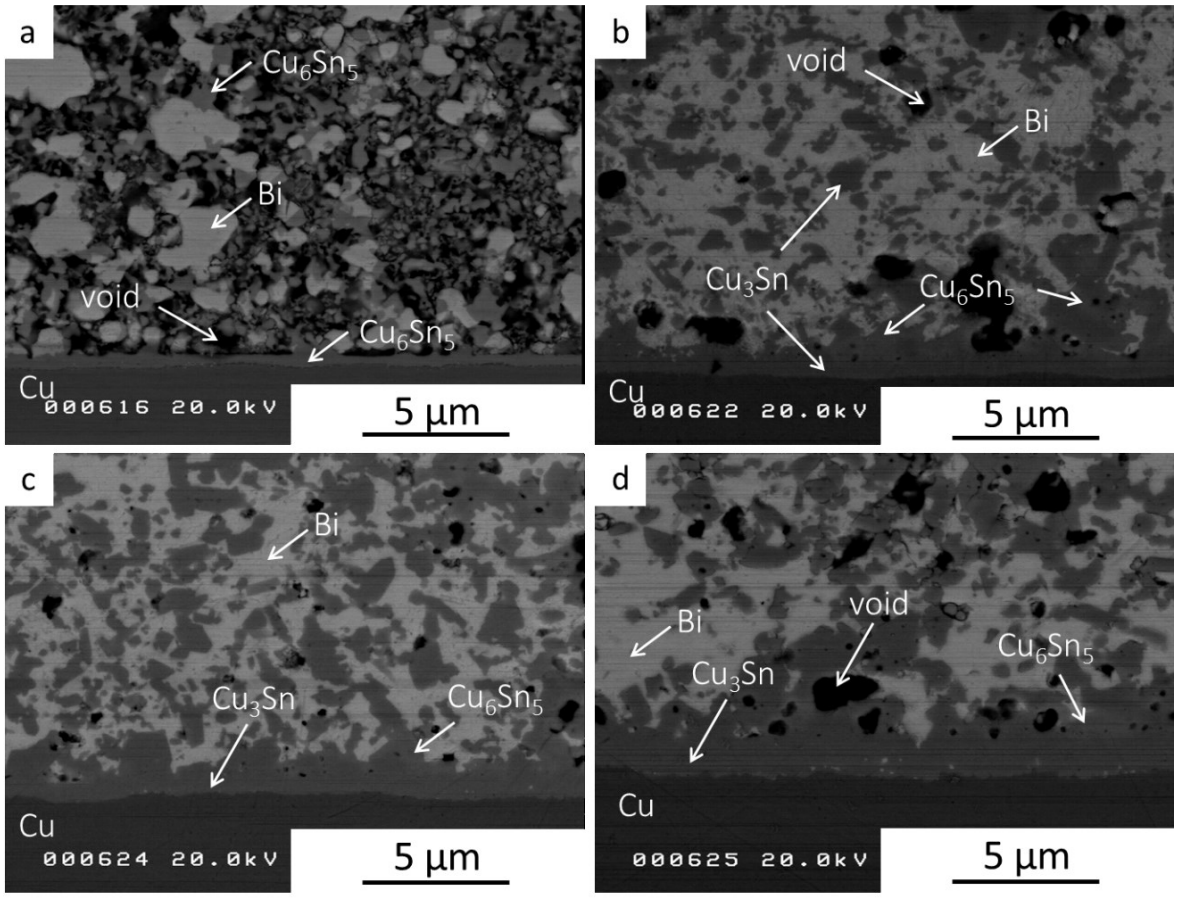

Figure 5.17 Cross-sectional SEM (BSE) images of Cu-65SnBi sintered at **a** 180 °C, **b** 200 °C, **c** 220 °C, and **d** 250 °C with same sintering holding time of 90 min

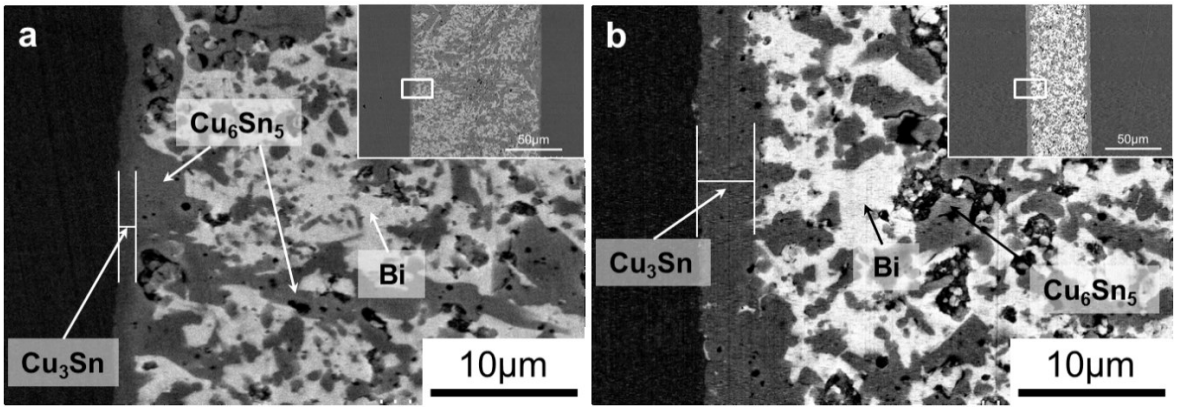

Figure 5.18 SEM images of cross-sections of Cu-65SnBi sintered at 90 min at sintering temperature of a 220°C, and b 250°C (images were magnified from the area as shown in inset)

Figure 5.18 shows SEM images of cross-sections of Cu-65SnBi bonded at 220°C and 250°C with sintering holding time of 90 min. Cu-65SnBi bonded at 220°C for 90 min (inset of Figure 5.18a) exhibited similar microstructure to the one bonded at 250°C for 0 min as shown in Figure 5.13a. Microscale voids were observed in the matrix for both sintering temperature conditions. In addition, at the interface, the thickness of planar-type Cu_3Sn IMCs were thinner when bonded at 220°C. These findings indicate that lower shear strength at lower sintering temperature might be attributed to the existence of scattered microscale voids in the matrix and/or poor interface strengthening. Nonetheless, the shear strength of Cu-65SnBi bonded at 220°C with 90 min sintering holding time were higher than 20 MPa, which fulfilled the requirement of MIL-STD-883K, and equivalent to the conventional Pb-solder as explained in earlier section.

Next, the effect of sintering temperature to the remelting temperature of the as-sintered Cu-65SnBi will be discussed. Figure 5.19a shows DSC results of Cu-65SnBi that was sintered at four different sintering temperatures. Figure 5.19b presents the magnified DSC results from Figure 5.19a within temperature range of 136 °C to 140°C. As can be seen in Figure 5.19a, regardless of sintering temperature, a new melting event at approximately 200 °C can be observed. This new melting event was assumed to be the result of reaction (5.6) as explained earlier. For Cu-65SnBi that was sintered at 180 °C, remelting event was only detected at one point, i.e. at approximately 200 °C. During sintering at 180 °C, reaction (5.6) was not initiated and the formed Cu_6Sn_5 and Bi-phase remained unreacted with each other until the sintering process was completed. Subsequence heating in DSC test up to 300 °C resulted in the reaction (5.6) to take place, hence, the observed endothermic peak at approximately 200 °C. Meanwhile, when Cu-65SnBi was sintered at 220 °C and 250 °C, a preceding remelting event at the proximity of eutectic temperature of Sn-Bi was detected, as can be confirmed from Figure 5.19b. The melting event at 138 °C is thought to be the melting of the solidified liquid phase that was generated in reaction (5.6). As explained earlier in Section 5.3.2, due to the non-equilibrium cooling stage, the liquid phase from reaction (5.6) is assumed to solidify as Sn-Bi hypereutectic and remelt again at the Sn-Bi eutectic temperature, as observed in Figure 5.19b for Cu-65SnBi sintered at 225 °C and 250 °C.

However, Cu-65SnBi that was sintered at 200 °C did not exhibit remelting event at Sn-Bi eutectic temperature albeit reaction (5.6) was thought to occur, as supported by the densified microstructure which is shown in Figure 5.17b. Since sintering at 200 °C was just slightly above the temperature of reaction (5.6), it is assumed that the volume fraction of the generated liquid phase and the subsequently solidified eutectic phase was too small to be detected by DSC. Accordingly, it is assumed that the volume fraction will increase with increasing sintering temperature.

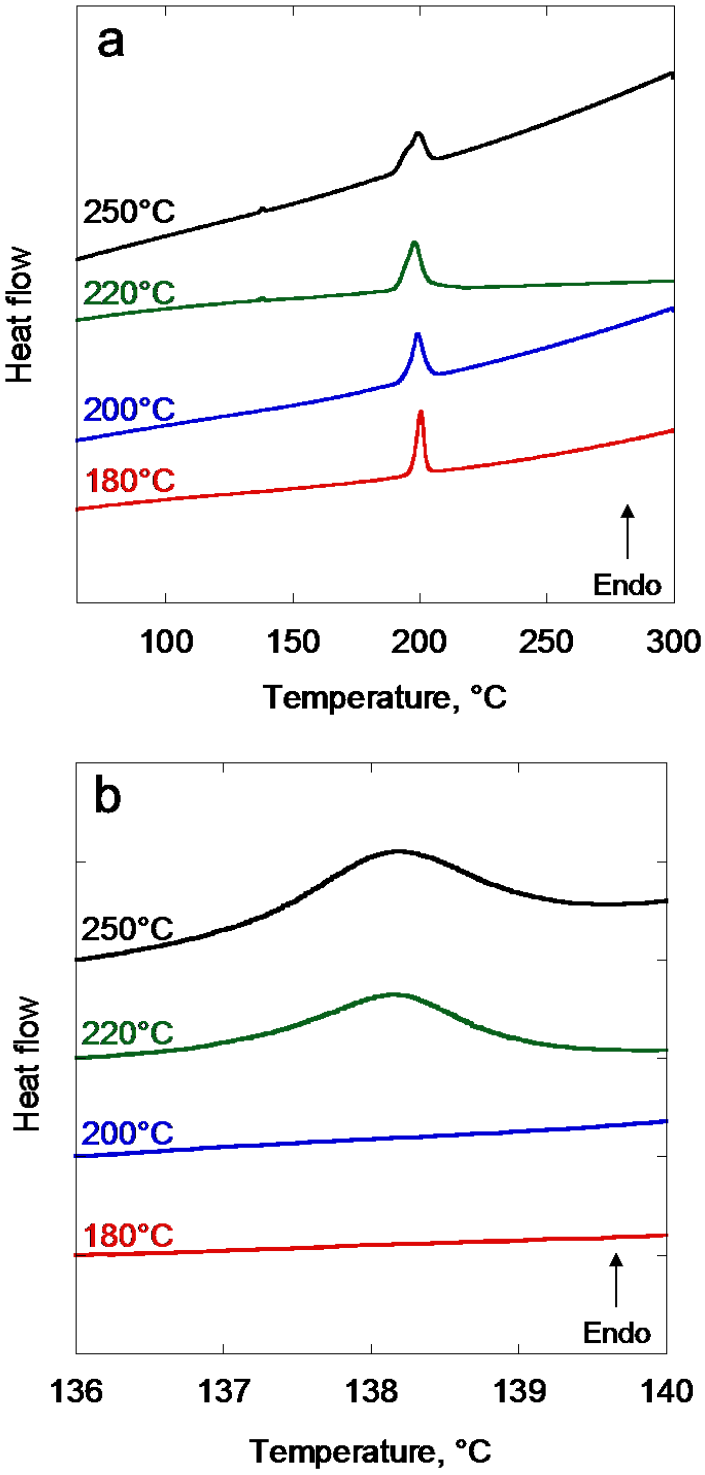

Figure 5.19 **a** DSC results of as-sintered Cu-65SnBi at four different temperatures, and **b** magnified DSC results of temperature range from 136°C to 140°C as illustrated in **a** (numbers shown in both graphs are sintering temperature)

Generally, the existence of liquid phase in solder during high temperature operation is detrimental as the strength of the solder will likely to drop. To investigate the effect of remelting temperature to the shear strength of Cu-65SnBi, additional high temperature shear test at 150 °C was conducted for Cu-65SnBi that was sintered at 200 °C, 220 °C, and 250 °C. The result is shown in Figure 5.20(a). For the sake of comparison, shear strength at r.t. from Figure 5.15 is incorporated in the graph. As can be seen from Figure 5.20(a), average shear strength at 150 °C of Cu-65SnBi that was sintered at 220 °C and 250°C decreased 28.6% and 26.6%, respectively, implying that the existence of liquid phase during shear test weakened the joint strength. Meanwhile, shear strength at 150 °C of Cu-65Sn-Bi that was sintered at 200 °C was almost equal to that of r.t., indicating that no liquid phase associated with the remelting event over than the Sn-Bi eutectic temperature was formed to decrease the joint strength.

Omid Mokhtari et al. calculated the required amount of Cu to completely convert the entire Sn-phase into Cu-Sn IMCs [2]. It was found that by the addition of 30wt% and above of Cu particles into Sn-Bi, all Sn-phase will completely reacted with Cu, resulting in no residual Sn-Bi eutectic phase. However, in the same study, the remelting event of 30 wt% Cu micro-particles (φ5 μm) added into Sn-Bi was observed at the Sn-Bi eutectic phase. The reason was thought to be that the Cu micro-particles was too large to entirely transform the Sn-phase into Cu-Sn IMCs, hence, resulting in residual Sn-Bi eutectic phase. Such remelting event at the Sn-Bi eutectic temperature will be unfavorable for the application in SiC-based module, which produces high heat-density compared to the conventional Si-based module. On the other hand, in our study, remelting event at Sn-Bi eutectic temperature was not detected for Cu-65SnBi that was sintered at 200 °C, supported by the equivalent shear strength at both r.t. and 150 °C. Firstly, this indicates that the usage of Cu nanoparticles (50 nm) accelerated the consumption of Sn-Bi, thus, no remelting event at Sn-Bi eutectic temperature. Secondly, by controlling the sintering temperature just slightly above the temperature of reaction (5.6),

the formation of liquid phase contributed to the densification and strengthening, nevertheless, the solidified Sn-Bi eutectic phase was too small in volume fraction and difficult to be detected by DSC. Correspondingly, almost no harm to the shear strength at high temperature up to 150 °C was revealed, as confirmed in Figure 5.20(a).

Aiming to increase the shear strength of Cu-65SnBi that was sintered at 200 °C, the sintering holding time was prolonged from 90 min to 180 min. It is assumed that at lower temperature, volume fraction of the liquid phase formed by reaction (5.6) was smaller, thus, prolonging sintering time is thought to facilitate the diffusion between liquid phase and also in the solid phase for further densification. Figure 5.20(b) presents the shear strength at r.t. and 150 °C of Cu-65SnBi sintered at 200 °C for 90 and 180 min sintering holding time. It is clear that with increasing sintering holding time at 200 °C, the shear strength was also increased. Interestingly, the shear strength at r.t. and 150 °C of Cu-65SnBi sintered for 180 min exhibited similar tendency to that of 90 min. The shear strength at 150 °C of Cu-65SnBi sintered for 180 min was almost unaffected as compared to that of r.t.

On contrary, Cu-70SnBi demonstrated an earlier remelting temperature prior to the temperature of reaction (5.6), i.e. at 138 °C. A comparison of the DSC test results of Cu-65SnBi and Cu-70SnBi that was sintered at 200 °C for 90 min is shown in Figure 5.21a. It is clear from Figure 5.21b that undercooling can be observed during cooling stage in DSC (-5 °C/min). This indicate that, the liquid phase from reaction (5.6) might solidify as hypereutectic Sn-Bi during the non-equilibrium cooling stage and remelt again at Sn-Bi eutectic temperature. As mentioned earlier, the remelting at the Sn-Bi eutectic temperature is detrimental for application above the eutectic temperature. Figure 5.22 compares shear strength of Cu-65SnBi and Cu-70SnBi that was sintered at 200 °C for 90 min. As can be seen, the shear strength at 150 °C of Cu-70SnBi dropped for approximately 30% when sintered at 200 °C, which implied that the existence of liquid phase of eutectic Sn-Bi might impose harm to the shear strength at high temperature up to 150 °C.

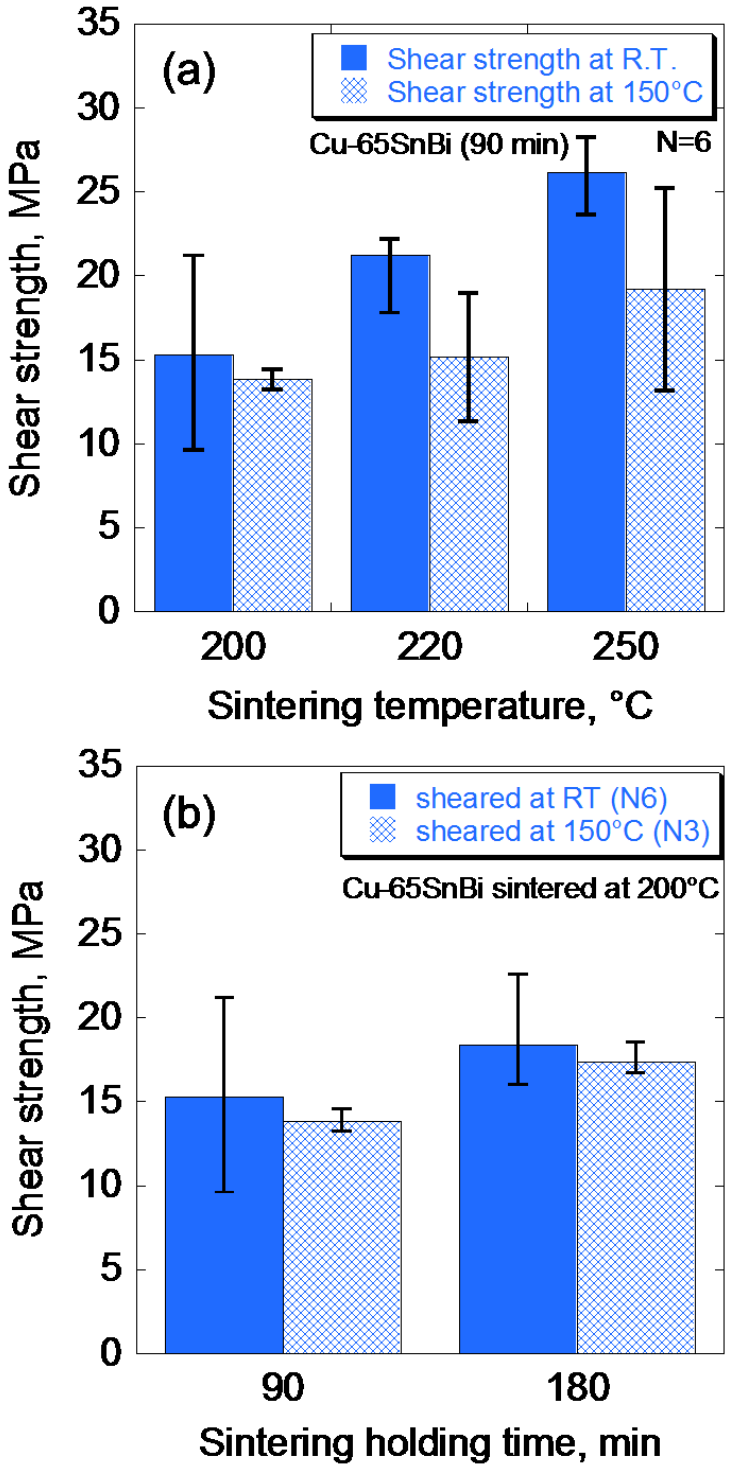

Figure 5.20 Shear strength at room temperature and 150 °C of Cu-65SnBi (a) sintered at different sintering temperature for 90 min sintering holding time, and (b) sintered at 200 °C with different sintering holding time

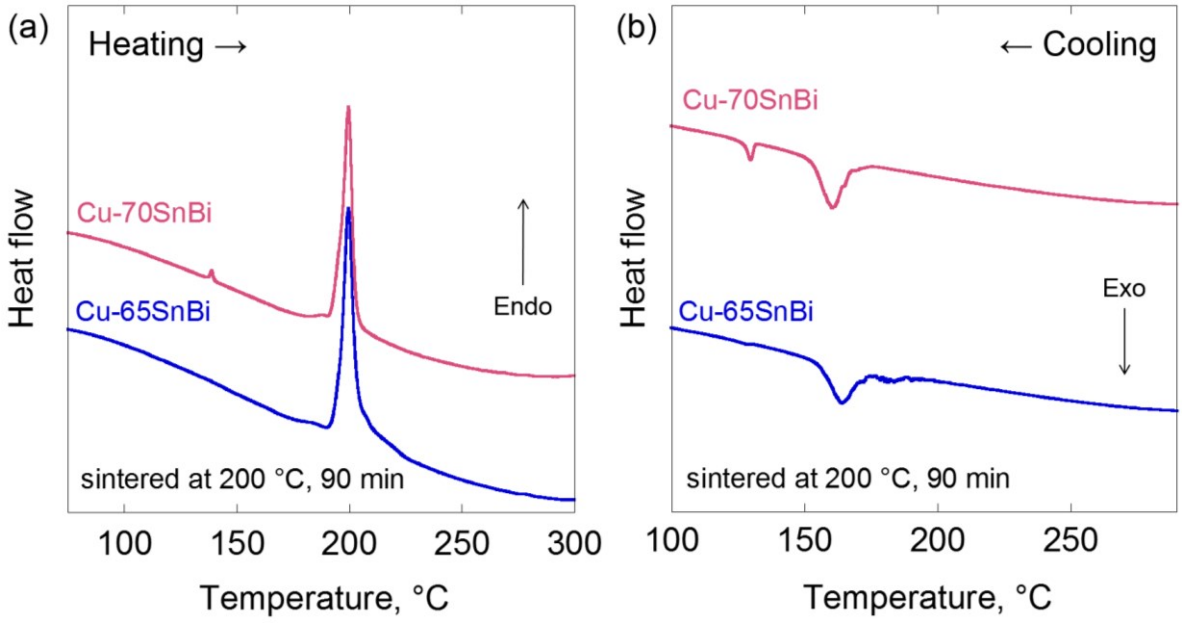

Figure 5.21 DSC analysis result of Cu-65SnBi and Cu-70SnBi sintered at 200 °C for 90 min sintering holding time: (a) heating curve, and (b) cooling curve

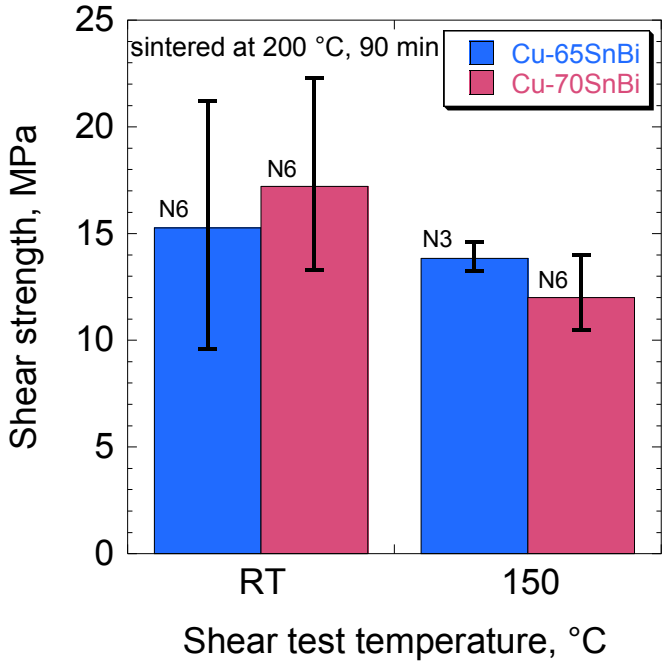

Figure 5.22 Shear strength at room temperature and 150 °C of Cu-65SnBi and Cu-70SnBi sintered at 200 °C for 90 min sintering holding time

5.4.3 Microstructure Evolution during Sintering Process

To elucidate the mechanism of TLPS of Cu mixed with Sn-Bi, similar investigation to Ag-based TLPS as explained in Chapter 4 Section 4.3.4 has been performed. The sintering conditions are shown in Figure 4.18. In this investigation, Cu-65SnBi and Cu-70SnBi, which exhibited shear strength higher than 20 MPa at r.t., as shown in Figure 5.8 was selected and evaluated.

Figure 5.23(a) and (b) shows the XRD pattern of Cu-65SnBi and Cu-70SnBi that was sintered using the sintering profile as shown in Figure 4.18, respectively. As can be seen at both compositions, the Sn (200) plane at 35.7 °, and Sn (101) plane at 37.3 ° were clearly detected at the sintering temperature of 150 °C from 0 to 15 min, i.e. the drying stage. Since at the drying stage formic gas was not yet introduced, even though the temperature of the drying stage was above the Sn-Bi eutectic temperature, the oxide layer existed on both Cu nanoparticles and Sn-Bi powders is assumed to hinder the wetting of Sn-Bi onto Cu nanoparticles. This residual unreacted Sn-Bi remelt during the DSC test as observed in Figure 5.24 and Figure 5.25, which will be described later. After the introduction of formic gas at temperature above 150 °C, the melted Sn-Bi began to wet the Cu nanoparticles and subsequently commencing isothermal solidification process by the solution of Cu particles into the molten Sn. From the XRD pattern of both compositions at 160 °C, Sn (200) and Sn (101) plane were no longer detected, implying that the isothermal solidification might be completed within 2 min after the introduction of formic gas (heating rate was 5 °C/min). For Cu-65SnBi, the peak at both Sn (200) and Sn (101) planes were almost not observed at other sintering conditions, although an extremely weak peak can be observed at sintering conditions of 250 °C and 90 min. Meanwhile, for Cu-70SnBi, Sn (200) and Sn (101) plane can be identified again at sintering temperature of 200 °C and above. This Sn-phase was thought to be the Sn-phase from the non-equilibria solidified liquid phase from reaction (5.6), as explained earlier in Section 5.3.2.

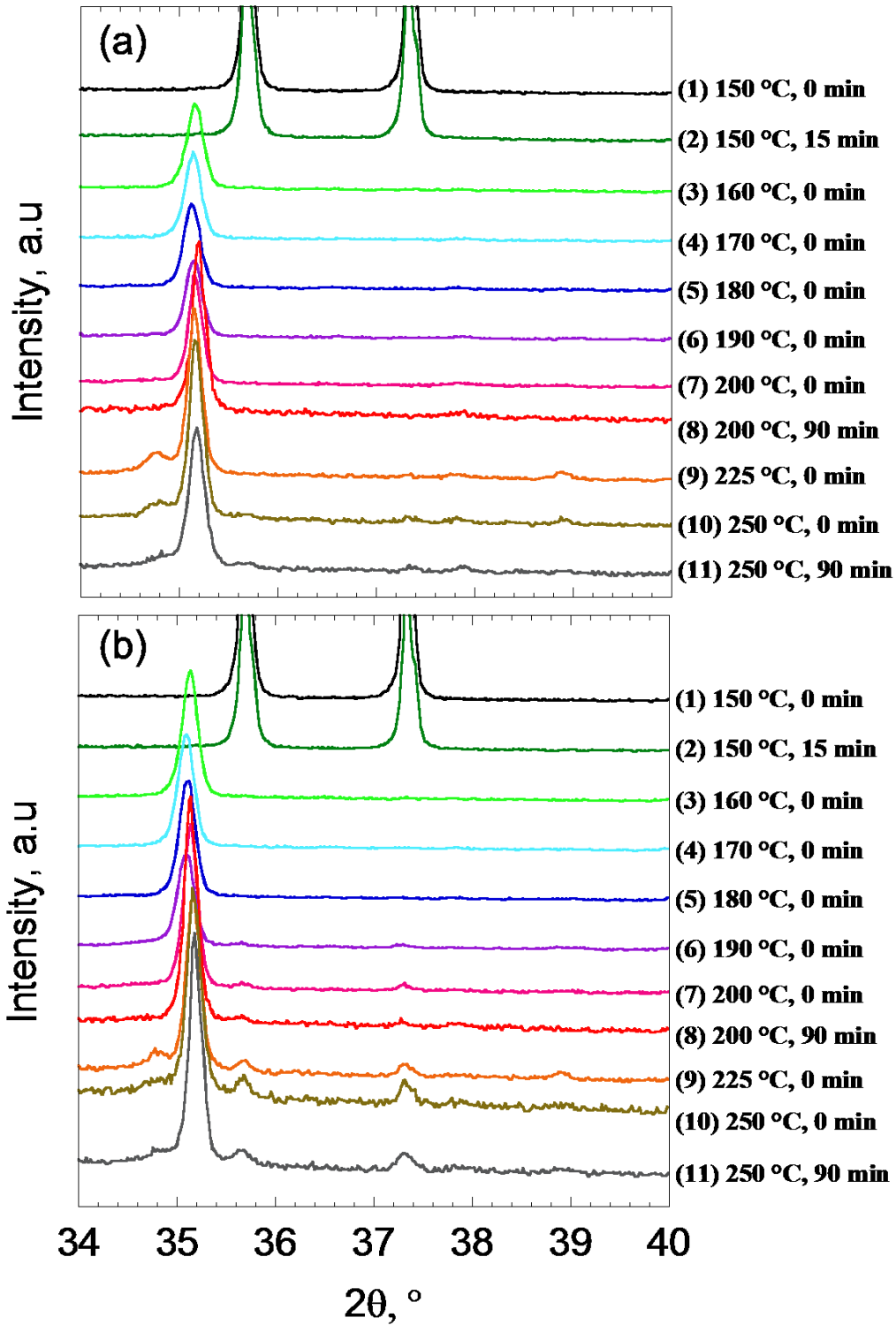

Figure 5.23 XRD pattern of (a) Cu-65SnBi, and (b) Cu-70SnBi sintered at different sintering conditions as shown in Figure 4.18

Figure 5.24, and Figure 5.25 illustrates the DSC test result of Cu-65SnBi and Cu-70SnBi sintered at certain sintering conditions as depicted in Figure 4.18, respectively. Onset and peak temperature of endothermic reaction at each condition investigated is summarized in Table 5.5 and Table 5.6. Cu-65SnBi and Cu-70SnBi depicted different behavior in remelting temperature when sintered at certain sintering temperature. As can be seen in Figure 5.24, isothermal solidification process in Cu-65SnBi is thought to be completed within 4 min after the introduction of formic gas at 150 °C and above. However, the remelting of Sn-Bi can still be observed in Cu-70SnBi sintered at 170 °C and 180 °C, as identified in Figure 5.25. The endothermic peak at Sn-Bi eutectic temperature when Cu-70SnBi was sintered above 150 °C was relatively weak compared to that of at 150 °C, but provide enough information that unreacted Sn-Bi eutectic phase might remained in the microstructure. Interestingly, the endothermic reaction peak at the same temperature was relatively larger when sintered at 200 °C, as identified in Figure 5.25(b). This might be attributed by the formation of additional Sn-Bi eutectic phase that was formed from the non-equilibria solidified liquid phase from reaction (5.6). However, for Cu-65SnBi, the remelting at Sn-Bi eutectic temperature was can only be observed again when sintered at 225 °C and 250 °C, but not at 200 °C. This is in good agreement with the findings in Figure 5.21, and showed good reproducibility despite the cooling rate in this DSC investigation was different to the investigation conducted in Section 5.4.3.

As shown in Figure 5.22, the factor that affected the drop in the shear strength at 150 °C of Cu-70SnBi as compared to Cu-65SnBi is assumed to be the residual Sn-Bi eutectic and the additional Sn-Bi phase from reaction (5.6). It has been proven from DSC result (Figure 5.21 and Figure 5.24(a)) of Cu-65SnBi that despite reaction (5.6) is thought to take place when sintered at 200 °C, the volume fraction of the liquid phase might be negligible small to be detected by DSC, and provided almost no harm to the shear strength at temperature higher than the Sn-Bi eutectic temperature.

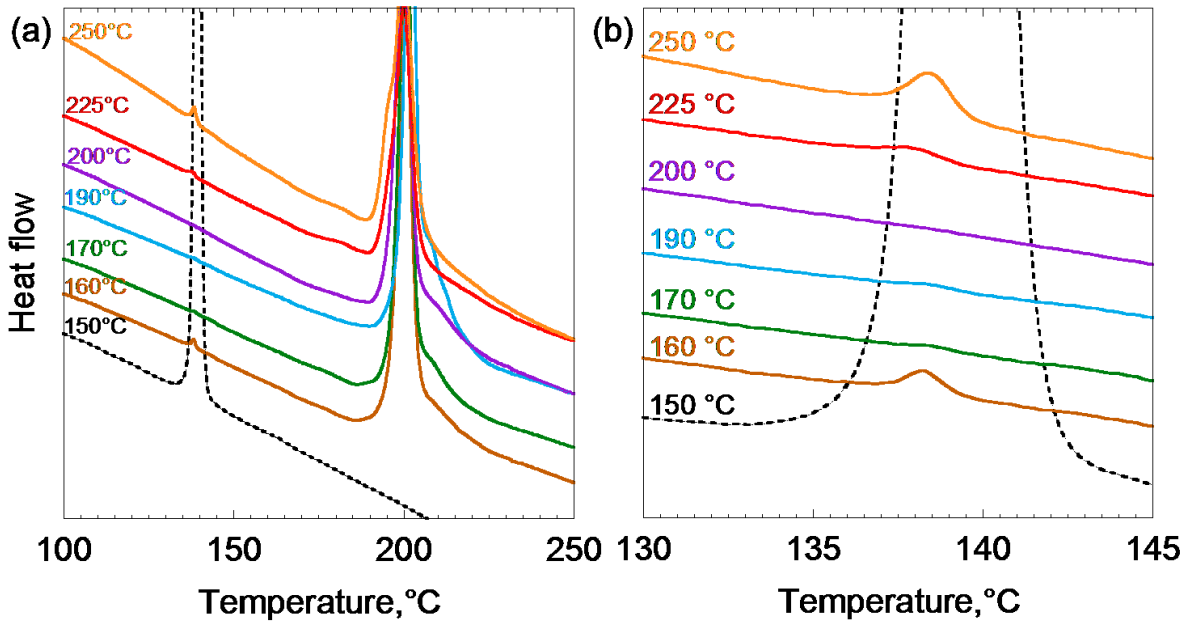

Figure 5.24 (a) DSC result of Cu-65SnBi sintered at different sintering conditions as shown in Figure 4.18, and (b) magnified DSC result at temperature range from 130 °C to 145 °C

Table 5.5 Onset temperature and peak temperature of endothermic reaction as observed in DSC analysis of Cu-65SnBi at each sintering conditions shown in Figure 4.18

No.	Sintering Condition		First melting event		Second melting event	
	Temperature °C	Holding time min	Onset temperature °C	Peak temperature °C	Onset temperature °C	Peak Temperature °C
1	150	0	137.92	139.94	-	-
2	150	15	137.80	139.80	-	-
3	160	0	137.06	138.27	196.50	200.53
4	170	0	-	-	196.46	200.81
5	180	0	-	-	197.99	201.60
6	190	0	-	-	198.47	202.00
7	200	0	-	-	195.24	199.89
8	200	90	-	-	195.26	199.68
9	225	0	134.38	137.80	194.94	200.04
10	250	0	137.05	138.45	194.40	199.95
11	250	90	137.42	138.79	190.11	199.03

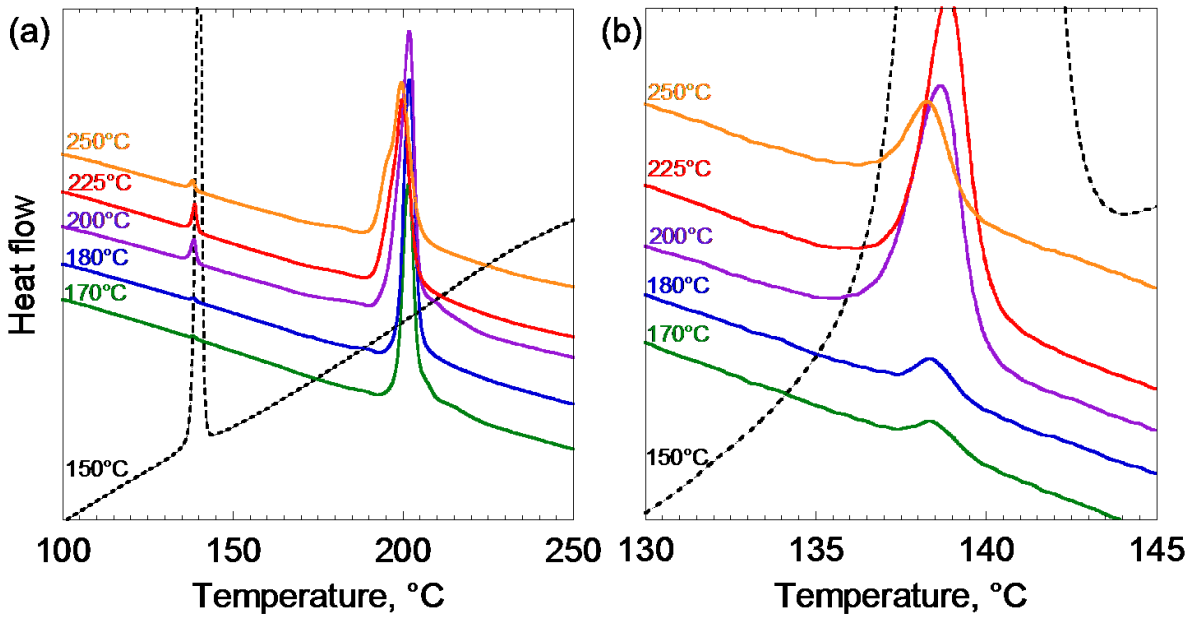

Figure 5.25 (a) DSC result of Cu-70SnBi sintered at different sintering conditions as shown in Figure 4.18, and (b) magnified DSC result at temperature range from 130 °C to 145 °C

Table 5.6 Onset temperature and peak temperature of endothermic reaction as observed in DSC analysis of Cu-70SnBi at each sintering conditions shown in Figure 4.18

No.	Sintering Condition		First melting event		Second melting event	
	Temperature °C	Holding time min	Onset temperature °C	Peak temperature °C	Onset temperature °C	Peak Temperature °C
1	150	0	138.48	140.33	-	-
2	150	15	138.38	140.38	-	-
3	160	0	137.13	138.56	198.87	202.33
4	170	0	136.44	138.45	198.41	201.73
5	180	0	137.37	138.42	198.77	201.93
6	190	0	137.27	138.33	199.85	202.97
7	200	0	136.82	138.69	196.45	201.95
8	200	90	137.55	138.96	195.06	199.72
9	225	0	137.43	138.90	194.42	199.90
10	250	0	136.85	138.31	194.13	199.61
11	250	90	137.24	138.60	189.62	198.68

Figure 5.26, and Figure 5.27 presents the SEM (SE) images of Cu-65SnBi, and Cu-70SnBi sintered at several sintering temperatures with 0 min sintering holding time, respectively. The observed surface from the sample of both compositions is depicted in Figure 4.18. It is clear from both figures that at 150 °C, the Sn-Bi powders was visible and the original sphere shape was almost unaffected. Cu particles was also observed at both compositions when sintered at 150 °C, but at the observation magnification of 3000× shown in Figure 5.26 and Figure 5.27, it is almost impossible to identify the Cu nanoparticles. The oxide layer on both Cu nanoparticles and Sn-Bi powders is thought to hinder the wetting of the latter on the former. However, by the introduction of the formic gas, the oxide layer was reduced, and the Sn-phase began to react with Cu to convert the Cu to Cu-Sn IMCs. At the sintering temperature of 160 °C and above, the initial Sn-Bi powders were not observed any longer. On the other hand, when Cu-65SnBi and Cu-70SnBi was sintered from 160 °C to 190 °C, the densification of the sintering microstructure can be observed, where the small particles was consumed by the larger particles as can be explained by the Ostwald ripening. At sintering temperature of 200 °C, owing to the formation of the liquid phase from reaction (5.6), the densification by the diffusion of atom via liquid phase was clearly visible at both compositions. At sintering temperature of 200 °C and higher, Cu-70SnBi showed fewer voids as compared to Cu-65SnBi. This might explain the higher shear strength at r.t. of the former as compared to latter.

The strengthening mechanism of Cu mixed Sn-Bi, in particular, the Cu-65SnBi and Cu-70SnBi is thought to be highly influenced by the densification of the microstructure. Particularly, owing to the formation of liquid phase at approximately 200 °C, the densification rate is assumed to multiple, as proven by the shear strength shown in Figure 5.15. It was also found that in order to achieve shear strength that almost unchanged at both r.t. and 150 °C, Cu-65SnBi, but Cu-70SnBi should be sintered at sintering temperature of 200 °C.

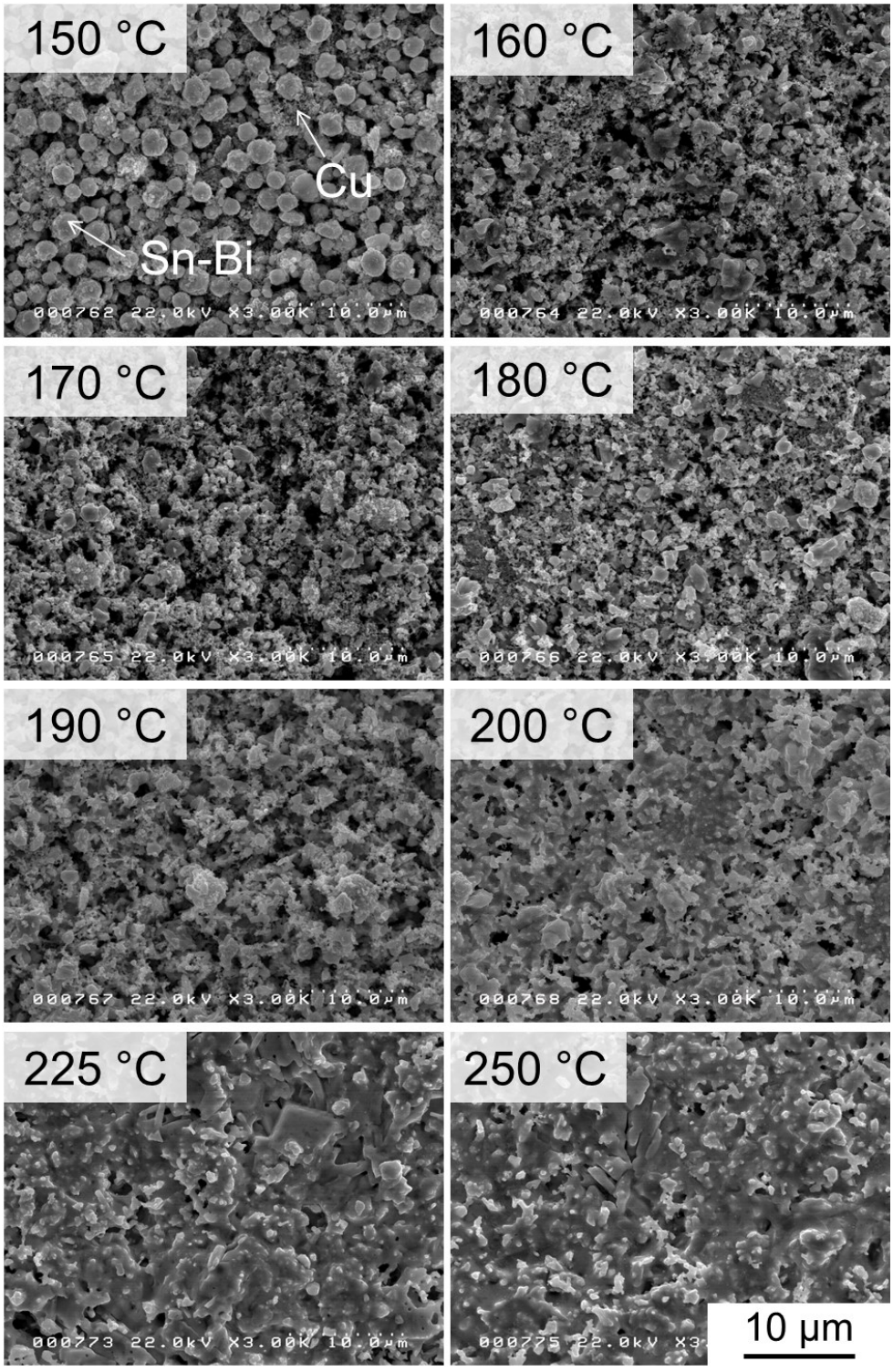

Figure 5.26 SEM (SE) image of Cu-65SnBi sintered at different sintering temperature (sintering holding time is 0 min for each condition)

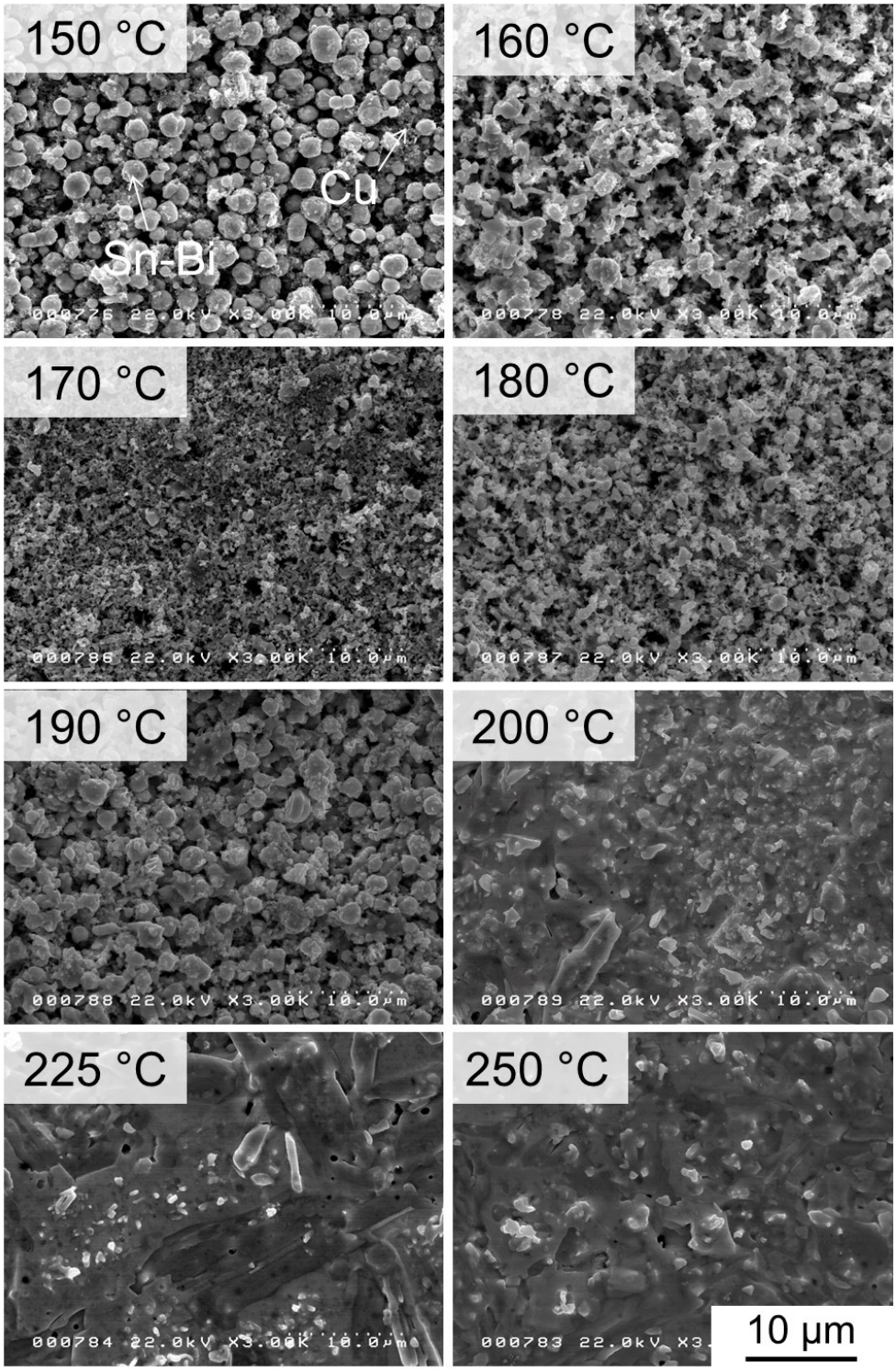

Figure 5.27 SEM (SE) image of Cu-70SnBi sintered at different sintering temperature (sintering holding time is 0 min for each condition)

5.5 Bonding with Ni plating

Up to this point, the aim of this study is to bond plateless Cu-Cu for the application of bonding DBC substrate of the module onto the Cu heat-spreader/sink. Thus, all investigations on the shear strength were conducted by bonding of plateless Cu-Cu substrate. As explained in Chapter 1 Section 1.2.3, the Cu heat-spreader that was attached on the Al heat-sink was aimed to spread the heat from the module to larger area before being cooled at the Al heat-sink, and also act as a buffer to reduce the thermomechanical stress due to the large CTE mismatch between Al heat-sink and ceramic substrate. However, the bonding of Cu heat spreader onto the Al heat sink is still an undergoing research and yet to be realized. On this account, the bonding of module onto a Ni-plated Al heat-sink is also demanded in the industry. On the other hand, Cu-65SnBi sintered at 200 °C has revealed similar shear strength at r.t. and 150 °C, as investigated in Section 5.4.2. To investigate the effect of Ni-plating on the bonding strength of the Cu-65SnBi, a preliminary experiment on plateless Cu and Ni-plated Cu (Cu-Ni/Cu) bonding was conducted. Plateless Cu disc with diameter of 5 mm and Ni-plated Cu substrate with dimension of 20 × 10 × t3 mm was bonded with Cu-65SnBi at 200 °C for 90 min.

Figure 5.28 shows the obtained shear strength of six samples that was bonded with Cu-65SnBi, and Figure 5.29 represents the corresponding fracture surface of each sheared sample. The average shear strength of Cu-65SnBi used to bond Cu-Ni/Cu was 12.9 MPa, which was approximately 16% lower than that of Cu-Cu bonding. Out of 6 samples, no sample demonstrated shear strength higher than 20 MPa. The observed fracture surface by optical micrograph as shown in Figure 5.29 revealed that the fracture mode was cohesive mode, indicating that a strong interface reaction layer might be formed between the Cu-65SnBi and the Ni-plating. Further investigation on the reaction that occurred at the interface is needed.

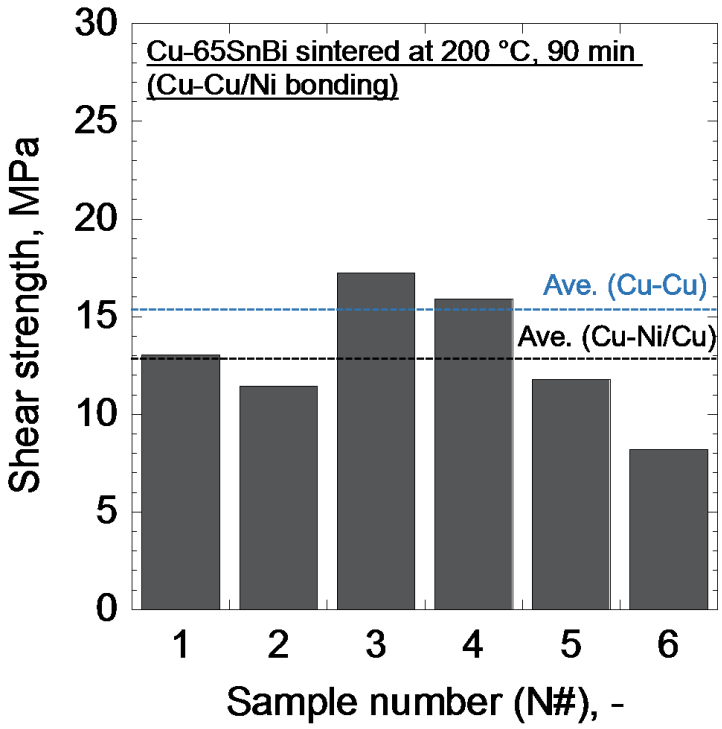

Figure 5.28 Shear strength of Cu-65SnBi used to bond Cu-Ni/Cu at sintering temperature of 200 °C and sintering holding time of 90 min

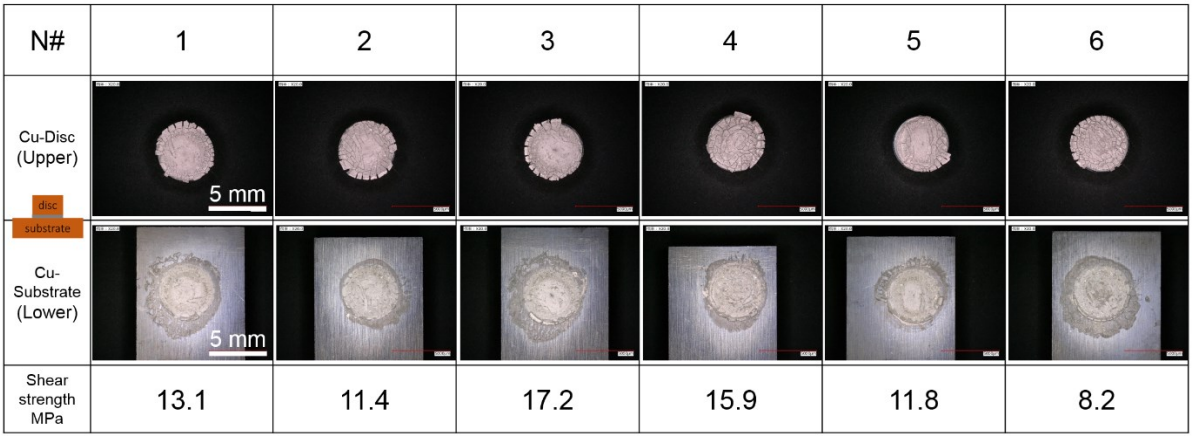

Figure 5.29 Optical micrograph image of fracture surface of Cu-65SnBi used to bond Cu-Ni/Cu at sintering temperature of 200 °C and sintering holding time of 90 min

5.5 Summary

In this chapter, bonding of plateless Cu-Cu substrates at temperature 250°C and low pressure of 0.1 MPa was achieved by TLPS of mixed Cu nanoparticles and Sn-Bi. In previous work on TLPS of Cu-SnBi, the remelting event at 139 °C due to the residual Sn-Bi was unavoidable, which will be unfavorable for the high temperature application of SiC-based module. This study is the first to develop a process in which the remelting temperature was completely shifted to around 200 °C. In this present study, at first, organic compounds selection method was discussed. Next, influences of composition, sintering holding time, and sintering temperature to the shear strength, microstructure, and remelting temperature were examined. Finally, compositions and sintering conditions that fulfilled the requirements in this study was selected to test the bonding of Cu-Ni/Cu. Alloy composition and sintering conditions that are thought to fulfill the requirements of this study are summarized in Table 5.7. The results obtained in this chapter are summarized as follows:

1. Based on the investigation conducted on Cu-70SnBi, the weight ratio of the particles to the organic compounds that showed the highest shear strength was defined as particles:TPO:EG = 87:11:2. This weight ratio was used to prepare the Cu-SnBi mixture paste for subsequent investigation in this study.
2. With increasing amount of Sn-Bi, shear strength was also increased. Cu-70SnBi exhibited the highest shear strength up to approximately 30 MPa when bonded at 250°C with 60 min sintering holding time. The shear strength obtained by Cu-65SnBi and Cu-70SnBi sintered at 250 °C exceeded conventional Pb-based solder and also fulfilled the requirement of MIL-STD-883K.
3. The remelting temperature of Cu-50SnBi and Cu-55SnBi sintered at 250 °C was found to be at the melting temperature of Bi-phase. On the other hand, Cu-60SnBi, Cu-65SnBi, and Cu-70SnBi demonstrated remelting temperature at lower temperature, i.e. at approximately

200 °C, as a result of the reaction (5.6). However, when sintered at 250 °C, Cu-65SnBi and Cu-70SnBi showed a small endothermic peak at Sn-Bi eutectic temperature, i.e. 139 °C.

4. At sintering temperature of 250°C, prolonging sintering holding time from 0 min to 60 min resulted in increasing shear strength of Cu-65SnBi. However, shear strength remained almost unaffected over 60 min to 90 min.
5. Shear strength of Cu-65SnBi when bonded at 180 °C for 90 min was lower than 5 MPa, but increased suddenly to 15 MPa with sintering temperature of 200 °C with the same sintering holding time, in which the highest shear strength recorded was over than 20 MPa. Subsequently, shear strength increased with increasing sintering temperature.
6. Cross-sectional SEM images of Cu-65SnBi sintered at 180 °C revealed a skeleton-type typical sintering structure, however, when the sintering temperature was 200 °C and higher, the microstructure was densified, which is thought to be the densification by the liquid phase that was created by reaction (5.6).
7. During sintering at 200 °C and higher, the reaction between Cu_6Sn_5 and Bi at approximately 200 °C was known to generate a liquid phase, which is thought to promote the densification of the microstructure and contribute to strengthening.
8. Remelting event of Cu-65SnBi that was sintered at 180 °C and 200 °C was observed at 200 °C, however, when sintered at 220 °C and 250 °C, remelting event was observed at approximately 138 °C and 200 °C, by DSC. On contrary, remelting event of Cu-70SnBi was always observed at the Sn-Bi eutectic temperature, regardless of sintering temperature, indicating residual Sn-Bi phase. As a result, the shear strength at 150 °C of Cu-70SnBi when sintered at 200 °C demonstrated a drop of about 30% as compared to that of r.t., while Cu-65SnBi with the same sintering condition showed almost no change in the shear strength at 150 °C.

Table 5.7 Alloy compositions of Cu-SnBi and sintering conditions that satisfied the requirement of processing conditions, and the obtained shear strength and remelting temperature

Alloy composition	Sintering conditions			Bonding Conditions		Shear strength MPa		Remelting temperature °C
	Temperature °C	Pressure MPa	Holding time min	Fluxless	Plateless Cu-Cu	≥ 20*	≥ 2.5**	(T_c max=125)
Target in this study	*≤ 200*	*≤ 0.1*	*n/a*	○	○	○	○	*≥ 200***
Cu-65SnBi	○ (200)	○ (0.1)	90	○	○	○ (21.2)	○	○ (200)
Cu-70SnBi	○ (200)	○ (0.1)	90	○	○	○ (22.3)	○	× (138)

* Equivalent to the Pb-based solder [16]

** MIL-STD-883K [17]

*** Considering $T_c = 0.85T_h$

A patent has been applied for the Cu-based TLPS that has been discussed in this chapter. The submitted patent application information is as follows (in Japanese):

Kato Ryoichi, Gohara Hiromichi, Ikeda Yasunari, Mochizuki Eiji, Takahashi Kazuyoshi, Yoshida Makoto, Muhammad Khairi Faiz, 2017-000281, Power Electronics Module Manufacturing Method and Power Electronics Module

References

[1] Omid Mokhtari, Hiroshi Nishikawa, J Mater Sci: Mater Electron 27, 4232 (2016)

[2] Omid Mokhtari, Hiroshi Nishikawa, The shear strength of transient liquid phase bonded Sn-Bi solder joint with added Cu particles, Adv Powder Technol 27, 1000 (2016)

[3] D.A. Porter, K.E. Easterling, Phase Transformations in Metals and Alloys, 2nd edn. (Nelson Thornes Ltd, Cheltenham, 2001), pp 44-47

[4] Molar volume of Cu, http://periodictable.com/Properties/A/MolarVolume.an.html

[5] Cu-Sn-Bi ternary system, http://www.metallurgy.nist.gov/phase/solder/bicusn.html (accessed on 31 August 2016)

[6] Lianwen Wang, Ai-Ping Xian, J Electron Mater 34, 1414 (2005)

[7] Data sheet of alpha-terpineol, https://goo.gl/ATcaJd (accessed on 31 August 2016)

[8] Yusuke Yasuda, Eiichi Ide and Toshiaki Morita, Low-Temperature Bonding Using Silver Nanoparticles Stabilized by Short-Chain Alkylamines, Japanese Journal of Applied Physics, Volume 48, Number 12R

[9] Tomohiro Yagishita, Tomo Ogura, Akio Hirose, Effect of polyethylene glycols with different polymer chain lengths on the bonding process involving in situ formation of silver nanoparticles from Ag2O, Materials Transactions, Vol. 54, No. 6 (2013) 866-871

[10] Yan Jianfeng, Zou Guisheng, Hu Anming, Y. Norman Zhou, Preparation of PVP coated Cu NPs and the application for low-temperature bonding, J. Mater. Chem., 2011, 21, 15981

[11] T. Ishizaki, T. Satoh, A. Kuno, A. Tane, M. Yanase, F. Osawa, Y. Yamada, Thermal characterization of Cu nanoparticle joints for power semiconductor devices, Microelectronics Reliability 53 (2013) 1543–1547

[12] Toshitaka Ishizaki and Ryota Watanabe, A new one pot method for the synthesis of Cu nanoparticles for low temperature bonding, J. Mater. Chem., 2012, 22, 25198

[13] Chengcai Luo, Yuhong Zhang, Xiaowei Zeng, Yuewu Zeng, Yanguang Wang, The role of poly(ethylene glycol) in the formation of silver nanoparticles, Journal of Colloid and Interface Science 288 (2005) 444–448

[14] Monica Popa, Trinitat Pradell, Daniel Crespo, Jose M. Calderon-Moreno, Stable silver colloidal dispersions using short chain polyethylene glycol, Colloids and Surfaces A: Physicochem. Eng. Aspects 303 (2007) 184–190

[15] Physical properties of Ethylene Glycols, https://goo.gl/Ha8V2z (accessed on 31 August 2017)

[16] Eiichi Ide, Akio Hirose, Kojiro F. Kobayashi, Influence of Bonding Condition on Bonding Process Using Ag Metallo-Organic Nanoparticles for High Temperature Lead-Free Packaging, Mater Trans 47, 211 (2006)

[17] MIL-STD-883K, EverySpec, http://everyspec.com/MIL-STD/MIL-STD-0800-0899/MIL-STD-883K_54326/ (Accessed on 10 October 2016)

[18] T. D'Hondt, S.F. Corbin, Thermal analysis of the compositional shift in a transient liquid phase during sintering of a ternary Cu-Sn-Bi powder mixture, Metall Mater Trans A 37A, 217 (2006)

[19] X. Deng, N. Chawla, K.K. Chawla, M. Koopman, Deformation behavior of (Cu, Ag)–Sn intermetallics by nanoindentation, Acta Mater 52, 4291 (2004)

[20] Yunhui Mei, Gang Chen, Yunjiao Cao, Xin Li, Dan Han, Xu Chen, Simplification of low temperature sintering nanosilver for power electronics packaging, J Electron Mater **42**, 1209 (2013)

[21] Doosoo Kim, Jong-hyeon Chang, Jungil Park, James Jungho Pak, Formation and behavior of Kirkendall voids within intermetallic layers of solder joints, J Mater Sci: Mater Electron (2011) 22: 703

[22] Toshitaka Ishizaki, Ryota Watanabe, Pressureless bonding by use of Cu and Sn mixed nanoparticles, J Electron Mater 43, 4413 (2014)

[23] Wenhua Yang, Masatake Akaike, Masahisa Fujino, Tadatomo Suga, A combined process of formic aced pretreatment for low-temperature bonding of copper electrodes, ECS J Solid State Sci Techn 2, 271 (2013)

[24] L. Samiee, M. Dehghani Mobarake, R. Karami, and M. Ayazi, Developing of Ethylene Glycol as a New Reducing Agent for Preparation of Pd-Ag/PSS Composite Membrane for Hydrogen Separation, Journal of Petroleum Science and Technology, Vol. 2, No. 2 (2012) 25-32

CHAPTER 6: COMPARISON OF TIN-BISMUTH ADDED SILVER-BASED AND COPPER-BASED TRANSIENT LIQUID PHASE SINTERING

6.1 Liquid Phase Volume Fraction

In this present study, based on the Ag-Bi and Cu-Bi binary phase diagrams, since Bi do not form solid solution neither with Ag nor Cu, the selection procedure of Sn-Bi addition amount has been conducted solely based on the Ag-Sn or Cu-Sn binary system. It is essential to completely convert the Sn-phase from the molten Sn-Bi to Ag-Sn and/or Cu-Sn IMC to prevent the remelting event at the proximity of Sn-Bi eutectic temperature, i.e. 139 °C. In Chapter 4 Section 4.1, according to the calculation based on the Ag-Sn binary system, it is important to control the Sn-Bi addition lower than 45 wt% (equivalent to 26 wt% of Sn) to completely convert the Sn-phase into Ag-Sn IMCs. Similarly, in Cu-based TLPS as explained in Chapter 5 Section 5.1, 80 wt% addition of Sn-Bi resulted in residual Sn-phase, thus, in this study, 70 wt% of Sn-Bi (equivalent to 51 wt%) has been selected as the maximum addition amount to be investigated. In both chapter, for the sake of convenience in conducting experiment, Sn-Bi addition amount has been described in weight percentage (wt%). However, in order to determine the factor that affecting the strengthening mechanism of the Sn-Bi added TLPS, it is necessary to describe the added Sn-Bi into liquid phase volume fraction, and its effects on solid fraction in both Ag-based and Cu-based TLPS should be discussed accordingly.

Lianweng Wang and Ai-Ping Xian measured the temperature-dependent density of liquid eutectic Sn-Bi by indirect Archimedean method [1]. The density of liquid Sn-Bi, ρ_L can be described according to the following equation (6.1), where T_m is the melting temperature and T is the temperature of interest in °C [1].

$$\rho_L = 8.51 - 10.9 \times 10^{-4}(T - T_m)\ [\text{g/cm}^3] \tag{6.1}$$

Taking into account that T_m=139 °C, the density of liquid Sn-Bi at 150 °C is calculated as 8.50 g/cm^3. On the other hand, the density of Ag and Cu is defined as 10.49 g/cm^3 and 8.96 g/cm^3, respectively. Using this value, the Sn-Bi liquid volume percentage is calculated and plotted against the obtained shear strength in Chapter 4 and Chapter 5.

Figure 6.1(a) shows the relationship between Sn-Bi liquid volume percentage and the shear strength of Ag-based and Cu-based TLPS used to bond Cu-Cu substrate at 250 °C for 60 min sintering holding time. As can be seen from Figure 6.1(a), there is no correlation between Sn-Bi liquid phase volume percentages to the shear strength of Ag-based and Cu-based TLPS. The shear strength was at peak when the Sn-Bi volume percentage was 34.6 % at Ag-based TLPS, however, in Cu-based TLPS, the shear strength increased with increasing Sn-Bi volume percentage. No definitive common volume fraction of Sn-Bi liquid phase that contribute to the strengthening in Ag-based and Cu-based TLPS can be defined. The difference in the shear strength shown by the Ag-based and Cu-based TLPS is thought to be attributed by the uniformly formed Cu-Sn interfacial reaction layer, and by the densification mechanism in the sintering structure, which will be summarized in the next section.

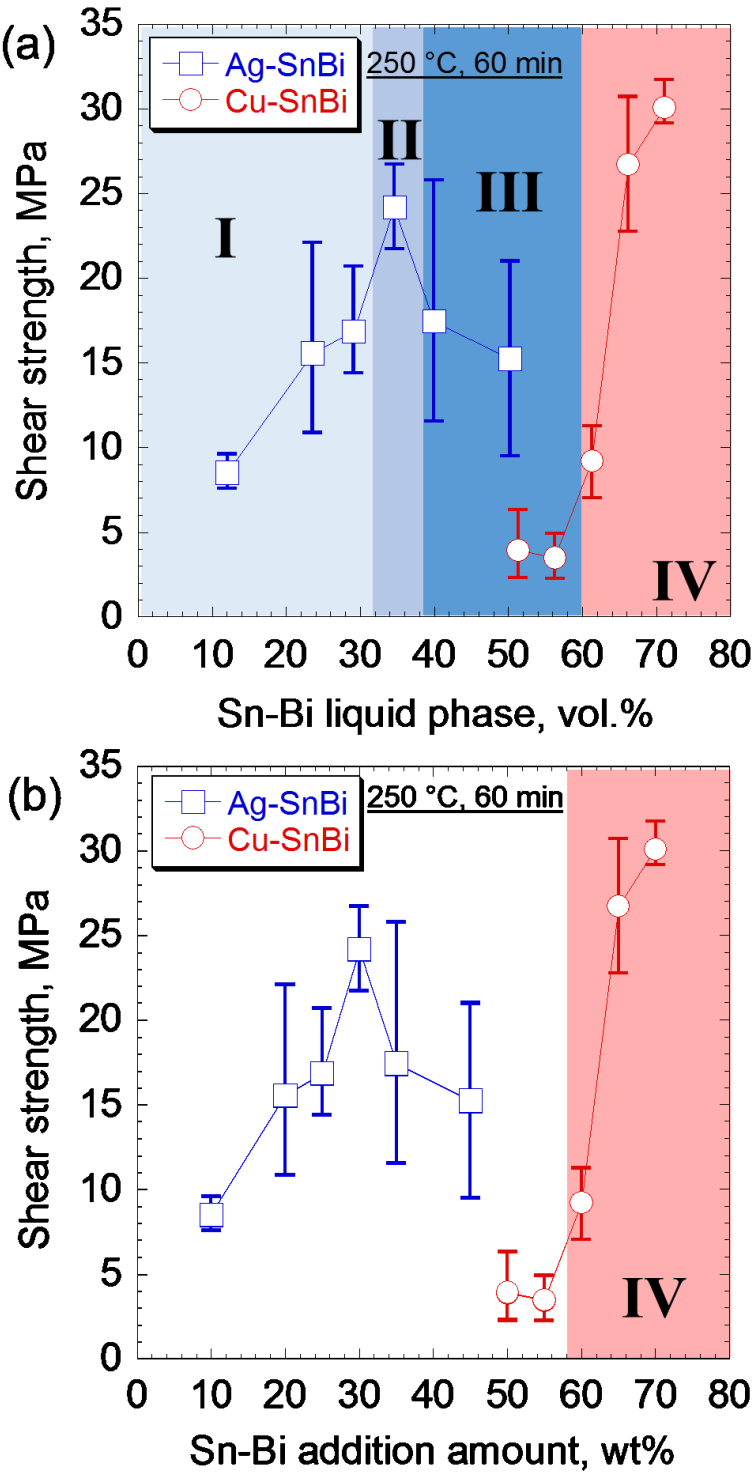

Figure 6.1 Influence of (a) Sn-Bi liquid phase volume percentage, and (b) Sn-Bi weight percentage on the shear strength of Ag-based and Cu-based TLPS sintered at 250 °C for 60 min

6.2 Strengthening Mechanism

The strengthening mechanism of Ag-based and Cu-based TLPS as investigated in this study was found to be distinctive to each other. Figure 6.1(a), and (b) represents the influence of Sn-Bi liquid volume percentage and Sn-Bi weight percentage on the shear strength of Cu-Cu joints bonded by Ag-based and Cu-based TLPS, respectively. Strengthening mechanism of both Ag-based and Cu-based TLPS referring to the Section I, II, III, and IV as categorized in the figure will be described in details as per below. Figure 6.1 (a) and (b) will be used interchangeably to explain the factors that affecting the shear strength, hereinafter. A schematic illustration of the cross-section microstructure referring to the sections described in the Figure 6.1 and a summary of the factor that influenced the shear strength of the joint is shown in Table 6.1.

Section I

In Ag-based TLPS, without the Ag-plating on the Cu substrate (plateless bonding), the Sn-phase from the Sn-Bi liquid eutectic is expected to react with the Cu substrate to form an interfacial reaction layer consisting of Cu-Sn IMCs. With increasing Sn-Bi eutectic liquid volume fraction, it is assumed that the formation of Cu-Sn IMCs interfacial reaction layer might be promoted. However, up to 29 vol.% of Sn-Bi eutectic liquid, the formation of the interfacial reaction layer is presumed to be non-uniform and the lack formation of this Cu-Sn layer is thought to result in the adhesive-type failure. The fracture path can be seen either at the interface of the Cu substrate and the Ag-SnBi matrix or within the thinly formed Cu-Sn IMCs interfacial reaction layer.

Section II

At approximately 35 vol% of Sn-Bi eutectic liquid, a uniformly formed Cu-Sn interface is thought to be the main factor of the strengthening at the interface. At this condition, no fracture was

observed at the interface. Accordingly, from the elemental mapping of the fracture surface as demonstrated in Figure 4.4, it was implied that the fracture took place within the sintering microstructure consisting of the Ag-Sn IMC and Bi. Figure 6.1 presents the shear strength of sample that was sintered at 250 °C. Ag-30wt%SnBi that was sintered at lower temperature, e.g. at 200 °C exhibited similar cohesive-type fracture although the obtained shear strength was lower compared to that of sintered at 250 °C. SEM image of the Ag-30wt%SnBi sintered at 200 °C and 250 °C, as shown in Figure 4.20 revealed that when sintered at the former, the sintering neck formation was limited but when sintered at the latter, the densified microstructure by the extensive formation of sintering necks is thought to contribute to the increase of shear strength with increasing sintering temperature.

Section III

In Ag-based TLPS, the Cu supply only came from the Cu substrate. Hence, during sintering process, the formerly formed Cu_6Sn_5 at the interface received the Cu supply from the Cu substrate to be transformed into Cu_3Sn. As a result, in 60 min sintering time, due to the difference of the diffusion coefficient between the Cu and Sn, the mass transportation of Cu atoms from the Cu substrate led to the formation of Kirkendall voids at the interface of Cu substrate and the subsequently formed Cu_3Sn. These Kirkendall voids is thought to be the crack initiation site and resulted in the decrease of the shear strength of Ag-based TLPS when the Sn-Bi weight percentage is higher than 30 wt% (Sn-Bi vol% higher than 35 vol%).

On contrary, in Cu-based TLPS, the Cu supply may come from within the Cu-SnBi matrix and also the Cu substrate. The abundance of Cu supply in the sintering microstructure (matrix) might prevent the mass transformation of Cu atoms from Cu substrate into the matrix, thus, suppressing the formation of Kirkendall voids, as opposed to the Ag-based TLPS. On the other hand, invariant reaction (5.6) explained in Chapter 5 as a result of locally concentrated Cu_6Sn_5 and Bi introduced a

new liquid phase at approximately 200 °C [2]. This liquid phase contributed to the densification of the sintering microstructure, as can be observed in Figure 5.17. However, when the Sn-Bi addition amount was less than 60 wt%, according to the lever rule, the expected phase to be formed was Cu_3Sn, as well as the precipitated Bi. Thus, reaction (5.6) might not be initiated in the case of Sn-Bi addition amount less than 60 wt%, where only Cu_3Sn and Bi existed. As a result, no densification by the new liquid phase was observed and resulted in porous microstructure, which led to low shear strength, as can be seen in Figure 5.11.

Section IV

As explained above, the invariant reaction (5.6) that initiates at temperature above 195 °C introduced a new liquid phase that contributed to the densification of the porous sintering microstructure. When the Sn-Bi addition amount is 60 wt% and higher, from the calculation based on the lever rule, the expected phase to form is Cu_6Sn_5, as well as the precipitated Bi. As a result, the increase of the shear strength may be observed when the Sn-Bi addition is higher than 60 wt% and the sintering temperature is above 200 °C, owing to the densified sintering microstructure by the introduction of the new liquid phase (Figure 5.11, 5.15, and 5.17)

Table 6.1 Schematic illustration of cross-section microstructure and the factor affecting the shear strength of the Cu-Cu joint referring to the sections shown in Figure 6.1 (a) and (b)

Section	Cross-sectional schematic illustration		Factors that influence the shear strength
	Ag-SnBi	Cu-SnBi	
I	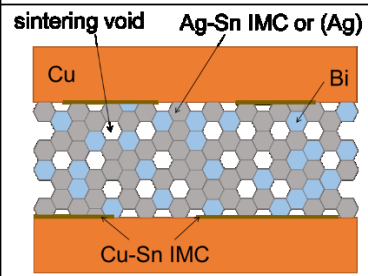	*Not investigated in this study*	▪ The lack formation of Cu-Sn IMC interfacial reaction layer weakened the interface
II	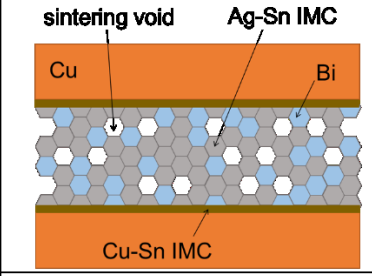	*Not investigated in this study*	▪ The uniformly formed Cu-Sn IMC interfacial reaction layer strengthened the interface, and accordingly contribute to cohesive-type failure
III	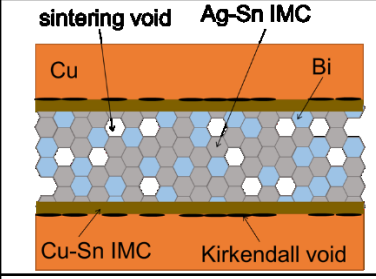	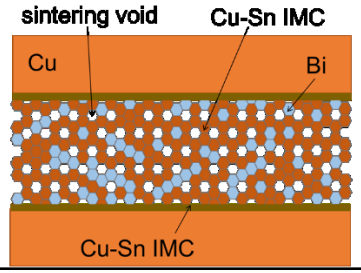	<u>Ag-SnBi</u> ▪ Kirkendall void formation weakened the interface and resulted in adhesive-type failure <u>Cu-SnBi</u> ▪ Porous microstructure resulted in low strength joint
IV	*Not investigated in this study*	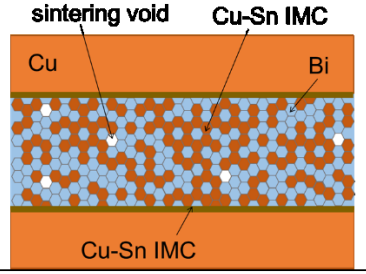	▪ Two-stages liquid phase sintering, particularly with the formation of liquid phase at about 200 °C contributed to the densification of the microstructure and strengthened the joint

6.3 Oxide Film Reduction Mechanism

In this present study, on realizing fluxless Cu-Cu bonding by Ag-based or Cu-based TLPS, formic acid environment was incorporated during the sintering process. This introduction of formic gas during sintering is assumed to reduce the oxide layer of Cu substrate and also the oxide layer of the particles. Oxide layer at Sn-Bi particles, Cu and Ag particles, will hinder the reaction to commence the isothermal solidification, meanwhile, the oxide layer on the Cu substrate will prevent the formation of Cu-Sn interfacial reaction layer.

Masahisa Fujino et al. reported that the reduction reaction of copper oxide by formic acid with Pt catalysis can be classified into three categories according to processing temperature: (1) reduction by H radicals that are generated from formic acid by Pt catalysis at temperature below 200 °C, (2) reduction by H_2 as a result of the decomposition of formic gas into H_2 and CO_2 at temperature range of 200-350 °C, and (3) reduction by CO as a result of the decomposition of formic gas into H_2O and CO at temperature above 350 °C [3]. In this study, all bonding process was conducted at temperature lower than 250 °C without the usage of Pt catalysis, hence the reduction by H_2 from the temperature range of 200-250 °C might be expected according to the above finding.

It can be implied from Figure 3.7 that almost all organic compounds in both Ag-based and Cu based sintering paste was vaporized at temperature higher than 120 °C. In addition, sintering profile that was used in this study (Figure 3.10) incorporated three-step gas exchange at the drying stage to assist the vaporized organic compounds out of the sintering paste. Hence, before the introduction of formic gas after the completion of drying stage, it can be assumed that almost no organic compound might be resided in the sintering paste. Once the formic gas is introduced at temperature higher than 150 °C, the oxide layer of both particles and Cu substrate is thought to be removed and facilitate the wetting and spreading of the Sn-Bi eutectic liquid.

References

[1] Lianwen Wang, Ai-Ping Xian, Journal of Electronic Materials, Vol. 34, No. 11 (2005) 1414-1419

[2] Cu-Sn-Bi ternary system, http://www.metallurgy.nist.gov/phase/solder/bicusn.html (accessed on 31 August 2016)

[3] Masahisa Fujino, Masatake Akaike, Naoya Matsuoka, Tadatomo Suga, Reduction reaction analysis of nanoparticle copper oxide for copper direct bonding using formic acid, Japanese Journal of Applied Physics 56, 04CC01 (2017)

CHAPTER 7: CONCLUDING REMARKS

7.1 Conclusions

In this study, low temperature and low pressure bonding of plateless Cu-Cu substrates has been achieved by utilizing transient liquid phase sintering of Ag or Cu with Sn-Bi eutectic alloy powders. In particular, bonding of plateless Cu-Cu substrates at temperature lower than 250 °C, pressure lower than 0.1 MPa has been successfully achieved without the usage of flux as reducing agent. Formic gas environment has been introduced to facilitate the reducing reaction of oxide layer of the added particles and the Cu substrates, as well as to help the wetting of Sn-Bi particles to both matrix grains and Cu substrates. A chapter-by-chapter summary of this dissertation is addressed as follows:

In ***Chapter 1***, based on the literature review, a new packaging solution of the next-generation SiC module replaced the silicone gel to a high-rigidity molding resin activated as strain dispersion structure, prior to bonding onto the heat-sink. Bonding requirements for this types of module, and the desired mechanical properties and remelting temperature are listed as follows:

i. Low bonding temperature to reduce the thermomechanical stress due to the CTE mismatch and also to prevent the thermal damage of the epoxy resin (≤ 200 °C)
ii. Pressure lower than 0.1 MPa to avoid premature cracking of the epoxy-molded module.
iii. Plateless Cu to Cu bonding as the metal plating deposition onto the module is difficult and as well as on contribute to cost-reduction
iv. Fluxless bonding so that post-processing flux-cleaning procedure can be omitted

v. Shear strength higher than 2.5 MPa, as the lowest minimum requirement considering the value of MIL-STD-883K, and preferably higher than 20 MPa, which is equivalent to the high temperature Pb-based solder.

vi. Remelting temperature higher than the Sn-Bi eutectic temperature, preferably ≥ 200 °C considering the rule of $0.85T_h$

Conventional bonding technology such as soldering, solid phase sintering, and transient liquid phase sintering was unable to accomplish all the above mentioned requirement, thus, a new bonding technology is highly desired.

In ***Chapter 2,*** on aiming to realize the bonding requirements as mentioned above, transient liquid phase sintering technology of Ag or Cu nanoparticles mixed with Sn-Bi powders has been proposed. The addition of Sn-Bi into the Ag or Cu is aimed to realize the plateless Cu-Cu bonding by the formation of IMC at the interface as an interface reaction layer, and also to achieve a highly densified matrix microstructure via the liquid phase. The isothermal solidification between Ag/Cu and the Sn-phase is assumed to shift the remelting temperature to temperature higher than the Sn-Bi eutectic temperature.

In ***Chapter 3***, all materials under test, sample preparations and evaluation methods that was applied to the investigation conducted in Chapter 4 and 5 has been described in details. Sn-Bi eutectic powders with 2 μm particle size has been adapted in this study to be added into commercially available Ag sintering paste and commercially available Cu nanoparticles ink. Sintering was conducted in a formic gas-comply reflow furnace, and shear strength evaluation was conducted with shear test apparatus that complies with the MIL-STD-883K, method 2019.9. MIL-STD-883K method 2019.9 has been used as a benchmark of shear strength in this study where for a die with bonding area

greater than 4 mm^2, shear force must exceed 2.5 kg. In this study, shear strength was evaluated in MPa, hence, since the shear test sample in this study has area of 19.6 mm^2, shear strength value that is needed to fulfill the specifications of this standard must be *greater than 2.5 MPa*. In addition, considering the maximum T_c in the SiC-based module to be 125 °C, the remelting temperature of the proposed Ag-based and Cu-based TLPS should be higher than 195 °C ($0.85T_h$). In this study, *remelting temperature higher than 200 °C* is set to be the criterion for the possibility in the application at high operation temperature.

Chapter 4 discussed about the Ag-based TLPS. The addition amount of Sn-Bi to the Ag influenced the shear strength. At low addition, i.e. 10wt% addition of Sn-Bi, the shear strength was at the lowest, even lower than that of without any addition. With increasing Sn-Bi addition amount, the shear strength was also increased, and reached its highest with the addition amount of 30wt%. The highest shear strength recorded for Ag-30SnBi sintered at 250 °C for 60 min was 26.7 MPa. On contrary, when the addition amount was higher than 30wt%, the shear strength drop again. The highest addition amount of Sn-Bi investigated in this study was 45wt%. The fracture mode shown by the Ag-30SnBi was cohesive mode, as compared to the other compositions investigated in this study which demonstrated adhesive failure. Lowering the sintering temperature of the Ag-30SnBi resulted in decreased shear strength, nevertheless, when sintered at 200 °C, the obtained shear strength, i.e. 9.0 MPa, passed the requirement of MIL-STD-883K. Prolonging the sintering holding time at sintering temperature of 200 °C revealed almost no change to the shear strength of Ag-30SnBi. It is interesting to note that the remelting temperature of all compositions investigated in this study was shifted to approximately 262 °C, implying the melting event of Bi-rich phase, as a result of complete conversion of Sn-phase to Ag-Sn IMCs. It was also found by DSC analysis that the isothermal solidification was assumed to be completed just right after the introduction of formic gas during the

sintering. Afterwards, with increasing sintering temperature and sintering holding time, the strengthening mechanism of Ag-30SnBi is thought to be attributed by the densification of the microstructure by solid-phase sintering. Higher sintering temperature, particularly at 250 °C, is thought to contribute to the densification, as observed by the SEM image of the sintered structure. In addition, the introduction of formic gas also contributed to the densification by assisting the formation of sintering neck with the reduction of oxide layer at the particles, as observed by SEM. Finally, using the Ag-30SnBi, a Cu to Ni-plated Cu bonding was conducted at 250 °C for 60 min, and it was found that the obtained shear strength was approximately 35% lower than that of Cu-Cu bonding. Nevertheless, the observed fracture surface revealed that the fracture path consist of the delamination of Ni-plating from the Cu substrate, indicating that the shear strength of Ag-30SnBi at Cu-Ni/Cu bonding might be influenced by the poor interface strength between Ni-plating and Cu-substrate.

Chapter 5 talked about the Cu-SnBi TLPS. In previous work on TLPS of Cu-SnBi, the remelting event at 139 °C due to the residual Sn-Bi was unavoidable, which will be unfavorable for the high temperature application of SiC-based module. This study is the first to develop a process in which the remelting temperature was completely shifted to around 200 °C. Cu-65SnBi and Cu-70SnBi that was sintered at 250 °C showed shear strength higher than 20 MPa at r.t. However, the observed remelting temperature was at 138 °C, for both composition. According to the Cu-Sn-Bi ternary system from the literature, it was clear that the invariant reaction of locally concentrated Cu_6Sn_5 and Bi at approximately 195 °C resulted in new liquid phase. This new liquid phase is assumed to contribute to the rapid densification in the microstructure. In addition, this liquid phase is thought to solidify as Sn-Bi eutectic phase in non-equilibrium state despite the ternary composition due to the low solubility of Cu. Nevertheless, by controlling the sintering temperature to be slightly above than the reaction temperature i.e. at 200 °C, Cu-65SnBi but Cu-70SnBi demonstrated no remelting event

at the Sn-Bi eutectic temperature. From the DSC analysis result, it was found that the remelting event at Sn-Bi eutectic temperature of Cu-70SnBi might be resulted from the residual Sn-Bi that was left unreacted after the introduction of formic gas during sintering. On the other hand, isothermal solidification of Cu-65SnBi was thought to be completed before the occurrence of the invariant reaction at 195 °C as mentioned above. From the SEM observation of the sintering surface and the cross-section, the densification of the microstructure in Cu-65SnBi was abruptly changed by the formation of liquid phase at 200 °C. Prolonging sintering holding time from 90 min to 180 min of Cu-65SnBi when sintered at 200 °C contributed to the increase in shear strength by 20%, indicating that providing sufficient time for the densification at low temperature may contribute in increasing shear strength. Finally, by using Cu-65SnBi, Cu-Ni/Cu bonding was performed at 200 °C for 90 min and revealed shear strength decrease by 16%, but still satisfying the requirement of MIL-STD-883K.

In ***Chapter 6***, Ag-based and Cu-based TLPS has been compared in term of Sn-Bi liquid phase volume fraction to determine the relationship between the liquid phase volume fractions with the shear strength of the proposed Sn-Bi added TLPS. It was found that no definitive common Sn-Bi liquid phase volume fraction can be defined to contribute to the strengthening of the both Ag-based and Cu-based TLPS. The strengthening mechanism depending to the Sn-Bi volume fraction and weight percentage can be categorized into four sections (I – IV):

I. *Sn-Bi liquid volume fraction < 29 vol%*:

   Lack formation of Cu-Sn IMC interfacial reaction layer resulted in weak interface and fracture at the interface of Cu substrate and Ag-SnBi matrix.

II. *Sn-Bi liquid volume fraction at approximately 35 vol%*:

   Uniformly formed Cu-Sn IMC interfacial reaction layer strengthened the interface of Ag-based TLPS. Fracture type was shifted from adhesive to cohesive-type (Ag-30wt%SnBi).

III. *Sn-Bi liquid volume fraction > 35 vol%, < 60 vol%*:

In Ag-based TLPS, the formation of Kirkendall voids at the interface of Cu substrate and Cu_3Sn is assumed to act as the crack initiation site and resulted in the adhesive-type failure. Meanwhile, in Cu-based TLPS, almost no Kirkendall voids was observed at the interface owing to the Cu mass transportation from the Cu substrate might be suppressed by the Cu supply form the Cu-SnBi (matrix). However, the void-dominant porous microstructure is thought to result in the low shear strength.

IV. *Sn-Bi volume fraction > 60 vol%, Sn-Bi weight percentage ≥ 60 wt%*:

The introduction of a new liquid phase at temperature above 195 °C in Cu-based TLPS contributed to the rapid densification of the porous sintering microstructure and increase the shear strength, accordingly.

Summary of alloys compositions and sintering conditions that fulfill the requirements as defined in this study is shown in Table 7.1. A patent has been applied for the Ag-based and Cu-based TLPS that have been discussed in this dissertation. The submitted patent application information is as follows (in Japanese):

Kato Ryoichi, Gohara Hiromichi, Ikeda Yasunari, Mochizuki Eiji, Takahashi Kazuyoshi, Yoshida Makoto, Muhammad Khairi Faiz, 2017-000281, Power Electronics Module Manufacturing Method and Power Electronics Module

Table 7.1 Alloy compositions and sintering conditions that satisfied the requirement of processing conditions, and the obtained shear strength and remelting temperature, as investigated in this study

Alloy composition	Sintering conditions			Bonding Conditions		Shear strength (Max.) MPa		Remelting temperature °C
	Temperature °C	Pressure MPa	Holding time min	Fluxless	Plateless Cu-Cu	≥ 20*	≥ 2.5**	(T_c max=125)
Target in this study	*≤ 200*	*≤ 0.1*	*n/a*	○	○	○	○	*≥ 200***
Ag-30SnBi	× (250)	○ (0.02)	60	○	○	○ (26.7)	○	○ (262)
Ag-30SnBi	○ (200)	○ (0.02)	60	○	○	× (12.7)	○	○ (262)
Cu-65SnBi	○ (200)	○ (0.1)	90	○	○	○ (21.2)	○	○ (200)
Cu-70SnBi	○ (200)	○ (0.1)	90	○	○	○ (22.3)	○	× (138)

* Equivalent to the Pb-based solder (Eiichi Ide et al., Mater. Trans. 47 (2006) p211)

** MIL-STD-883K (2.0 ×)

*** Considering $T_c = 0.85T_h$

7.2 Future Works

Transient liquid phase sintering technology developed in this study is anticipated to be exploited for the application on bonding epoxy-molded SiC-based power module to the Cu heat spreader/sink. Future works for the TLPS of Ag or Cu mixed with Sn-Bi in this study are described as follows:

i. Ag-SnBi and Cu-SnBi TLPS developed in this study was evaluated solely on the shear strength properties, and remelting temperature event measurement to confirm the high thermal stability of the proposed bonding material. However, as the proposed materials is expected to be applied adjoining to the heat sink, thermal conductivity is one of significant parameters that will determine the worthiness of applying the proposed TLPS technology as thermal interface material. Thermal conductivity and specific heat are the parameters that should be obtained in the future.

ii. Thermal interface material is used to transport the heat from the module to be dissipated into the heat sink. Hence, the TLPS materials is expected to be exposed to repetitive heating and cooling at both sides. Hence, effects of thermal cycle to the fatigue behavior and fatigue life is in great concern. Thermal cycle test or thermal shock test may be used to investigate the phenomenon of fatigue in IMCs-rich joints.

iii. On reducing cost and evaluation time, numerical analysis such as finite element method analysis has been used broadly to investigate the deformation mechanisms of materials under certain conditions and constrains. Mechanical properties of the materials developed in this study is not acquired yet, hence, in order to construct a constitutive model of the proposed TLPS materials, tensile shear test or any other test suitable to acquire the mechanical properties should be conducted.

ACKNOWLEDGMENT

Alhamdulillah, Praise be to God, *Al-Alim* wa *Ar-Rashid*, The All-Knowing, and The Guide, Infallible Teacher and Knower; as no gratitude should surpass the praise to Him. Undoubtedly, without His grace and mercy, I am incapable of finishing this PhD journey.

I would like to express my sincerest appreciation to Professor Yoshida Makoto, my PhD dissertation supervisor for his undivided support and constant research guidance. I am indebted to him for accepting me as his student after the loss of my master thesis supervisor, the late Professor Horibe Susumu. Professor Yoshida has shown me a great deal of enthusiasm towards science and engineering, and his firm standing that any research should benefit the mankind and not for just self-satisfaction, has my utmost respect.

I would also like to thank the other referees, Professor Miyashita Tomoyuki from Waseda University, and Professor Suga Tadatomo from The University of Tokyo, for offering me thoughtful advice and guidance. Those fruitful discussions have allowed me to improvise the contents of this dissertation.

I am grateful to Dr. Takahashi Yoshikazu, Dr. Ikeda Yoshinari, Mr. Gohara Hiromichi, and Mr. Kato Ryoichi from Fuji Electric Co., Ltd. It is not an exaggeration to mention that this research would not first take place without them. They came to our lab bringing a head-scratching problem on the need of low temperature bonding, but fortunately they also came with a large sum of money to conduct the research so that this can be realized.

My special thanks go to Mr. Yoshinari Goro and Mr. Mochizuki Akihiro from Alent Japan Company for allowing me to use the reflow system in the early stage of this study. Without them, I might still stuck at the problem of removing the oxide layer of the particles. I would also like to acknowledge the staff at Waseda University from Materials Characterization Central Laboratory and Kagami Memorial Research Institute for Materials Science and Technology for their kind assistance during conducting the analysis.

Throughout my time as a PhD candidate in the Yoshida Lab, I have had the pleasure of working with and getting to know many interesting and talented people, both research-wise and life-wise. I would like thank my other PhD-mates, Dr. Takai Ryosuke and Dr. Matsushita Akira. Both of you are truly an example of great researcher and friend, whose kind support has put me at ease during my turbulence time.

To my supportive Power Module Group member: Marumoto Yumi (formerly Yamauchi Yumi), Ahmad Sufian, Bansyo Kazuma, Yamamoto Takehiro, Asakura Yo, Ashida Hajime, Abe Yuki, Maita Hiroko, and Kobayashi Satoshi; I am deeply indebted with all of you, and thank you for sharing your knowledge and experience with me. Not to forget, Kan Xuan, Ishizaki, Kotaki, Naoki, Iwamoto, Uehara, Ito, Sano, Someya, Nagata, and other Yoshida Lab members to name a few, your friendship means the world to me. Special thanks also go to my Penguin-mates who have been great companions during high and low, up and downs, happy and sad; you know who you are.

I also would like to acknowledge Yayasan Pelajaran Mara, Malaysia for providing the scholarship starting from my undergraduate study in University of Selangor until my PhD study in Waseda University. Without this scholarship, I cannot imagine myself now. Coming from a moderate-income family from the rural east-coast Peninsular Malaysia, pursuing my higher education to a foreign country was just a dream, and for that, I will forever be grateful.

Most importantly, I would like to dedicate this work to my family, whose encouragement and support have gotten me to where I am today. To Mama, Latifah binti Ismail, Abah, Ahmad Hairuddin bin Mokhtar, and also my brother, Muhammad Khairi Fadhil, literally, no words can describe how much I owe you for your unconditional love and unyielding support. I love you all very much.

This dissertation is based on the results obtained from a project subsidized by the New Energy and Industrial Technology Development Organization (NEDO), Japan.

October 2017

Muhammad Khairi Faiz Bin Ahmad Hairuddin

LIST OF PUBLICATIONS

Publications related to this dissertation

Original Research Article

1. Muhammad Khairi Faiz, Takehiro Yamamoto, Makoto Yoshida, Low temperature and low pressure bonding of plateless Cu-Cu substrates by Ag-based transient liquid phase sintering, Journal of Materials Science: Materials in Electronics 28 (2017) 9351-9362

2. M. Khairi Faiz, Kazuma Bansho, Tadatomo Suga, Tomoyuki Miyashita, Makoto Yoshida, Low temperature Cu-Cu bonding by transient liquid phase sintering of mixed Cu nanoparticles and Sn-Bi eutectic powders, Journal of Materials Science: Materials in Electronics, *published online (20 July 2017)*

Conference and Proceeding

3. M. Khairi Faiz, Takehiro Yamamoto, Makoto Yoshida, Sn-Bi added Ag-based transient liquid phase sintering for low temperature bonding, 2017 5th International Workshop on Low Temperature Bonding for 3D Integration (LTB-3D), May 16-18, Tokyo, Japan, p34

4. M. Khairi Faiz, Takehiro Yamamoto, Makoto Yoshida, Low temperature and low pressure fluxless Cu-Cu bonding by Ag-based transient liquid phase sintering for high temperature application, IEEE CPMT Symposium Japan 2017, November 20-22, *Accepted for oral presentation in regular session*

5. Takehiro Yamamoto, M. Khairi Faiz, Makoto Yoshida, Low temperature low pressure fluxless and plateless Cu-Cu bonding by Cu nano particle transient liquid phase sintering, IEEE CPMT Symposium Japan 2017, November 20-22, *Accepted for Early Career Researcher's (ECR) poster presentation session*

Patent (in Japanese)

6. 加藤遼一，郷原広道，池田良成，望月英司，高橋良和，吉田誠，ムハマド ハイリ ファイズ，2017-000281，半導体装置の製造方法及び半導体装置
(Power Electronics Module Manufacturing Method and Power Electronics Module)

Others (Publication unrelated to this dissertation)

Original Research Article

7. Hiroyuki Shimano, M. Khairi Faiz, Asato Hara, Kyoko Yoshizumi, Makoto Yoshida, Susumu Horibe, Analysis of partially pulsating fatigue process on carbon steel with microstructural observation, Materials Science & Engineering A 651 (2016) 83-88